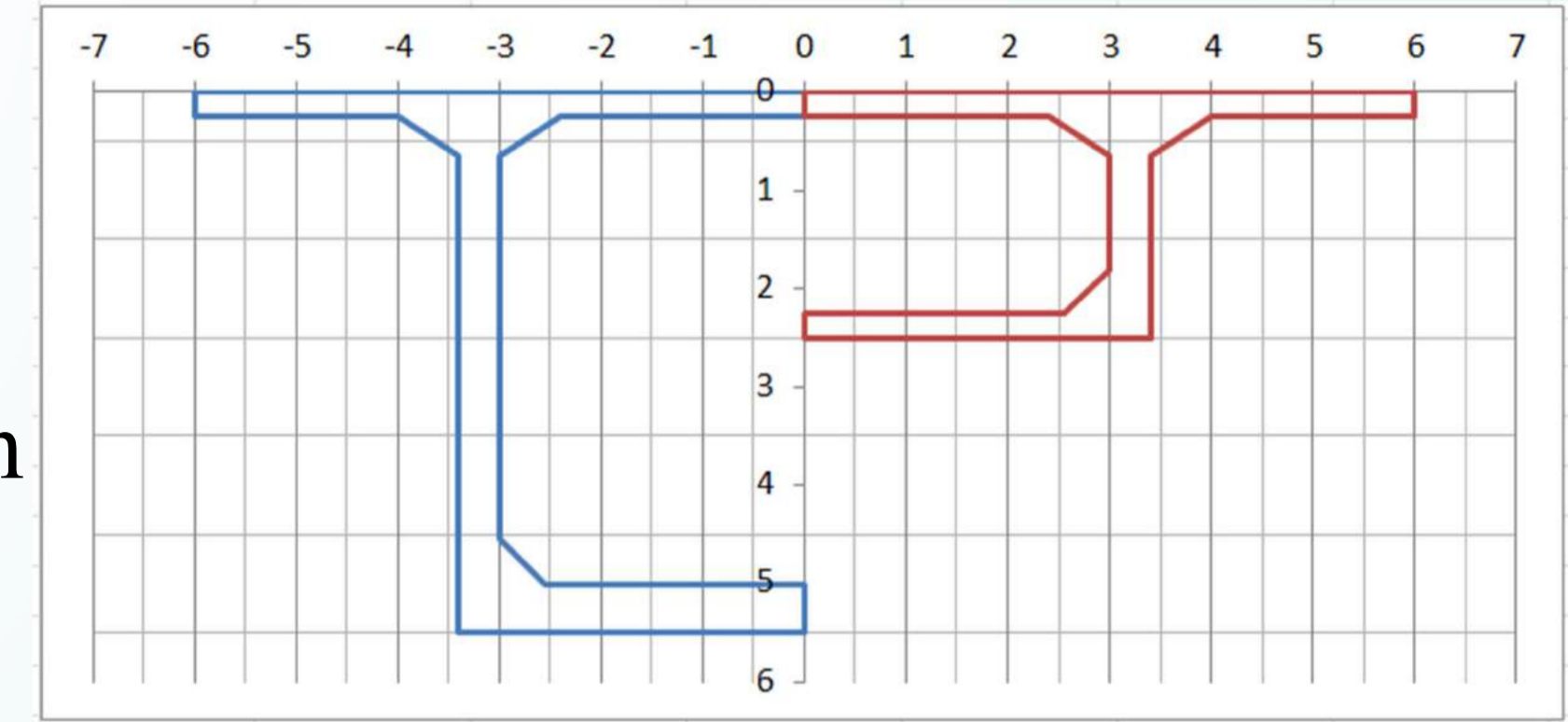


Target

Optimization of prestressed concrete bridges aiming to minimize the cost while maintaining the bridge's functionality, has long occupied the mind of many researchers.

Objectives set for this study:

- Resolution of a multi-span beam with variable stiffness using a new developed analytical approach
- Introducing the new pivot rule in fully and partially prestressed concrete sections (SLS & ULS)
- Develop new methods of optimization for the design of prestressed concrete Bridges



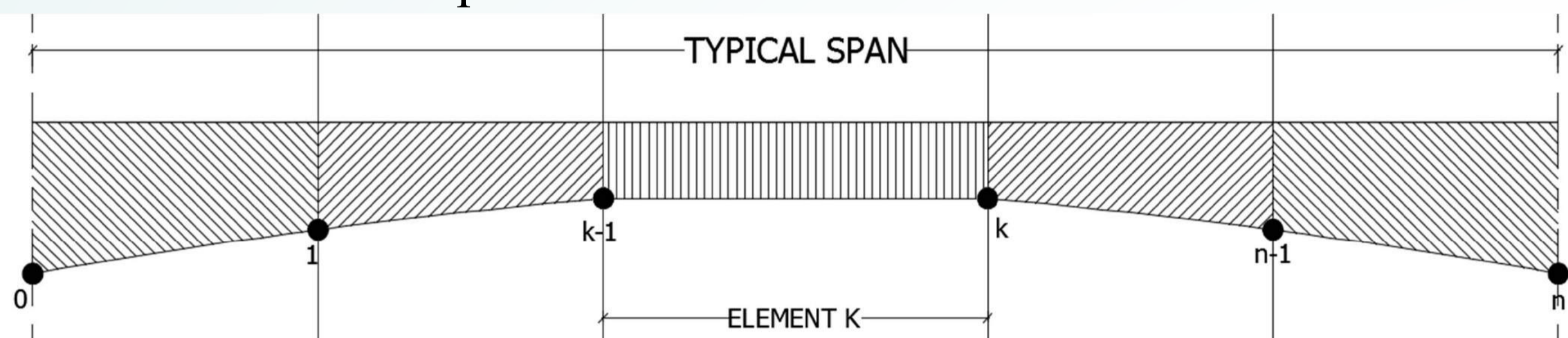
Methodology

New "Transfer Matrix" Method For Continuous Beams :

$$S_n = \int_0^l \frac{x^n}{l^n} \frac{dx}{EI}$$

Main principles behind this Method:

1. Use the integral S_n for the calculation of the Mechanical Constants (a, b & c) and the Rotations δ_i of the 3-Moment equation.
2. Choose the proper segmentation along the beam. ("Beam Meshing")
3. Convert the S_n expression into a "Matrix"



$$S_{k,n} = S_{k-1,n} + \sum_{j=0}^n \binom{n}{j} \beta_k^n \alpha_k^{n-j} (1 - \alpha_k)^j \times I_{k,j}$$

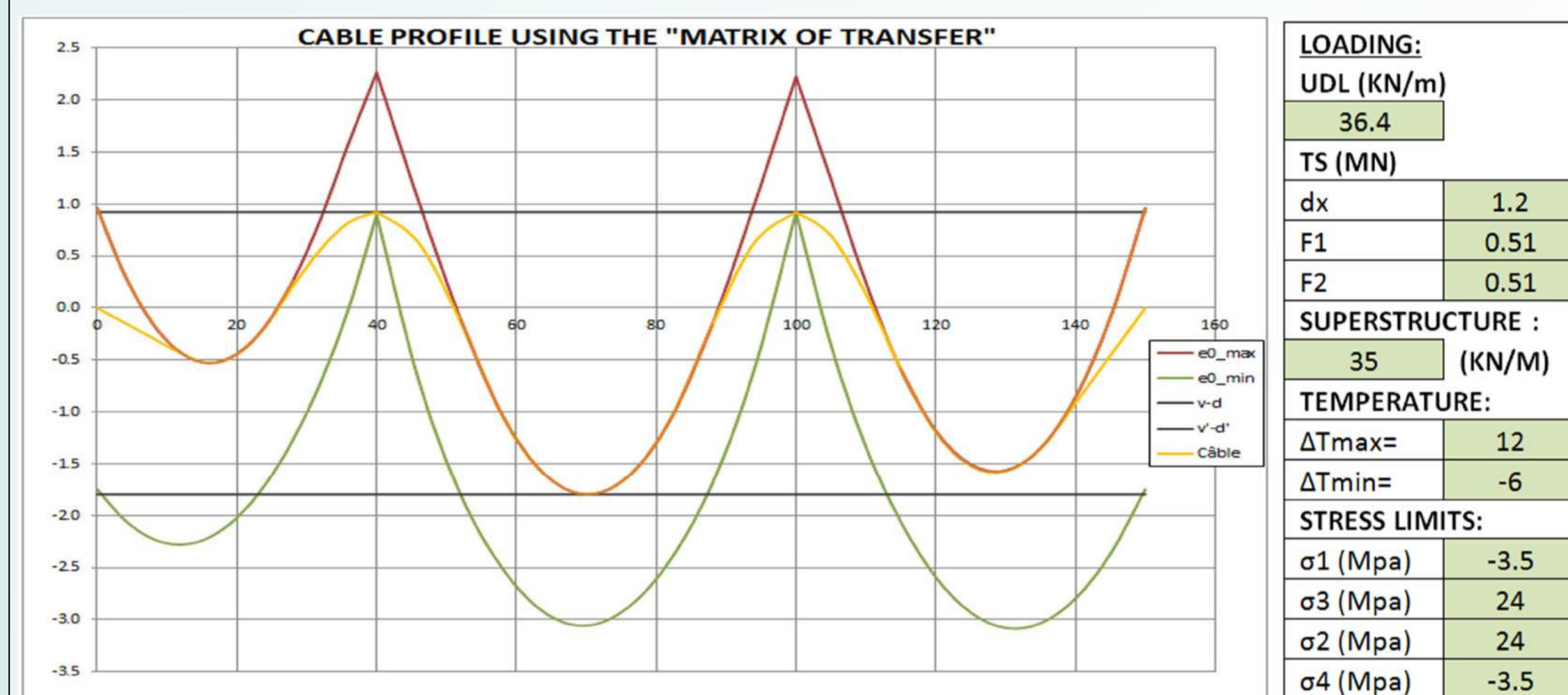
$$\frac{x_k^n}{l^n} = \beta_k^n$$

$$\frac{x_{k-1}}{x_k} = \alpha_k$$

$$\begin{bmatrix} S_{k,0} \\ S_{k,1} \\ S_{k,2} \\ S_{k,3} \end{bmatrix} = \begin{bmatrix} S_{k-1,0} \\ S_{k-1,1} \\ S_{k-1,2} \\ S_{k-1,3} \end{bmatrix} + A(\beta_k, \alpha_k) \begin{bmatrix} I_{k,0} \\ I_{k,1} \\ I_{k,2} \\ I_{k,3} \end{bmatrix}$$

Results

Multi-Span PT beam using the "Matrix of Transfer":



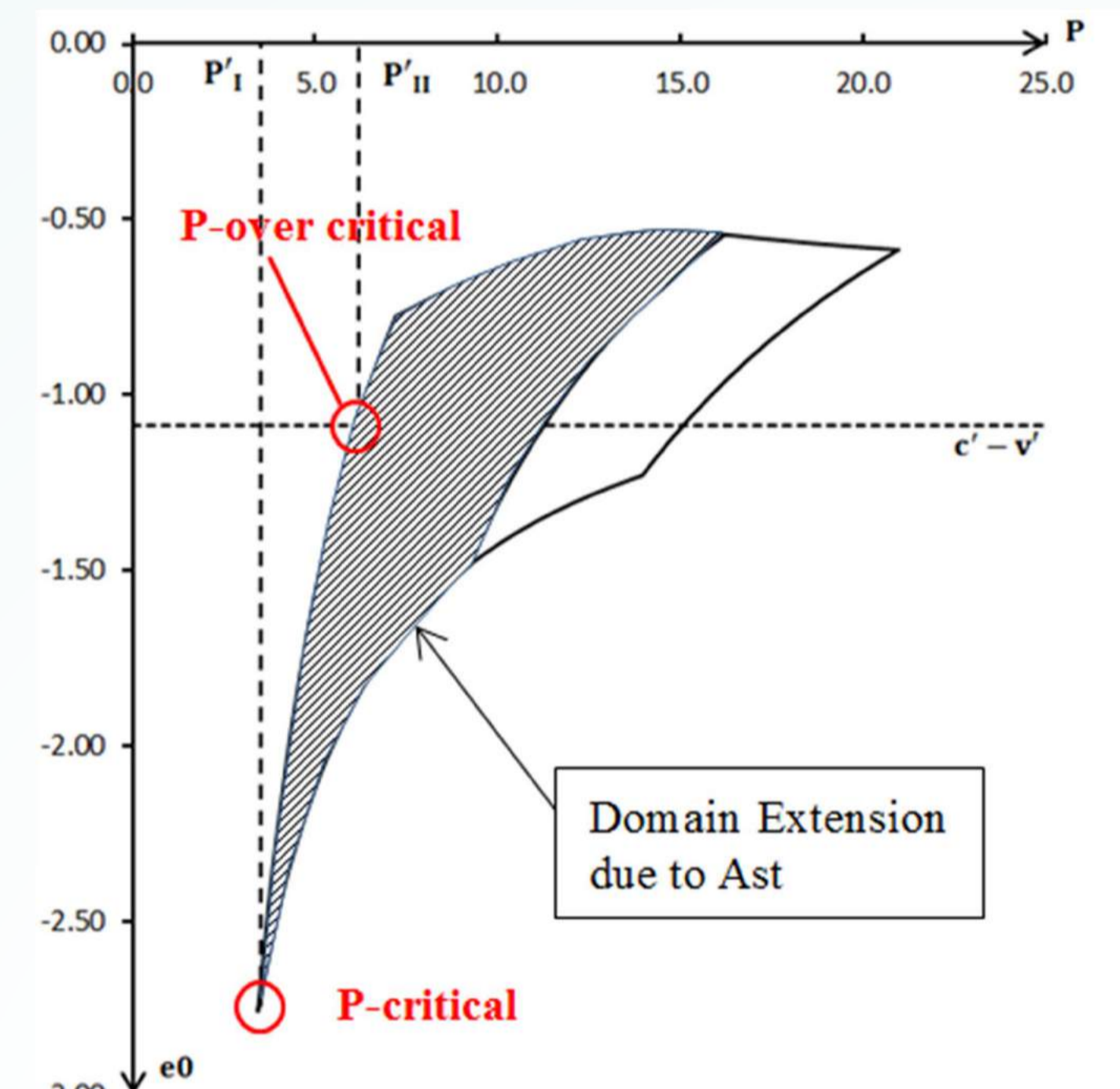
Problem solved without the need of Numerical Methods!!

Rotation due to Prestressing moment formulated Using the "Matrix of Transfer"

$$\delta_i = \int_0^{l_{i+1}} \left(1 - \frac{x}{l_{i+1}}\right) e_0(x) \frac{dx}{EI} + \int_0^{l_i} \frac{x}{l_i} \frac{dx}{EI} = (S_0 - S_1)_{i+1} + S_1$$

Optimization of Partial prestressing force P using Pivot Rule:

Geometry		Stress Limits		
b	2 m	$\bar{\sigma}_1$	-2	Mpa
h	2.5 m	$\bar{\sigma}_2$	24	Mpa
b_w	0.24 m	$\bar{\sigma}_3$	24	Mpa
h_f	0.16 m	$\bar{\sigma}_4$	0	Mpa
b_t	0.8 m	W_k	2	mm
h_t	0.4 m	Material		
h_g	0.2 m	f_{ck}	40	MPa
b_g	0.4 m	$f_{ct,eff}$	3.5	MPa
e_g	0.2 m	E_s	200	GPa
Cover		α_e	5.70	
Moments				
c	0.2 m	M_{min}	2	MN.m
c'	0.2 m	M_{max}	12	MN.m
c_p	0.04 m			



Results under ELS-car:

	Case 1	Case 2	Case 3	Case 4
$A_{st}(\%)$	0	0.5	1	1.5
$\bar{\sigma}_{st}(Mpa)$	0	197	238	257
P(MN)	12.20	8.03	6.12	4.15

Significate Reduction of P in Partially Prestressed Concrete = 60% for a 1.5% of Ast

New Pivot Rule for Fully and Partially Pre-stressed Concrete:

Main Equations to be satisfied by the EN:

Stress Limitation

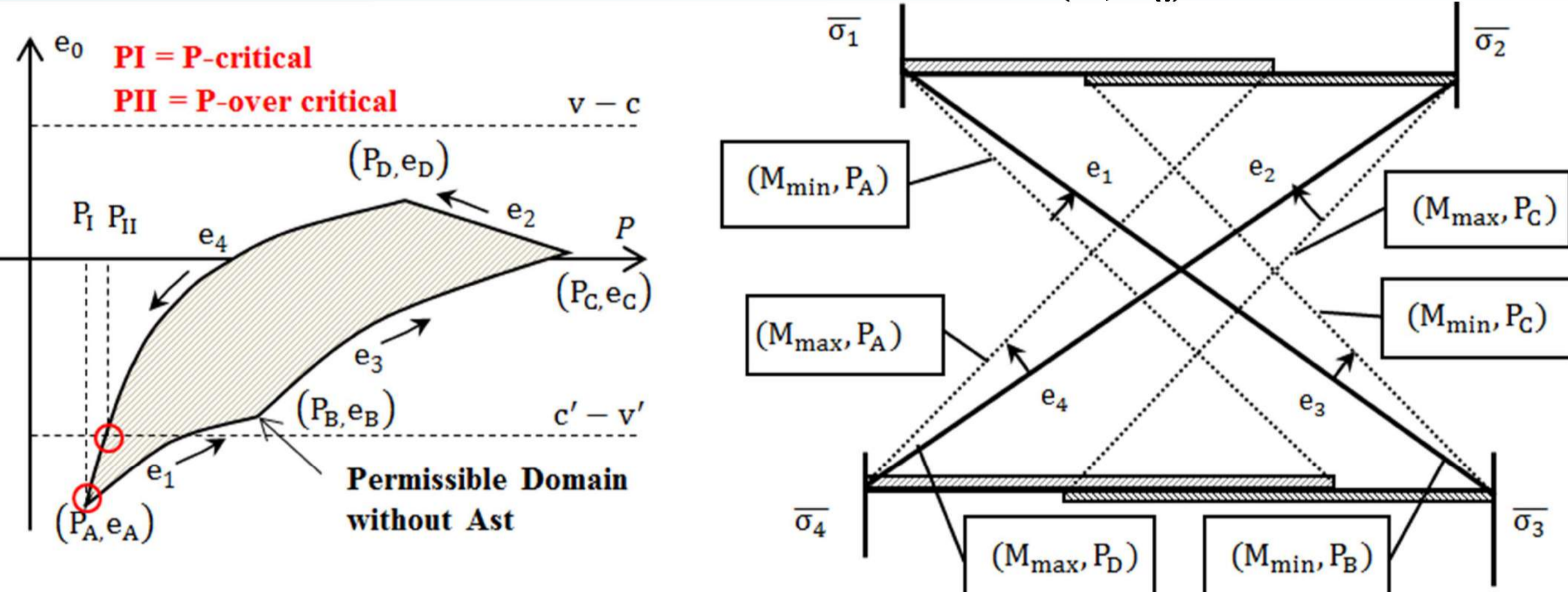
$$\bar{\sigma}_1 \leq \sigma_{sup}(M_{min}) \leq \sigma_{sup}(M_{max}) \leq \bar{\sigma}_2$$

$$\bar{\sigma}_4 \leq \sigma_{inf}(M_{max}) \leq \sigma_{inf}(M_{min}) \leq \bar{\sigma}_3$$

Cover Limitation

$$-(v' - c') \leq e_0 \leq v - c$$

Permissible domain of (P, e_0):



- Along each Hyperbola e_i , Only **1 constraint** is satisfied
- At Intersection Points, **2 constraints** are satisfied **simultaneously**

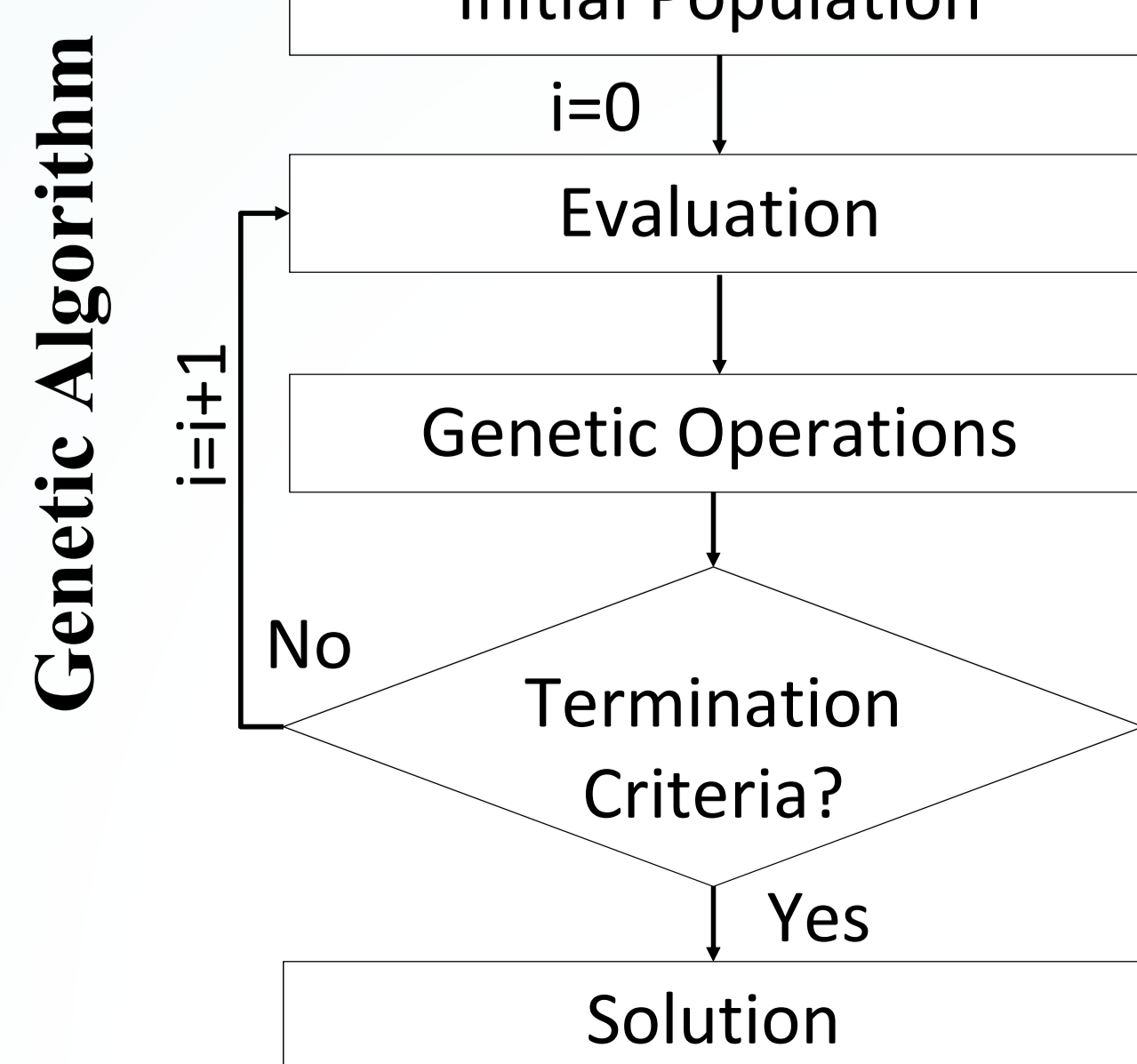
Optimization Method

Optimizing an objective function (Cost, P, A_c ...) using either Analytical or Numerical Methods.

Minimize $f(X)$

Subject to $g_j(X) < 0$
 $h_k(X) = 0$
 $x_{i,lower} < x_i < x_{i,upper}$

$$f: C_{conc} A_{conc} + C_{Ast} A_{Ast} + C_{Ap} A_{Ap} + \sum w_i \text{Constraint}_i$$



Expected Results

- Find the portion of moment to be resisted by Ast for an optimal solution in Partial Prestressed Concrete
- Apply analytical optimization methods for 2 and 3 spans beams
- Develop numerical optimization tool, based on Genetic Algorithm, for a multi span prestressed beam with constant inertia and for a cantilevered bridge with variable inertia



Bibliography

1. [EC2 05] EUROCODES., NF EN 1992-1-1, AFNOR, 2005
2. [NIL 77] NILSON A.H., « Flexural Stresses after Cracking in Partially Prestressed Beams », PCI Journal, vol. 21, n° 4, 1977, p. 72-81.
3. Z. Aydm and Y. Ayvaz, "Optimum topology and shape design of prestressed concrete bridge girders using genetic algorithms," Struc Multidisc Optim, no. 41, pp. 151-162, 2010.
4. [DIL 86] DILGER W.H., SURI K.M., « Steel stresses in Partially Prestressed Concrete Members », PCI Journal, vol. 31, n° 3, 1986, p. 88-112.

Bending creep of notched beams in sheltered outdoors conditions: applications on Gabonese and European wooden species



M. ASSEKO ELLA^{1,2}, R. MOUTOU PITTI^{1,3}, J. GRIL^{1,4}, G. GODI¹, E. Fournely¹



Ecole doctorale Sciences Pour l'Ingénieur

¹Université Clermont Auvergne, CNRS, SIGMA Clermont, Institut Pascal, Clermont Ferrand, France, martian.asseko_ella@etu.uca.fr

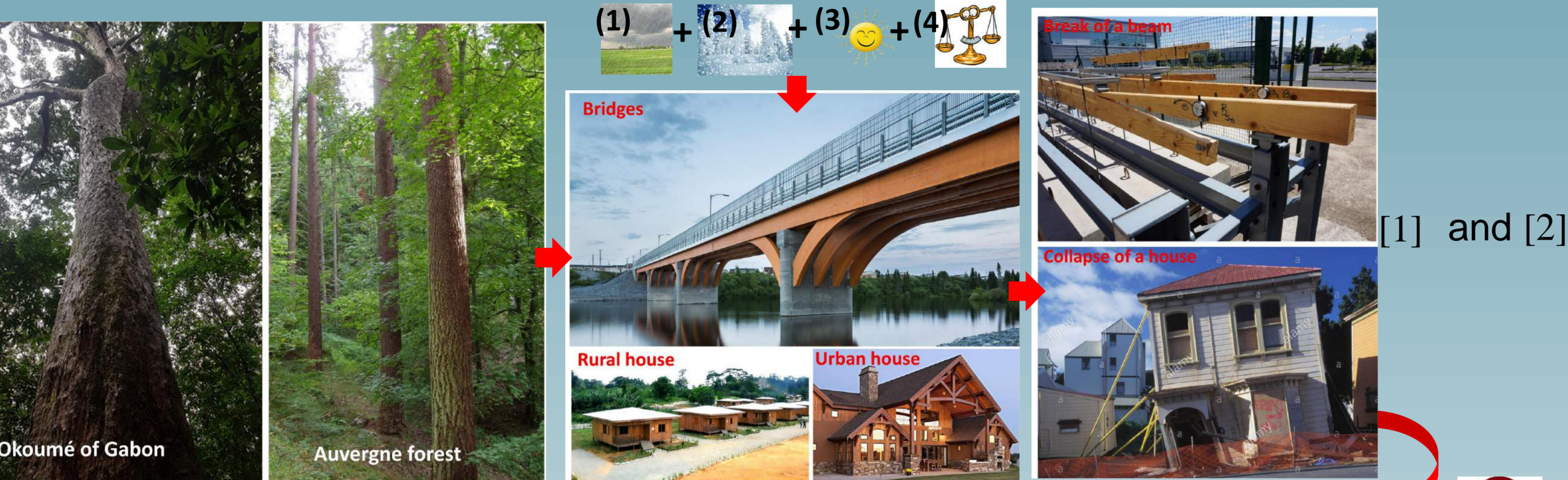
²Ecole Nationale des Eaux et Forêts (ENEF), Libreville, Gabon ;

³CENAREST, IRT, Libreville, Gabon

⁴Université Clermont Auvergne, INRA, UMR PIAF, Clermont Ferrand, France

1.Context

Interactions between climatic variations (1, 2, 3) and mechanical loads (4)



Interactions between climatic variations (1, 2, 3) and mechanical loads (4), **coupling with crack process**

3.Methods

The characterization is done on tropical wood Iroko (Fig.1a) Padouk (Fig.1b) and Okume (Fig.1c). Specimens (L=680 x 40x60 mm) were brought back from Gabon to Clermont-Ferrand.

Fig 1: Raw beams of tropical species brought back from Gabon: (a) Iroko (b); Padouk (c); Okume



Determination of specimen geometry:

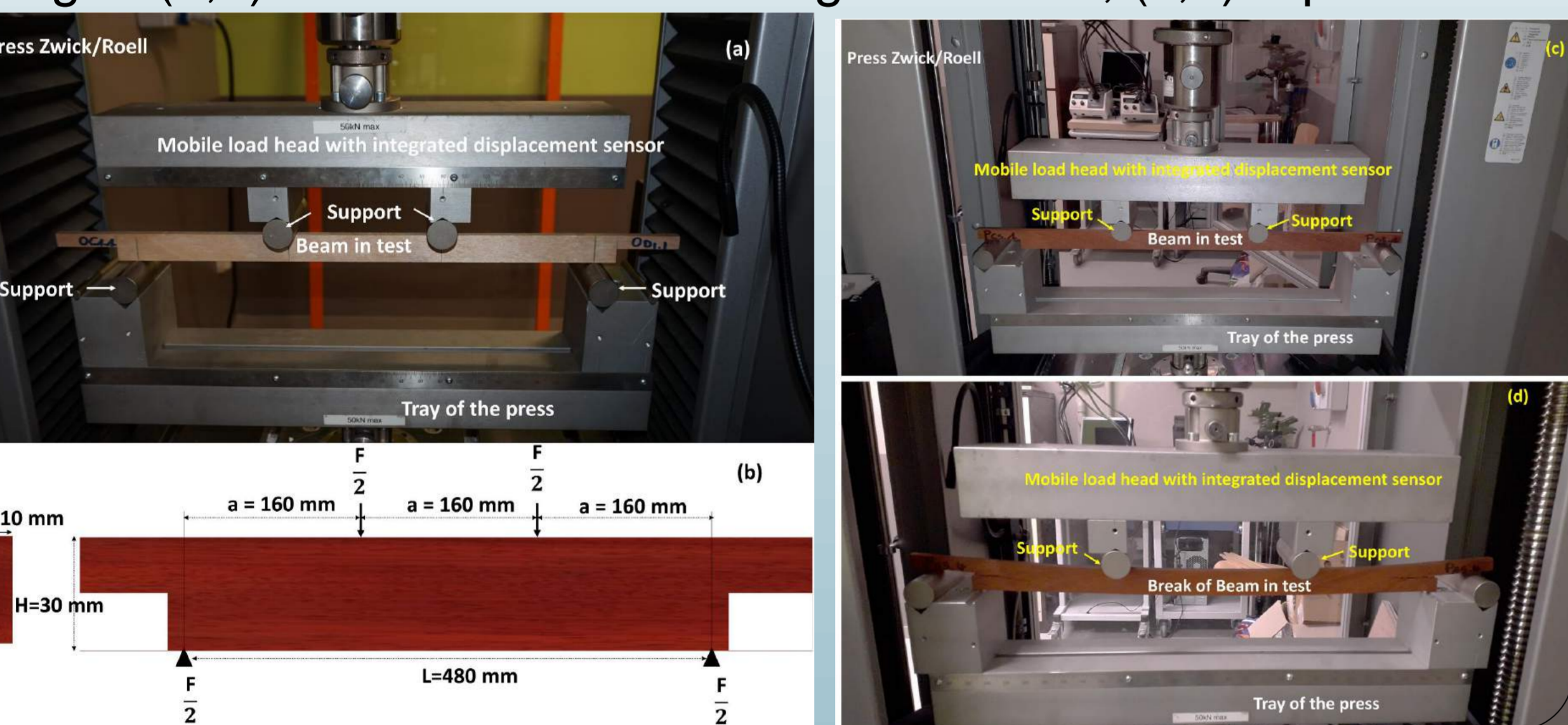
(9) allowed us to validate the geometry of the beams presented in (Fig. 2) $l = 38,3 \text{ mm}$ and $Lr = 63,3 \text{ mm}$.

Fig 2. Geometry of test specimens (a); Padouk (b) Iroko (c); okume



3.2. Experimental approach

Fig.3: (a,b) Measurement of Young's modulus; (c,d) rupture test



$$E_L = \frac{5L^3 (F_2 - F_1)}{324I_0(U_2 - U_1)} \quad (10)$$

$$F_{load} = \frac{bH^2 E_L \varepsilon_{load}}{L} \quad (11)$$

$$\varepsilon = \frac{864H}{167L^2} y \quad (12)$$

$$y = \frac{FL^3}{E_L I_0} \left(\frac{5}{324} + \frac{7}{48} \left(\frac{1}{\alpha} \right)^3 \right) \quad (13)$$

4.Results

Wood	Density	MC (%)	$E_{L(10)}$ (MPa)
Okume	0,47(0,03)	13,11(0,58)	7 694(421)
Padouk	0,77(0,09)	10,44(1,12)	10 898(748)
Iroko	0,60(0,06)	10,96 (0,56)	10 194(277)

In ()=Standard deviation; MC =moisture content, $E_{L(10)}$ =Longitudinal Young's modulus given by (10)

(a): measuring of Young's modulus
(b,c,d) rupture tests

Wood	ε_e (%)	ε_{c1} (%)	ε_b (%)	ε_{load} (%)	F_{load} (daN)	F_{c1} (daN)	F_b (daN)
Okoumé	0,183(0,015)	0,313(0,051)	0,51 (0,096)	0,26	29,64	36,6(39)	51,1(67)
Padouk	0,234(0,023)	0,394(0,064)	0,509(0,062)	0,27	43,42	59,7(97)	68,8(130)
Iroko	0,157(0,017)	0,202(0,026)	0,203(0,024)	0,16	25,34	30,4(30)	30,4(30)

In ()=Standard deviation ; F_{c1} =critical force; F_b =rupture force ; ε_e =elastic limit ε_{c1} =; critical strain ε_b =rupture strain; y =deflection; ε = strain of the beam during the test ; F_{load} =Loading force for creep test; ε_{load} = Loading strain for creep test

6. Conclusion

This study presents the dimensioning and the characterization of the beams in outdoor conditions. It is based on strength of materials and experimental approaches. This approaches enabled us to validate the specimens geometry and to estimate the loading strain and the loading forces for the creep test.

2.Objective

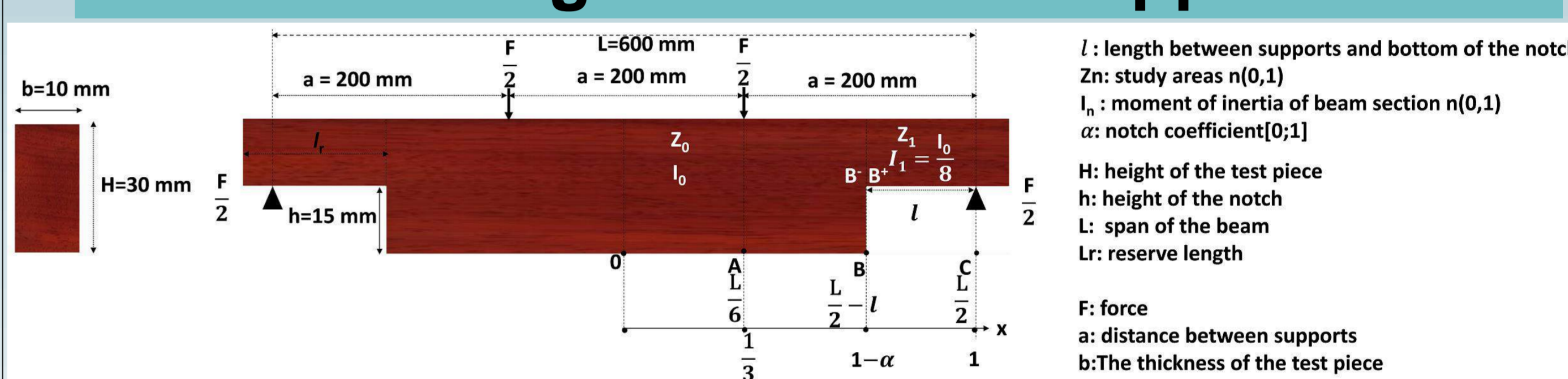
General objective:

- Evaluate the influence of initial defects on the structural response and crack propagation, and adapt the design codes to the context of structural use of wood in tropical and temperate environments

Specific objectives:

- creep tests in 4-point bending of notched beams in sheltered outdoor conditions
- Characterization of diffusion process
- Coupling between rupture, creep and sorption

3.1. Strength of Materials approach



$$\sigma_0 = \frac{HM_0}{2I_0} \quad (1)$$

$$\sigma_1^{B-} = \frac{3HM_0}{4I_0} \alpha \quad (2)$$

$$\sigma_1^{B+} = \frac{3HM_0}{I_0} \alpha \quad (3)$$

$$\sigma_1^{B-} \leq \sigma_1^{B+} \quad (4)$$

$$\text{if } \sigma_1^{B+} = \sigma_0 \rightarrow \alpha = \frac{1}{6}$$

$$(7) \rightarrow l = \frac{L}{12}$$

$$I_0 = \frac{BH^3}{12} \quad (5)$$

$$M_0 = \frac{FL}{6} \quad (6)$$

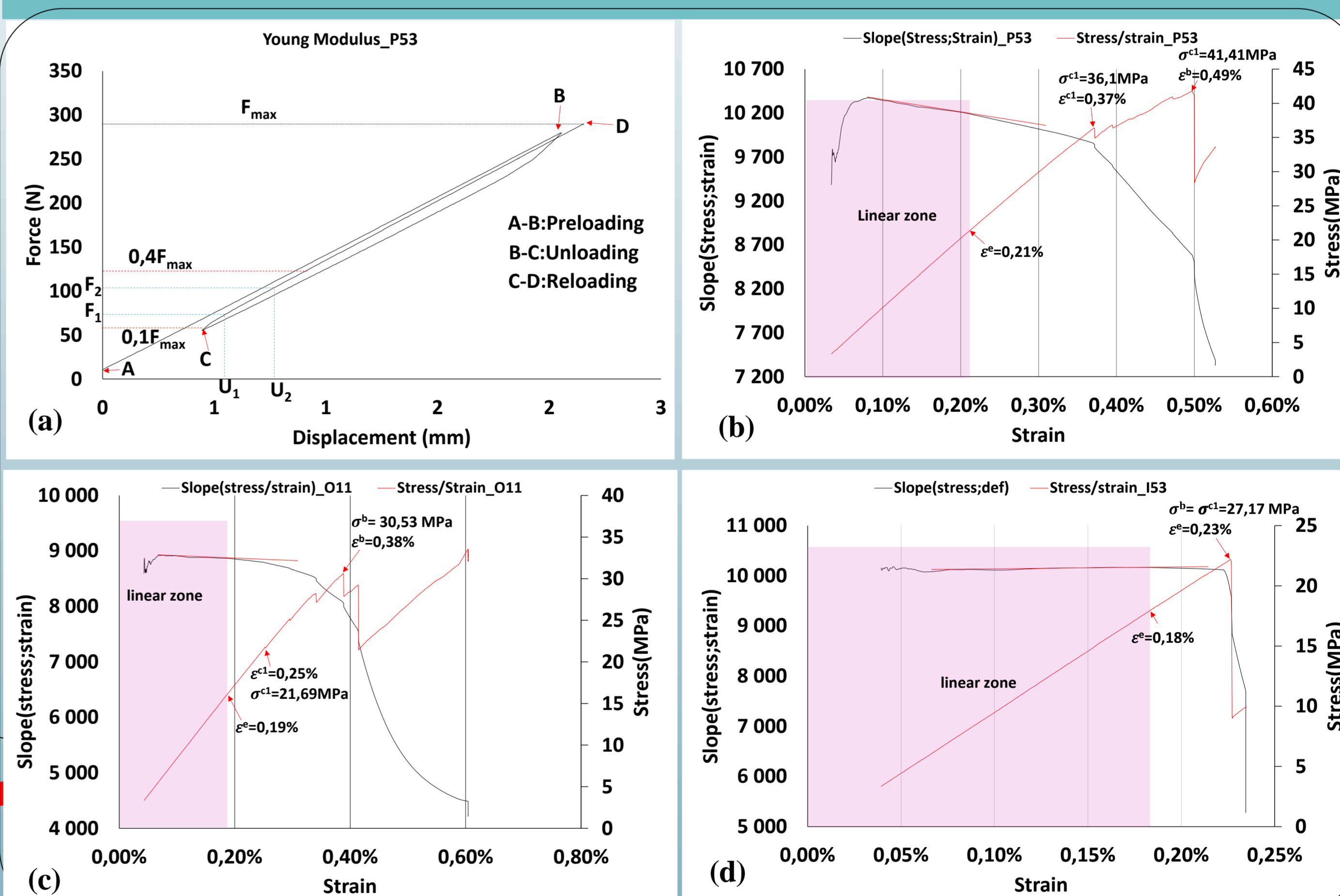
$$l = C - B = \frac{\alpha L}{2} \quad (7)$$

$$\alpha = 1 - \frac{2x(B^+)}{L} \quad (8)$$

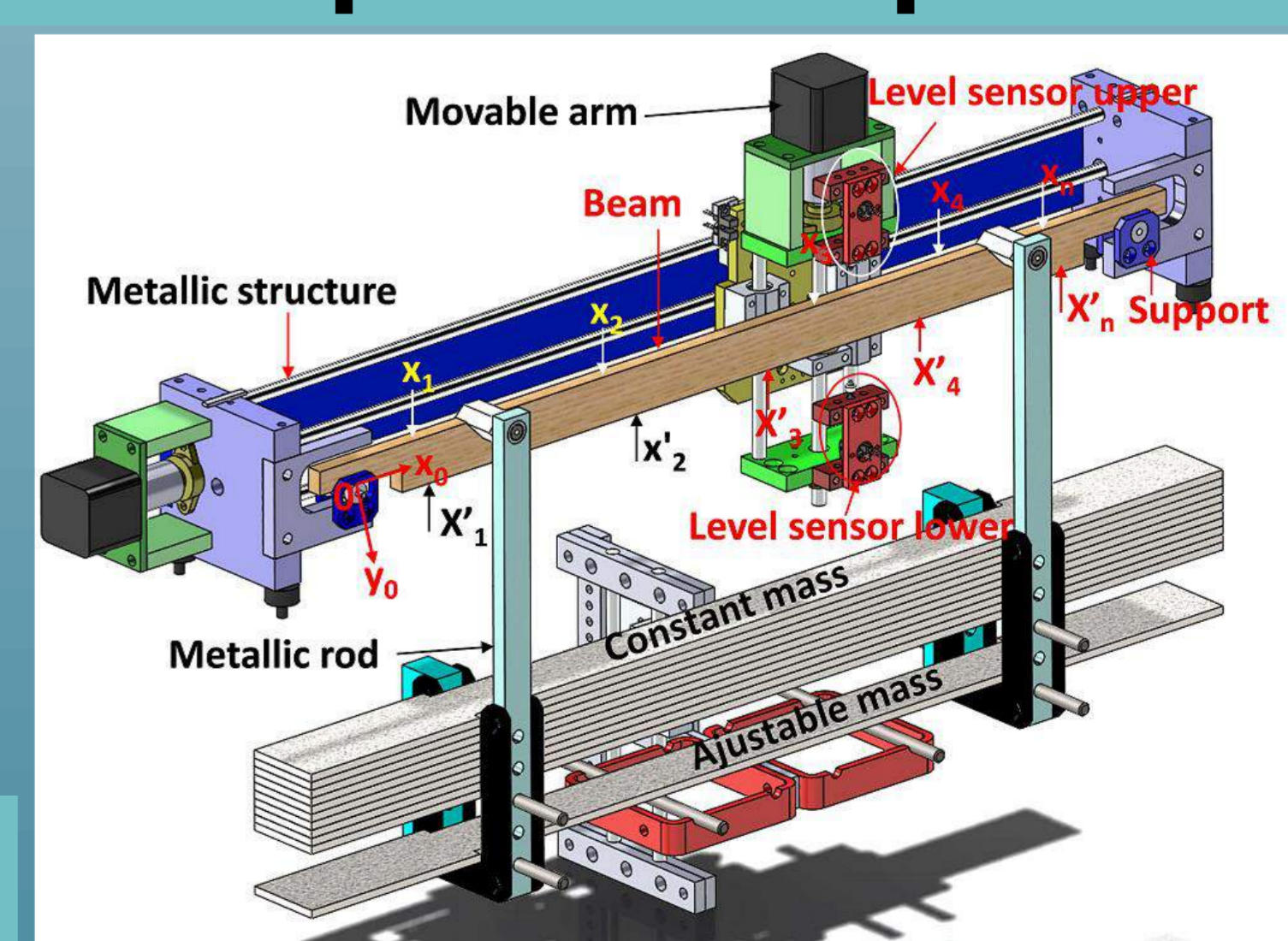
For $\alpha < 1/6$, the stress in Z_1 is lower than in Z_0 : $\sigma_1^{B+} \leq \sigma_0$

For this the condition on l is: $l \leq \frac{L}{12} = 50 \text{ mm}$ (9)

4.Results



5. Experimental setup for creep tests



Bibliography

- [1] H. Randriambololona., Modélisation du comportement diffère du bois en environnement variable. Thèse de doctorat Université de Limoges, 2003.
- [2] N. Angellier, F. Dubois, R. Moutou Pitti, M. Diakhaté, R. Spero Adjovi Loko, Influence of hydrothermal effects in the fracture process in wood under creep loading, Engineering Fracture Mechanics 177 (2017) 153–166.

General objectives

1. **Dichotomy.** To find the necessary and the sufficient conditions for a complexity class to have dichotomy.
2. **Description.** To find logical languages that describe certain complexity classes.

P and NP classes

- ▶ **P.** A problem belongs to the class P if there exists an algorithm that solves it in the time polynomial of the size of the input of the problem.
- ▶ **NP.** A problem belongs to the class NP if there exists an algorithm that checks if the proposed solution to the problem is correct in the time polynomial of the size of the input of the problem.

Logical description

Let \mathcal{L} be a logic i.e. a set of logical sentences; and let \mathcal{C} be a complexity class i.e. a set of problems. We say that \mathcal{L} *describes* \mathcal{C} if there is a two-sided polynomial time reduction φ_1, φ_2 from \mathcal{L} to \mathcal{C} i.e. the following hold:

- ▶ For every sentence $\Phi \in \mathcal{L}$ it is possible to find in polynomial time a problem $\mathcal{A} \in \mathcal{C}$ such that for all graphs G :

$$G \models \Phi \Leftrightarrow \varphi_1(G) \in \mathcal{A}$$

- ▶ For every problem $\mathcal{A} \in \mathcal{C}$ it is possible to find in polynomial time a sentence $\Phi \in \mathcal{L}$ such that for all graphs G :

$$G \models \Phi \Leftrightarrow \varphi_2(G) \in \mathcal{A}$$

MMSNP logic

The class $MMSNP$ consists of formulas of the form:

$$\exists P_1, \dots, P_n \forall x_1, \dots, x_m \bigwedge_i \neg(\alpha_i \wedge \beta_i)$$

where

- ▶ α_i is a conjunction of atoms of the form $E(x_i, x_j)$ where $E(\cdot, \cdot)$ is an input edge relation.
- ▶ β_i is a conjunction of atoms of the form $P_i(x_j)$ or $\neg P_i(x_j)$ where $P_i(\cdot)$ is a unary existentially defined relation on the graph vertices.

Known results

- ▶ The class NP doesn't have dichotomy. See [Lad75].
- ▶ The class CSP has dichotomy. See [Zhu17] and [Bul17].
- ▶ The logic $MMSNP$ describes the class CSP . See [FV99].

MMSNP* as a candidate for M-partition

The class $MMSNP^*$ consists of formulas of the same form as $MMSNP$:

$$\exists P_1, \dots, P_n \forall x_1, \dots, x_m \bigwedge_i \neg(\alpha_i \wedge \beta_i)$$

with the only difference: α_i is either a conjunction of atoms $E(x_i, x_j)$ or a conjunction of negated atoms $\neg E(x_i, x_j)$.

The sketch of possible proof is below:



Here:

- ▶ Each arrow stands for two-sided polynomial time reduction.
 - ▶ \mathfrak{F}_1 – the class of families of graphs such that for every $\varphi \in MMSNP^*$ there exists a family $\mathcal{F}_\varphi \in \mathfrak{F}_1$ such that the set $\mathcal{L}_\varphi = \{G - \text{graph} : G \models \varphi\}$ coincides with the set $Forb(\mathcal{F}_\varphi) = \{G - \text{graph} : \forall G' \in \mathcal{F}_\varphi. G' \not\models G\}$.
 - ▶ \mathfrak{F}_2 – the class of families of graphs such that for every problem \mathcal{M} from M -partition there exists a family $\mathcal{F}_\mathcal{M} \in \mathfrak{F}_2$ such that the set $\mathcal{L}_\mathcal{M} = \{G - \text{graph} : G \text{ satisfies } \mathcal{M}\text{-partition}\}$ coincides with the set $Forb(\mathcal{F}_\mathcal{M}) = \{G - \text{graph} : \forall G' \in \mathcal{F}_\mathcal{M}. G' \not\models G\}$.
- This approach was used to show that $MMSNP$ describes CSP in [KN08].

Particular objectives

1. **Dichotomy.** To check if the complexity class M -partition has dichotomy or not.
2. **Description.** To find a logical language that describes the complexity class M -partition.

P-time reduction and NP-completeness

- ▶ **P-time reduction.** A problem \mathcal{A} is said to be *reducible* to a problem \mathcal{B} if there is a polynomial time algorithm φ that maps instances of the problem \mathcal{A} to instances of \mathcal{B} such that for every instance A of \mathcal{A} the following is true:

$$A \text{ is true in } \mathcal{A} \Leftrightarrow \varphi(A) \text{ is true in } \mathcal{B}$$

- ▶ **NP-completeness.** A problem \mathcal{C} belongs to the class NP -complete if the following conditions hold:

- ▶ \mathcal{C} belongs to the class NP .
- ▶ Every problem from NP is reducible to \mathcal{C} .

Dichotomy

Let \mathcal{C} be a complexity class. We say that \mathcal{C} *has dichotomy* if

$$\mathcal{C} \subseteq P \sqcup NP\text{-complete}$$

We assume that $P \neq NP$ because otherwise this concept has no sense.

CSP class

Let G and H be graphs. We say that a map $h : G \rightarrow H$ is a *homomorphism between G and H* if for every $u, v \in G$:

$$(u, v) \text{ is an edge of } G \Rightarrow (h(u), h(v)) \text{ is an edge of } H.$$

Let H be fixed. The problem that decides if there is a homomorphism from the input G to H is denoted by $CSP(H)$.

M-partition

Let M be an $n \times n$ matrix with elements from $\{0, 1, *\}$. We say that a graph G *satisfies M-partition* if there is a partition of its vertices into n classes M_1, \dots, M_n such that the following is preserved:

- ▶ if an element m_{ij} of M equals 0 then for any $u \in M_i$ and $v \in M_j$ there is no edge (u, v) in G ;
- ▶ if $m_{ij} = 1$ then for any $u \in M_i$ and $v \in M_j$ (u, v) is an edge of G ;
- ▶ if $m_{ij} = *$ then there is no restriction for any $u \in M_i$ and $v \in M_j$.

Let matrix M be fixed. The problem that decides if a given as an input graph G satisfies M -partition is called an M -partition problem.

References

- [Bul17] A. A. Bulatov. A Dichotomy Theorem for Nonuniform CSPs. *FOCS*, pages 319–330, 2017.
- [FV99] T. Feder and M. Vardi. The computational structure of monotone monadic SNP and constraint satisfaction: A study through Datalog and group theory. *SIAM J. Comput.*, 28(1):57–104, 1999.
- [KN08] G. Kun and J. Nešetřil. Forbidden lifts (NP and CSP for combinatorialists). *Eur. J. Comb.*, 29(4):930–945, 2008.
- [Lad75] R. E. Ladner. On the structure of polynomial time reducibility. *J. Assoc. Comput. Mach.*, 22:155–171, 1975.
- [Zhu17] D. Zhuk. A Proof of CSP Dichotomy Conjecture. *FOCS*, pages 331–342, 2017.

Contact Information

Email: alexey.barsukov@uca.fr

Introduction

A behavioural model of a system is useful to help engineers understand how a system is functioning and audit it. However, create such a model by hands is a long and error prone task. *Model learning* methods are methods that infer a behavioural model of a system. There exist two types of model learning methods :

- *Active methods* [1], query directly the system or the user to obtain observations, used to build or improve a model. This type of method does not work on every system, like uncontrollable systems or systems that cannot be reset like IoT systems.

- *Passive methods* [2], deduce a model from data extracted from the system like for example execution traces. These methods can return incomplete model, and huge model difficult to understand.

IoT systems are generally composed of many reusable components, and model these components separately can lead to smaller and more understandable models.

CONfECT (CORrelate EXtract COMpose) is a passive model learning method that generates model of each component of the system from execution traces of the system. A more detailed presentation of this work can be found in [3]

The CONfECT Method

We suppose that the events of the log have the following form :
<label>(parm1, param2,...).

```
e1: /devices (Verb, Uri)
e2: /json.htm (param, svalue)
e3: Response (response)
e4: Response (response, data)
e5: /json.htm (param, svalue)
e6: Response (response)
e7: /devices (Verb, Uri)
e8: Response (response, data)
e9: /hardware (Verb, Uri)
e10: Response (response, data)
e11: /config (Verb, Uri)
e12: /json.htm (param, switchcmd)
e13: Response (response)
e14: Response (response, data)
e15: /tools (Verb, Uri)
e16: Response (response, data)
```

Figure 1. Example of formatted traces.

The CONfECT method is separated into 4 steps : Trace Extraction, LTS Generation, LTS Synchronization, and state merging.

STEP 1 : Trace Extraction:

In this step, we try to separate the events that come from different components. For that we use a *correlation coefficient*, used to determine if two events in a trace come from the same component. This coefficient is defined by the user and depends of the system, for example, it can be based on frequency of the events. We use this coefficient to separate each trace into sequences of consecutive events with a high correlation. Then, we remove of the trace each sequence that come from an other component than the first event of the trace, and replace it by synchronization event *call_Ci* and *return_Ci*.

Trace T1:	Trace T2:
e1: /devices (Verb, Uri)	call_C2
call_C2	/json.htm (param, svalue)
return_C2	Response (response)
e4: Response (response, data)	return_C2
call_C3	
return_C3	Trace T3:
e7: /devices (Verb, Uri)	call_C3
e8: Response (response, data)	e5: /json.htm (param, svalue)
e9: /hardware (Verb, Uri)	e6: Response (response)
e10: Response (response, data)	return_C3
e11: /config (Verb, Uri)	
call_C4	Trace T4:
return_C4	call_C4
e14: Response (response, data)	e12: /json.htm (param, switchcmd)
e15: /tools (Verb, Uri)	e13: Response (response)
e16: Response (response, data)	return_C4

Figure 2. Trace Extraction Step.

STEP 2 : LTS Generation:

In this step, we generate for each the trace T_i , a LTS C_i with only one path that correspond of the trace, where each event is modelled by a transition.

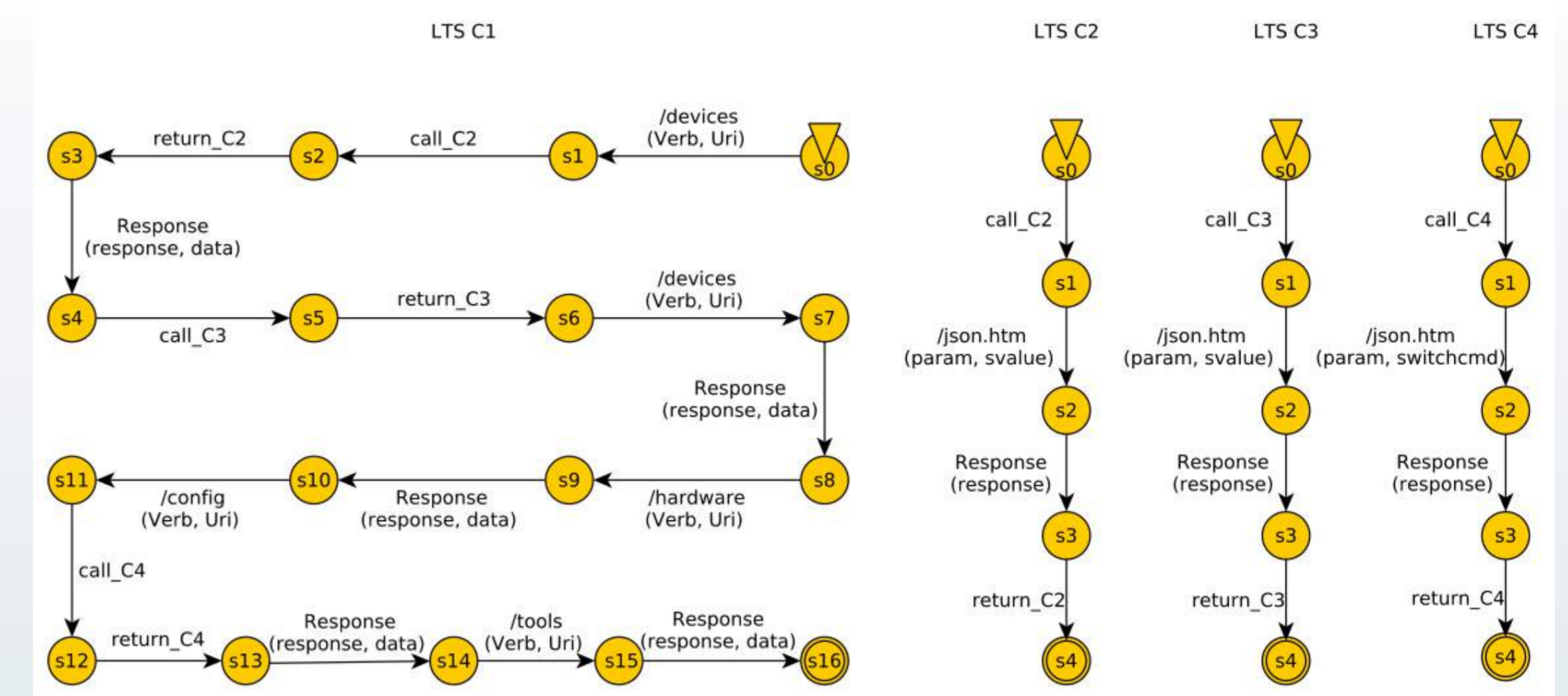


Figure 3. LTSs generated from the four previous traces.

STEP 3 : LTSs Synchronization:

Different synchronization strategies are proposed for our models. Here only the *weak* strategy is showed, where we merge the similar LTSs that come from the same component, with the help of clustering technique and generalize the models by letting a component call an other many times in a row (modelled by a loop *call_Ci return_Ci*).

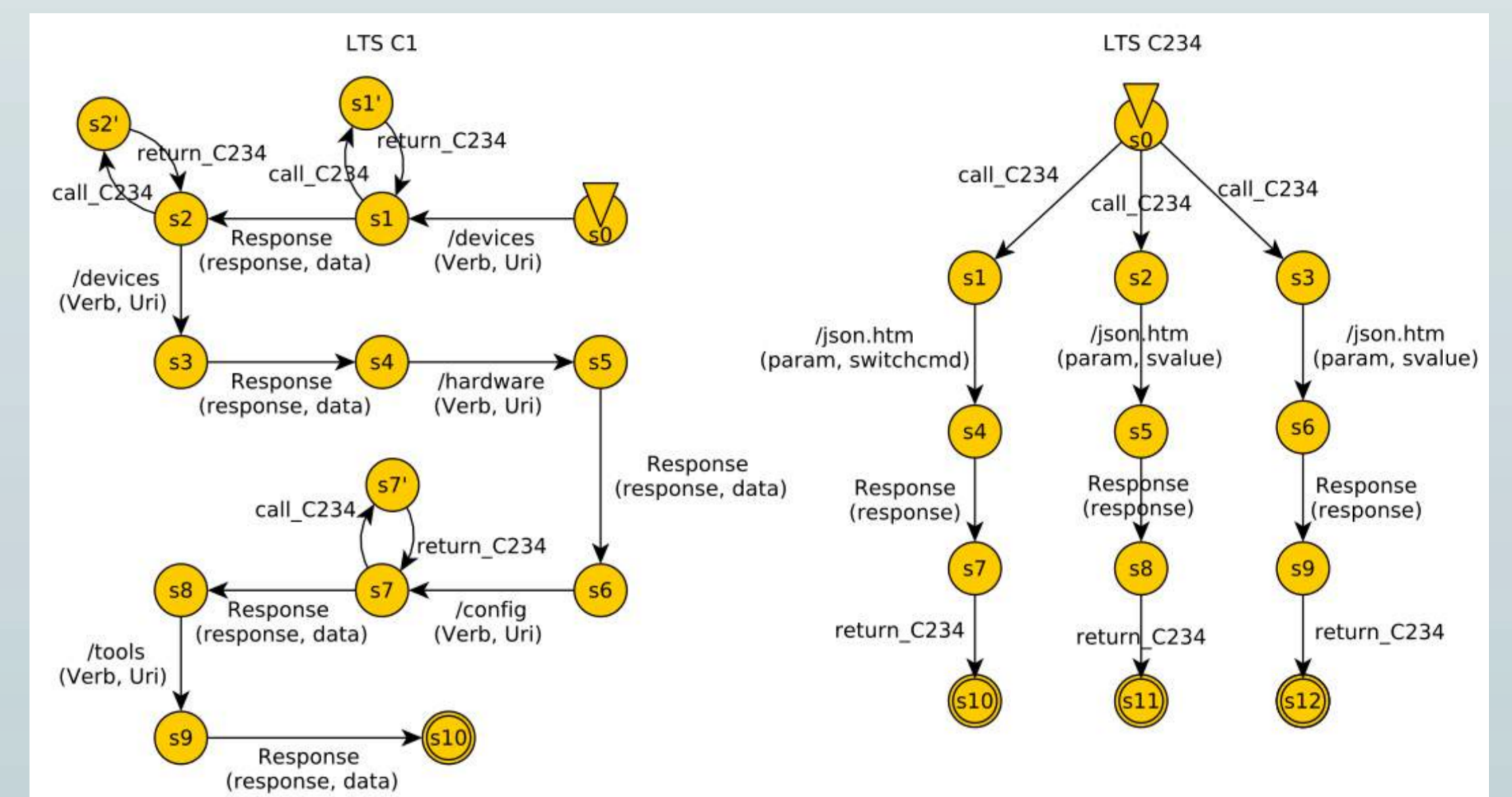


Figure 4. Generalization of the weak strategy of CONfECT.

STEP 4 : State Merging:

In this step we merge the equivalent states with the help of kTail[2] with $k=2$, that merges states that have the same future of length k .

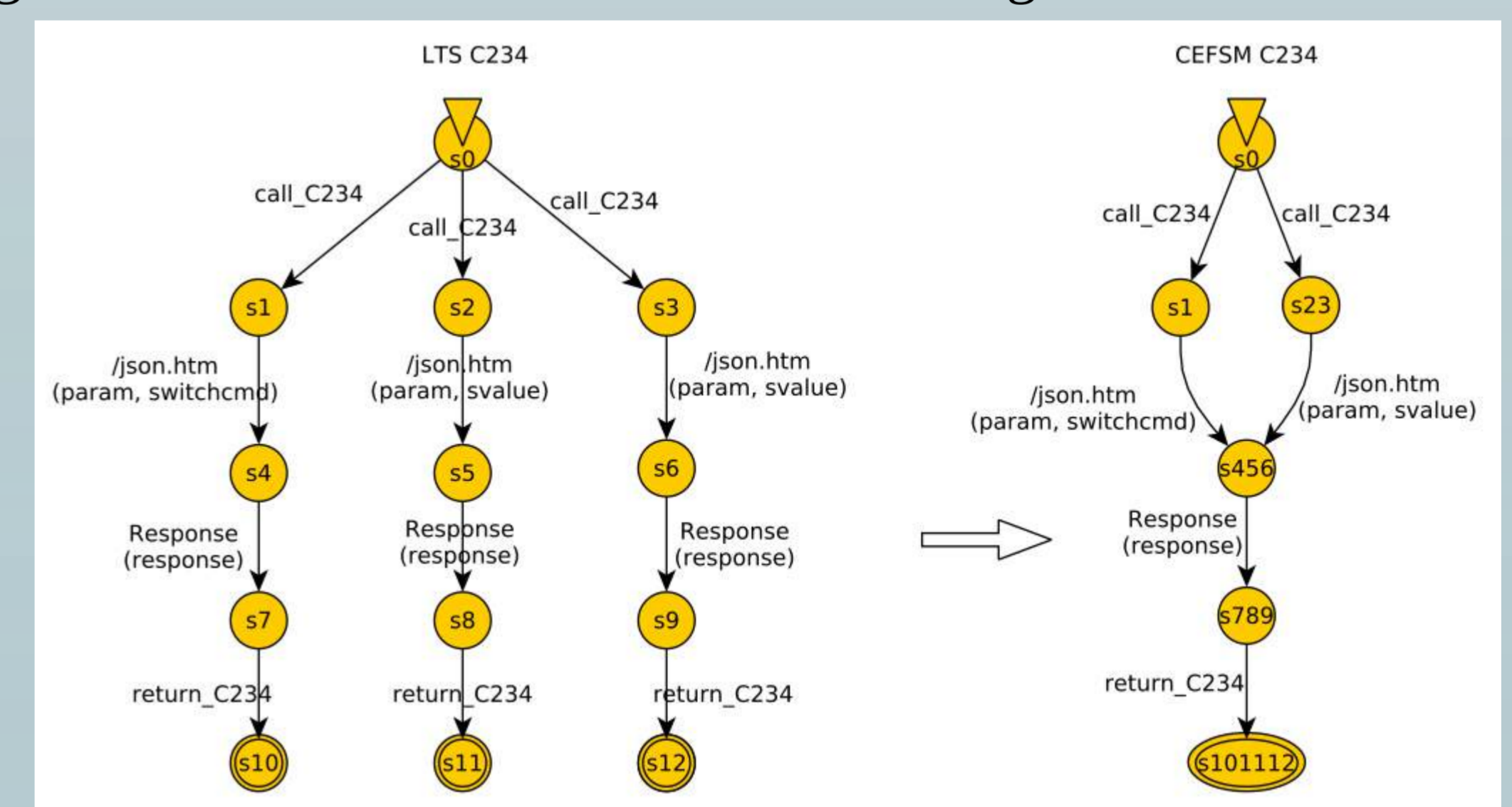


Figure 5. Result of kTail on the LTS C234 (C1 stay unchanged).

Conclusion

The CONfECT method can generate the model of the different component of the system. These models can be used to analyze the whole system, with the help of the synchronization events *call_Ci* and *return_Ci*, or to analyze a specific component of the system by hiding these events.

In term of perspective, we plan to use these models, to verify some security property.

Bibliography

1. Dana Angluin. Learning regular sets from queries and counterexamples. *Information and Computation*, 75(2):87-106, 1987
2. A.W. Biermann and J.A. Feldman. On the synthesis of finite-state machines from sample of their behavior. *Computers, IEEE Transactions*, 592-597, June 1972
3. Sébastien Salva, Elliott Blot. CONfECT: An Approach to Learn Models of Component-based Systems. *ICSOFT 2018*: 298-305

Objectives

1. To analyse the evolution of agricultural practices in water catchment areas
2. To study the impact of the characteristics of protection programs on water quality

Context

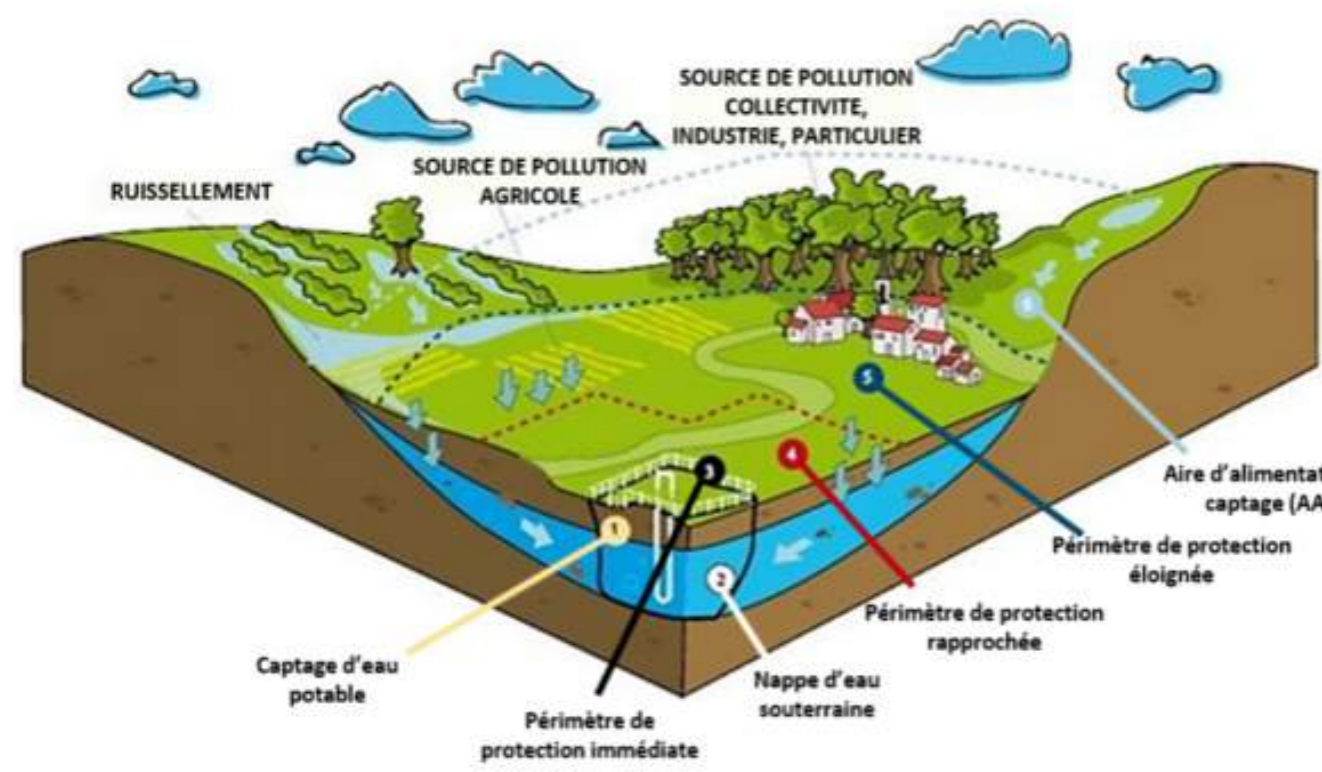


Figure 1: Water catchment area (source: Agence de l'Eau Seine-Normandie)

- ▶ Diffuse pollution from agricultural practices → major threat to water quality.
- ▶ One option for the public policies: promoting farming practices protecting water quality.
- ▶ Protection program → **voluntary commitment** of farmers.

Methods

- ▶ **Agent-based modelling** Computational systems with autonomous entities with dynamic behavior (agent) who operate in an environment and interact with each other and with the environment.

- ▶ **Social-ecological systems frameworks** Conceptual framework developed to represent and study complex systems around natural resource management [1].

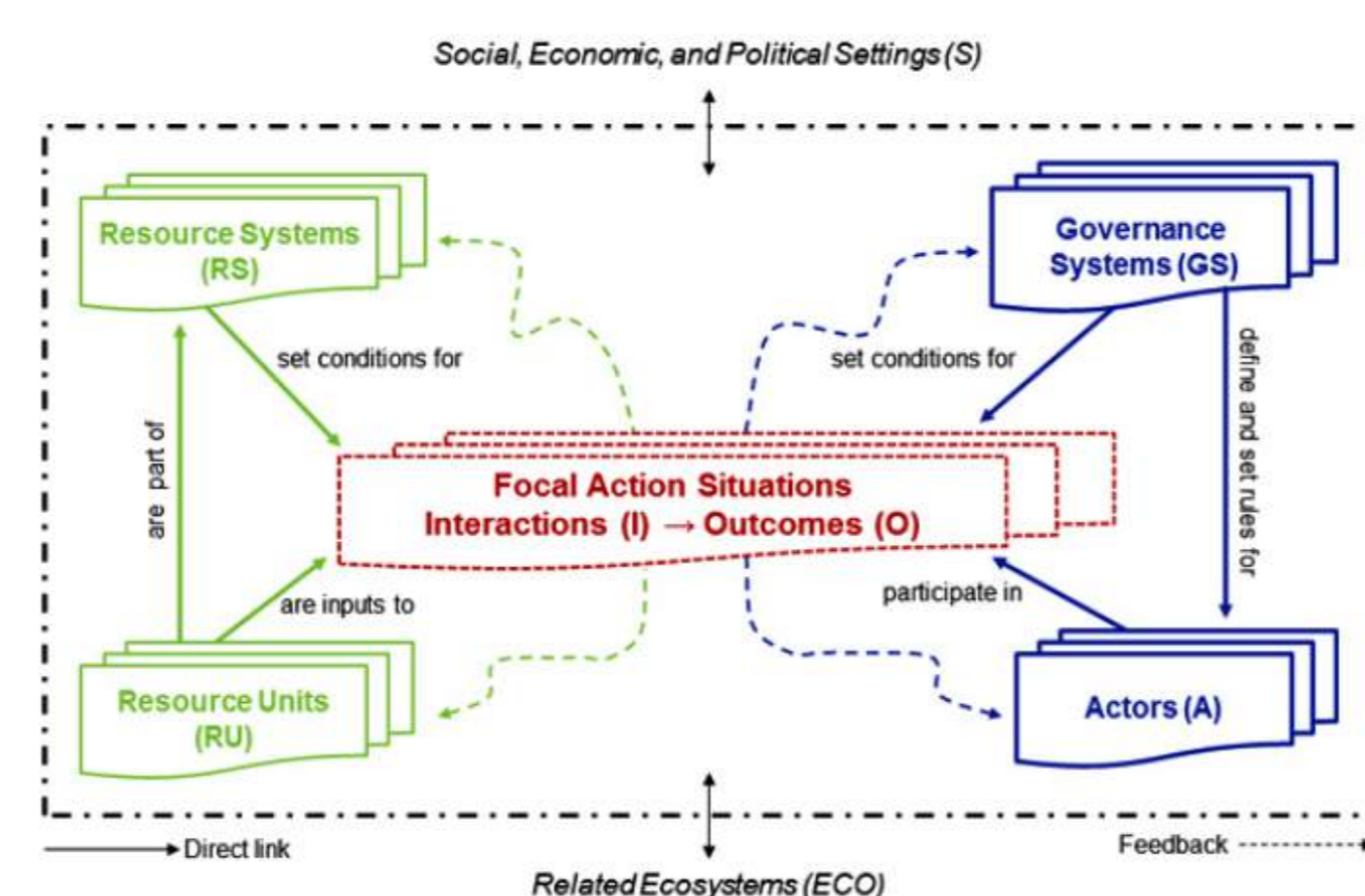


Figure 2: SES framework [1]

- ▶ **Theory of planned behaviour (TPB)** [2] Intention towards a behaviour is predicted by:
 - ▷ *attitude towards behaviour*, judgment about the desirability of the behaviour and its consequences
 - ▷ *subjective norm*, considerations about the influence and opinions of others on that behaviour
 - ▷ *perceived behavioural control*, beliefs about the individual's ability to succeed in the behaviour.

Model description

- ▶ **Resource system** → **Groundwater table**

- ▷ A water flow feeds (E) and exits (D) the groundwater. The concentration by polluting in water in mg/l (C) is used as a proxy to measure water quality.

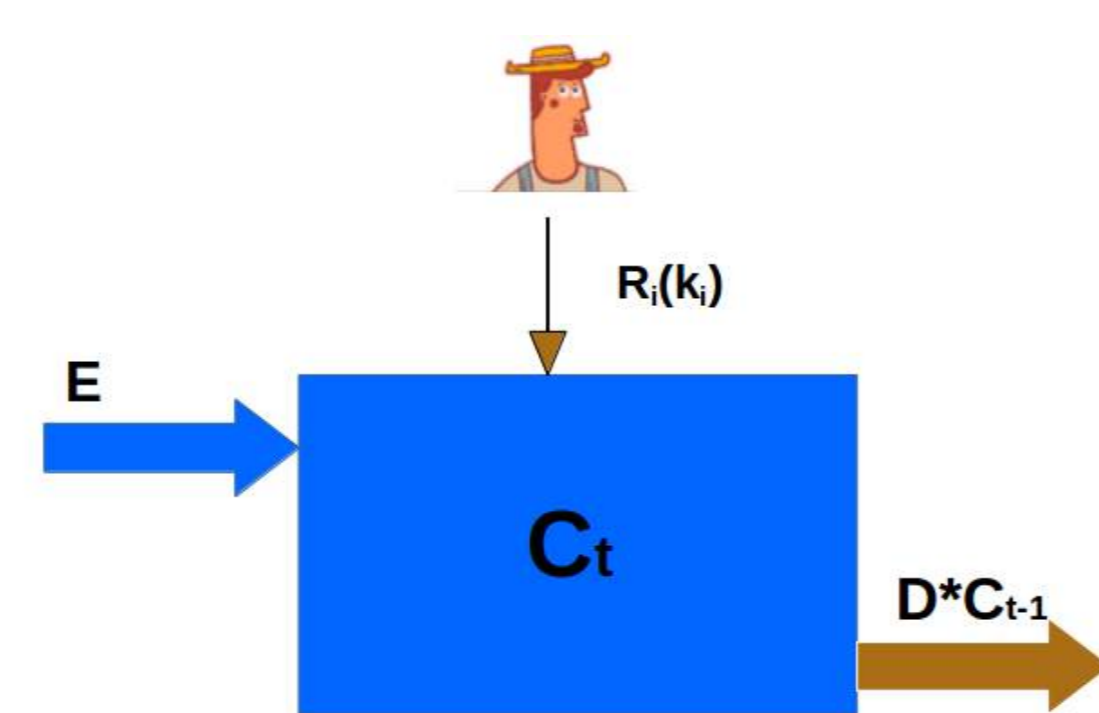


Figure 3: Representation of water and pollution flow

- ▶ **Actors system**

- ▷ 2 farming practices (k) with different quantities of input more or less polluting for the water resource (R): *bio* and *conventional*.
- ▷ 2 agent types: *eco-friendly* and *economicus* with different attitudes' weights.
- ▷ Behavior (B) [3]:

$$B = Att * \gamma_{Att} + SN * \gamma_{SN} + PC * \gamma_{PC}$$

where *Att* attitude towards a behaviour; *SN* subjective norm; *PC* perceived behavioural control; γ variable weighting.

- ▶ **Governance system**

- ▷ Protection program = combinaison of 2 measures
 - ▶ measure 1: agri-environmental measure (financial compensation)
 - ▶ measure 2: training measure

Simulation 1 - Results

Actors behaviour

- ▶ *Simulation*: Test of different weights of the variables affecting the intention of behaviour with a specific measure.
- ▶ *Results*: a) Results in terms of water quality and number of farmers changing their farming practice are different. b) The higher the weight of subjective norm is, the lower the adherence of protection program is. c) Attitude influences agent types differently.

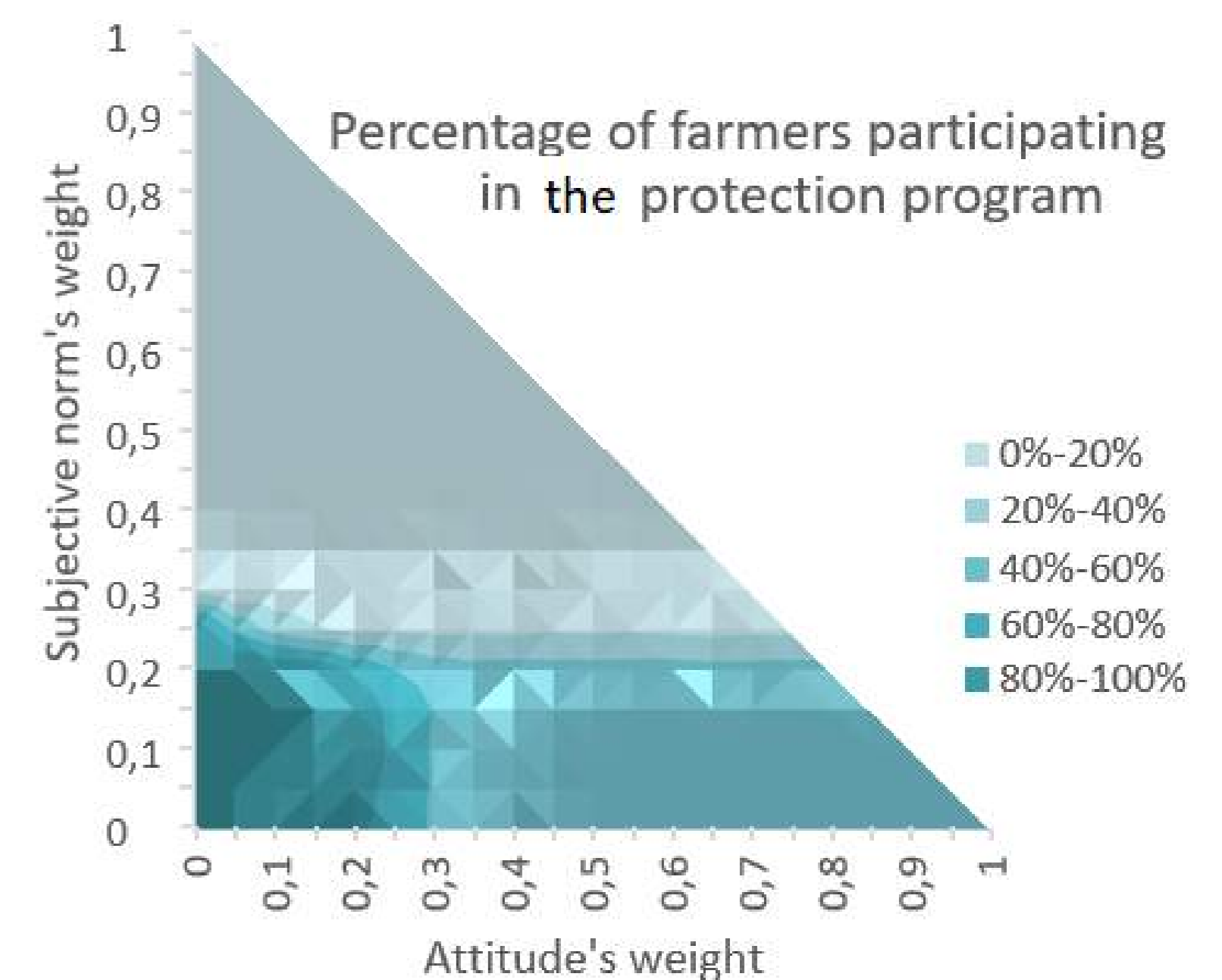


Figure 4: Percentage of farmers participating in the program depending on weight's variables of TPB

Simulation 2 - Results

Influence of the program's characteristics

- ▶ *Simulation*: With a set of weights, test of measures included in protection programs.
- ▶ *Results*: a) The bigger subsidies or the level of training proposed, the higher the percentage of farmers participating in the program. b) Existence of a minimum levels. c) Different combinations of the two measures lead to the same result.

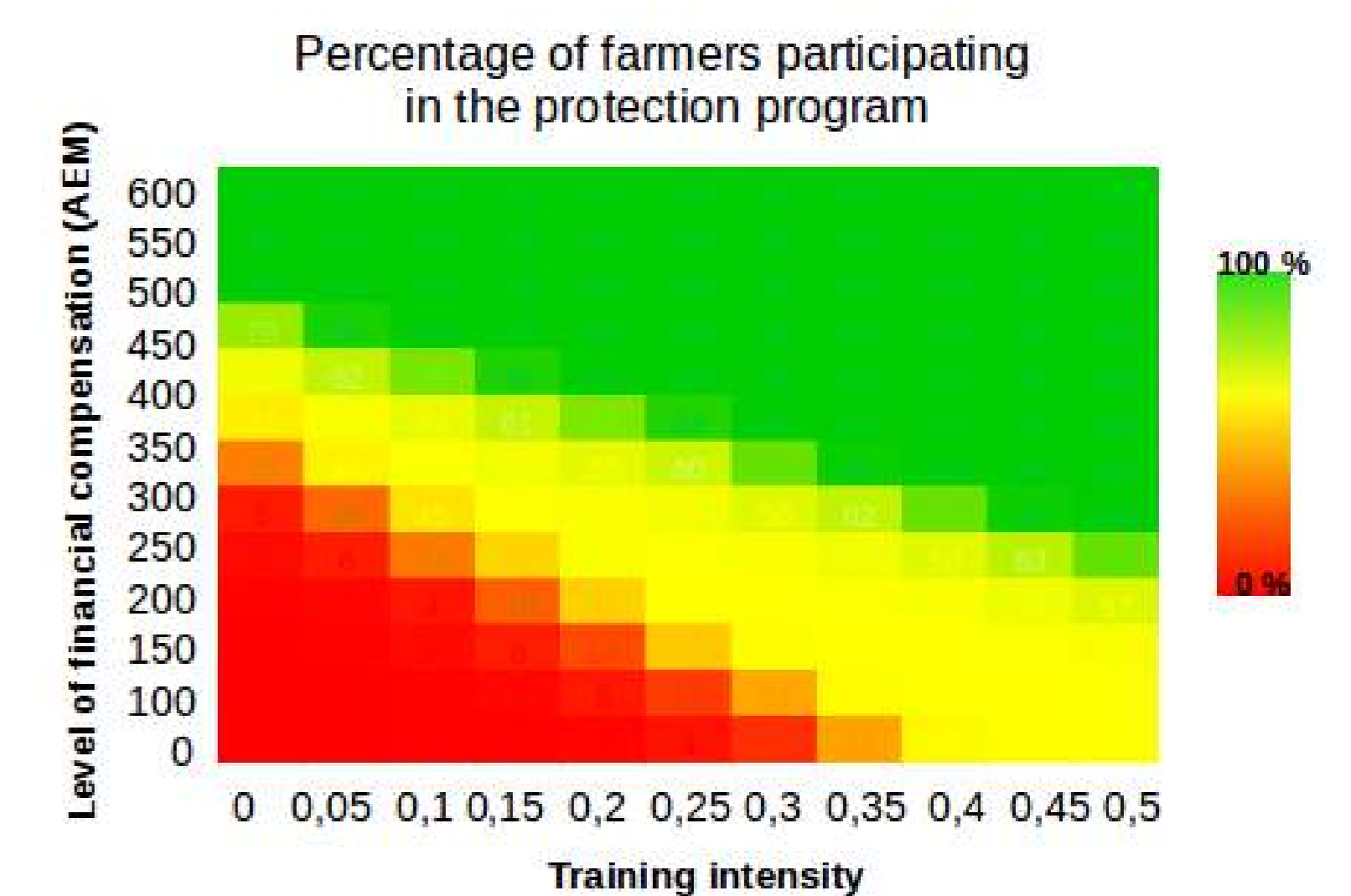


Figure 5: Percentage of farmers participating in the program depending the levels of measures' program

Conclusion

- ▶ This study allows us to understand how behavioural specifications influence farmers involvement and water quality results.
- ▶ In terms of public policy, this model enables us to highlight the trade-off between different measures.

References

1. McGinnis, M. D., and E. Ostrom. 2014. Social-Ecological System Framework: Initial Changes and Continuing Challenges. *Ecology and Society* 19 (2): 30. <https://doi.org/10.5751/ES-06387-190230>.
2. Ajzen, I. 1991. The Theory of Planned Behavior. *Organizational Behavior and Human Decision Processes* 50: 179211.
3. Beedell, J., and T. Rehman. 2000. Using Social-Psychology Models to Understand Farmers Conservation Behaviour. *Journal of Rural Studies* 16.

Acknowledgments

- ▶ This research has been funded by the ANR (Agence Nationale de la Recherche) under the VIRGO project (ANR-16-CE03-0003) and the I-Site CAP 20-25 project from Investissement d'avenir II program.

Contact Information

- ▶ Web: <https://virgo.irstea.fr/>
- ▶ Email: amelie.bourceret@irstea.fr

Quantifying the vulnerability of buildings exposed to the risk of debris flows and flash floods by numerical modelling

1. Introduction

Lahars are gravitational flows of sediment and water, originating from volcanoes. The city of Arequipa (Peru) is our case study, which is located 17 km of the summit of the El Misti volcano. Arequipa is exposed to many natural hazards, especially volcano related hazards such as high rainfall and volcanic ash that form lahars. This city includes poor populations and the structures are made of rudimentary masonry and suffers from disorderly and poorly planned growth, therefore vulnerability measurement is needed to map risks.



+



2. Objectifs

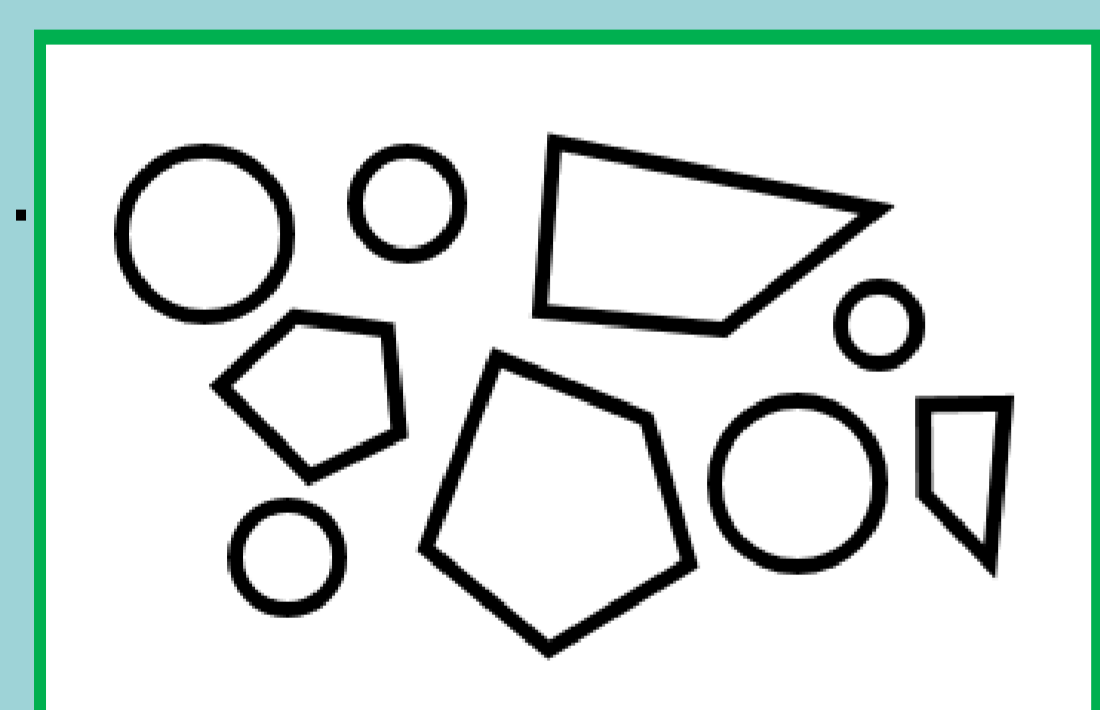
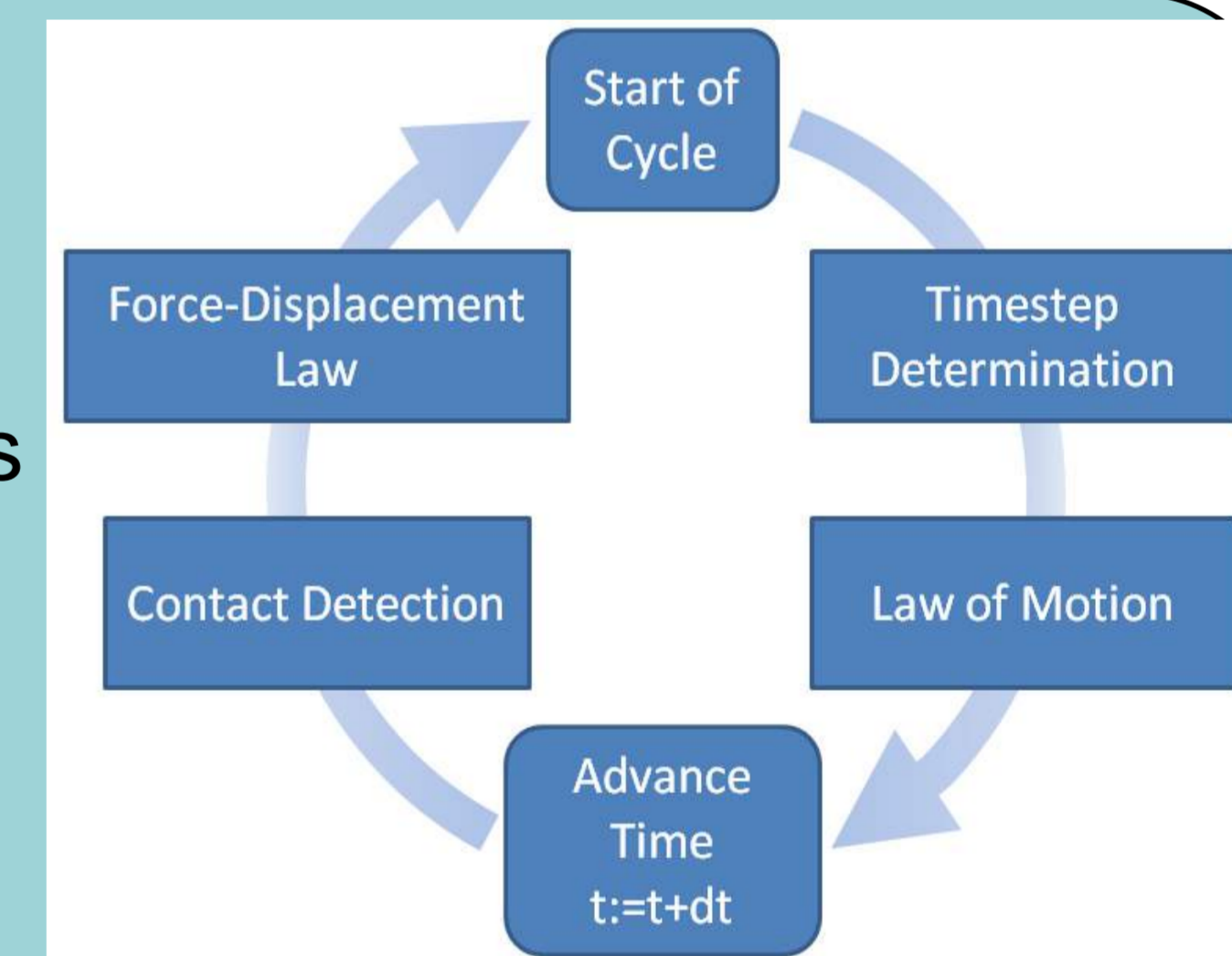
1. Propose a lahar modeling that better describes the effect of blocks.
2. Model the lahars interaction with typical structures (residential/infra).
3. Assess the vulnerability of its structures.



3. Methods

Numerical approach is used to model the impact of boulders generated by the flows on structures:

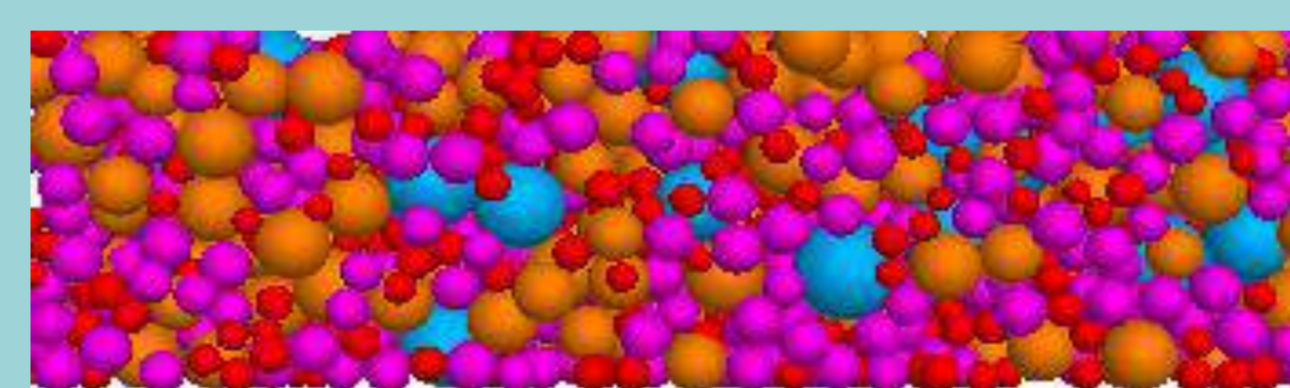
- ✓ Distinct element method (**DEM**): allows to model a set of particles without any limitations in terms of rotations, displacements or large deformations.
- ✓ Software used: **PFC3D** (to model solid phase of the flow-spherical particles) + **FLAC3D** (Darcy model shows fluid flow in a porous media in order to compute the orientation of the fluid velocity vectors in the channel).



Blocks

Explicitly modelled by
PFC-DEM

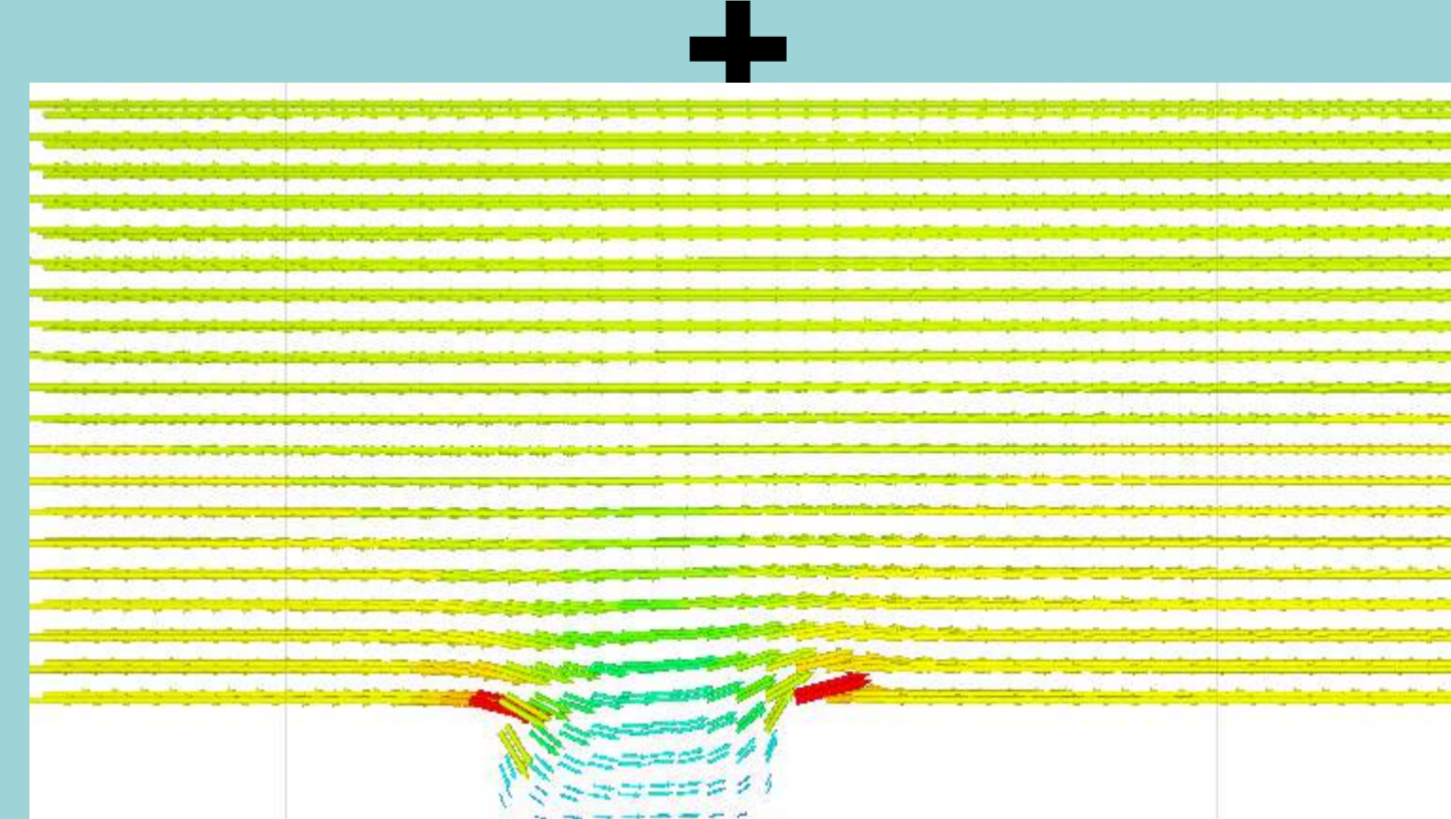
Spherical particles



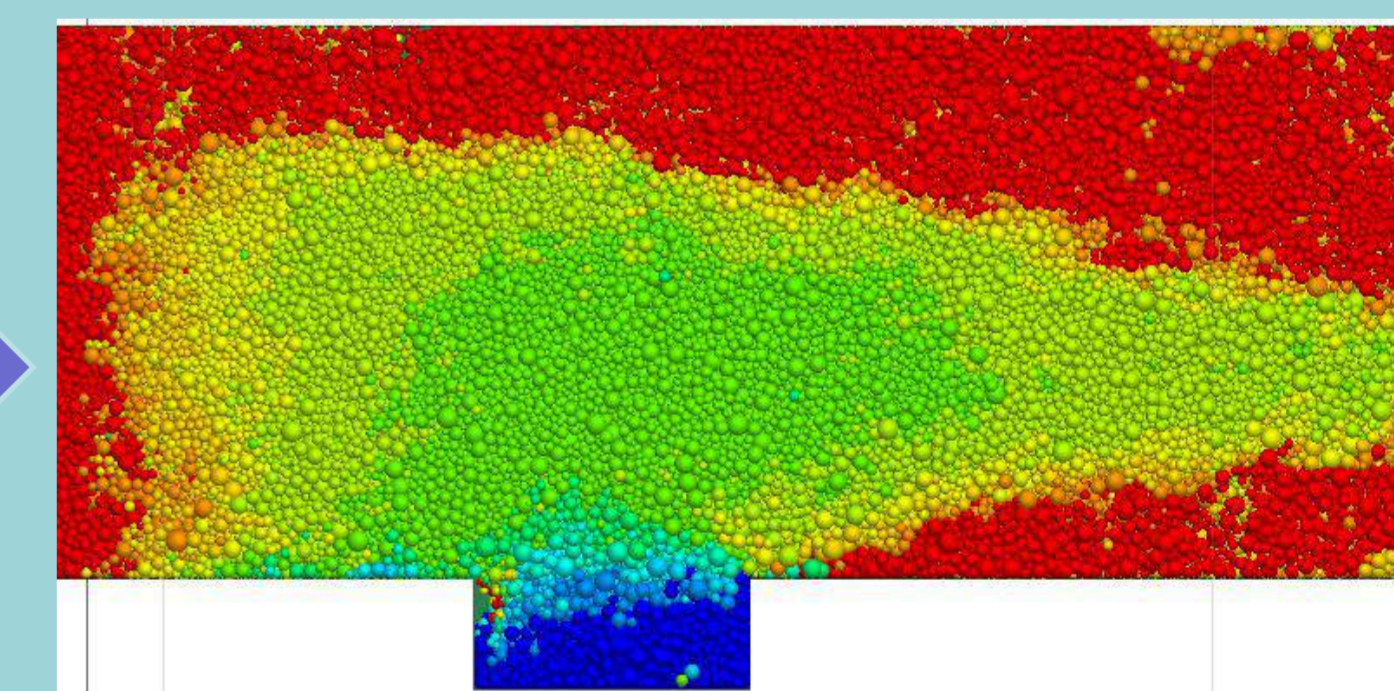
Water
+
Fines

Modeling of the fluid
and/or its effects by
FLAC3D

Coupling



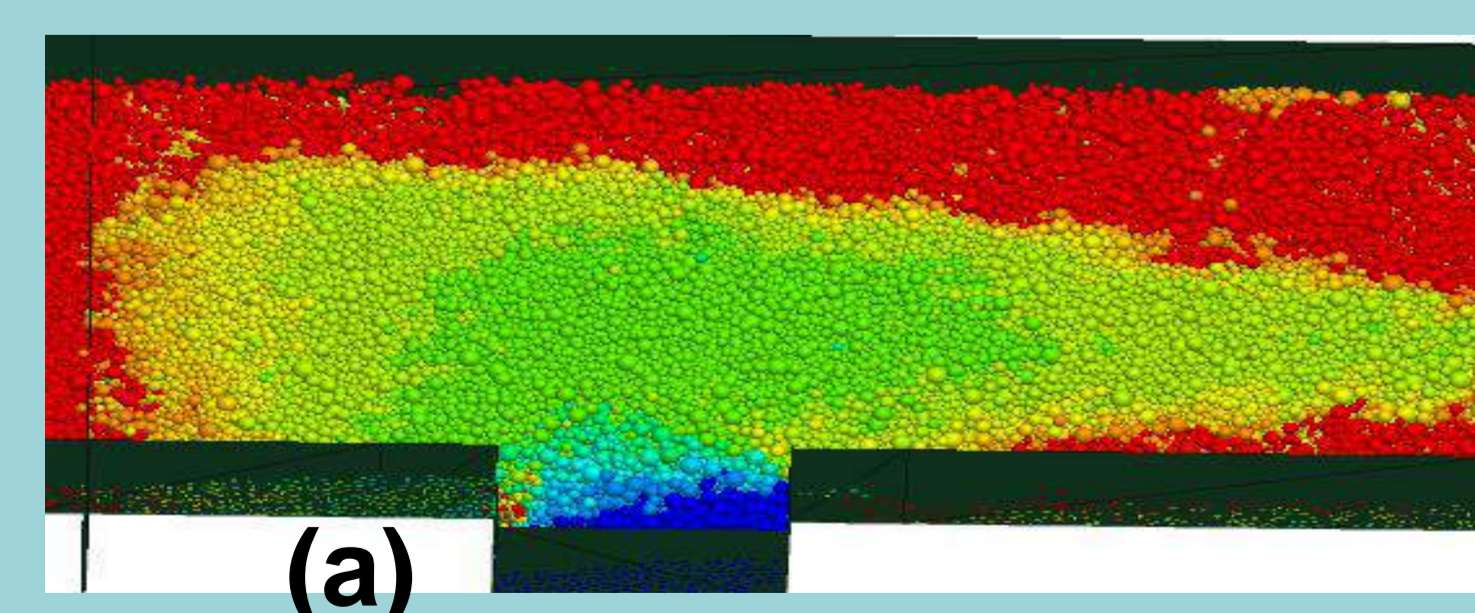
Velocity vectors



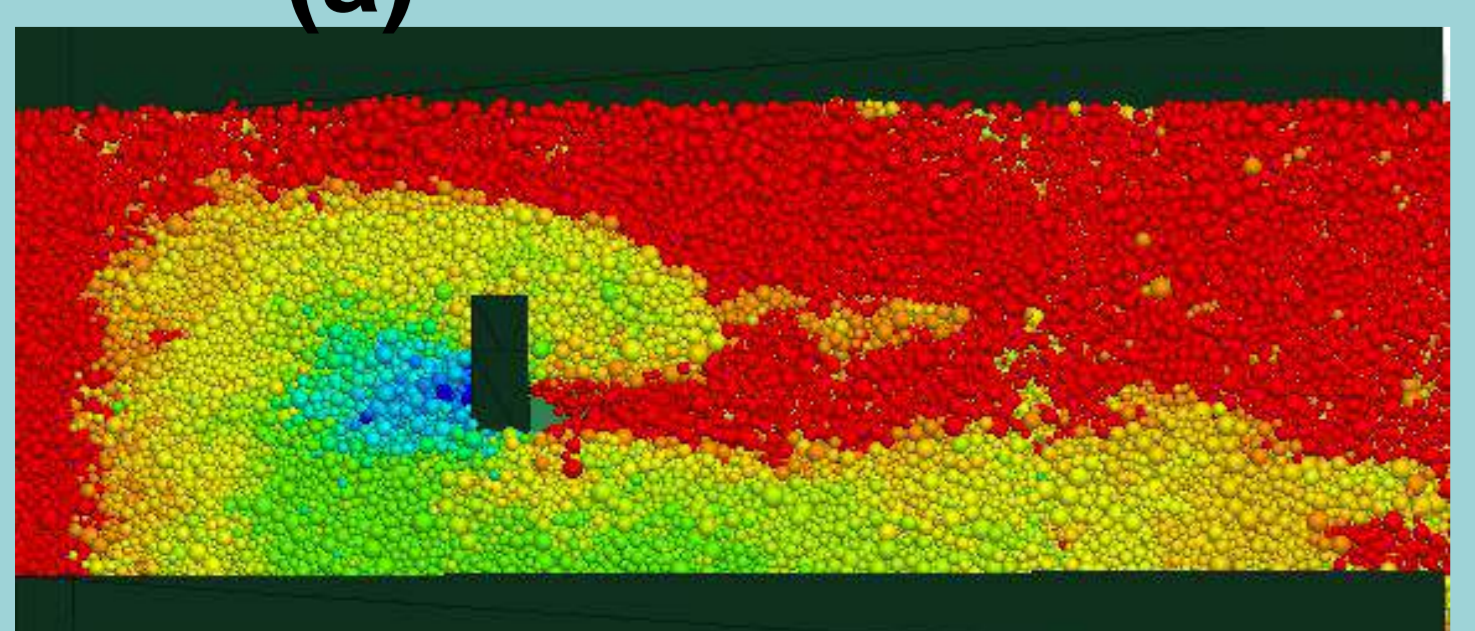
Simulated flow in the channel

4. Results

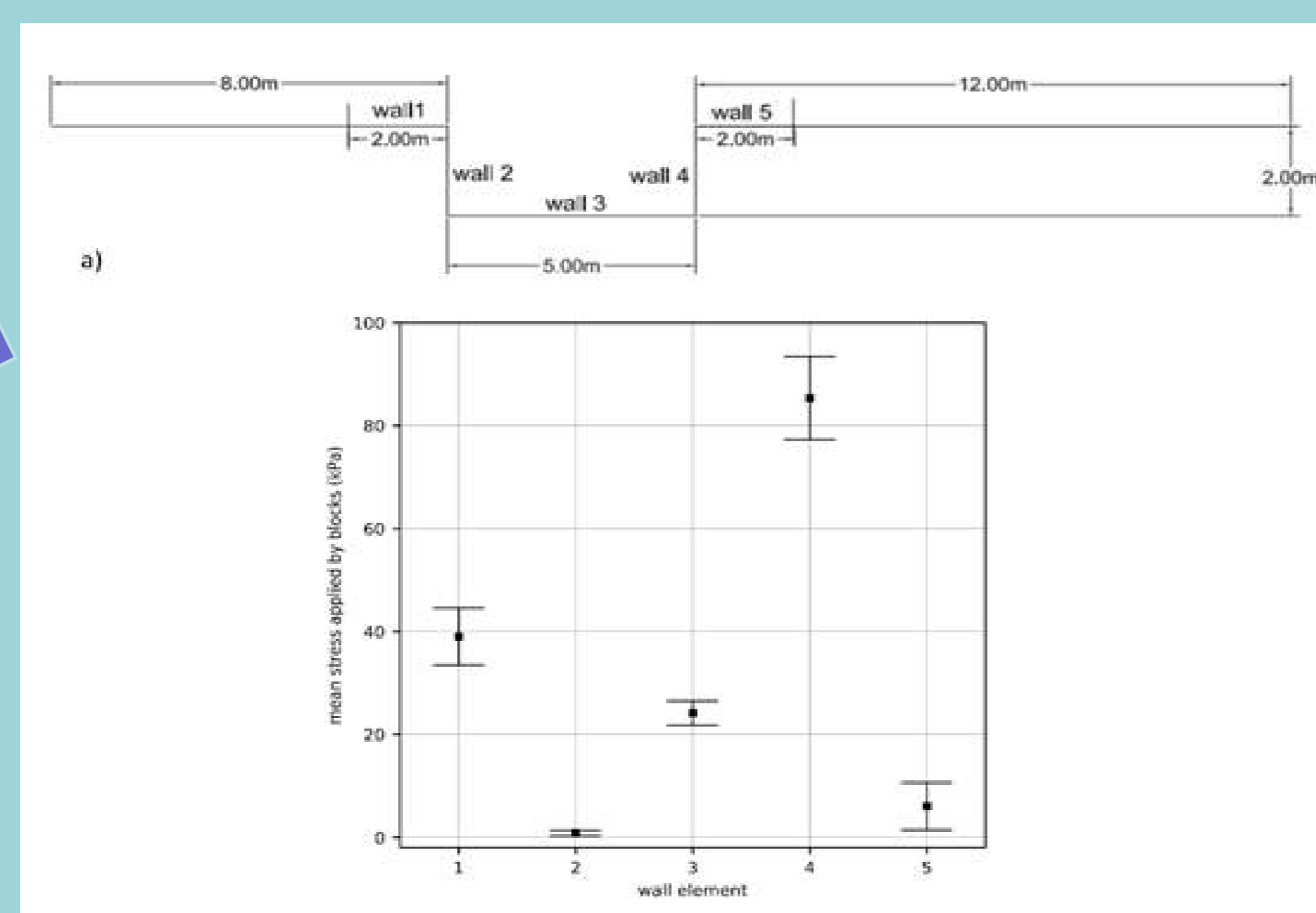
The impact stresses induced by the blocks can be measured during the simulation: (a) on wall element located along the flow path or (b) on the obstacle located in the middle of the channel.



(a)



(b)



5. Conclusion

A numerical model of debris flows is developed and validated in order to find the desired flow corresponding to Arequipa. Once the flow is modelled, the forces induced by the blocks on the structure can be measured and can be added to the effect of the fluid phase. Then, total impact pressure can be used to assess the vulnerability of structures.

Bibliography

- [1] Iverson, R. M., 1997. The physics of debris flows. *Reviews of Geophysics*, 35, 245-296.
- [2] Manville, V., Major, J. J., Fagents, S. A., 2013. Chapter 14: Modeling lahar behavior and hazards, in: Fagents, S. A., Gregg, T. K. P., Lopes, R. M. C. (Eds) *Modeling volcanic processes: the physics and mathematics of volcanism*. Cambridge University Press, 300-330.
- [3] Mead, S.R., Magill, C., Lemiale, V., Thouret, J.-C., Prakash, M., 2017. Examining the impact of lahars on buildings using numerical modeling. *Natural Hazard and Earth System Sciences*, 17, 703-719.

Introduction

A new type of floor, called Shallow-Floor, have been developed in the 1990s, using the advantages of composite construction and offering flexible spaces without dropdown beam with reduced floor thicknesses. This type of floor is made possible thanks to the use of slabs embedded in the height of a metallic beam, as Deltabeam. The most common is the use of Hollow Core slabs with Deltabeam that can more than 12 meters of span.

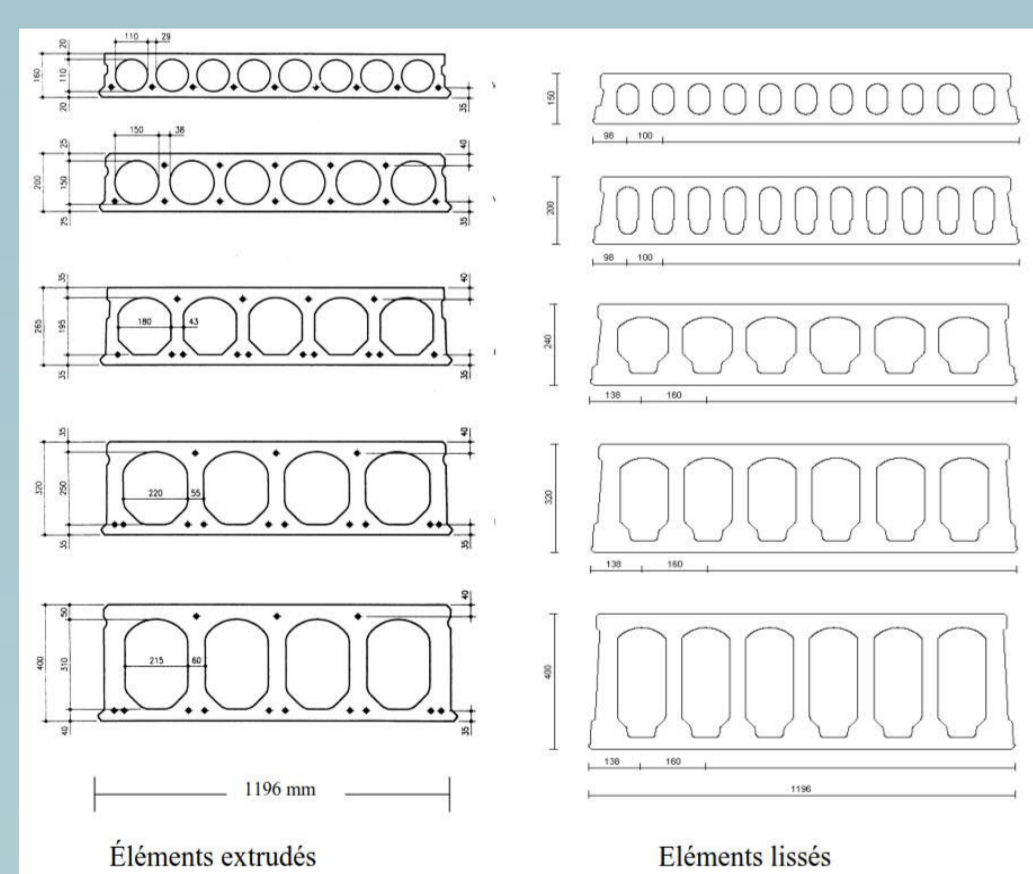
However, initially Hollow Core slabs were used and designed for rigid bearings, such as walls. With the introduction of column-beam structure and also the Shallow-Floor, the Hollow Core slabs are now being used on supports qualified as flexible.

At current, the behavior and design of these slabs on flexible bearings aren't very popular in some countries, particularly in France, and aren't included in the European regulations^{3&4}. Furthermore, the application of Shallow-Floor is currently not very widespread in the French construction.



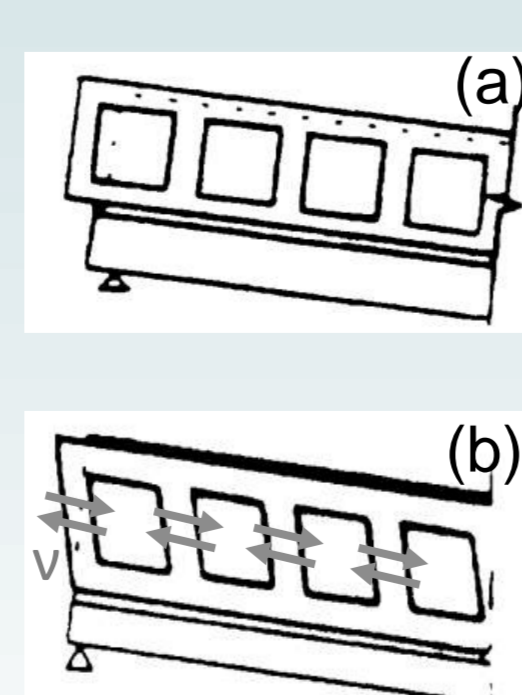
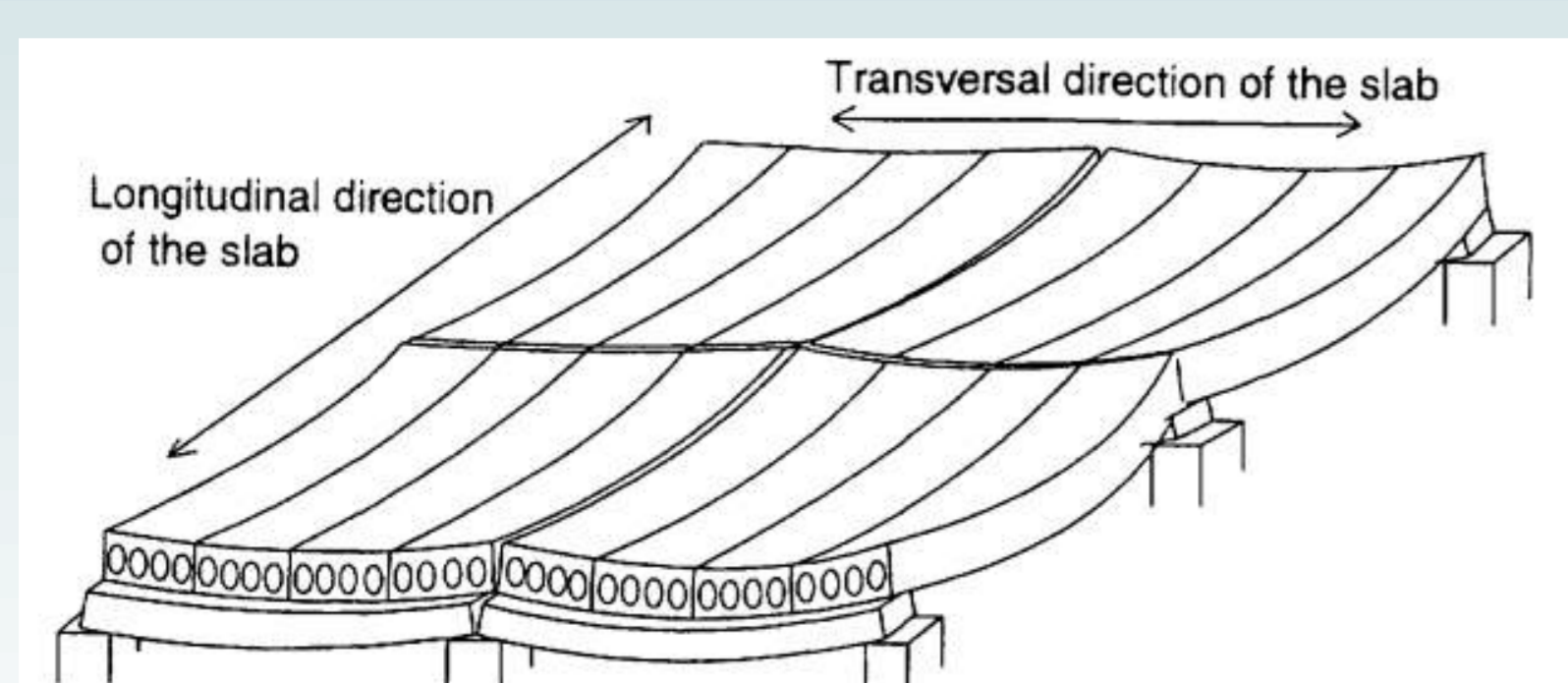
State-of-the-art

The Hollow Core slabs are traditional products for the construction of prefabricated floor. They are generally made of prestressed concrete with longitudinal strands and have holes in their direction of span. The characteristics of the Hollow Core slabs allow to obtain lighter slabs with a high degree of mechanical performance.



Originally designed for rigid supports, the emergence of column-beam structure has led to the use of Hollow Core slabs on flexible bearings and it was in 1990 that the first research on the behavior of Hollow Core slabs on flexible supports began in the Finnish Technical Center VTT, by Pajari. Then, they continued throughout Scandinavia and Germany. All in all, 20 large-scale tests were made public by Pajari in his publication VTT n°148⁶ in 2005.

In all experimental tests, a reduction of up to 60 % in the shear resistance of Hollow Core slabs on flexible supports is observed compared with rigid bearings. This decrease is caused by a failure of the webs in the Hollow Core slabs due to the formation of a transverse shear flow in the slabs, noted v . Specifically, this flow is due to a double curvature of the prefabricated slabs induced by the deformation of the beam when the floor is subjected to a uniformly distributed load. But also due to a composite action between the elements that avoids the progressive displacement of the Hollow Core slabs towards the outside of the beam during the bending of the beam (See (a) without composite action and (b) with composite action).



Examples of the webs failures by transverse shear in VTT n°148⁶:

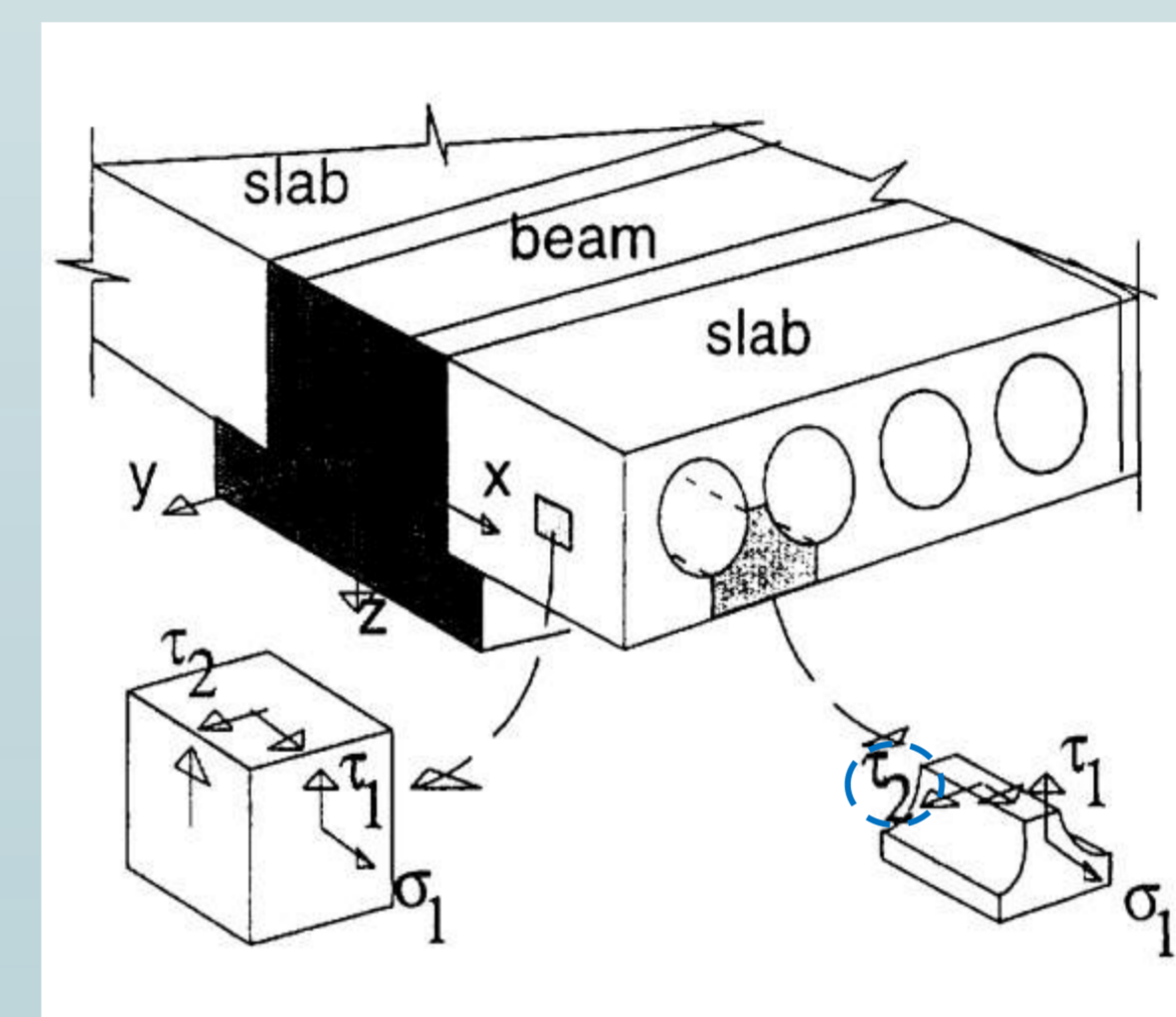


Test VTT PC INT.500.2006



Test VTT CR.DELTA.500.2005

Then, based on the many available researches, different design models have been developed to take into account this transverse shear flow occurring in the webs of Hollow Core slabs on flexible supports. An example is the Pajari's design model, which has been used in many scientific publications, such as the Fib Bulletin n°6⁵.



$$\sigma_{ps} = \frac{\sigma_1}{2} + \sqrt{\left(\frac{\sigma_1}{2}\right)^2 + \tau_1^2 + \tau_2^2}$$

σ_1 : Normal stress due to prestressing force, is determined in analogy with the formula for prestressed concrete beam (as in rigid supports)

τ_1 : Vertical shear stress due to the vertical shear force determined according to the beam theory (as in rigid supports)

τ_2 : Transverse shear stress, due to shear flow in the transverse direction, is determined from the beam theory applied to a section including the support beam, the composite section, the slab section and the top concrete slab if present

The different methods proposed for the behavior of the Hollow Core slabs on flexible supports are still being discussed. One of the reasons is that the reduction in the shear capacity of the slabs isn't caused only by the deformation of the beam. But also according to other important parameters, such as the composite properties between slabs and beam and the slab cross section (shape of the voids, webs thickness, prestressed, etc.).

Moreover so far, no general, standardized and precise design model allows the design of Hollow Core slabs on flexible bearings in Europe. And the distinction between rigid and flexible supports is often not clear.

However, in some countries, there are codifications for this design to better avoid transverse shear in Hollow Core slabs. Especially in Finland, with the Code Card¹, which is based on the Pajari's Model. Also, in Germany regulation, Dibt Z-15.10-279², with 4 requirements to limit damage in these prefabricated slabs on flexible floors (Reduction of 50% for the shear strength calculated on rigid supports, cambering limited to L/300, concrete in the void in the slabs near the support beam, support on elastomer tape).

Contributions envisaged

We plan to investigate in more details the behavior of Hollow Core slabs with transverse shear, in particular with Deltabeam, in accordance with the European regulations^{3&4} and also following the good practice in France.

In addition, we plan to study the complete functioning of traditional floors (concrete beam + Hollow Core slabs) into the transmission of the forces until the vertical elements, thanks in particular to the connection and diaphragm effect in normal and seismic situations. In order to offer similar effective and durable solutions for complete composite floors (Deltabeam + Hollow Core slabs).

So, the overall objective is to show the good cooperation and functioning of Hollow Core slabs with shallow and mixed beam (such as Deltabeam).

Bibliography

1. CODE CARD N°18, *Design of Hollow Core slabs supported on beams*, English Edition for Peikko Group Oy with updates 25.11.2012-2.8.2017, 2017
2. DIBt Z-15.10-279, *Verwendung von Spannbeton-Holplatten nach DIN EN 1168:2011-12 und DIN EN 1992-2-2:2011-01 System BRESPA*, 2014
3. EN 1168 : 2005 + A2 :2009, *Precast concrete products : Hollow Core slabs*, 2005
4. EUROCODE 2, EN 1992-1-1, *Design of concrete structure: Part 1-1 : General rules and rules for buildings*, 2003
5. FIB, *Special design considerations for precast prestressed Hollow Core floors*, Guide to good practice, Bulletin 6, Janvier 2000
6. PAJARI MATTI, *Resistance of prestressed Hollow Core slabs against web shear failure*, VTT Research Notes 2292, 2005
7. PEIKKO GROUP CORPORATION, *PG 0917 Behavior and design of steel-concrete composite structure*, First Edition, 2017

Introduction

Digital geometry is the field of mathematics that studies the geometry of points with integer coordinates, also known as *lattice points* [1]. Convexity is a fundamental concept in digital geometry, as well as in continuous geometry [2]. From a historical perspective, the study of digital convexity dates back to the works of Minkowski [3] and it is the main subject of the mathematical field of geometry of numbers. While convexity has a unique well stated definition in any linear space, different definitions have been investigated in \mathbb{Z}^2 and \mathbb{Z}^3 . In two dimensions, we encounter at least five different approaches, called respectively digital line, triangle, HV (for Horizontal and Vertical), and Q (for Quadrant) convexities. These definitions were created in order to guarantee that a digital convex set is connected (in terms of the induced grid subgraph), which simplifies several algorithmic problems.

Definition

The original definition of digital convexity in the geometry of number does not guarantee connectivity of the grid subgraph, but provides several other important mathematical properties, such as being preserved under certain affine transformations (Fig. 1). The definition is the following.

digital convex: A set of lattice points $S \subset \mathbb{Z}^d$ is *digital convex* if $\text{conv}(S) \cap \mathbb{Z}^d = S$, where $\text{conv}(S)$ denotes the convex hull of S .

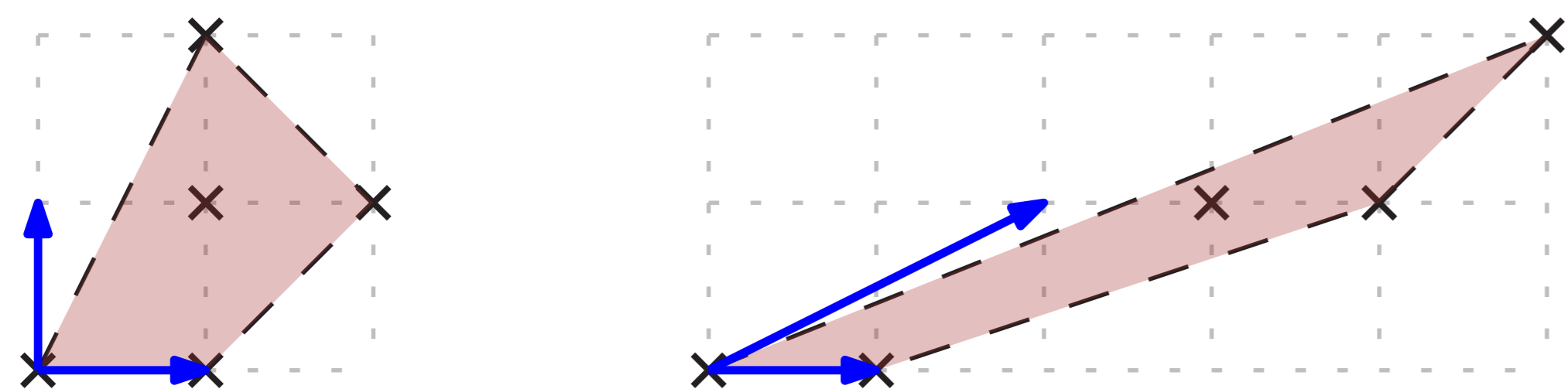


Figure 1: **Shearing a digital convex set.** Example of a set whose connectivity is lost after a linear shear.

Problems considered

Here are a few of the problems considered: Given set of lattice:

- Is the set digital convex ?

Problem Test Convexity(S)

Input: Set $S \subset \mathbb{Z}^d$ of n lattice points given by their coordinates.

Output: Determine whether S is digital convex or not.

- What is the largest digital convex subset ?

Problem Digital Potato Peeling (S)

Input: Set $S \subset \mathbb{Z}^2$ of n lattice points given by their coordinates.

Output: Determine the *largest* set $K \subseteq S$ that is digital convex (i.e., $\text{conv}(K) \cap \mathbb{Z}^2 = K$), where largest refers to the area of $\text{conv}(K)$.

- What is the largest union of k digital convex subsets ?

Problem Digital k -Potato Peeling (S)

Input: Set $S \subset \mathbb{Z}^2$ of n lattice points given by their coordinates.

Output: Determine the *largest* union of sets $K = K_1 \cup K_2 \cup \dots \cup K_k$ such that $\forall i \in [1..k] : K_i \subseteq S$ is digital convex.

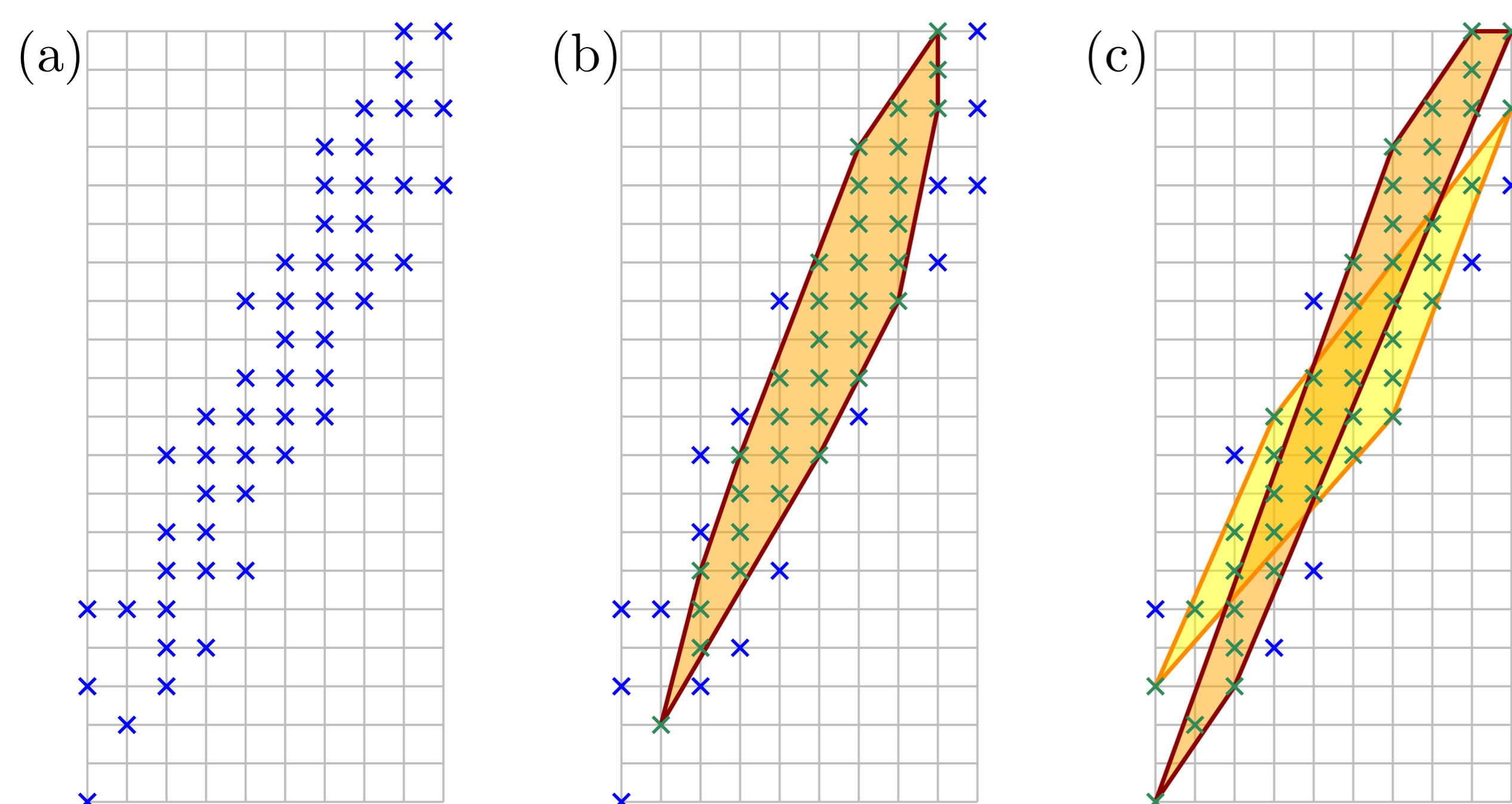


Figure 2: (a) Input lattice set S . (b) Largest digital convex subset of S . (c) Largest union of two digital convex subsets of S .

Results and Conclusion

Many problems in the intersection of digital, convex, and computational geometry remain open. Our study falls in the following framework of problems, all of which receive as input a set of n lattice points $S \subset \mathbb{Z}^d$ for constant d and are based on a fixed parameter $k \geq 1$.

1. Is S the union of at most k digital convex sets?
2. What is the smallest superset of S that is the union of at most k digital convex sets?
3. What is the largest subset of S that is the union of at most k digital convex sets?

In [4] we considered the first problem for $k = 1$, presenting polynomial time solutions (which may still leave room for major improvements for $d > 3$). We are not aware of any previous solutions for $k > 1$. In contrast, the continuous version of the problem is well studied. The case of $k = 1$ can be solved easily by a convex hull computation or by linear programming. Polynomial algorithms are known for $d = 2$ and $k \leq 3$ [5, 6], as well as for $d = 3$ and $k \leq 2$ [7]. The problem is already NP-complete for $d = k = 3$ [7]. Hence, the continuous version remains open only for $d = 2$ and fixed $k > 3$.

It is easy to obtain polynomial time algorithms for the second problem when $k = 1$, since the solution consists of all points in the convex hull of S . The continuous version for $d = k = 2$ can be solved in $O(n^4 \log n)$ time [8]. Also, the orthogonal version of the problem is well studied (see for example [9]). We know of no results for the digital version.

In a yet to be published paper, we considered the digital version of the third problem for $d = 2$ and $k = 1, 2$, proposing algorithms with respective running times of $O(n^3 + n^2 \log r)$ and $O(n^9 + n^6 r)$, where r is the diameter of S . Since the first problem trivially reduces to the third problem, we also solved the first problem for $k = d = 2$ in $O(n^9 + n^6 r)$ time. It is surprising that we are not aware of any faster algorithm for the first problem in this particular case.

The third problem for $d > 2$ or $k > 2$ remains open. Surprisingly, even the continuous version seems to be unresolved for $d > 2$ or $k \geq 2$.

References

- [1] Reinhard Klette and Azriel Rosenfeld. *Digital geometry: Geometric methods for digital picture analysis*. Elsevier, 2004.
- [2] Christian Ronse. A bibliography on digital and computational convexity (1961-1988). *IEEE Transactions on Pattern Analysis and Machine Intelligence*, 11(2):181-190, February 1989.
- [3] H. Minkowski. *Geometrie der Zahlen*. Number vol. 2 in *Geometrie der Zahlen*. B.G. Teubner, 1910.
- [4] Loïc Crombez, Guilherme D. da Fonseca, and Yan Gérard. Efficient algorithms to test digital convexity. In Michel Couprie, Jean Cousty, Yukiko Kenmochi, and Nabil Mustafa, editors, *Discrete Geometry for Computer Imagery*, pages 409-419, Cham, 2019. Springer International Publishing.
- [5] Patrice Belleville. On restricted boundary covers and convex three-covers. In *5th Canadian Conference on Computational Geometry (CCCG)*, pages 467-472, 1993.
- [6] Thomas C. Shermer. On recognizing unions of two convex polygons and related problems. *Pattern Recognition Letters*, 14(9), pages 737-745, 1993.
- [7] Patrice Belleville. Convex covers in higher dimensions. In *7th Canadian Conference on Computational Geometry (CCCG)*, pages 145-150, 1995.
- [8] Sang Won Bae, Hwan-Gue Cho, William Evans, Noushin Saeedi, and Chan-Su Shin. Covering points with convex sets of minimum size. *Theoretical Computer Science*, 718:14-23, 2018.
- [9] Cem Evrendilek, Burak Genç, and Brahim Hnich. Covering points with minimum/maximum area orthogonally convex polygons. *Computational Geometry*, 54:32-44, 2016.

Acknowledgments

This work has been sponsored by the French government research program "Investissements d'Avenir" through the IDEX-ISITE initiative 16-IDEX-0001 (CAP 20-25).

Enumeration problems

Typical question:

"Given input I , list all objects of type X in I ."

- ▶ cycles, cliques, independent sets, dominating sets, etc. of a graph
- ▶ transversals of a hypergraph
- ▶ elements of the (dual) antichain of a lattice
- ▶ variable assignments satisfying a formula
- ▶ trains to Paris leaving tomorrow before 10:00
- ▶ shortest paths from Montpellier to Marseille, etc.

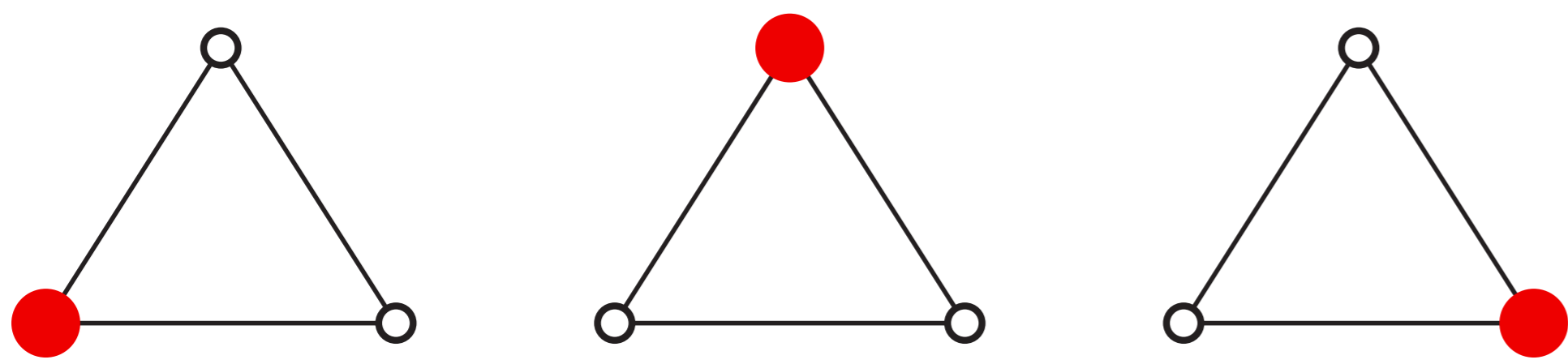
Applications

Mainly in database theory (query answering, repairing), AI, bioinformatics.

Possibly many objects: an example on graphs

Definition: Let $G = (V, E)$ be a graph.

A subset $D \subseteq V$ of vertices of G is a **dominating set** if every vertex of G is either in D , or adjacent to a vertex of D . It is called **minimal** if it is minimal by inclusion, i.e., no vertex can be removed while remaining a dominating set.



Observation: there are graphs with $3^{n/3} \approx 1.44^n$ minimal dominating sets, where n is the number of vertices (best known upper bound is 1.71^n).

Complexity measures

Input-sensitive: in terms of input size

There is an algorithm enumerating the minimal dominating sets of a n -vertex graph in $O(1.71^n)$ time. [Fomin, Grandoni and Pyatkin, 2008]

Output-sensitive: in terms of input+output size

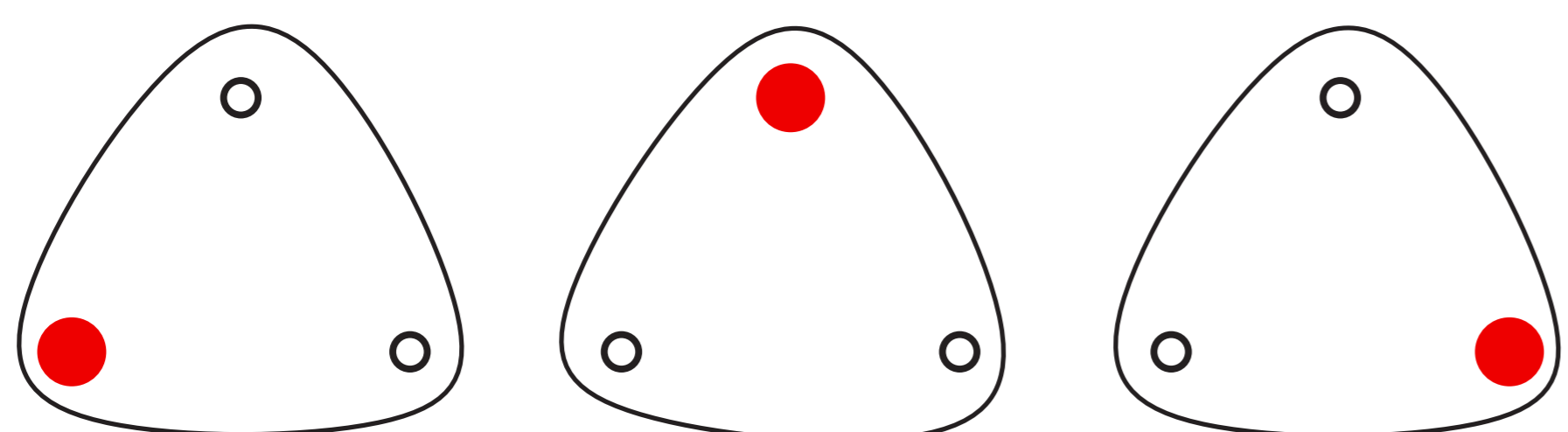
There is an algorithm enumerating the minimal dominating sets of a n -vertex graph in $O(N^{\log N})$ time, where $N = n + d$ and d is the number of minimal dominating sets of G . [Fredman and Khachiyan, 1996]

Polynomial equivalence: two enumeration problems Π_1 and Π_2 are **polynomially equivalent** if there is an output-polynomial time algorithm solving Π_1 if and only if there is one solving Π_2 .

A transversal problem

Definition: Let $\mathcal{H} = (V, \mathcal{E})$ be a hypergraph.

A subset $T \subseteq V$ of vertices of \mathcal{H} is a **transversal** if it intersects every hyperedge of \mathcal{H} . It is called **minimal** if it is minimal by inclusion, i.e., no vertex can be removed while remaining a transversal.



Observation: enumerating the minimal dominating sets of a graph amounts to enumerate the minimal transversals of its **hypergraph of (min.) neighborhoods**. In fact, both problems are **equivalent** [Kanté et al., 2014].

Open problems

Is there an output-polynomial algorithm for Trans-Enum/Dom-Enum?

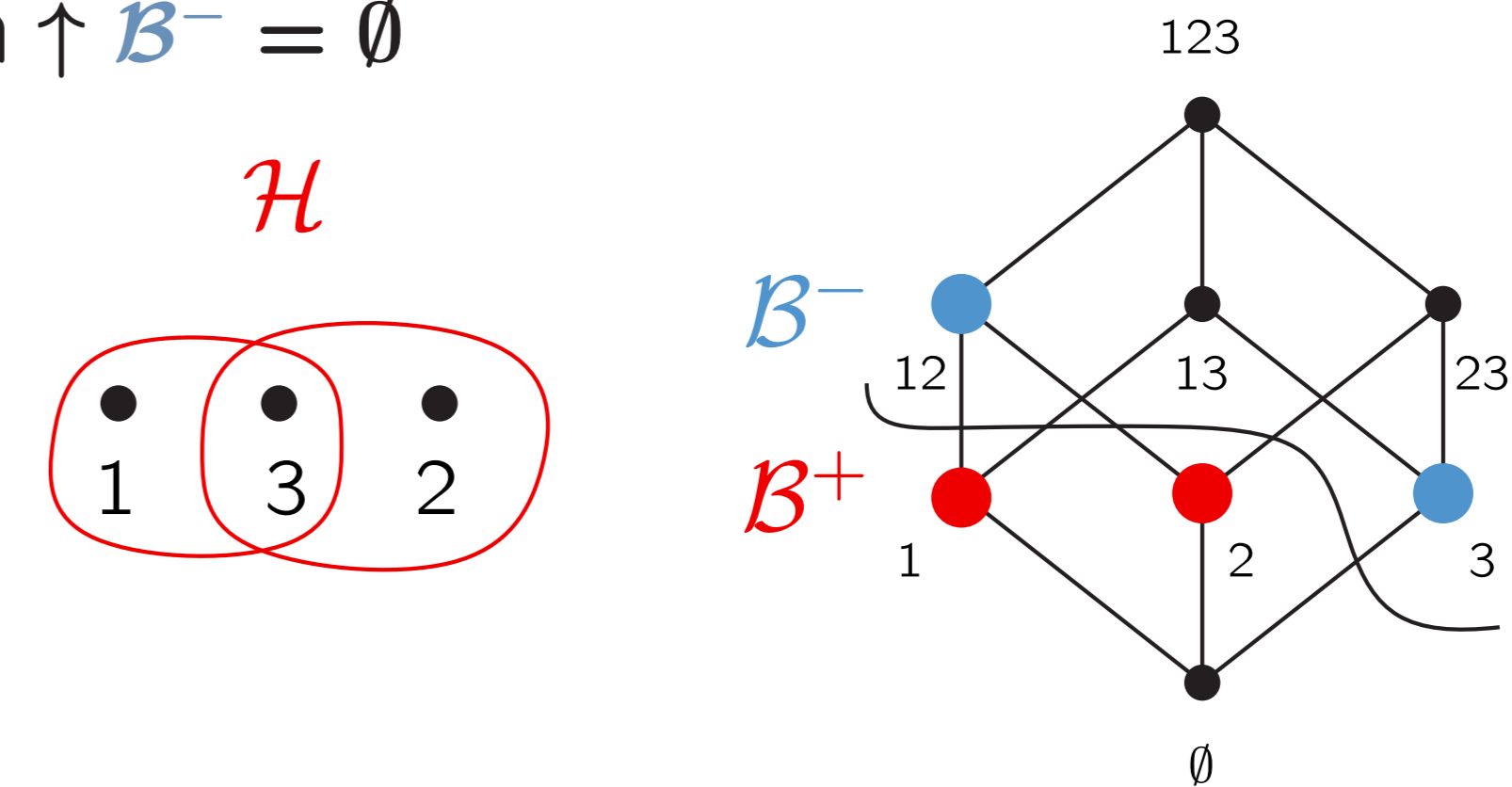
- ▶ what if the graph is bipartite? output-poly even for K_t -free! [1, 2].
- ▶ has no cycle of size four?
- ▶ enumeration with linear delay? in P_7 -free chordal graphs! [3].

Dualization in Boolean lattices

Definitions: Let $P = (X, \leq)$ be a poset.

The **ideal** of x in P is $\downarrow x = \{y \mid y \leq x\}$. The **filter** of x in P is the dual $\uparrow x = \{y \in X \mid x \leq y\}$. If $S \subseteq X$ then $\downarrow S = \bigcup_{x \in S} \downarrow x$ and $\uparrow S = \bigcap_{x \in S} \uparrow x$. An **antichain** of P is a subset of elements that are not comparable. Two antichains \mathcal{B}^+ and \mathcal{B}^- are **dual** if:

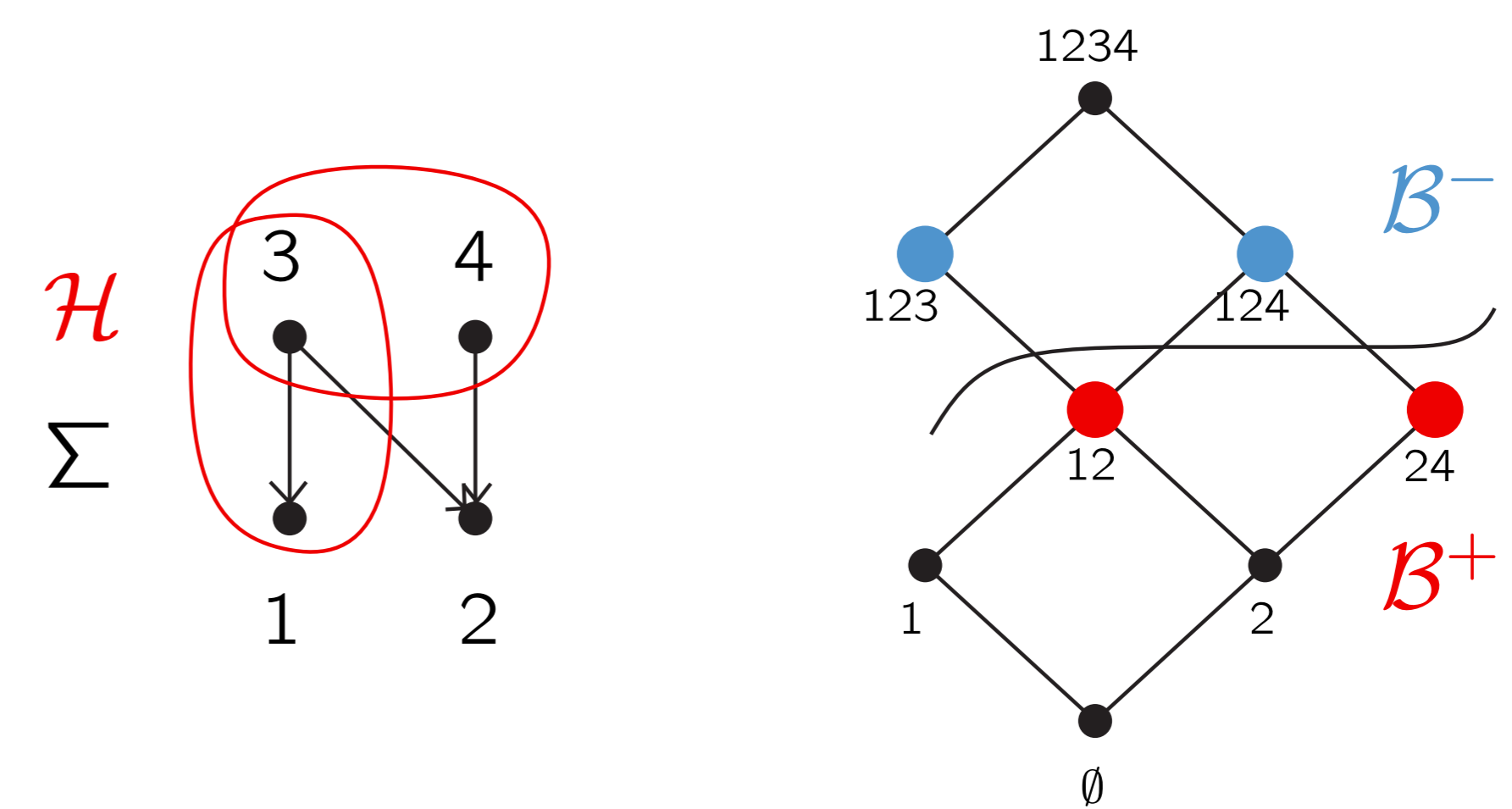
- ▶ $\downarrow \mathcal{B}^+ \cup \uparrow \mathcal{B}^- = X$
- ▶ $\downarrow \mathcal{B}^+ \cap \uparrow \mathcal{B}^- = \emptyset$



Observation: enumerating the minimal transversals of a hypergraph $\mathcal{H} = (V, \mathcal{E})$ amounts to compute the dual antichain of its complementary $\mathcal{B}^+ = \{V \setminus E \mid E \in \mathcal{E}\}$ in the **Boolean lattice** obtained by ordering all subsets of V by inclusion, i.e., $P = (X, \subseteq)$ where $X = 2^V$.

Generalization to other lattices?

When generalized to other lattices, the lattice can be given by an **implicational base** Σ and consists of all sets that are **closed** according to the implications in Σ . The lattices is **distributive** if implications are of size one. In the figure below, **14** does not belong to the lattice as it is not closed in Σ .



Observation: given the antichain \mathcal{B}^+ of a distributive lattice, computing its dual antichain \mathcal{B}^- amounts to compute the minimal closed (in Σ) transversals of its complementary $\mathcal{B}^+ = \{V \setminus E \mid E \in \mathcal{E}\}$.

Complexity status

Distributive lattices: open in general. The problem is equivalent to the **Boolean** case if the graph of implications is of bounded induced matching [4]. Output-polynomial are known under various restriction on the antichain and the implicational base coding the lattice [5].

General lattices: the dualization is impossible in output-polynomial time unless $P = NP$, even when the implicational base coding the lattice is of dimension two [4].

References

- [1] Marthe Bonamy, Oscar Defrain, Marc Heinrich, and Jean-Florent Raymond. Enumerating minimal dominating sets in triangle-free graphs. In *36th International Symposium on Theoretical Aspects of Computer Science*, pages 16:1–16:12. Springer, 2019.
- [2] Marthe Bonamy, Oscar Defrain, Marc Heinrich, Michał Pilipczuk, and Jean-Florent Raymond. Enumerating minimal dominating sets in K_t -free graphs and variants. *arXiv preprint arXiv:1810.00789*, 2019.
- [3] Oscar Defrain and Lhouari Nourine. Neighborhood preferences for minimal dominating sets enumeration. *arXiv preprint arXiv:1805.02412*, 2018.
- [4] Oscar Defrain and Lhouari Nourine. Dualization in lattices given by implicational bases. To appear in *ICFCA*, 2019.
- [5] Oscar Defrain, Lhouari Nourine, and Takeaki Uno. On the dualization in distributive lattices and related problems. *arXiv preprint arXiv:1902.07004*, 2019.

Objectives

- ▶ Study complex vehicle routing problems with inventory and loading constraints.
- ▶ Propose exact approaches : Mixed Integer Programming (MIP), Constraint Programming (CP) ...
- ▶ Propose heuristic approaches : metaheuristics, hybrid methods ...

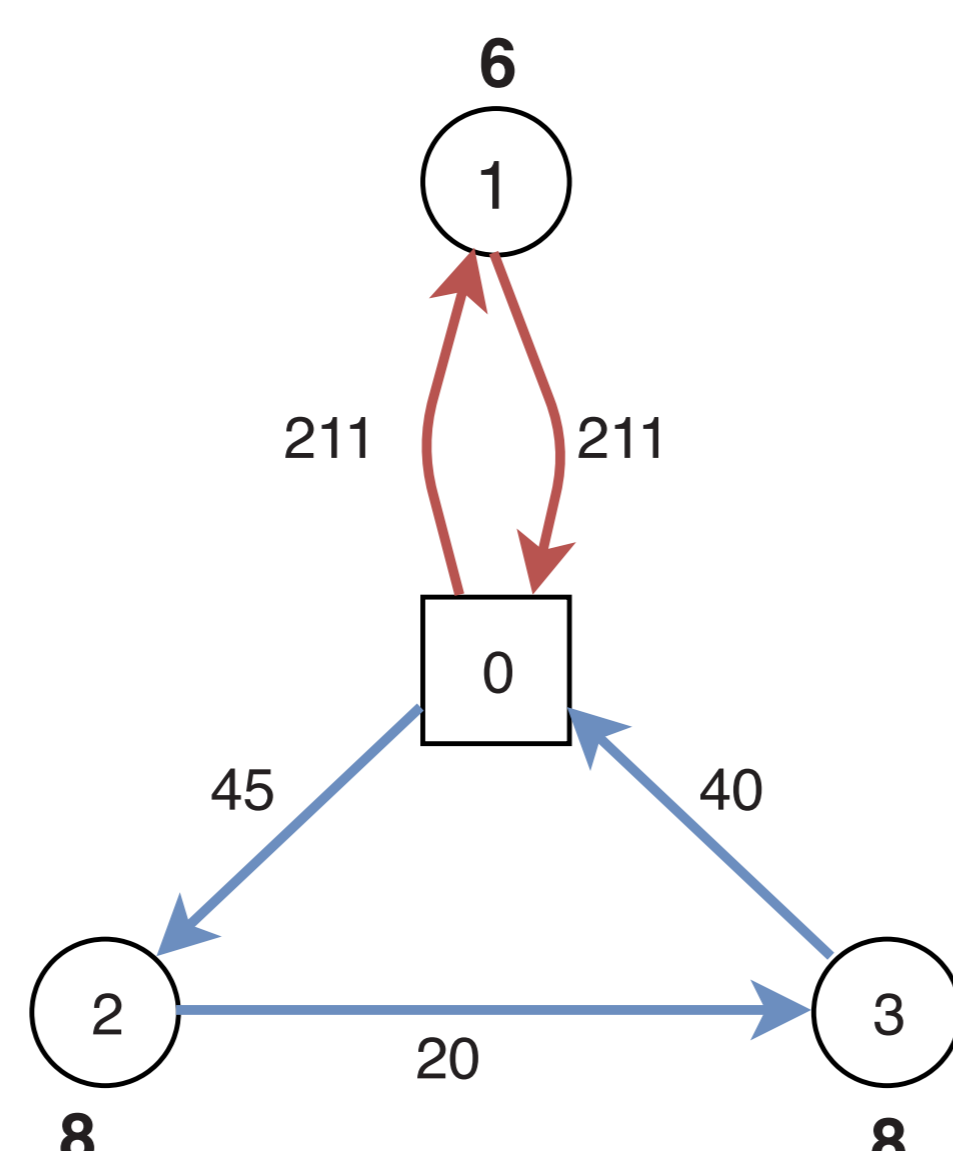
First studied problem

- ▶ Multivehicle Inventory Routing Problem = Capacitated Vehicle Routing Problem + Inventory management
- ▶ Handle inventory level over time.
- ▶ Schedule transportation of products.

Capacitated Vehicle Routing Problem (CVRP)

Data :

1. Complete weighted graph : $G = (V, E)$
2. Weight of edge $(i, j) \in E : C_{i,j}$
3. $V = \{0, \dots, N\}$
4. Number of nodes : N
5. Special node 0 : depot
6. Nodes $i \geq 1$: customers
7. Fleet of K vehicles with capacity Q
8. Demand at each node $i \geq 1$: R_i



Variables:

1. Vehicle assignment of node $i \geq 1$: v_i
2. Successor of node $i \geq 1$ in its route : x_i
3. First visited node of vehicle k : x_0^k

Objective: Minimize

$$\text{Transportation cost} : \sum_{i \geq 1} C_{i,x_i} + \sum_{k \in K} C_{0,x_0^k}$$

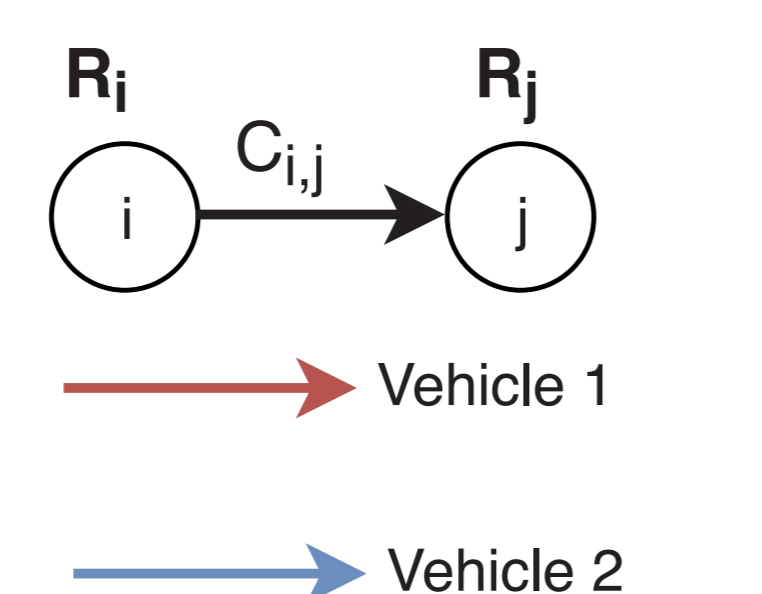


Figure 1: CVRP

Inventory management (IM)

Data :

1. Discrete time horizon : $\mathcal{T} = \{1, \dots, T\}$
2. Demand at each node $i \geq 1$ (retailers) and period t : R_i^t
3. Production at the supplier and period t : R_0^t
4. Inventory bounds at node i : $[\mathcal{L}_i, \mathcal{U}_i]$
5. Inventory cost of node i at period t : \mathcal{H}_i^t
6. Initial inventory level at node t : \mathcal{I}_i^0

Variables:

1. Inventory level of node i at period t route : s_i^t
2. Delivery of node $i \geq 1$ at period t : q_i^t

Objective: Minimize

$$\text{Inventory cost} : \sum_{t \in \mathcal{T}} \sum_{i=0}^N \mathcal{H}_i^t s_i^t$$

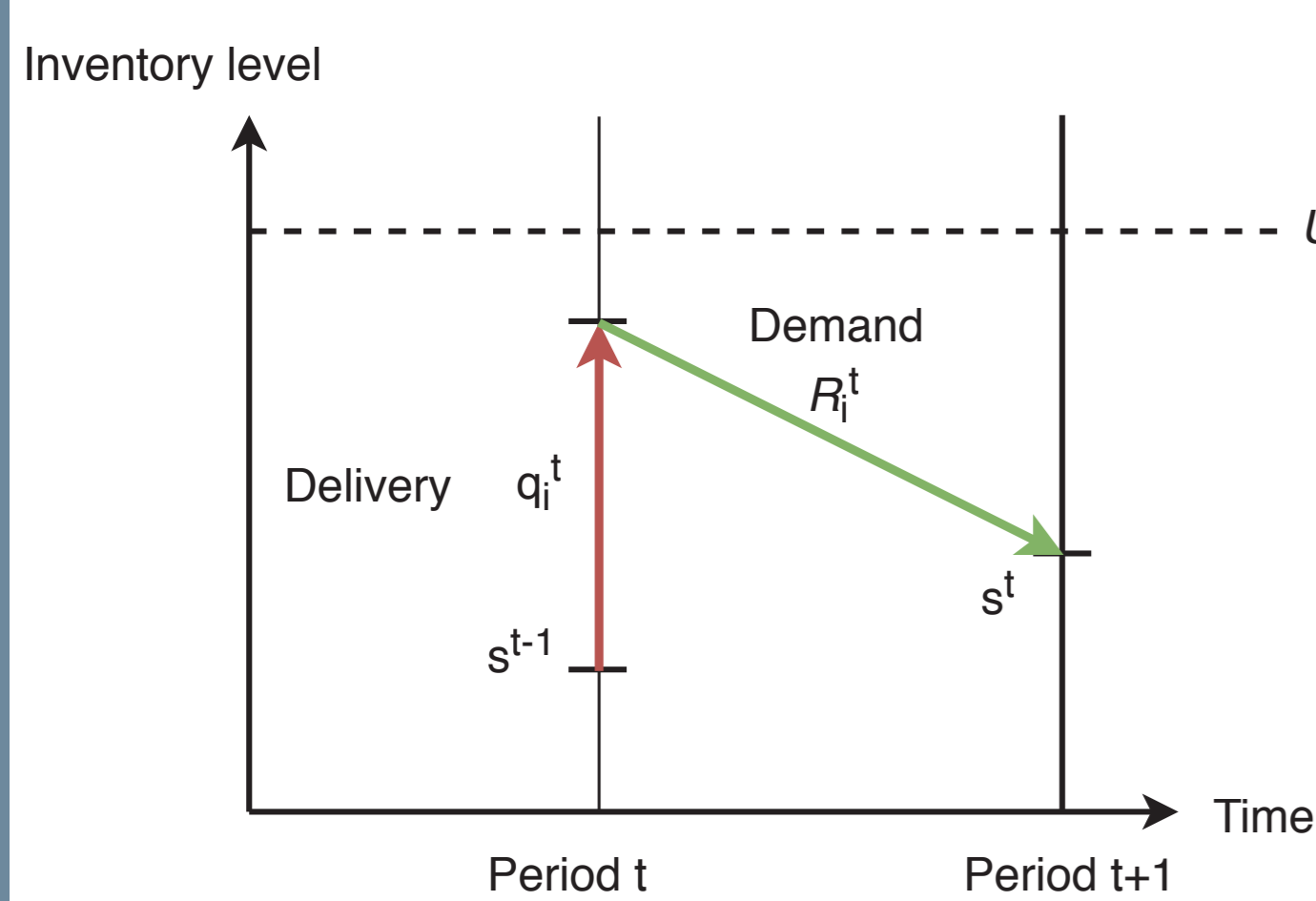


Figure 2: Inventory flow for one retailer

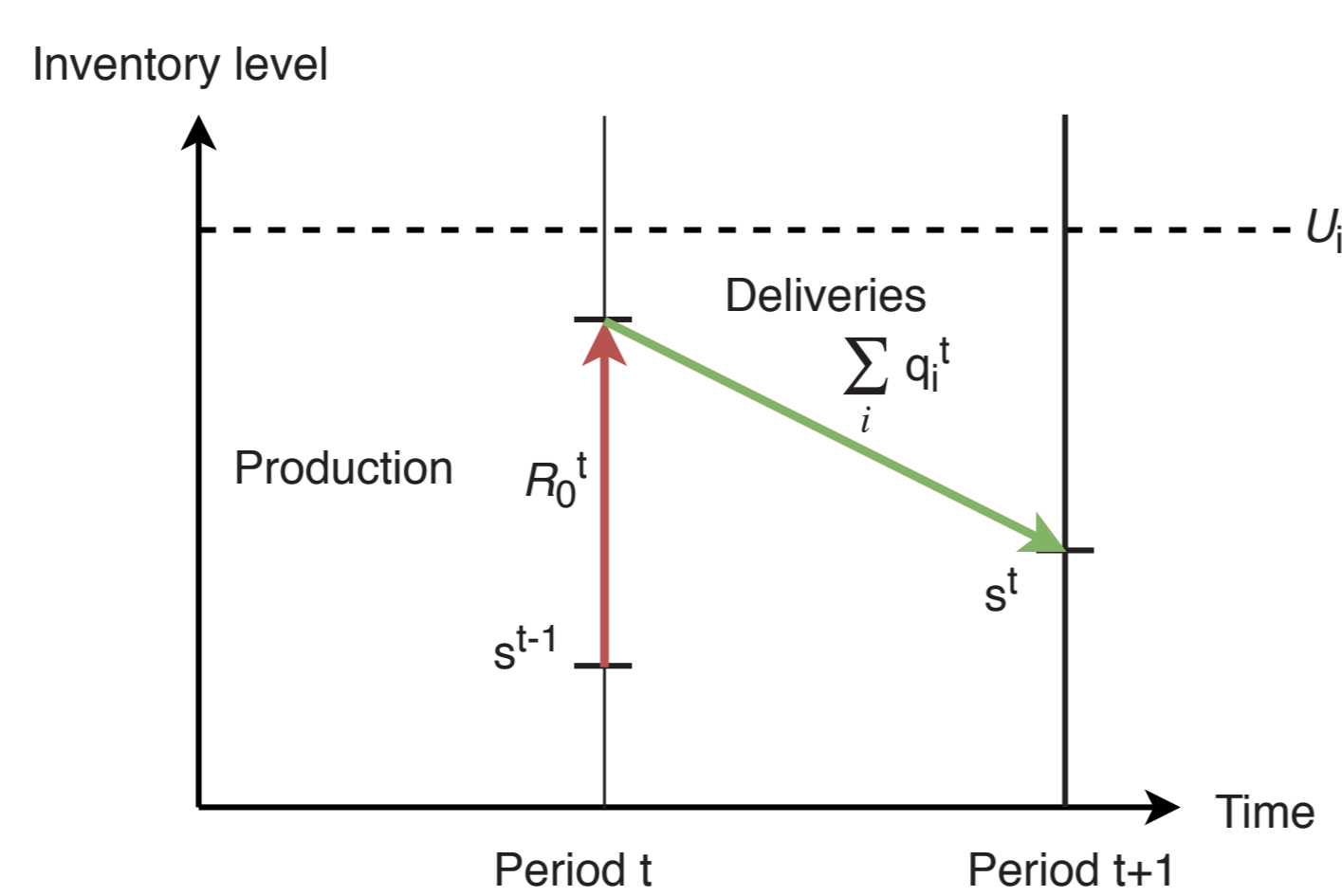


Figure 3: Inventory flow for the supplier

Resolution scheme

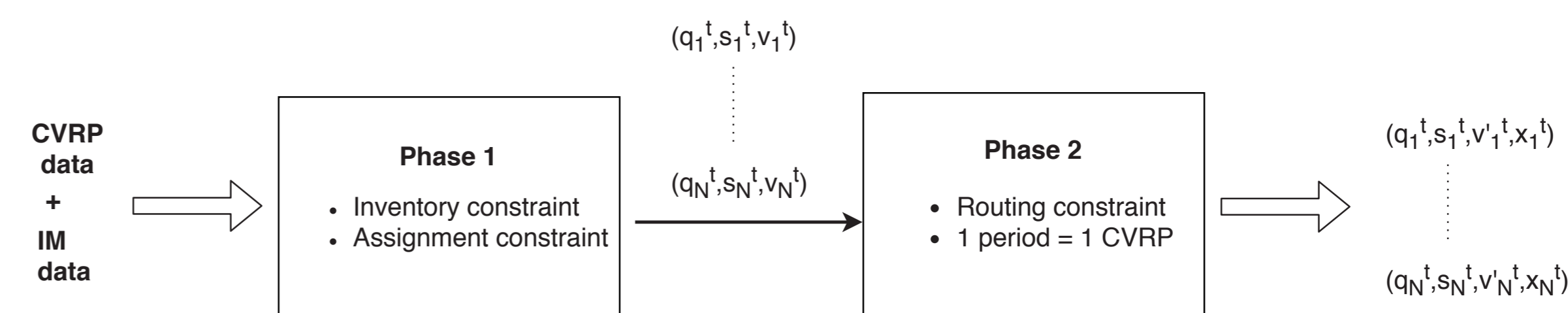


Figure 4: Global resolution scheme

Phase 1 : Feasible inventory solution

Solved using CP (OR-Tools : <https://developers.google.com/optimization/>)

Inventory constraints:

- ▶ $s_i^1 = \mathcal{I}_i^0 - \mathcal{R}_i^1 + q_i^1$
- $\forall t \in \mathcal{T} \setminus \{1\}, s_i^t = s_i^{t-1} - \mathcal{R}_i^t + q_i^t$
- ▶ $s_0^1 = \mathcal{I}_0^0 + \mathcal{R}_0^1 - \sum_{i \in \mathcal{V}'} q_i^1$
- $\forall t \in \mathcal{T} \setminus \{1\}, s_0^t = s_0^{t-1} + \mathcal{R}_0^t - \sum_{i \in \mathcal{V}'} q_i^t$

Assignment constraints:

- ▶ $\forall t \in \mathcal{T}, \text{assignment}(\{v_i^t | i \in \mathcal{V}'\}, \{q_i^t | i \in \mathcal{V}'\}, K + 1, Q)$

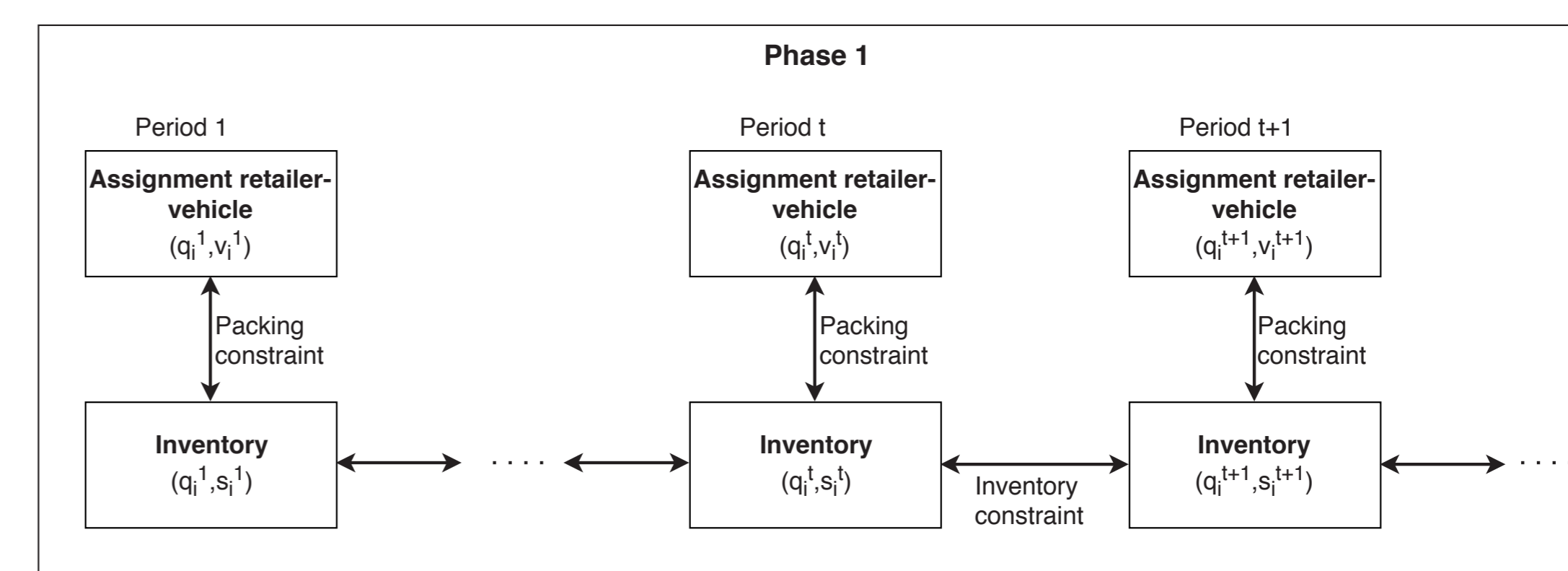


Figure 5: Phase 1 scheme

Phase 2 : Routing

Solved using metaheuristics (OR-Tools)

1 period = 1 CVRP problem such that :

1. $\mathcal{V} = \{0\} \cup \{i | q_i^t > 0\}$
2. Special node 0 : supplier
3. $\{i | q_i^t > 0\}$: retailers
4. Demand at each node i : $\mathcal{R}_i = q_i^t$

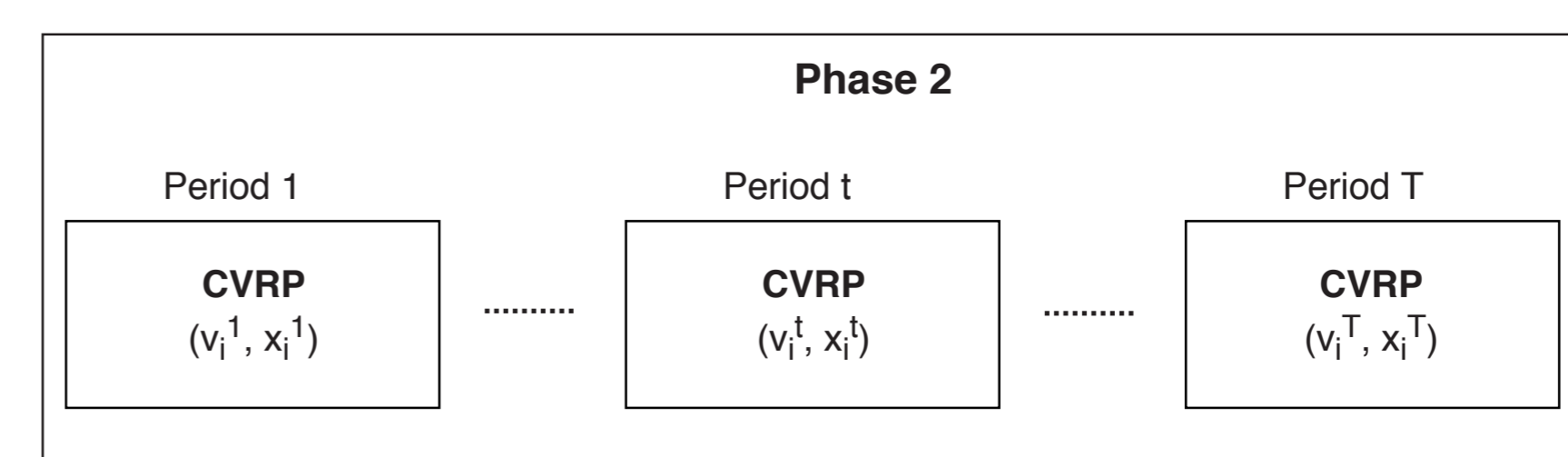


Figure 6: Phase 2 scheme

Results

Instance		[1]	[2]	our approach
S3PHC	Avg Time (s)	399.45	-	0.02
	Gap w.r.t best known solution	6.48%	36.8 %	17.25 %
	# sol	188	200	200
S6PHC	Avg Time (s)	504.30	-	0.02
	Gap w.r.t best known solution	11.85 %	36.13 %	27.51 %
	# sol (s)	102	119	119
B6PHC	Avg Time (s)	-	-	1.30
	Gap w.r.t best known solution	-	31.76	14.55
	# sol (s)	-	120	120

References

- [1] Claudia Archetti, Natasha Boland, and M. Grazia Speranza. A Matheuristic for the Multivehicle Inventory Routing Problem. *INFORMS Journal on Computing*, 29(3):377–387, aug 2017.
- [2] Aldair Alvarez, Pedro Munari, and Reinaldo Morabito. Iterated local search and simulated annealing algorithms for the inventory routing problem. *International Transactions in Operational Research*, 25(6):1785–1809, nov 2018.
- [3] Claudia Archetti, Luca Bertazzi, Alain Hertz, and M. Grazia Speranza. A Hybrid Heuristic for an Inventory Routing Problem. *INFORMS Journal on Computing*, 24(1):101–116, feb 2012.

Contact Information

- ▶ Web: <https://fc.isima.fr/~axdelsol/>
- ▶ Email: axel.delsol@isima.fr

Objectives

1. Determining new life factors that impact on dementia (Ex. Alzheimer).
2. Development of machine learning algorithms to handle categorical data.
3. development of machine learning algorithms to handle mix data (numeric and categorical).

Introduction

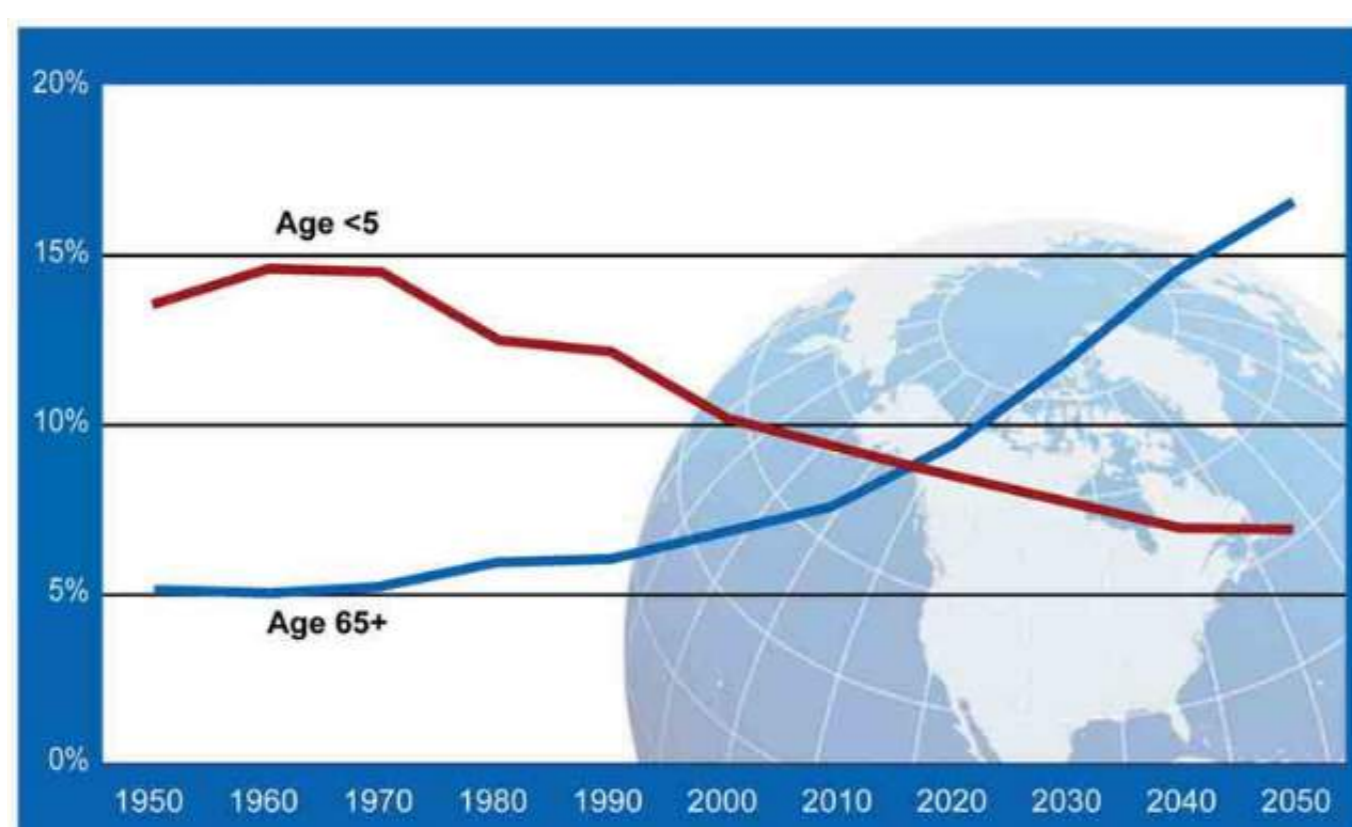


Figure 1: Projection of young and older adults [1]

- ▶ 131 million of persons are expected to be living with dementia by 2050 [2].
- ▶ Economic impact: 1 trillion total worldwide cost of dementia [2].
- ▶ A need of understanding dementia.

Background

Clustering is a family method of machine that aims to group a set of objects based on their similarity and dissimilarity. Given a number of clusters in:

- ▶ Crisp clustering, a data point must belong to at most one.
 - ▷ Ex. K-Means
- ▶ Fuzzy clustering, a data point could belong to many clusters.
 - ▷ Ex. Fuzzy C-Means
- ▶ Probabilistic clustering, certain models (Gaussian, Poisson) are used to cluster data.
 - ▷ Ex. Expectation-Maximization
- ▶ Evidential clustering, generalize crisp, fuzzy and probabilistic clustering.
 - ▷ Ex. Evidential C-Means [3]

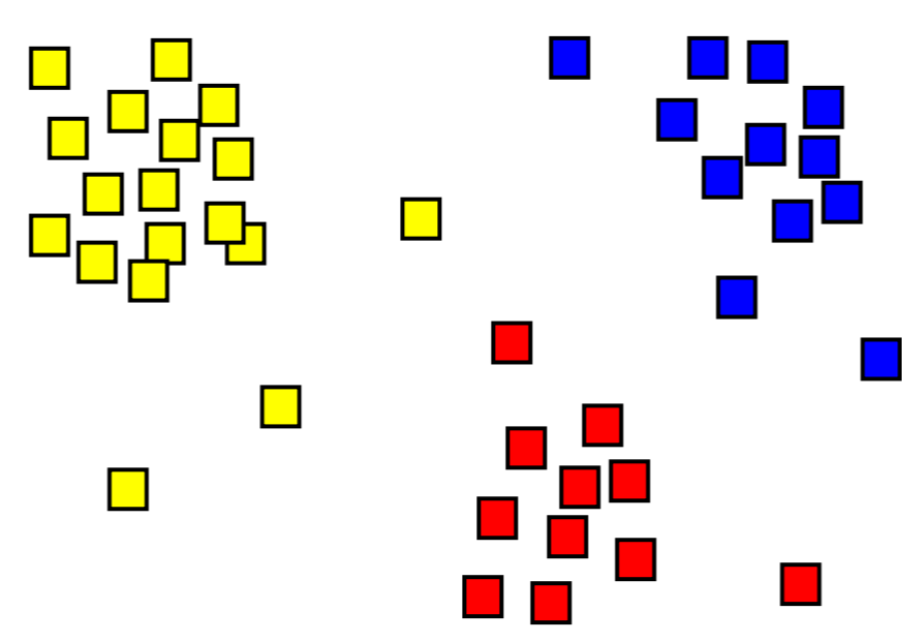


Figure 2: Example of 3 clusters

Methodology

- ▶ State-of-the-art.
- ▶ Defining dissimilarity measures.
- ▶ Defining clusters prototypes.
- ▶ Optimize the objective function.
- ▶ Experimentation.

Mathematical Section

- ▶ Objective function
The evidential c-means (ECM) algorithm searches for a partition called credal M and the set of prototypes V that minimize intra-cluster variance:

$$\begin{cases} J_{ECM}(M, V) = \sum_{i=1}^n \sum_{A_j \subseteq \Omega, A_j \neq \emptyset} |A_j|^\alpha m_{ij}^\beta d_{ij}^2 + \sum_{i=1}^n \rho^2 m_{i\emptyset}^\beta \\ s.t \sum_{j/A_j \subseteq \Omega, A_j \neq \emptyset} m_{ij} + m_{i\emptyset} = \mathbf{1}, \quad \forall i = \{1, \dots, n\} \end{cases} \quad (1)$$

With α : the weighting exponent for cardinality, β : the weighting exponent for the fuzziness, δ the distance to the empty set.

- ▶ Optimization process
 - ▷ NP-Hard problem.
 - ▷ Fix M , and optimize V .
 - ▷ Fix V , and optimize M .

Example of evidential clustering application

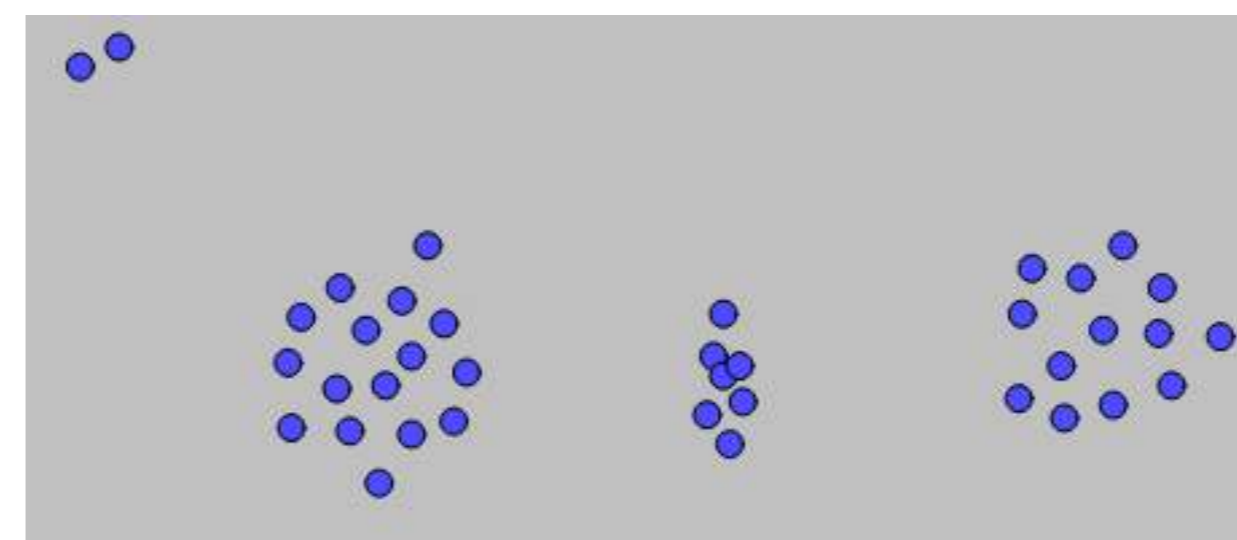


Figure 3: Data points to cluster

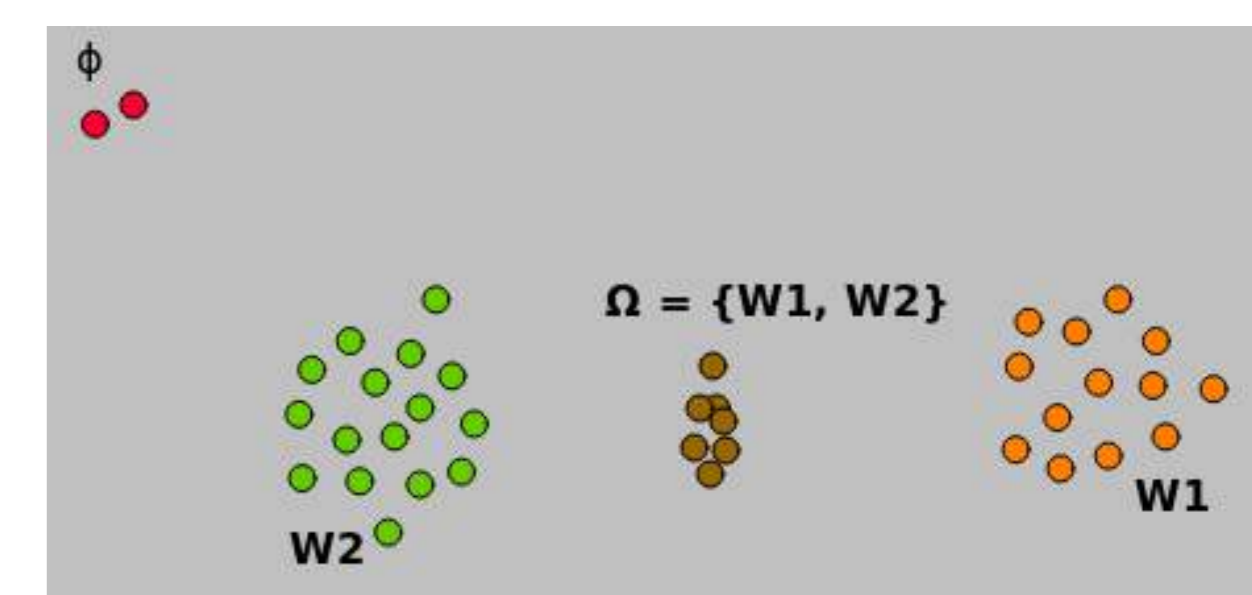


Figure 4: Results of ECM

- Real-world applications:
- ▶ **Green class**: persons with Alzheimer.
 - ▶ **Orange class**: persons without Alzheimer (normal).
 - ▶ **Brown class**: persons that begin to have Alzheimer's symptoms.
 - ▶ **Red class**: persons with lost of memory but not due to Alzheimer.

Challenges with categorical data

Let's consider the follow data set:

Sex	AgeGroup	MemoryLost	RepeatedQuestionsOrStatements
M	35-45	No	No
F	65-75	Yes	Yes
M	55-65	Yes	No
F	45-55	No	No

- ▶ How to define clusters prototypes ? (ex. Barycenter with numeric data)
- ▶ How to define distance between data points and clusters ? (ex. Euclidian distance with numeric data)

Contributions

Our paper 'Evidential clustering for categorical data' is accepted for publication at the international conference FUZZ-IEEE. The main contributions are the following:

- ▶ New cluster prototypes representation.
- ▶ New dissimilarity measure between clusters and data points.

Conclusion & Perspectives

- ▶ Dementia remains a big challenge in the world.
- ▶ Machine learning approach to determine life factors that affect dementia.pOSTER
- ▶ Development of new robust methods that can handle numeric and categorical data.
- ▶ Perspectives
 - ▷ Defining new dissimilarity measure (the proposed one gives crisp cluster centers).
 - ▷ Mix evidential clustering to handle categorical and numeric data.

References

- [1] United Nations. World Population Prospects: The 2010 Revision.
- [2] Alzheimers Disease International. September 2016.
- [3] M. Masson and T. Denœux. ECM: An evidential version of the fuzzy c-means algorithm. *Pattern Recognition*, 41(4):1384-1397, 2008.

Acknowledgments

- ▶ This thesis is supported by the Agence Nationale de la Recherche of the French government throught the program "Investissements d'Avenir" (16-IDEX-0001 CAP 20-25).

Contact Information

- ▶ Web: <http://www.limos.fr>
- ▶ Email: abdoul_jalil.djiberou_mahamadou@uca.fr
- ▶ Phone: +33 (0) 473 40 53 70

Improvement and automatization of an image analysis tool to characterize the plant 3D nucleus

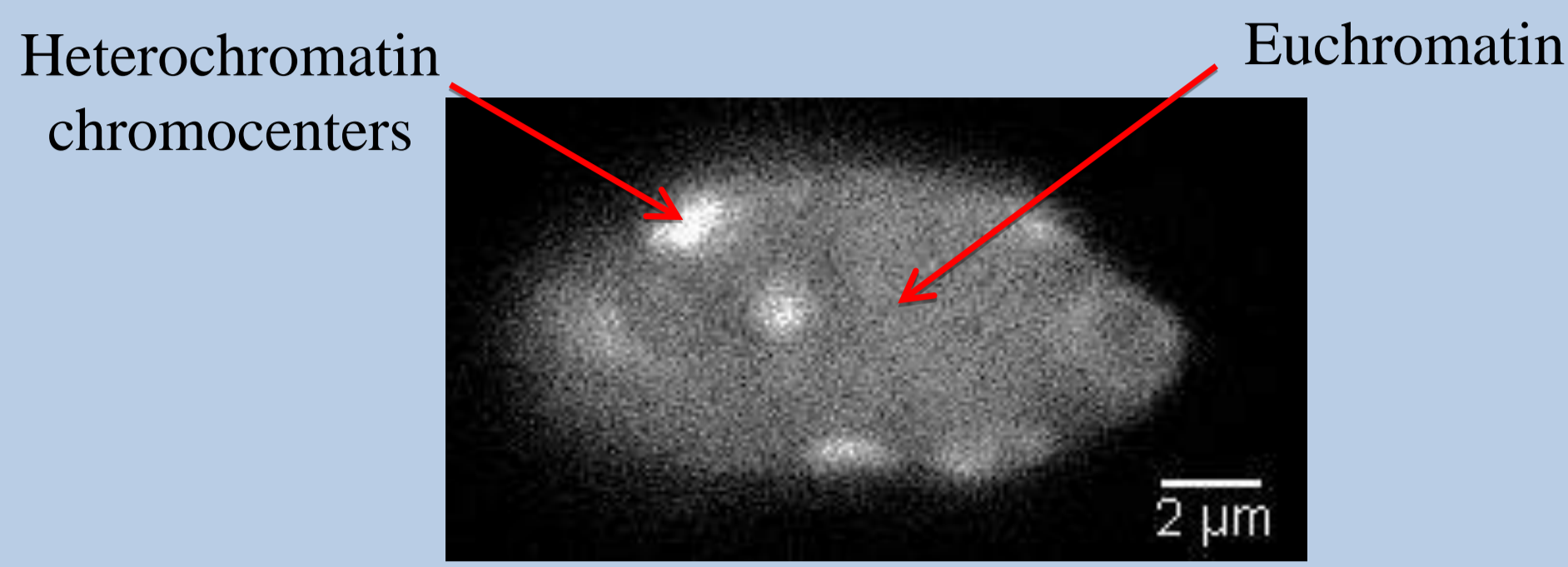
DUBOS Tristan^{1,2}, MALGOUYRES Rémy², POULET Axel³, GONTHIER Céline¹, POUCHIN Pierre¹, PROBST Aline¹, TATOUT Christophe¹ and DESSET Sophie¹

¹ Université Clermont Auvergne, Laboratoire GReD, Clermont-Ferrand, France

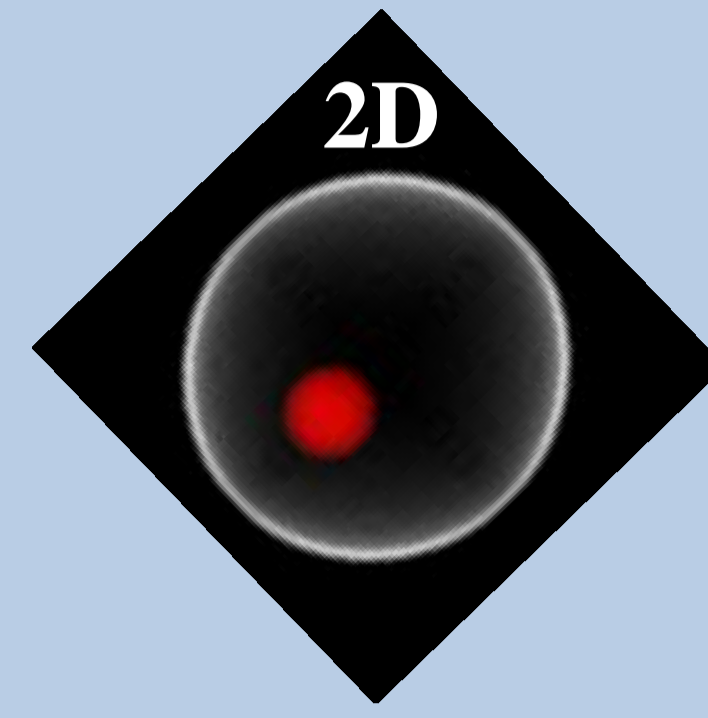
² Université Clermont Auvergne, Laboratoire LIMOS, Aubière, France

³ Emory University, Department of Biostatistics and Bioinformatics, Atlanta, USA

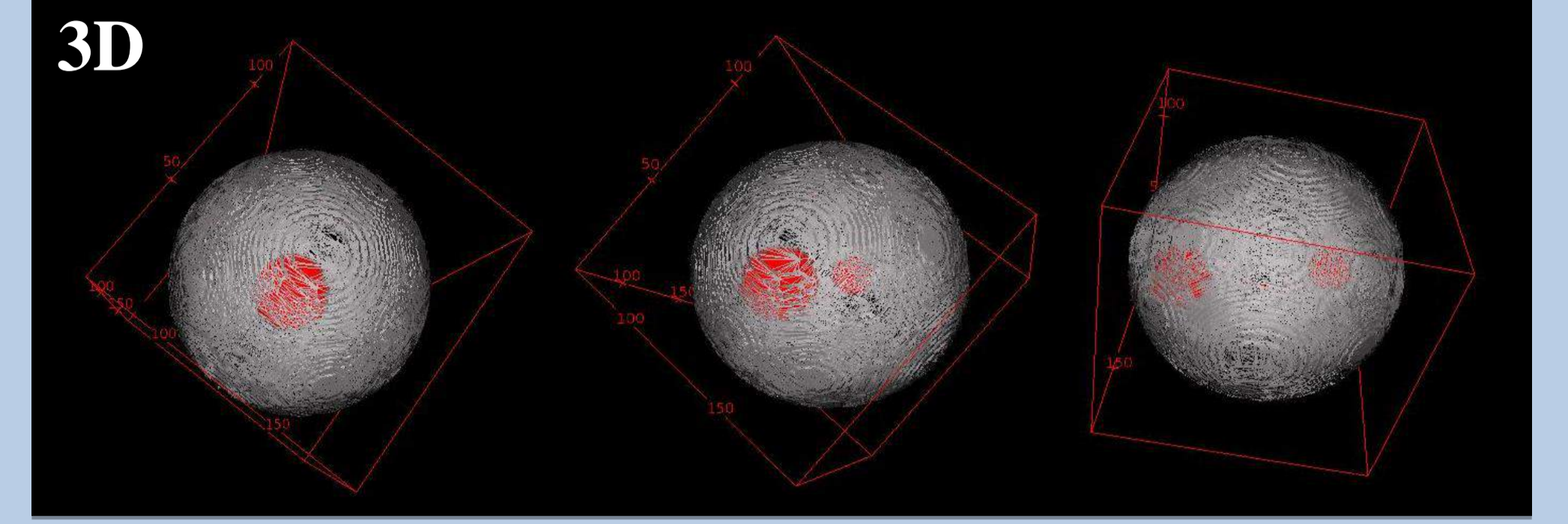
I. Objective: study nuclear organization (nuclear morphology and chromatin organization) in 3D



Parameters to characterize a nucleus?
Volume, shape, heterochromatin density & position,...



2D: only 1 chromocentre (red object) can be detected in the center of a nucleus (white circle)



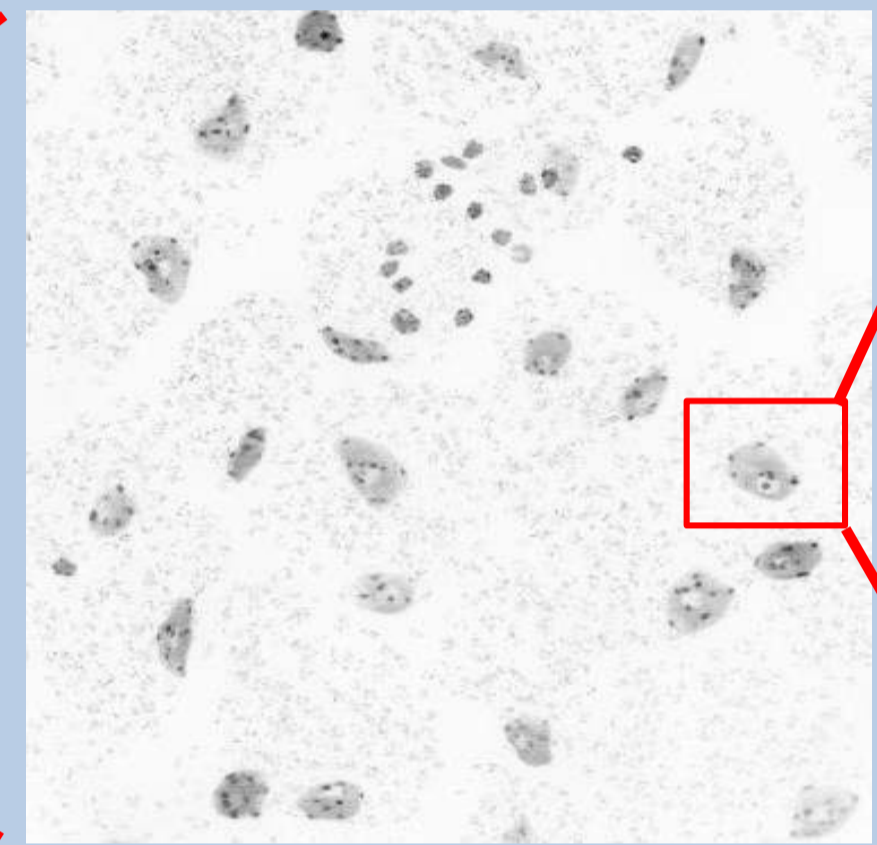
3D: reveals a second chromocentre behind the first one, and both are close to the nuclear periphery.

Aim : implement a workflow to compute 3D morphometric from Plant nuclei

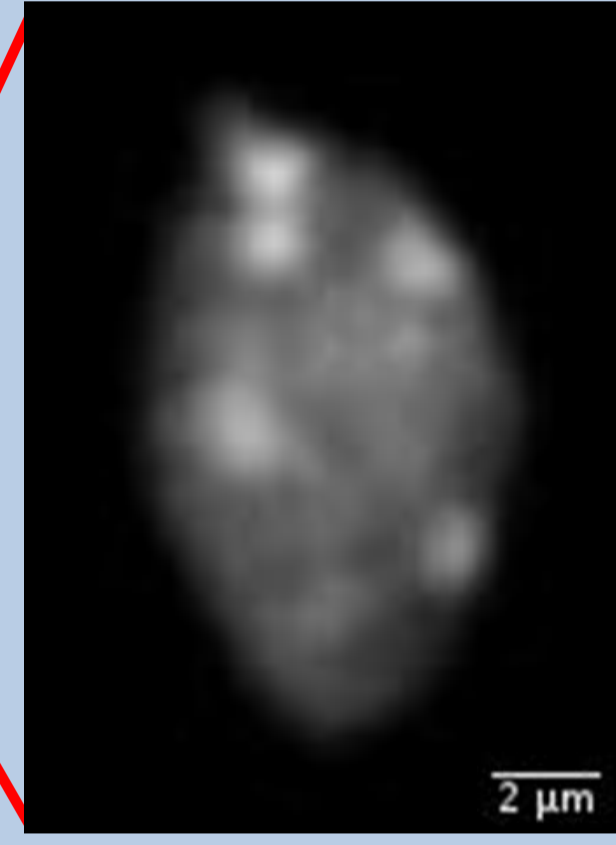
II. Method: Wide field images acquisition and general image process analyses through the *NucleusJ* plugin



Whole-mount preparation
Fixed-tissue + DNA dye (DAPI)



Wide field microscopy
3D image stack
(MMAF+ optigrd)



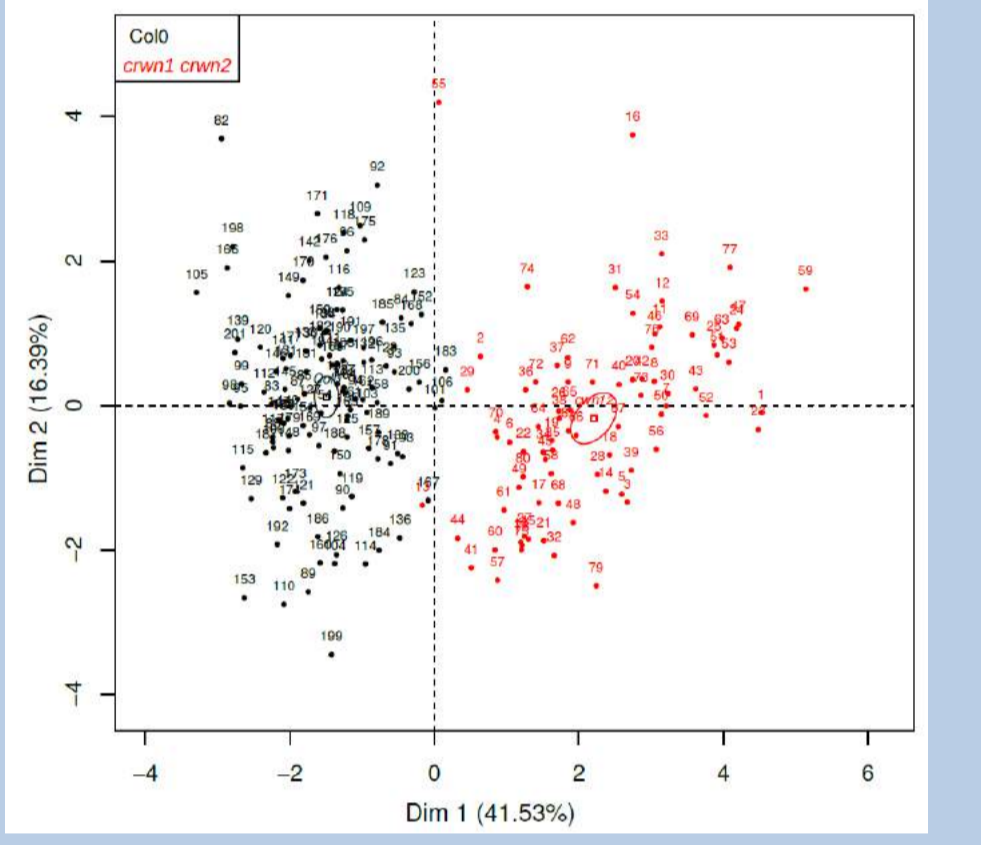
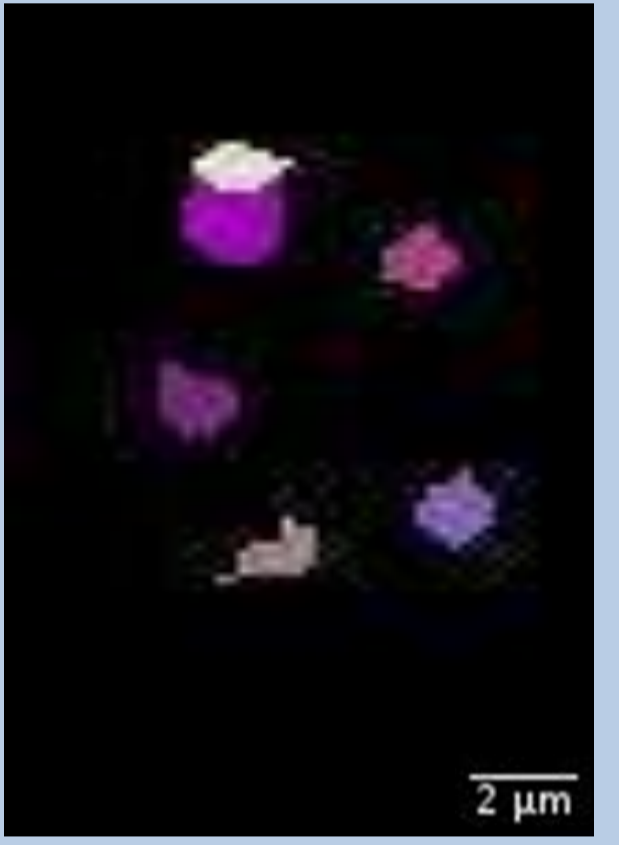
Automated
isolation of nuclei
(Autocrop)



Nuclei
segmentation
(Otsu modified)



Chromocenters segmentation
with manual thresholding
(3D watershed + thresholding)

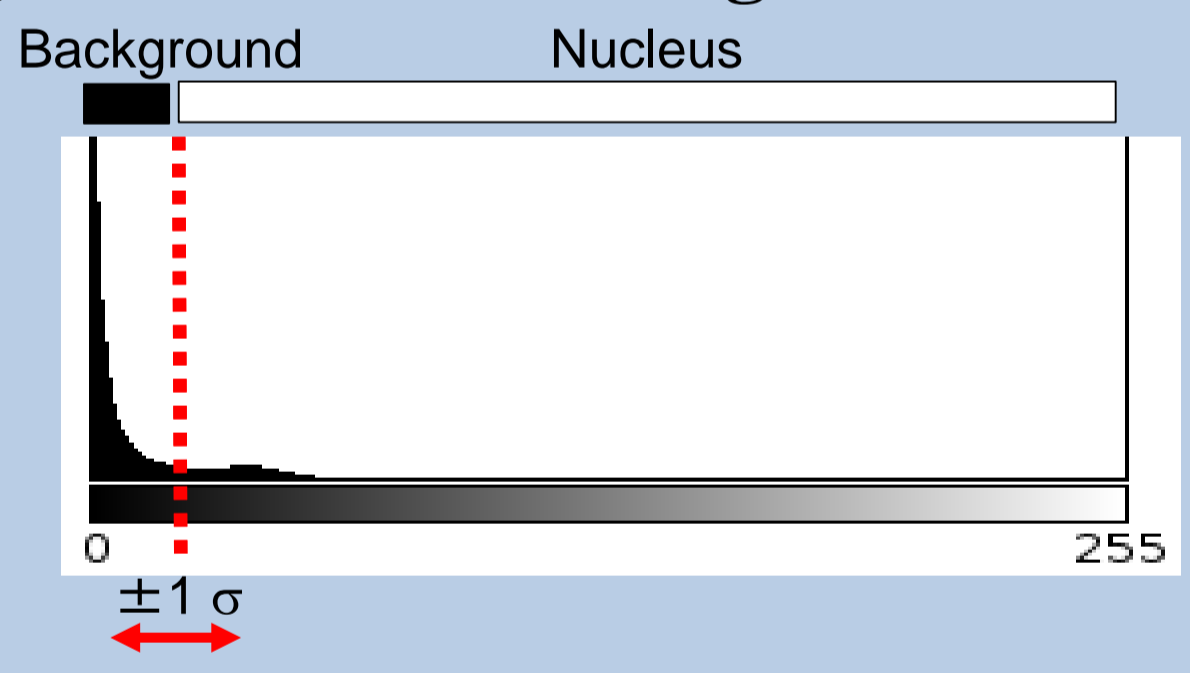


Output: 15 parameters
(sphericity, distance,
volume...)

NucleusJ is functional (see Poulet et al., *Bioinformatics* 2017, *J. Cell Science* 2017) but needs automated segmentation processes

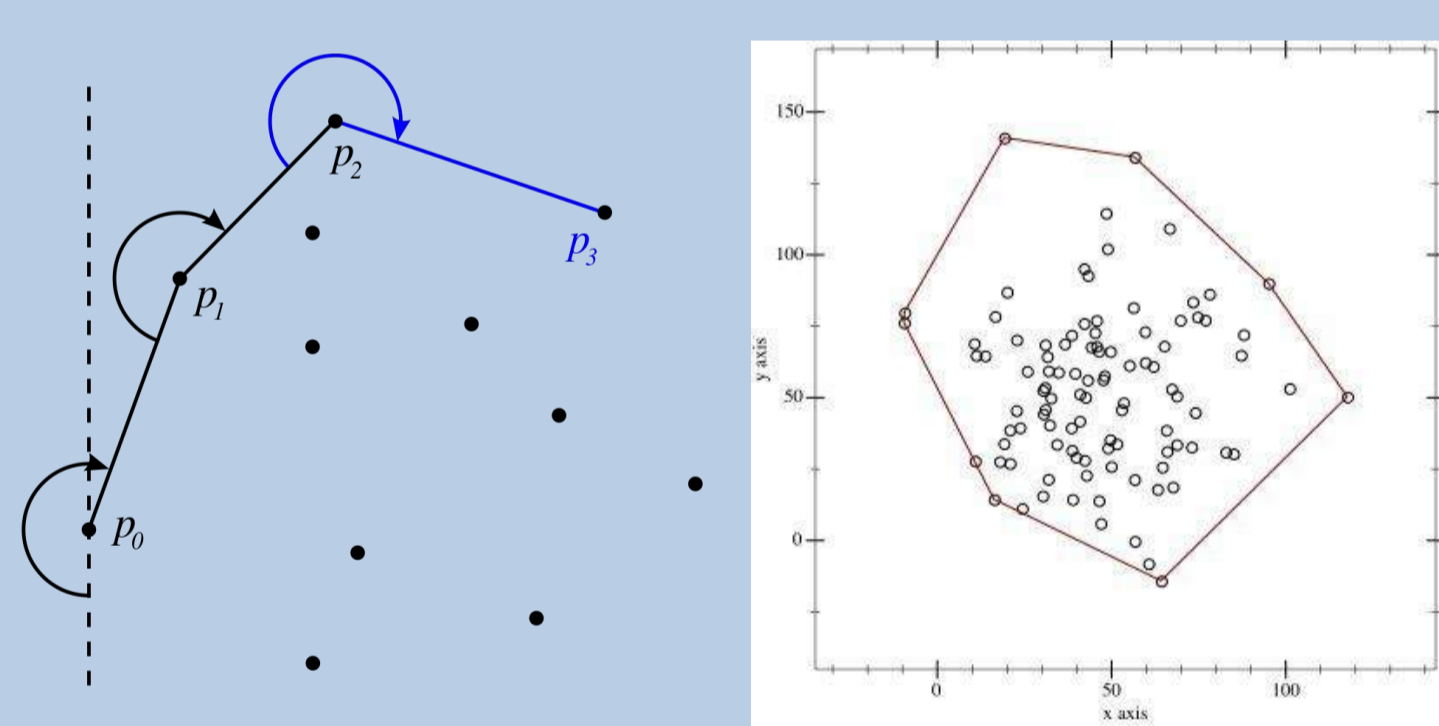
III. Improvement of NucleusJ

A) Modified OSTU segmentation



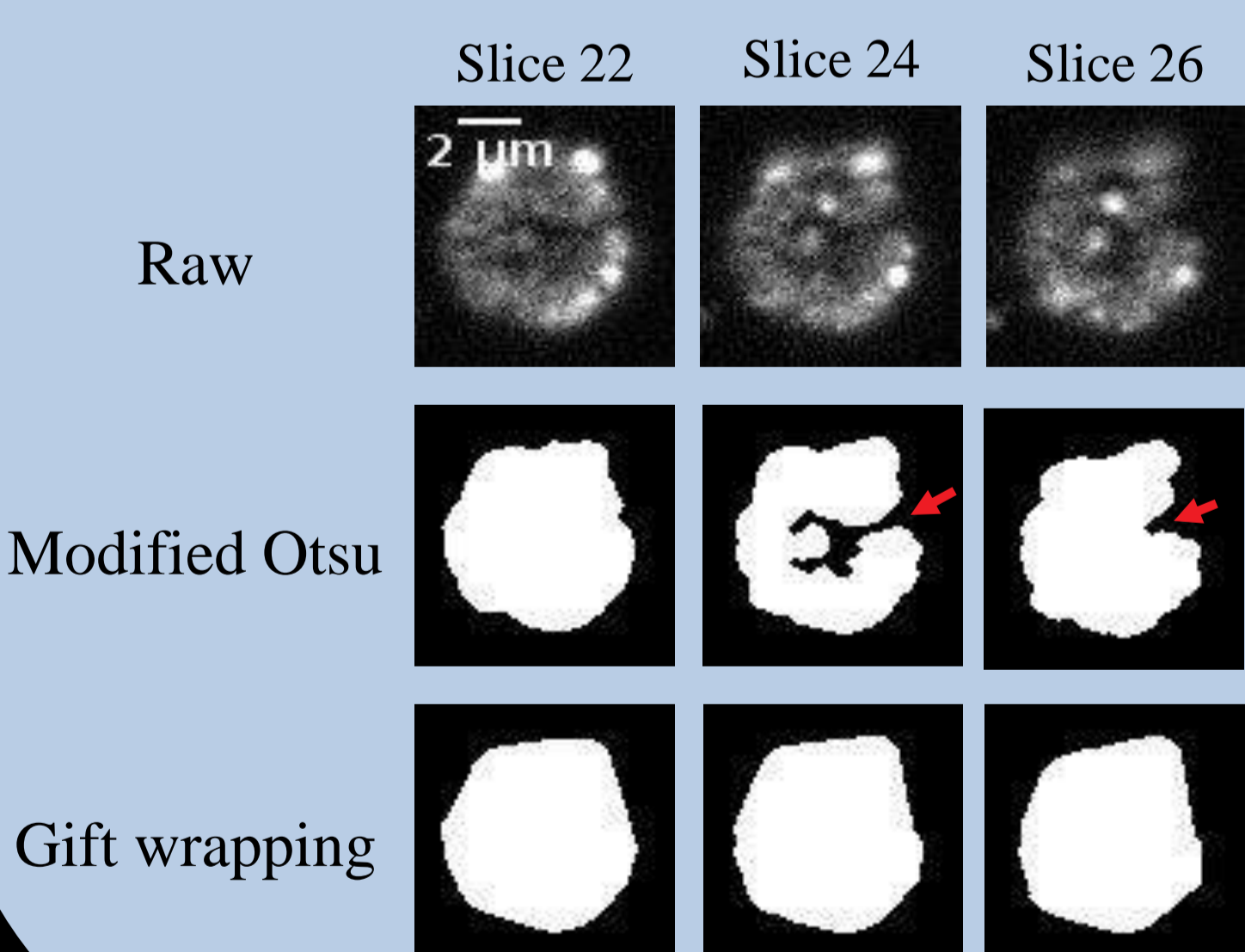
Optimized Otsu threshold maximized sphericity

B) Gift wrapping segmentation



Implementation of Jarvis march algorithm

C) Application on nuclei



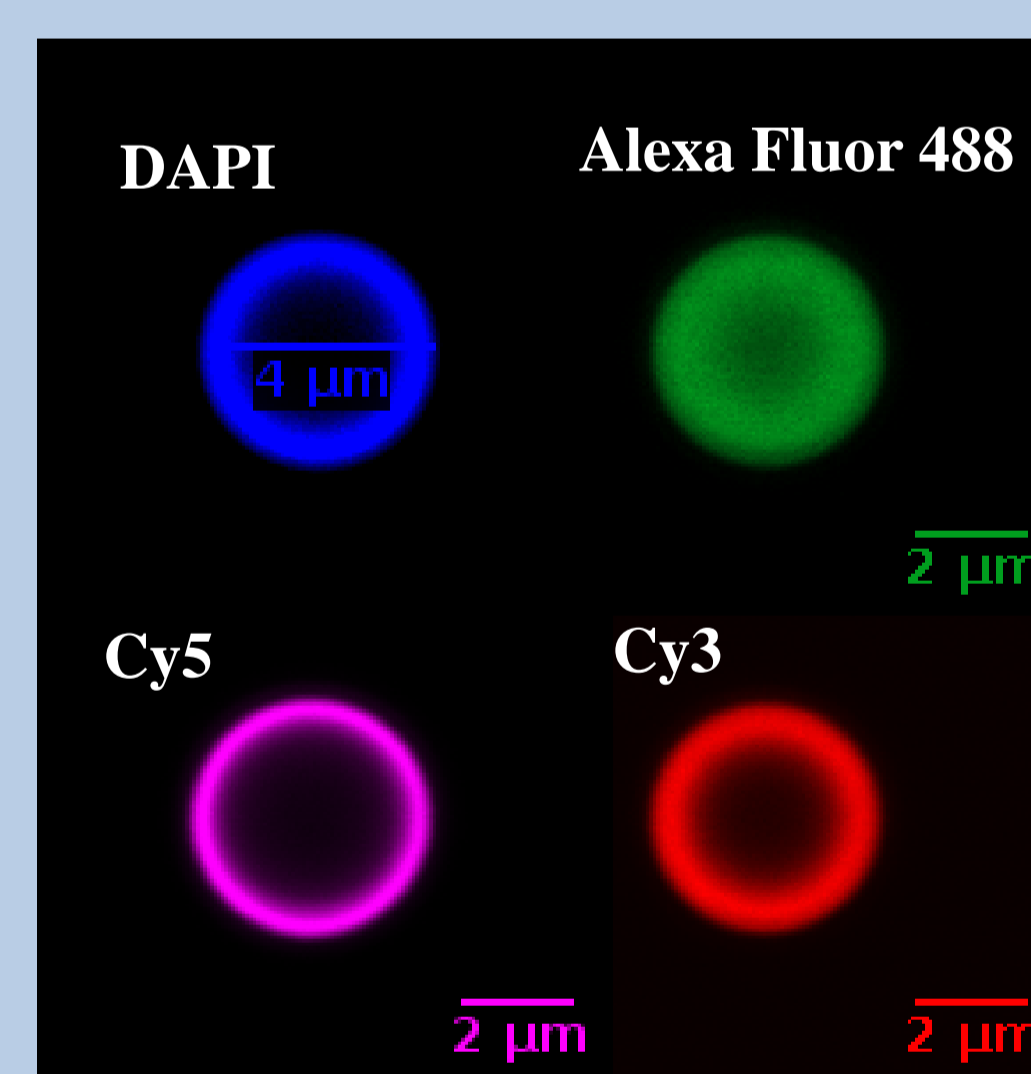
Nucleolus (no DNA = no staining)
Boundaries: Irregularities due to poor DAPI staining

Nucleolus (hole)
Indentations & irregularities at boundaries

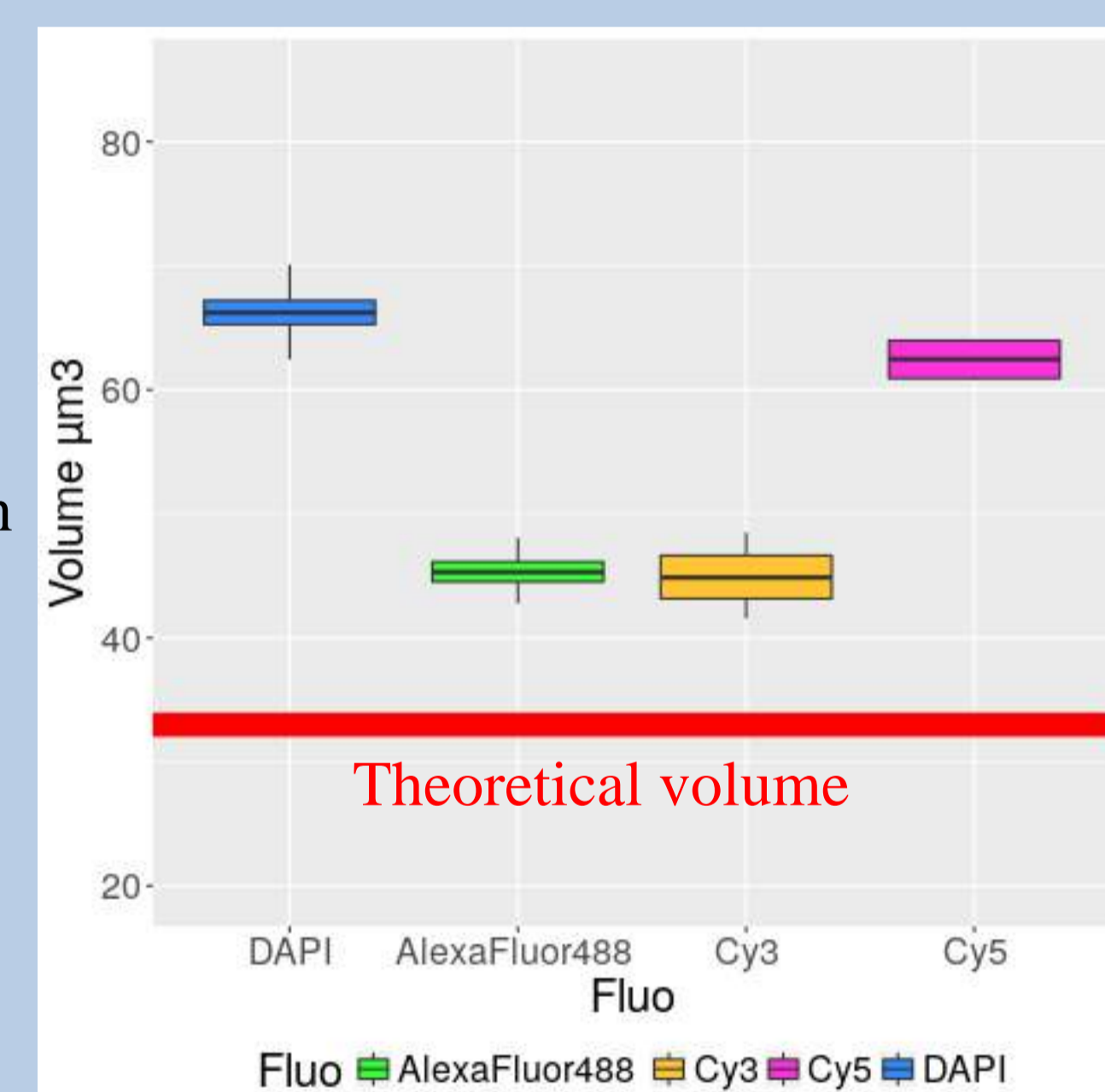
Nucleolus is filled (no hole)
Reduction of indentations & irregularities at boundaries
BUT
Over estimation of the volume

IV. Validation

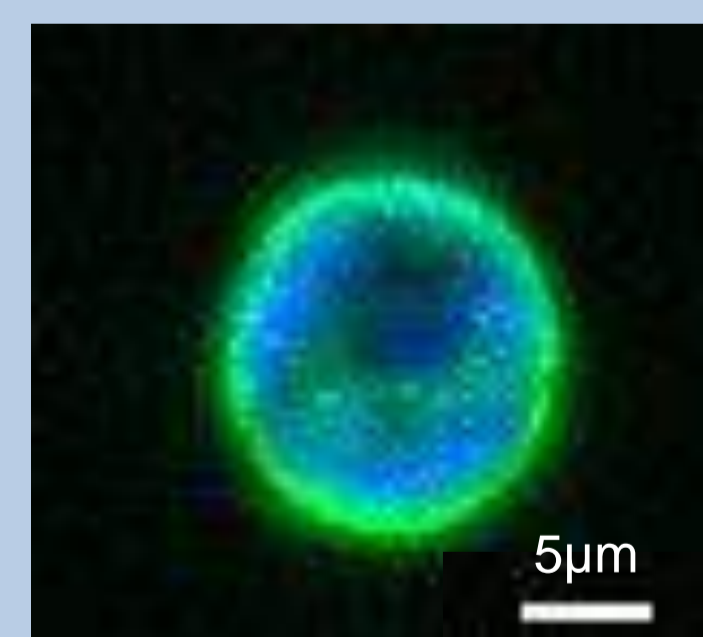
A) Using polychrome beads 4µm Ø



Segmentation
Volume
computation



B) Using mutant with periphery marker (in progress)



SUN2-GFP marker : protein localized at the Nuclear periphery (nuclear envelope marker)

DAPI : DNA binding molecule

V- Conclusion & Perspectives

We select a set of segmentation methods to assess quantitative parameters to describe nuclear organization.

Future directions:

- Correction of the segmentation methods (theoretical objects, marked mutant ...)
- Use of other model species (ex: spermatozoid nucleus compaction)
- Exploration of new method to automatize chromocenters segmentation (3D watershed -> Deep learning, machine learning ?)
- Adaptation to 3D DNA-FISH analyses

ProFan

ProFan is a projet which takes part in the action « Innovation numérique pour l'excellence éducative ». The core of this project is an experiment conducted over 20 000 professional high-school students with the help of more than 1000 teachers. Those students are undertaking one of those high-school majors related to technical fields :

- « Accompagnement, Soins et Services à la Personne » (ASSP),
- « Métiers de l'Electricité et de ses Environnements Connectés » (MELEC),
- « Commerce » (COM)

It aims to evaluate the effectiveness of collaborative learning through Jigsaw method. Along with scholar results, progression is also measured with activity like Text coping, Brainstorming...

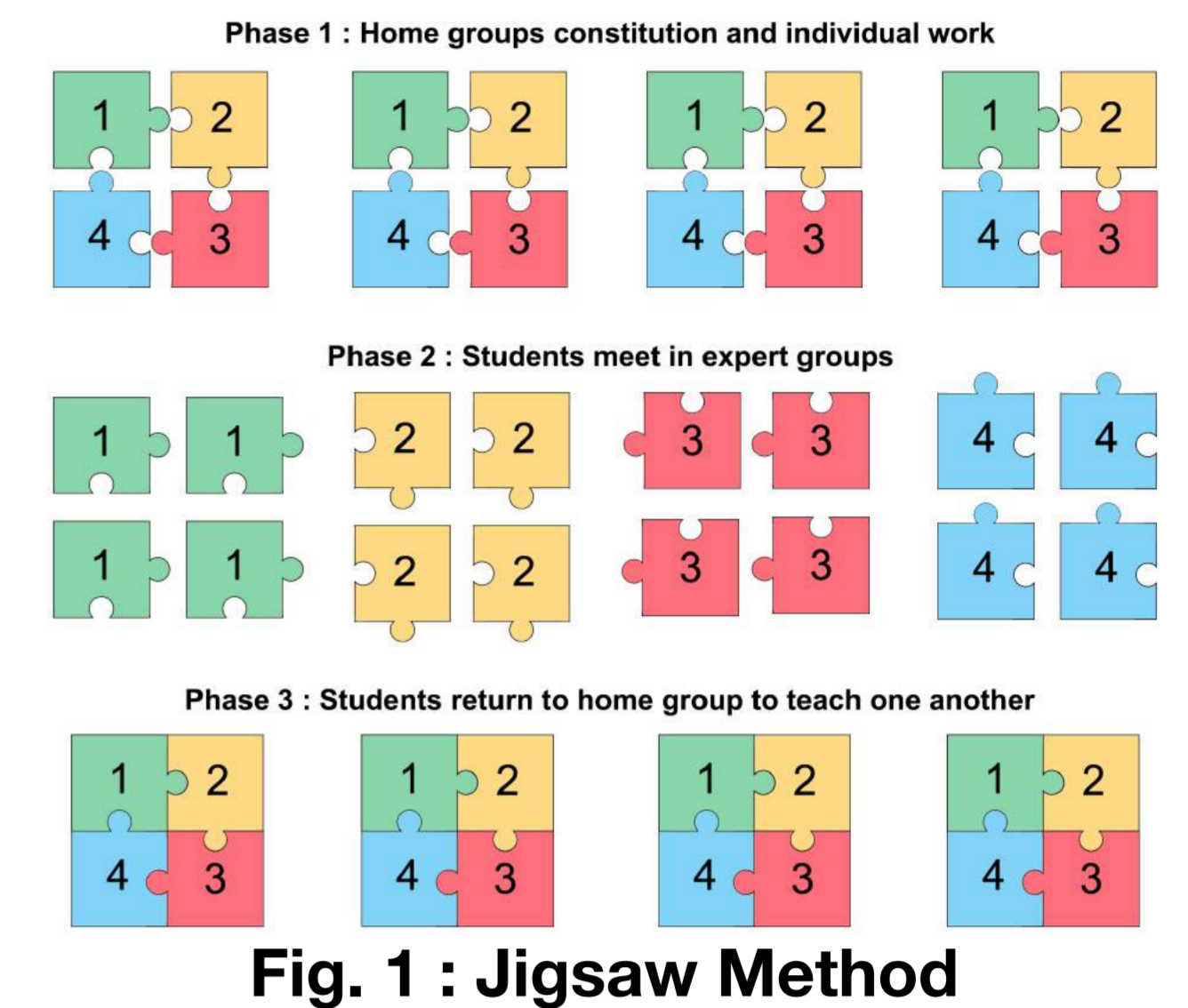


Fig. 1 : Jigsaw Method

Brainstorming data overview

Brainstorming activity produced chat conversation processed to determine the idea of each line. Based on that, three criteria evaluate creativity : flexibility, fluidity and originality.

- Large number of data available (> 50k annotated lines)
- Annotations provided by experts
- Features : - Poor context
 - Unusual spelling (mistakes, abbreviations,...)
 - Reality representative

Elève	Contribution	Idée	Catégorie
A	un photophore	Photophore	Décoration
B	je connais pas		
A	tu sais c'est un truc avec une bougie a l'interieur		
B	heummm nan je vois pas		
B	on pourrait faire des cannettes telephone	Téléphone	Electronique
C	les resicler	Recyclage	Autre

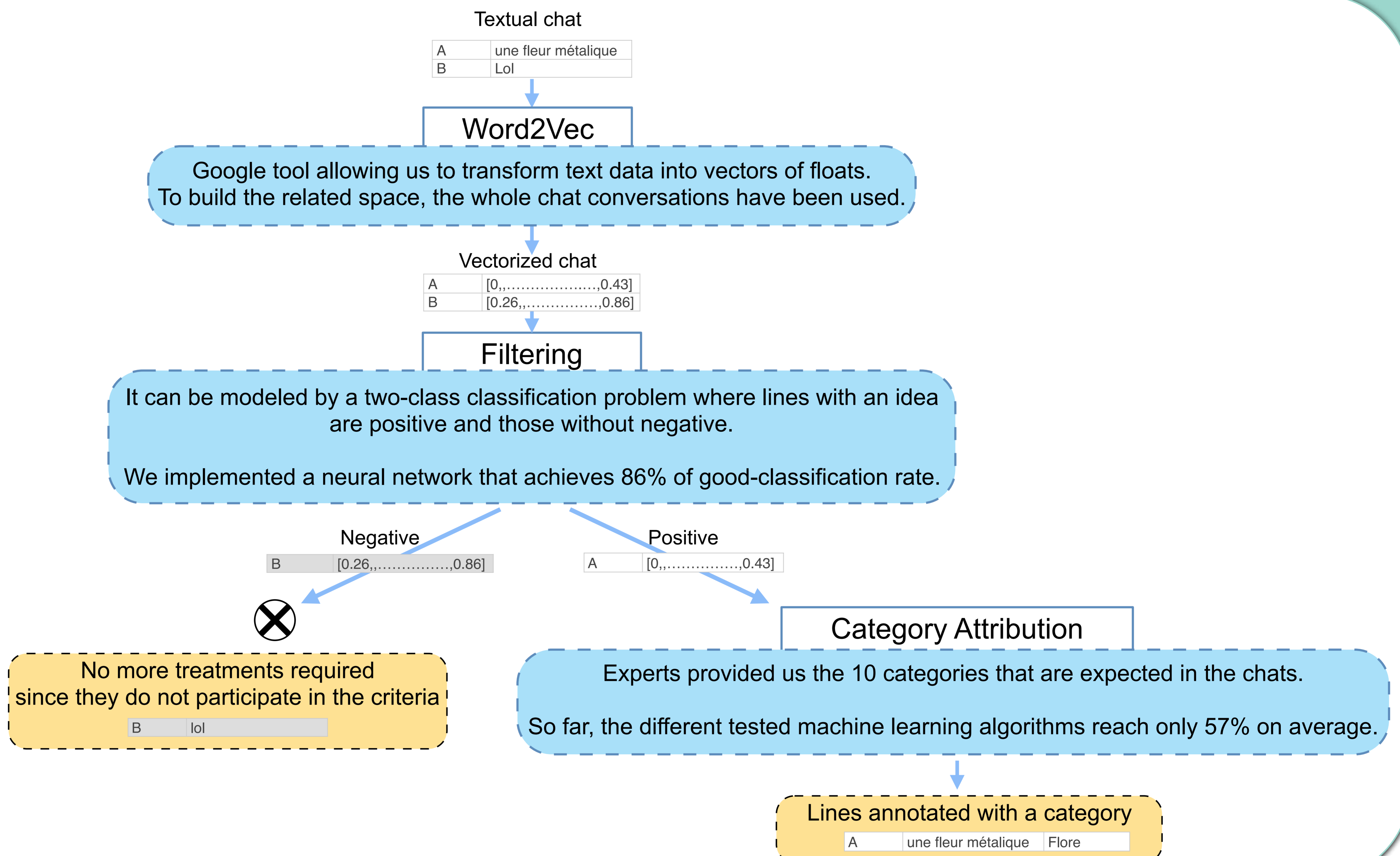
Fig. 2 : Annotated chat extract

Objectives

Computerize annotating process

- The following sub-goals have been identified :
- Separate lines with idea from those without
 - Find a way to give annotations to lines with idea
 - Compute criteria according to expert's formula

A first approach using machine learning



Results

In order to avoid, for now, noise from the classification mistake of the Filtering step, we extracted only the true positive data. They have been used to build a first classifier that aims to differentiate the categories. Among the 23 133 lines available, 4 627 composed the testing set.

The global accuracy reaches 58% which is low. However, the confusion matrix has an interesting feature : outside the first class, the mistake are very few as shown in Fig. 3.

After investigating, it was revealed that some of the first class predicted were in fact undetermined. They are easily identifiable so we can retrieve them which produces the Fig. 4.

Those results are encouraging because ~66% of the initial data are determined with high accuracy. Nonetheless, there are still ~34% to work on and other needs for the criteria that makes it unsatisfying.

912	2	1	6	0	2	1	0	2	0	1
207	261	3	3	0	2	1	0	1	0	1
160	0	149	2	0	8	1	0	1	0	0
228	2	0	151	0	1	0	0	1	0	1
46	0	0	39	2	0	0	0	0	0	1
361	3	2	6	1	659	0	1	3	0	0
134	0	0	0	1	1	246	0	0	0	1
70	1	0	0	0	1	0	122	0	0	0
183	2	0	2	0	0	1	0	180	0	0
75	0	1	1	0	0	1	0	0	160	0
104	1	0	0	1	1	0	0	3	1	98

Fig. 3 : Confusion matrix

667	2	1	6	0	2	1	0	2	0	1
12	261	3	3	0	2	1	0	1	0	1
6	0	149	2	0	8	1	0	1	0	0
9	2	0	151	0	1	0	0	1	0	1
1	0	0	39	2	0	0	0	0	0	1
11	3	2	6	1	659	0	1	3	0	0
3	0	0	0	1	1	246	0	0	0	1
1	1	0	0	0	1	0	122	0	0	0
4	2	0	2	0	0	1	0	180	0	0
2	0	1	1	0	0	1	0	0	160	0
5	1	0	0	1	1	0	0	3	1	98

Fig. 4 : Same matrix without « undetermined »

Introduction

Aqueous mixtures of carbohydrates and polyols play an important part in the majority of the formulation of food products (i.e in bakery, ice cream and sweeteners industries) and in several food processes.

The knowledge of physicochemical properties of such aqueous mixtures is mandatory for developing controlled and optimized processes.

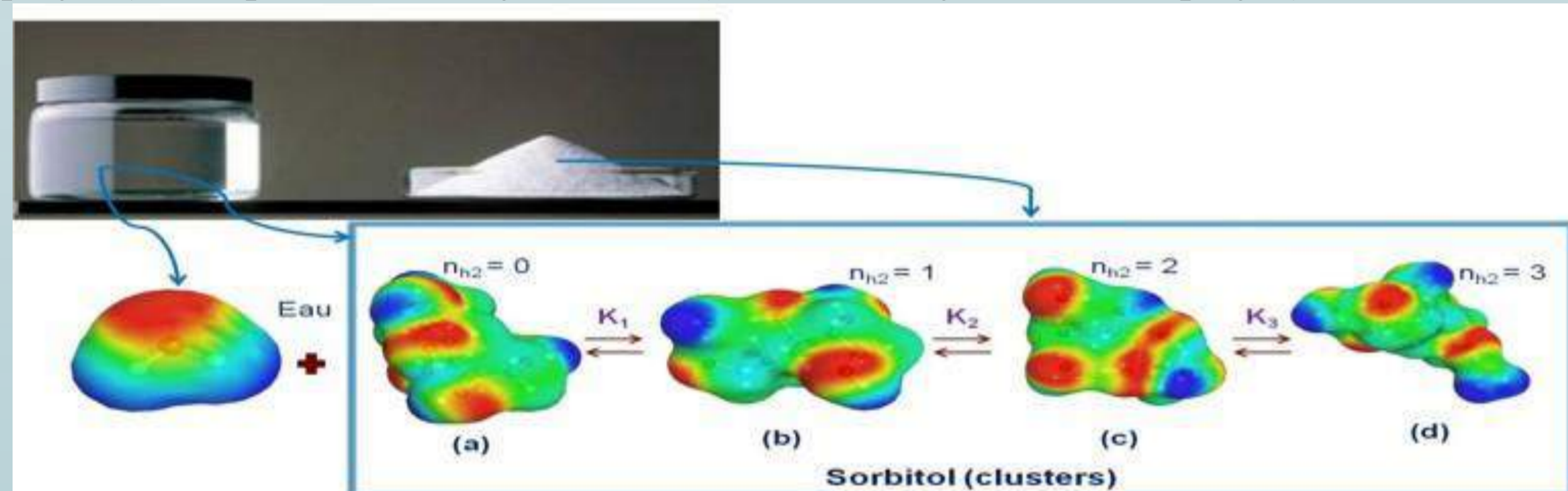
Raman spectroscopy has been intensively used experimentally since 1950 to investigate the behavior of bulk water [1,2], solid carbohydrates [3,4] and aqueous mixtures containing carbohydrates [5,6,7].

Today, simulation tools are able to compute Raman spectra of a custom molecule provided that the space arrangement of the atoms and bonds are given. This procedure allows us to compute Raman spectrum of one up to several molecules interacting with each other.

The most likely geometry can be found by making a link between computed and experimental data. Thus this geometry can be used to perform thermodynamics calculation (i.e COSMO-RS-PDHS model)[8].

The aim of this work is to use Raman spectroscopy to investigate **interactions between water and carbohydrates** (especially the hydration phenomena)

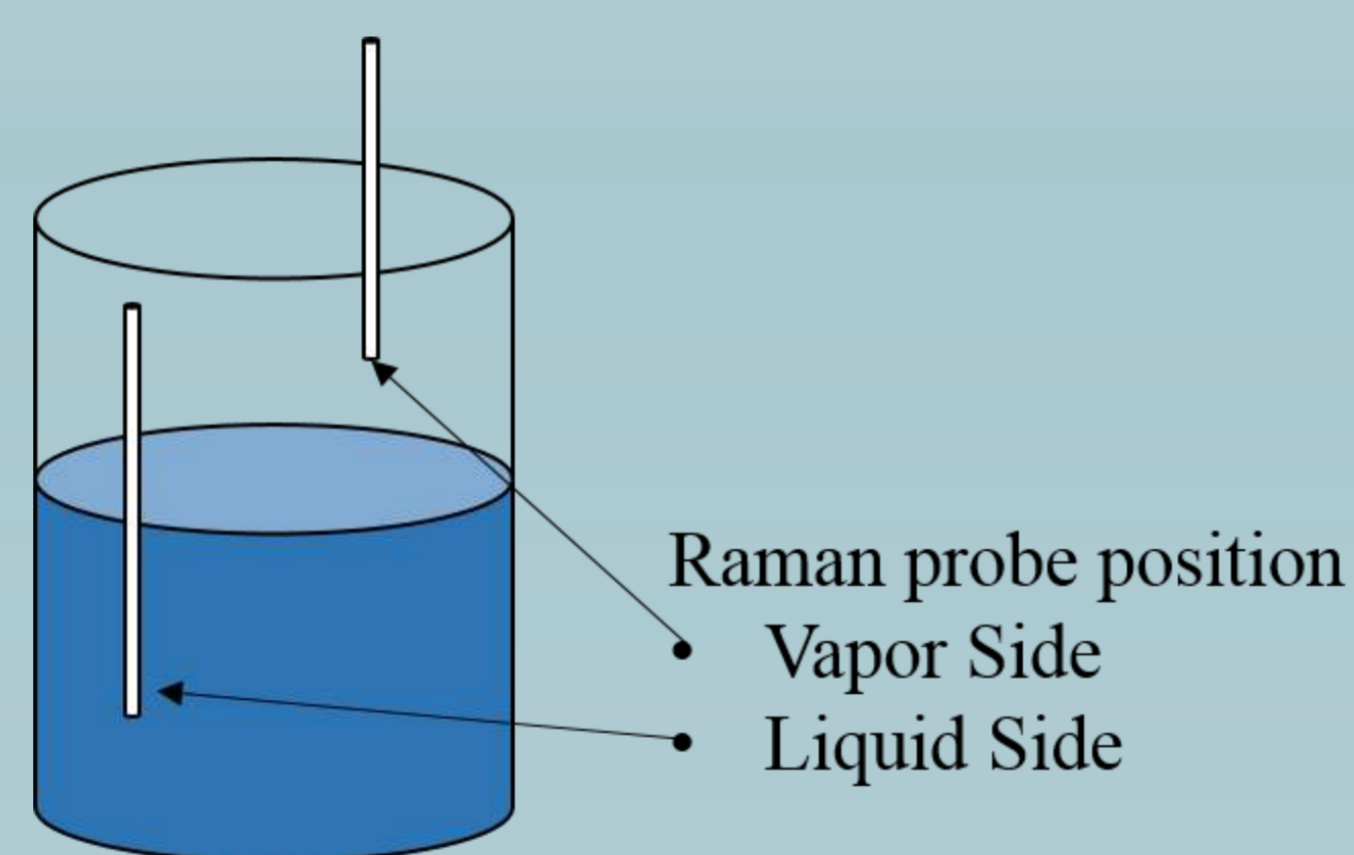
This poster presents preliminary results: Raman spectra of pure compounds (water, carbohydrates and polyols) and spectra of binary mixtures (water-carbohydrate, water-polyol).



Material and Methods

Experimental means:

The experimental Raman setup contains an 'in situ' Raman spectrometer supplied by ocean optics. The system includes a 532 nm laser beam, all Raman spectra have been recorded in the [50-4000]cm⁻¹ range using the in situ probe which allows us to take Raman spectra of liquid and gases both at Liquid-Vapor equilibrium.

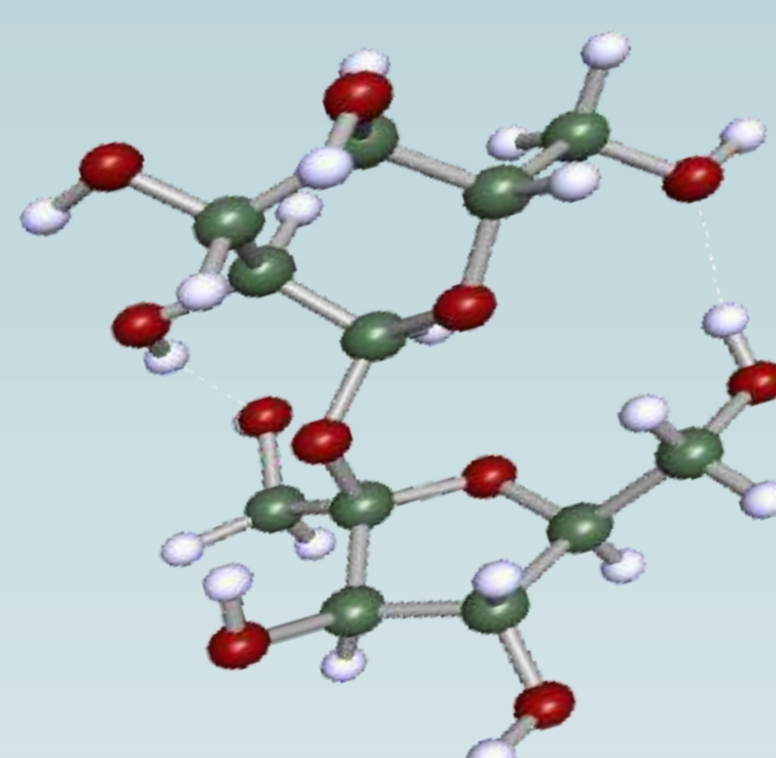


Simulation mean :

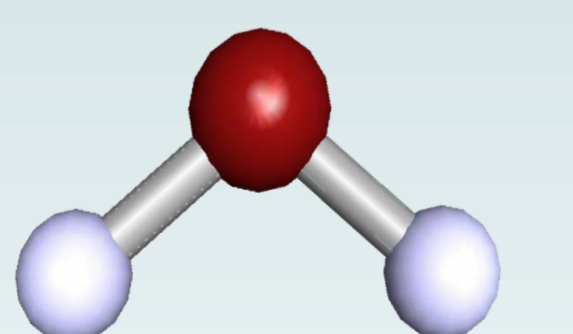
Our simulation tool is the TmoleX software which can be used to compute Raman spectra of compound of interest.

The procedure is listed below :

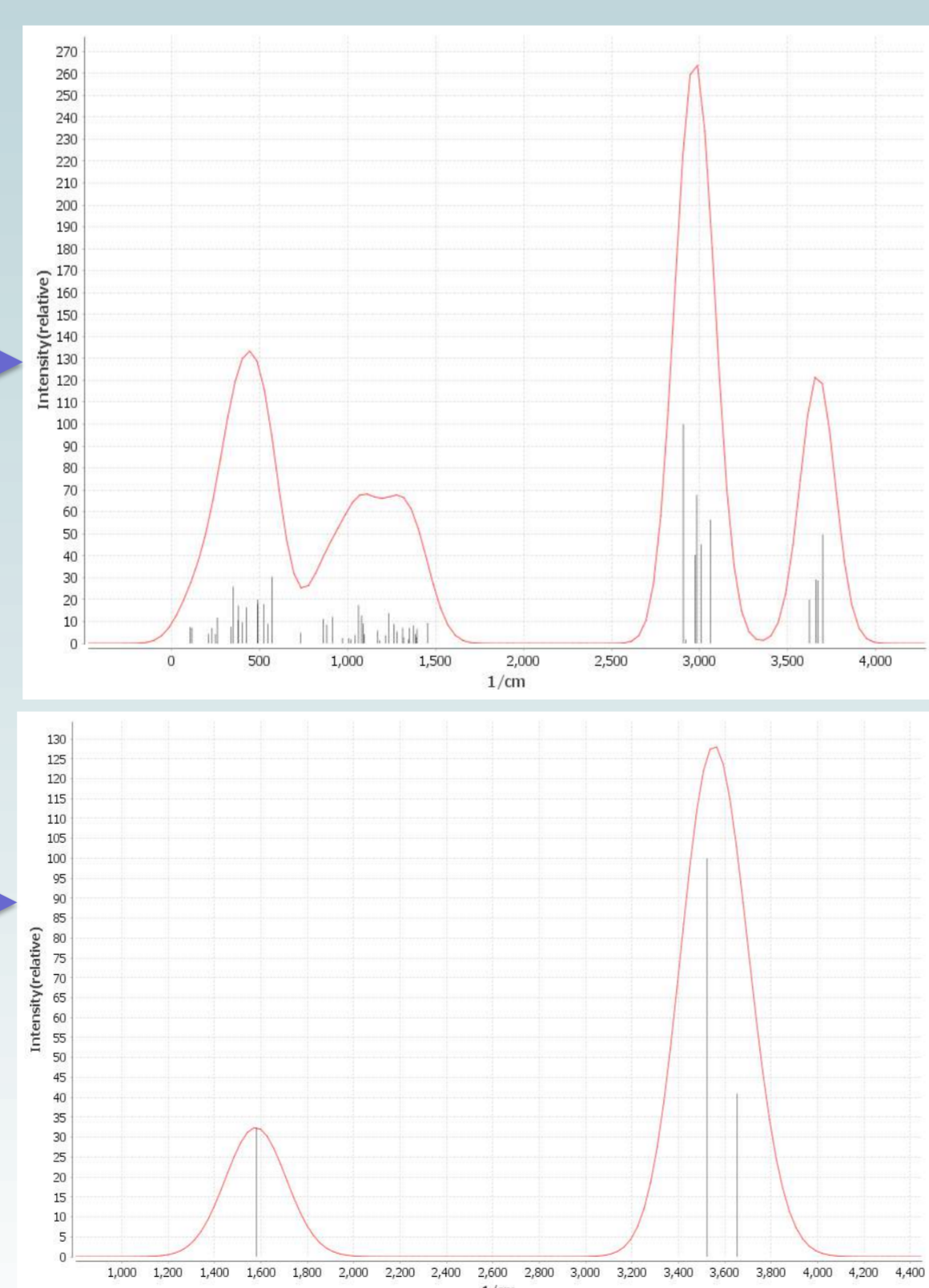
- Drawing of the desired geometry
- Energy calculation (DFT-RI + TZVP) with BP86 functional
- Computation of the vibrational frequencies (x-axis) and scattering cross sections (y-axis)



Exemple of a possible geometry of a sugar



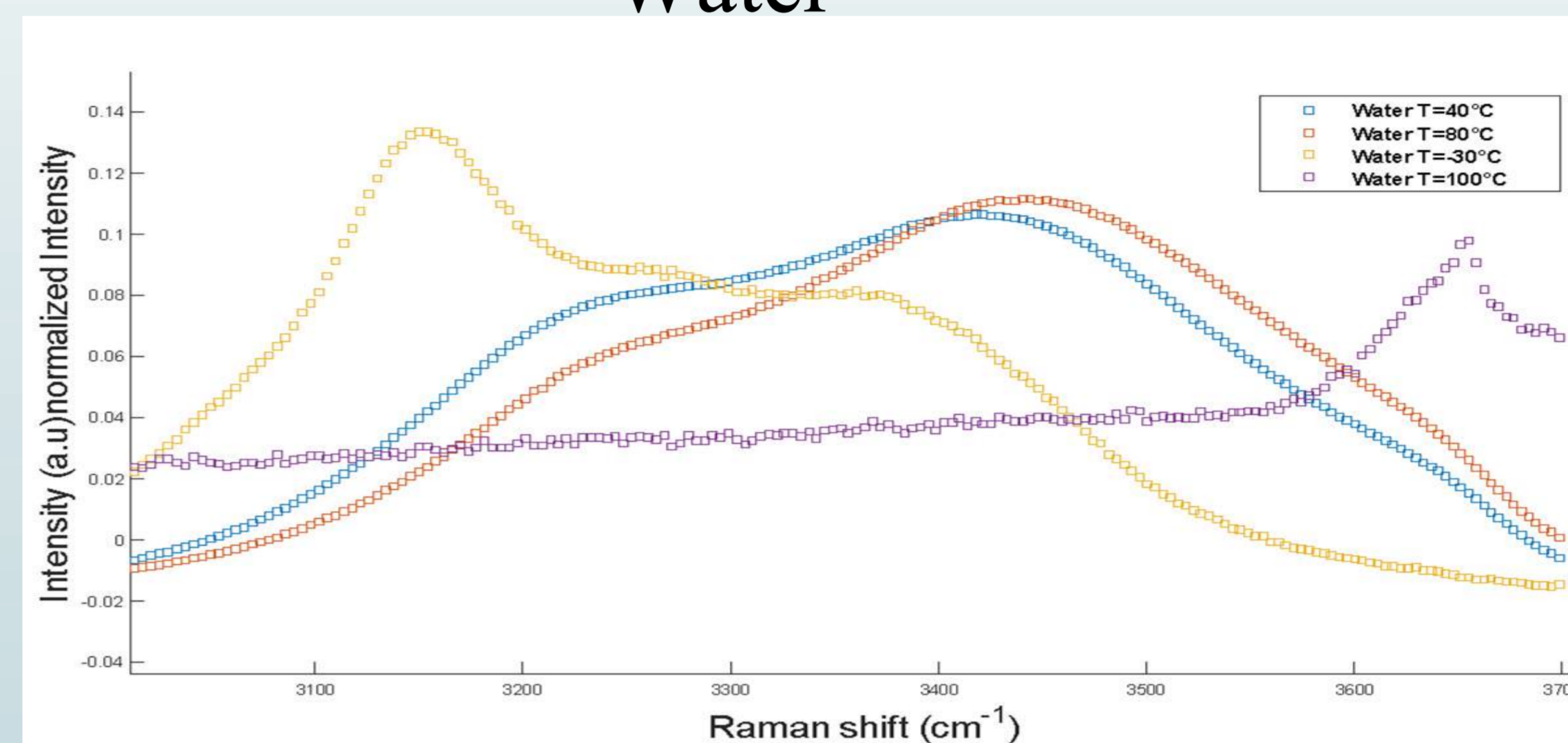
Exemple of a water molecule



Preliminary Results

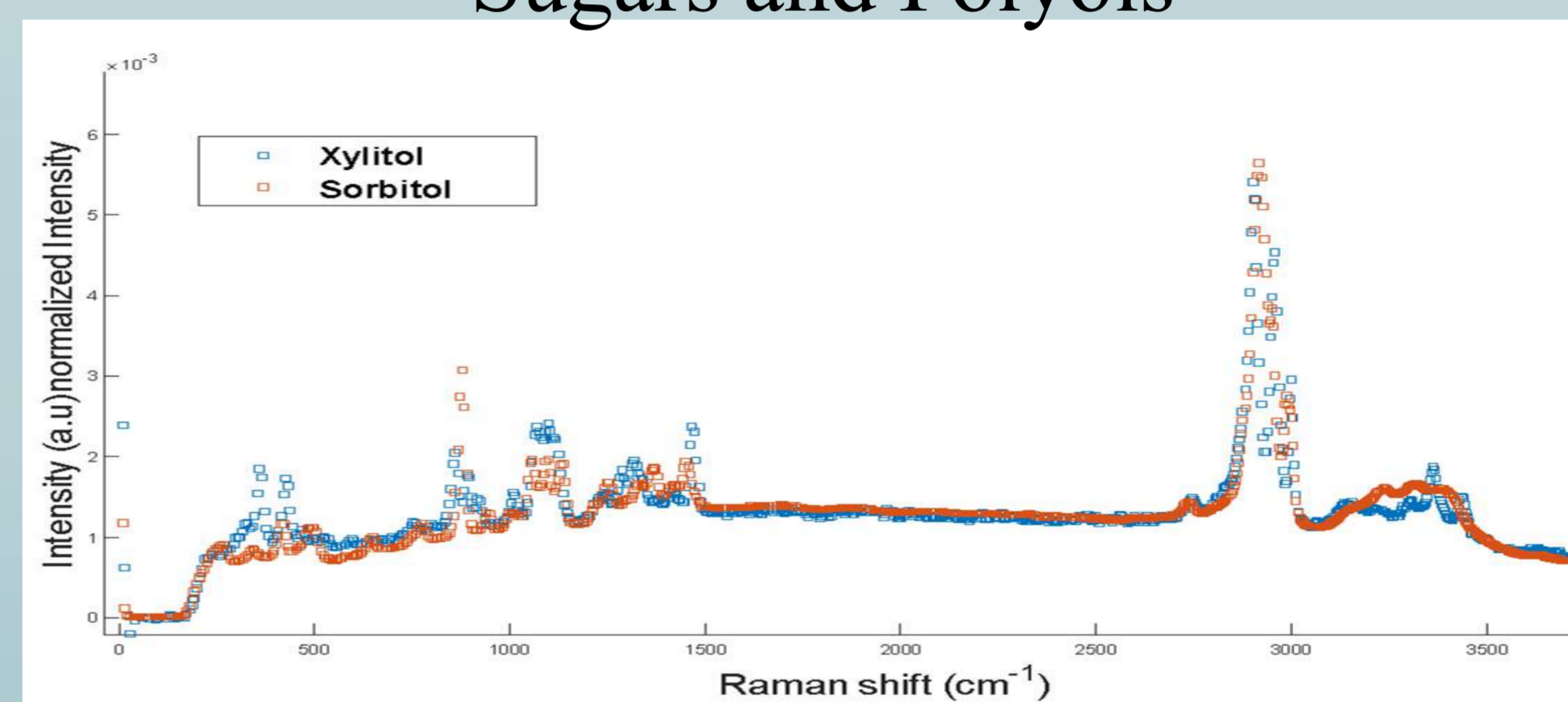
This poster aim is to present preliminary results concerning experimental spectra of pure water in its different state (vapor, liquid, solid), solid carbohydrates and aqueous mixture of carbohydrate

Water



Raman spectra of ice at -30°C, liquid water at 40°C and 80°C and water at vapor/liquid equilibrium at 100°C are presented. Liquid water presents two very strong bands at 3220 cm⁻¹, 3435 cm⁻¹ and a weak band at 1600 cm⁻¹. Solid water reveals two strong bands at 3100 cm⁻¹ and 3400 cm⁻¹ whereas vapor water shows two weak bands at 1450 cm⁻¹ and 3645 cm⁻¹. As temperature increases, two strong bands of liquid water are shifted and the intensity of peak at 3200 cm⁻¹ decreases.

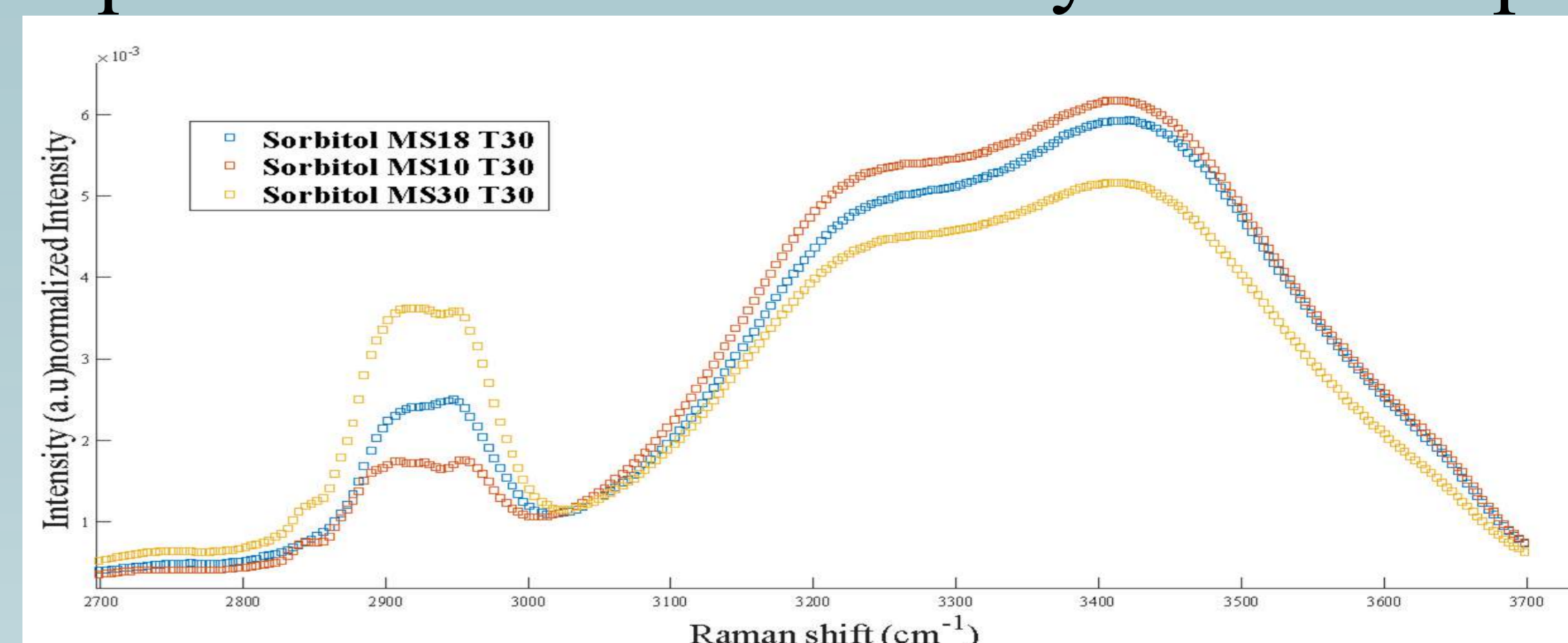
Sugars and Polyols



Unlike water, carbohydrates present weak shifts in the [500-1500] cm⁻¹, [3000-3600] cm⁻¹ range and strong shifts in [2700-2900] cm⁻¹ range. Like water, the [3000-3600] cm⁻¹ area allows the discrimination of solid/liquid carbohydrates and may be used to investigate the interactions between water and carbohydrates.

Fluorescence greatly impacts the measured Raman spectra and needs to be treated without altering the initial information provided by the Raman effect.

Aqueous mixtures of carbohydrates and polyols



Interactions between water-carbohydrate and water-polyol lead to modifications in the Raman spectra of mixture containing 30% of DS at 30°C

Raman spectra of aqueous mixtures containing respectively 10%, 18%, 30% DS of sorbitol are presented. As the weight ratio of carbohydrate increases, the intensity of the [2800-3000] cm⁻¹ spectral range (C-H band) increases and the intensity of the [3100-3500] cm⁻¹ region (O-H band) decreases.

The shift at 1600 cm⁻¹ occurs when liquid water is mixed with carbohydrates (Picture 5). However, Carbohydrates don't have bands in this spectral region, this information might be useful when searching for water content in such mixtures.

Conclusions

Raman spectroscopy detects structural modifications between the structure of pure compound such as water, carbohydrate-polyol and the structure of binary mixtures : water-carbohydrates, water-polyols.

Regarding pure water, these structural modifications are the consequence of a change of state. In the case of binary mixtures, the structural modifications are the result of water-carbohydrate and water-polyol interactions. Thus, Raman spectroscopy appears as a promising tool to investigate the hydration phenomena regarding carbohydrates and polyols.

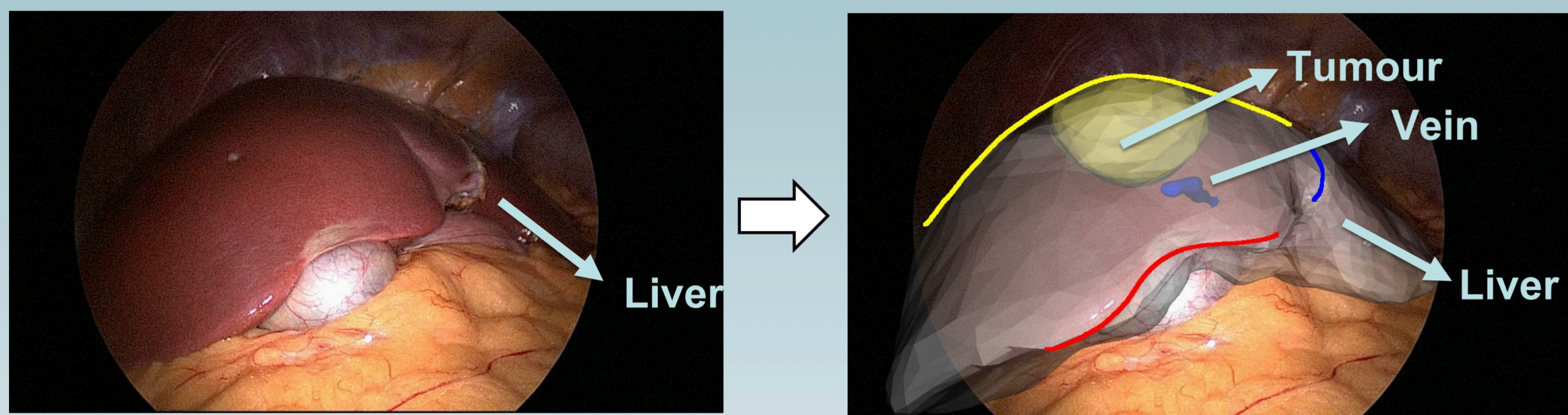
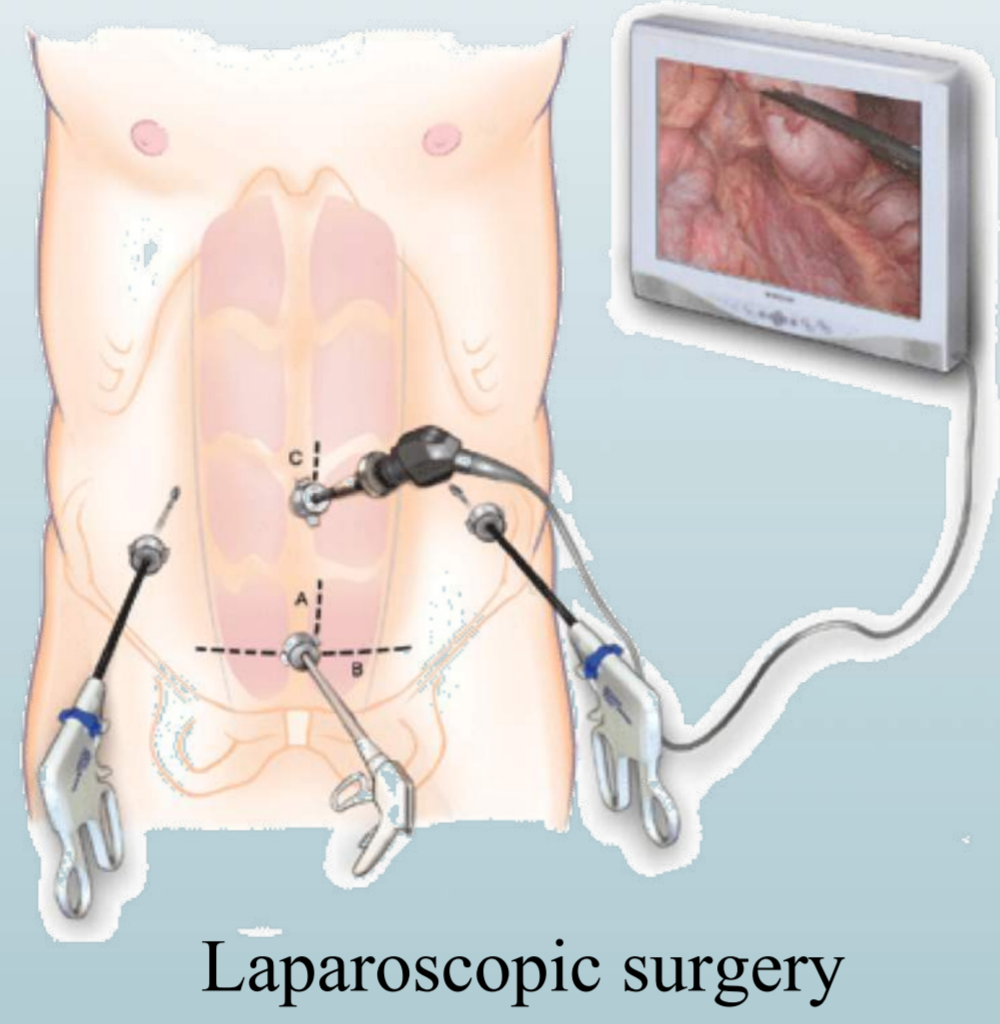
Bibliography

1. M. Magat (1934), J. Phys. Radium, 5 (7) Carbohydrate Research, 44
2. M. Starzak and M. Mathlouthi (2003). Food Chemistry, 82(1)
3. Wiercigrochet et al. (2017), Spectrochimica Acta, 185,
4. E. Palomäki et al (2016), International Journal of Pharmaceutics

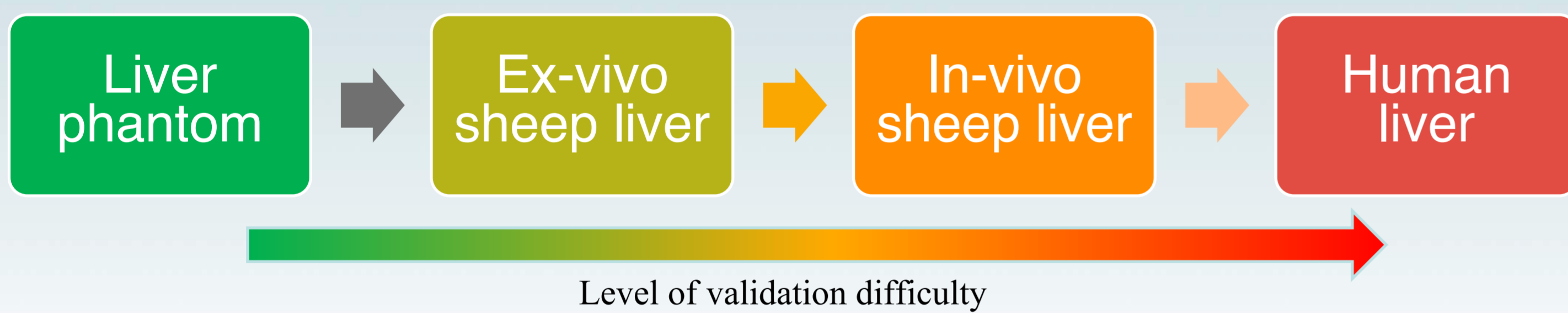
5. H. Hong et al (2010), Organic Process Research and Development
6. M. Mathlouthi and D.V. Luu, (1980), Carbohydrate Research, 78
7. M. Mathlouthi and al, (1986), Carbohydrate Research, 44
8. Toure, O., Lebert, A., & Dussap, C.-G. (2016). Fluid Phase Equilibria

Introduction

- Laparoscopy is a technique to perform minimal invasive surgery through the usage of a small camera and thin, light instruments.
- It requires small incisions and thus is less traumatizing.
- The large size of the liver and the reduced camera's field of view makes it difficult to locate tumours and vessels.
- Augmented Reality (AR) tries to solve this problem by adding this invisible information on top of the laparoscopic video stream.
- This is done by registering a set of preoperative 3D models obtained from radiological data into the laparoscopic images [1].

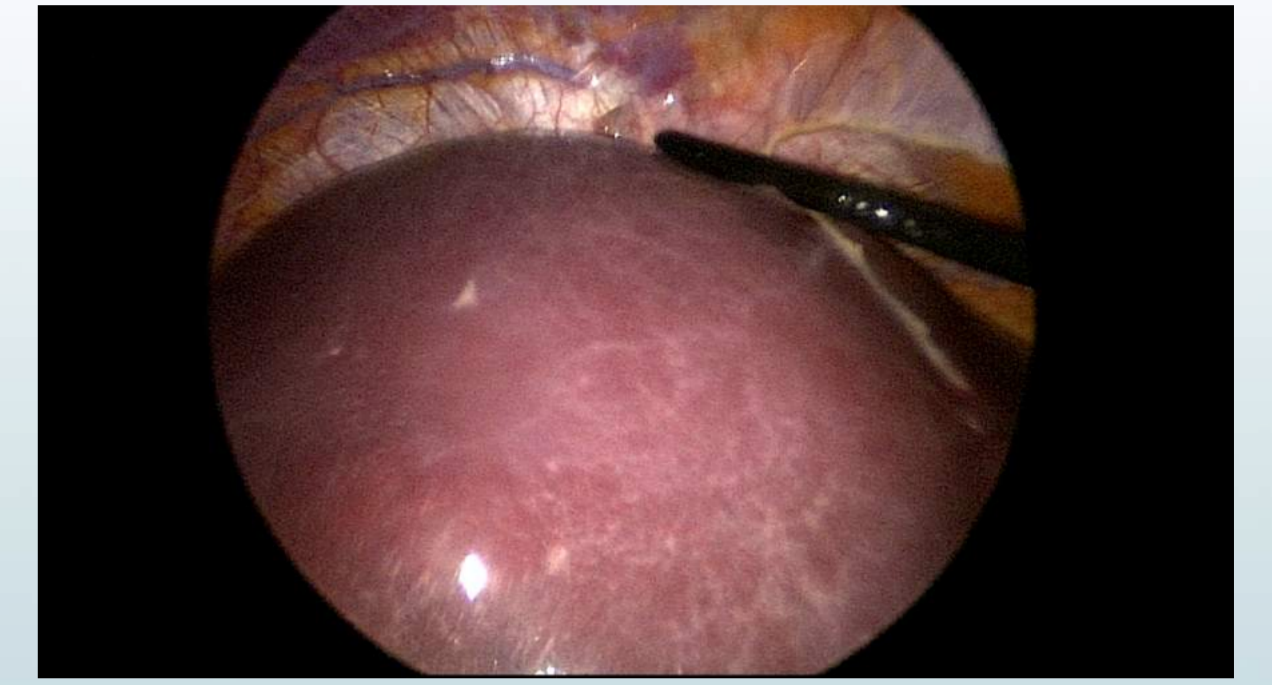


- How to measure quantitatively (validate) the accuracy of AR?



- How can we perform automatic AR on the liver?

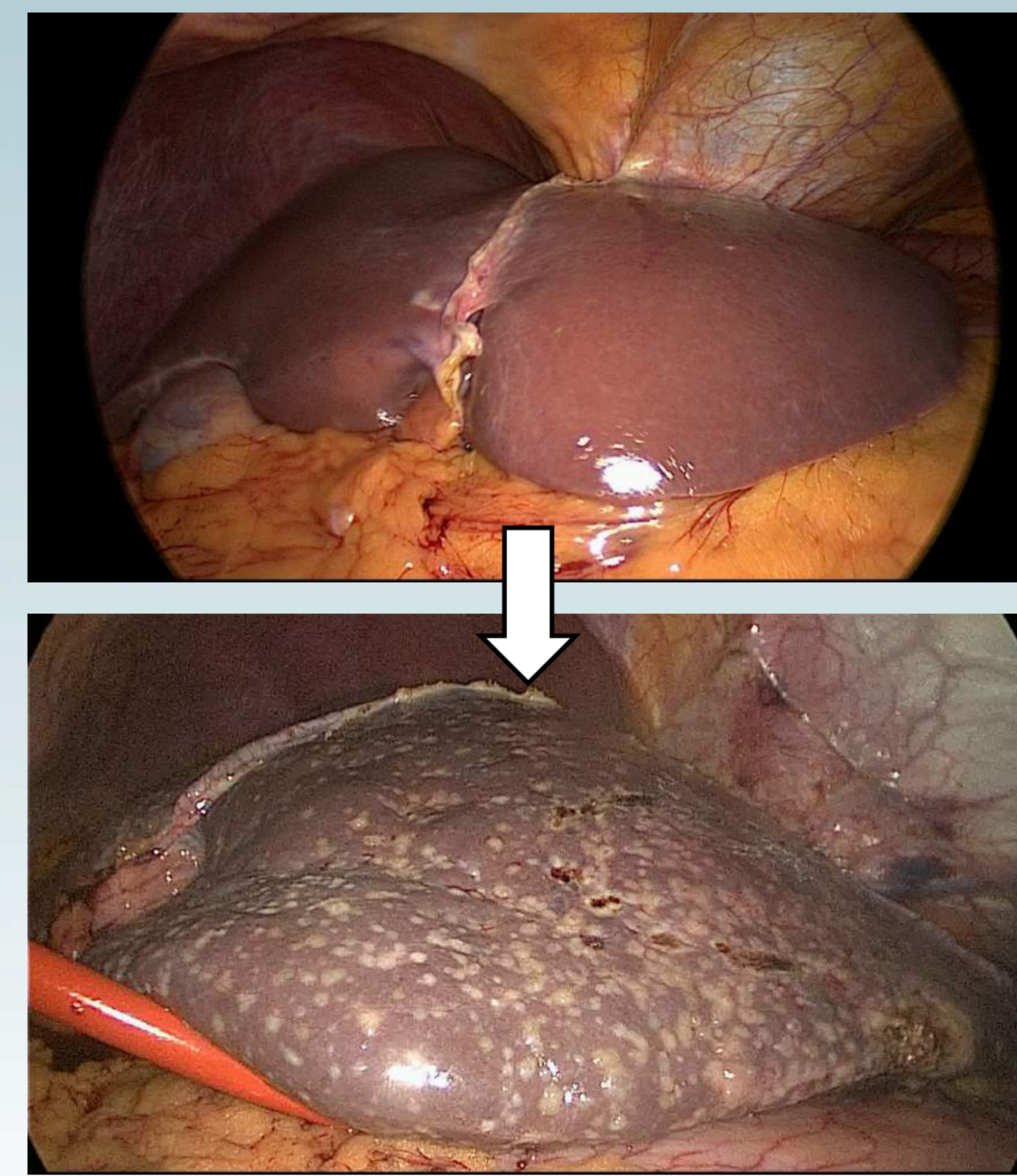
- Cases such as registrations with a lack of visual cues must be evaluated.
- What if we have to register with a very partial view of the liver?
- Inter-surgeon registration variability to assess the robustness of our method.



Partial view of the liver with lack of visual cues

LIVER DETECTION AND TRACKING:

- To place the preoperative models automatically in the images, features must be detected and matched, letting us to compute movement changes from both liver and camera.
- A common strategy for automatic AR on laparoscopy is to take an initial video footage of the organ before starting the surgery.
- This footage lets to reconstruct a map of the organ's surface and bring the preoperative models to where the reconstructed map is located [2].



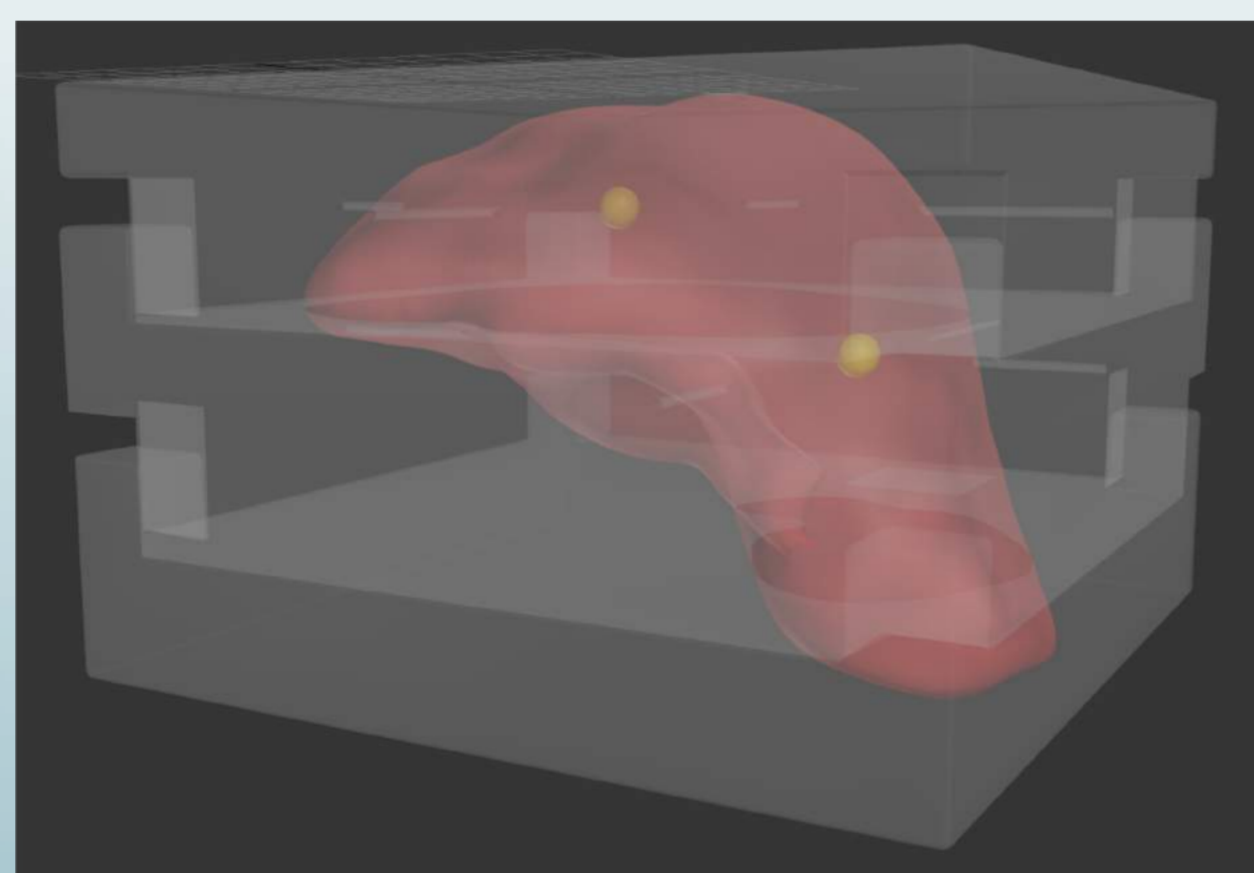
Healthy vs. cirrhotic liver

- Texture of a normal healthy liver is very uniform, while a cirrhotic one has visible spots.
- A robust way to detect features in the liver should be found in this case.
- How to quickly deform the preoperative models such that they fit with the real liver?

Methods

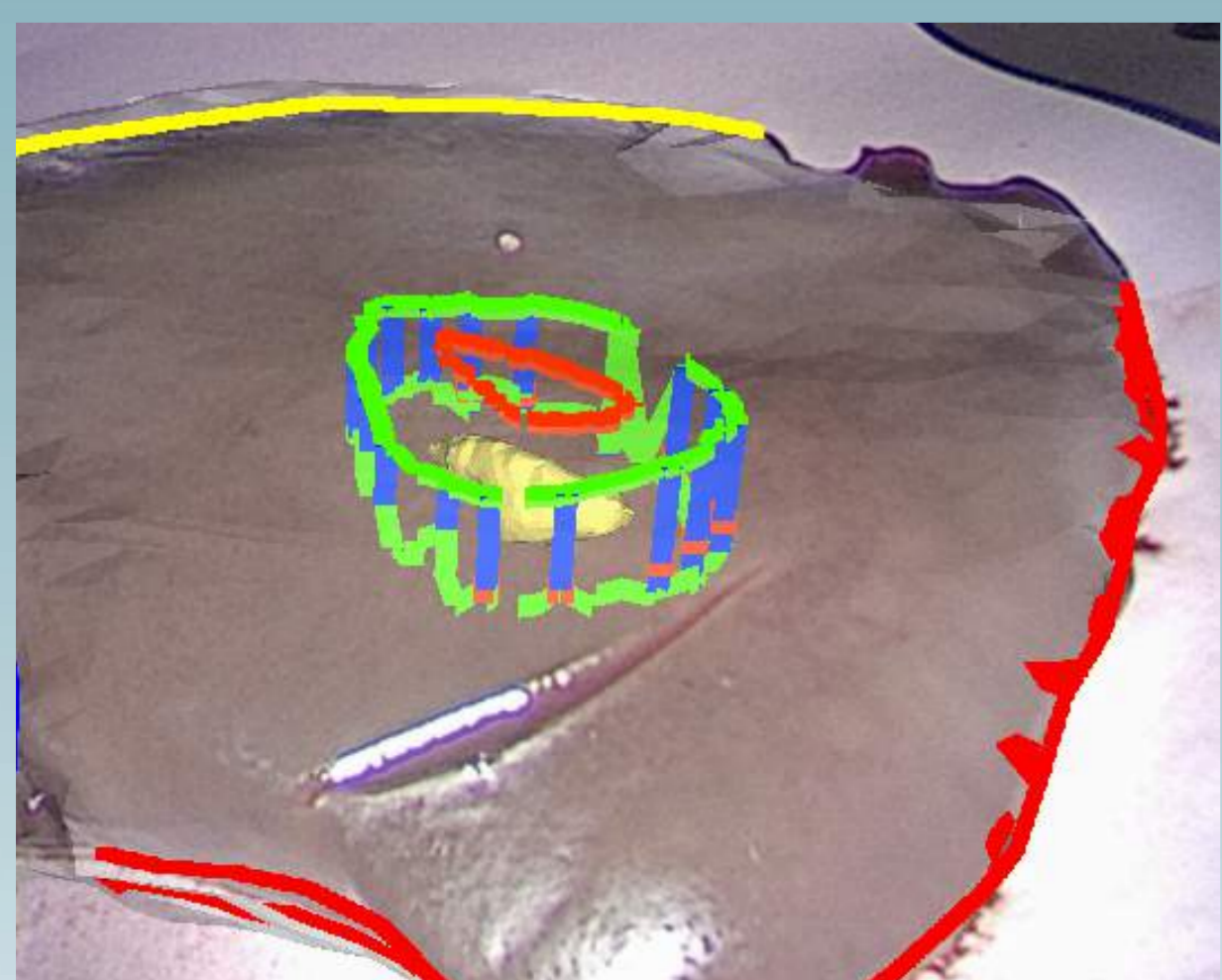
VALIDATION WITH LIVER PHANTOM:

- We created a model with two endophytic tumours.
- Phantom is deformed in several ways and registrations are made for each.
- Tumour positions shown by the augmentation are compared with the real positions of the CAD models.



Model of liver phantom with endophytic tumours and mold for 3D printing

VALIDATION WITH EX-VIVO LIVER:



Sheep liver with augmented tumour (in yellow) and generated resection mark (in green)

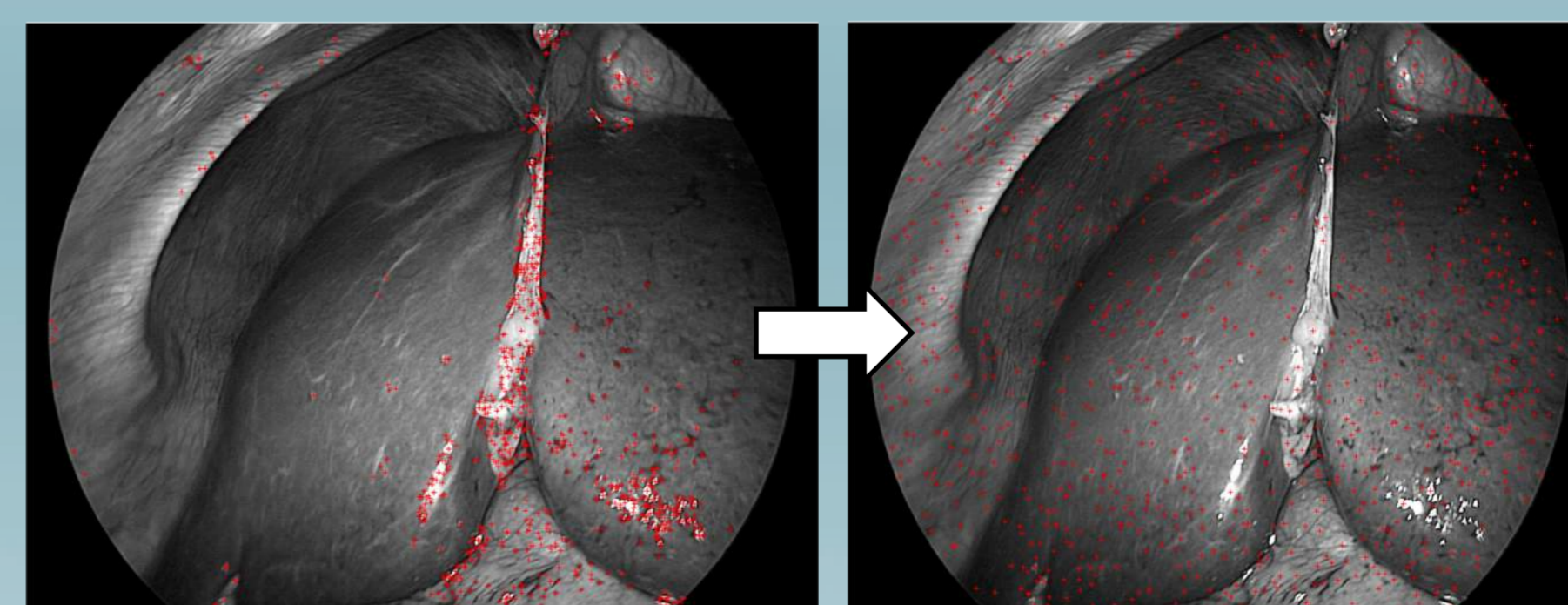
- For validation on ex-vivo and in-vivo animal livers, alginate is injected to create artificial tumours.
- CT scans are made to obtain the preoperative models.
- Resections are made as in a real surgery.
- Registration errors are measured, along with rate of successful resections using no US/AR, using US only, and AR only.

Results and Conclusions

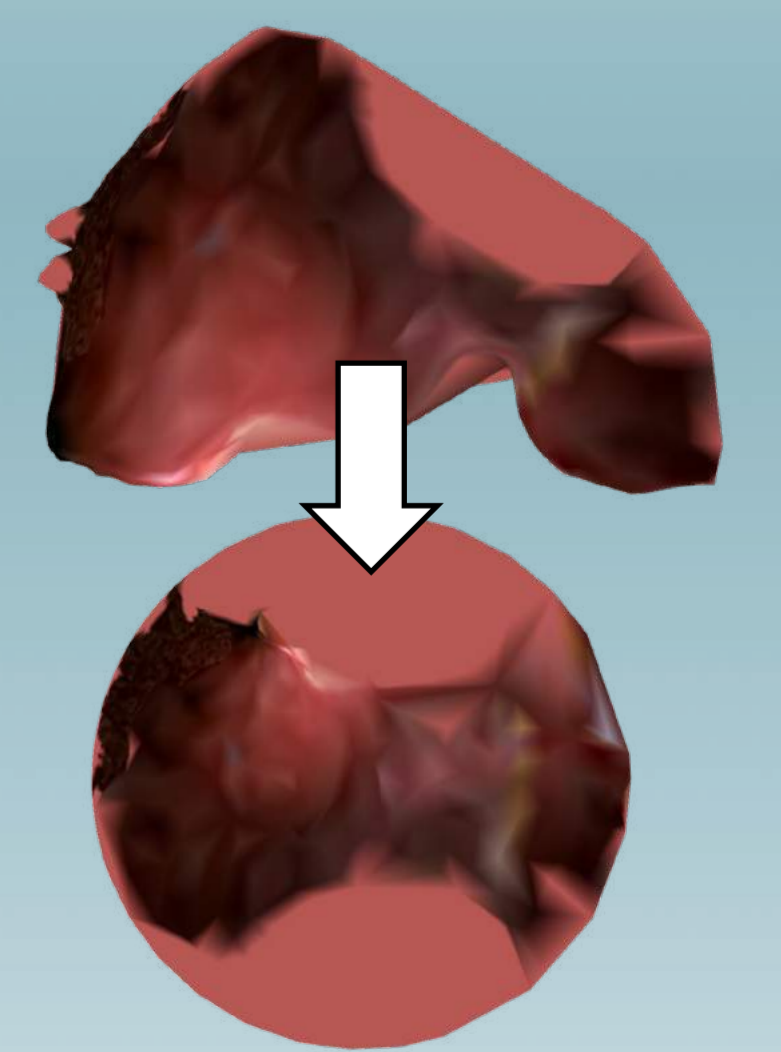
- SIFT descriptors deal better with changes in illumination and contrast.
- Flattening the liver texture through conformal mapping can help preserving a similarity transformation between features.

INCOMING TASKS:

- We will compare the matched features from in the original and the flattened textures to evaluate the convenience of this strategy.
- A first rigid tracking strategy will be implemented using SIFT features, assessing the results and possible improvements for deformable registration.



SURF features vs SIFT features. SURF features are highly localized around bright areas, compared to the more spread SIFT features



Conformal mapping of liver texture

Bibliography

- Espinel, Y., Olgur, E., Calvet, L., Le Roy, B., Buc, E., Bartoli, A. Combining Visual Cues with Interactions for 3D-2D Registration in Liver Laparoscopy. IPICAI, 2019.
- Collins, T., Chauvet, P., Debize, C., Pizarro, D., Bartoli, A., Canis, M., Bourdel, N. A System for Augmented Reality Guided Laparoscopic Tumour Resection with Quantitative Ex-Vivo User Evaluation. CARE - MICCAI, 2016.

C. F. Oliveira^{1,2},

P. Breul¹ ; C. Bacconnet¹ ; B. Chevalier¹ ; M. A. Benz-Navarrete²

¹ Institut Pascal, Civil Engineering Department

² Sol Solution, RiD Department

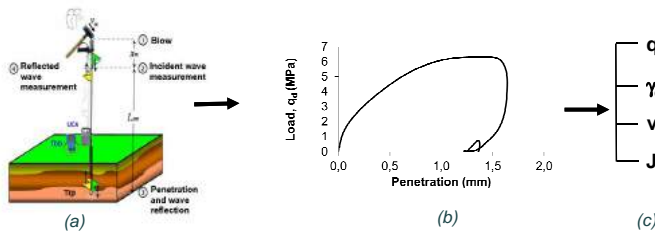
Thèse CIFRE

Ecole Doctorale
Sciences Pour
l'Ingénieur

Introduction

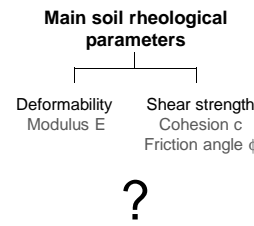
Soil characterization is an essential task to design foundations in civil engineering. Dynamic penetration test is a widely used technique due to its versatility, low cost and reliability. In the current state of knowledge, it doesn't allow to obtain directly intrinsic soil parameters.

Background

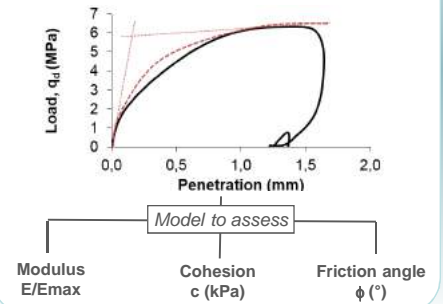


(a) Lightweight dynamic penetrometer Panda 3® and its principle (b) Load-penetration curve, (c) Soil parameters determined during penetrometer driving

Current problem

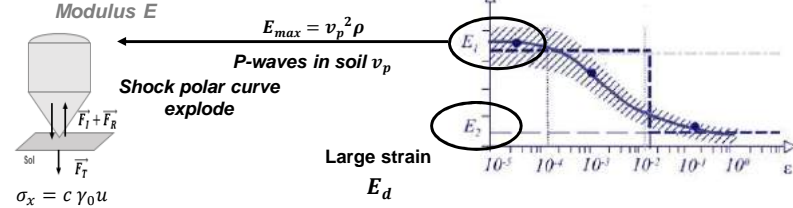


Objective

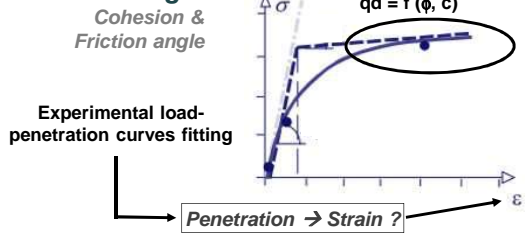


General Methodology

Deformability



Shear strength



Experimental

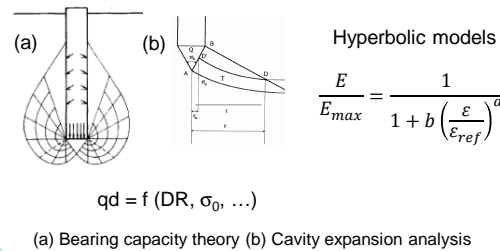
Panda 3® test
In calibration
chamber



Physical characterization
Triaxial tests
Geophysical

Analytical

Penetration models and constitutive models



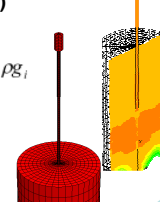
Numerical

Panda 3® test modelling in calibration chamber

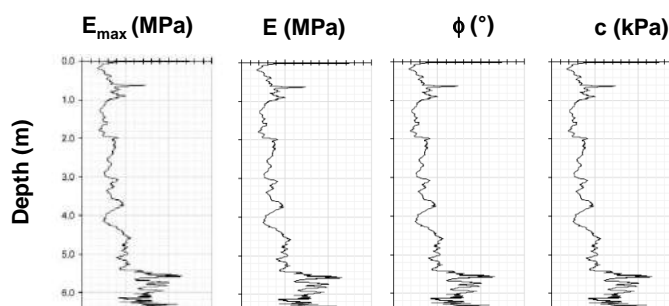
Finite Difference Method (FDM)

Equation of motion: $\rho \frac{\partial u_i}{\partial t} = \frac{\partial \sigma_{ij}}{\partial x_j} + \rho g_i$

Constitutive model: $\bar{\sigma} = f(\bar{\epsilon})$



Expected results



Bibliography

- Aussedat, G., 1970. *Sollicitations rapides des sols*. Thèse doctorale. Université de Grenoble
- Benz-Navarrete, M. A., 2009. Benz-Navarrete, M. A., Mesures dynamiques lors du battage du pénétromètre PANDA 2, thèse, Université Blaise Pascal-Clermont-Ferrand II.
- Escobar, E., 2015. Mise au point et exploitation d'une nouvelle technique pour la reconnaissance des sols: le PANDA 3, s.l.: PhD thèse, Université Blaise Pascal Clermont-Ferrand II.
- Gourvès R., Pénétrromètre dynamique léger à énergie variable, (LERMES CUST, Université Blaise Pascal, Clermont-Ferrand, France, 1991).
- Salgado, R. & Randolph, M. F., 2001. Analysis of cavity expansion in sand. *International Journal of Geomechanics*, 1(2), pp. 175-192.
- Tran, Q. A., 2015. *Modélisation numérique du comportement des milieux granulaires à partir de signaux pénétrométriques : approche micromécanique par la méthode des éléments discrets*, thèse, Université Blaise Pascal-Clermont-Ferrand II.

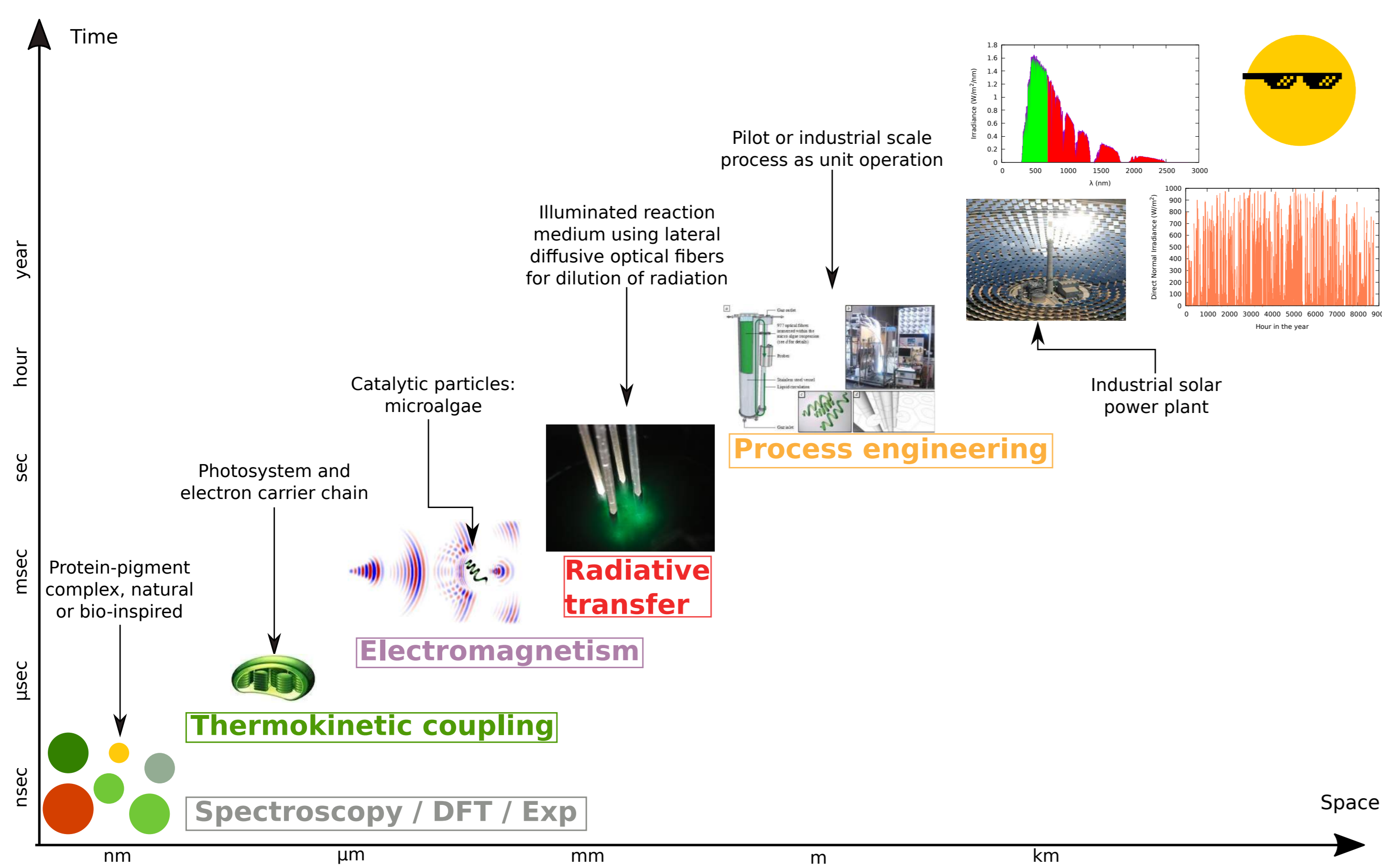
Introduction

Design and/or optimization of processes require the development of knowledge models. These models can involve several bodies of physics, chemistry and/or biology all coupled, sometimes non-linearly: this is generally referred to a **multi-scale model** (and sometimes also to a **multiphysics model**) [1]. Calculating a quantity at the scale of the process involves in general a sequential approach (the solution at a given level requires input data from the underlying level) that generates two difficulties involving calculation time issues:

- Geometry management at different scales
- Exchange of information between solvers using couplers

The main objective of this work is to develop **statistical approaches** to handle all scales through a single Monte Carlo algorithm. These approaches are developed in the field of photo-reactive processes enabling to produce renewable third generation of biofuels or synthetic fuels (H_2 , CH_4 Syngas, CH_3OH) from solar energy. The example of a **solar photobioreactor** that produces *Arthrospira platensis* is presented here.

Multi-scale model



Biomass annual productivity $\langle r_x \rangle$ is written as a path integral for the multi-scale model solution. At this state of our research, we use some approximations in order to tackle difficulties one by one:

- Linear thermokinetic coupling

$$\langle r_x \rangle = \int_{\Delta t} dt p_{\Delta t}(t) \int_{\Delta \lambda} d\lambda p_{\Delta \lambda}(\lambda) \int_{\partial V} \frac{d\vec{x}_s}{S} \int_0^\infty dl k_{a,\lambda} e^{-k_{a,\lambda} l} H(\vec{x} \in V) \omega$$

- Purely absorbing medium (no scattering) with Schiff approximation of electromagnetism for the absorption coefficient

$$k_{a,\nu} = C_x \int_{4\pi} \frac{d\vec{e}_0}{4\pi} \int_{\Delta R} dR p_{\Delta R} \int_P \int_P d\vec{x}_m \left[1 - e^{(-a_\nu L_m(\vec{x}_m, \vec{e}_0, R))} \right]$$

- Refractive index given by the sum of pigments' contributions

$$a_\nu = \sum_p E_{a,\nu,p} C_p = \sum_p a_{\nu,pig,p}$$

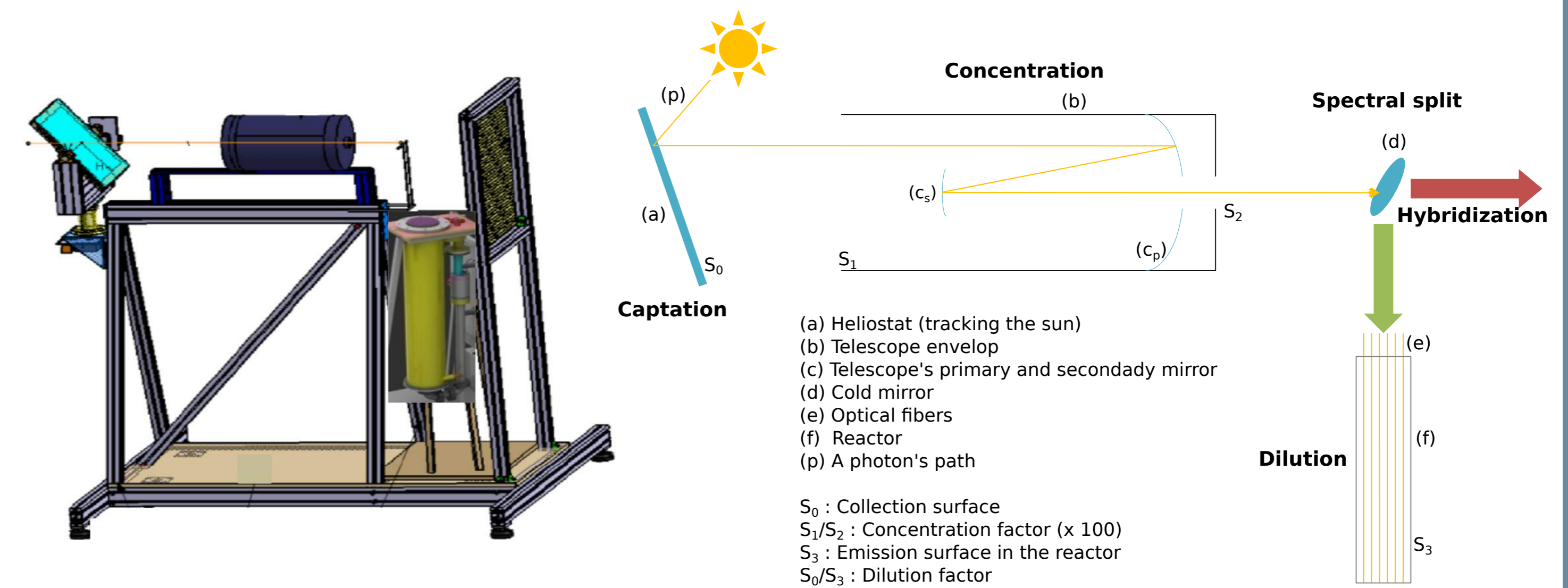
Monte Carlo (MC) method

Monte Carlo method is a statistical approach that offers suitable advantages:

- Management of infinite dimensions
- Meshless (in volume)
- Access to numerical error
- Possibility to compute sensitivities
- **Complex geometries** easily handled with advanced computer-graphics-tools [2]

An issue is to manage multi-scale non-linearities thanks to recent Monte Carlo advances (null collisions, ...) [3,4].

The developed DiCoFluV-Hy prototype



Main results

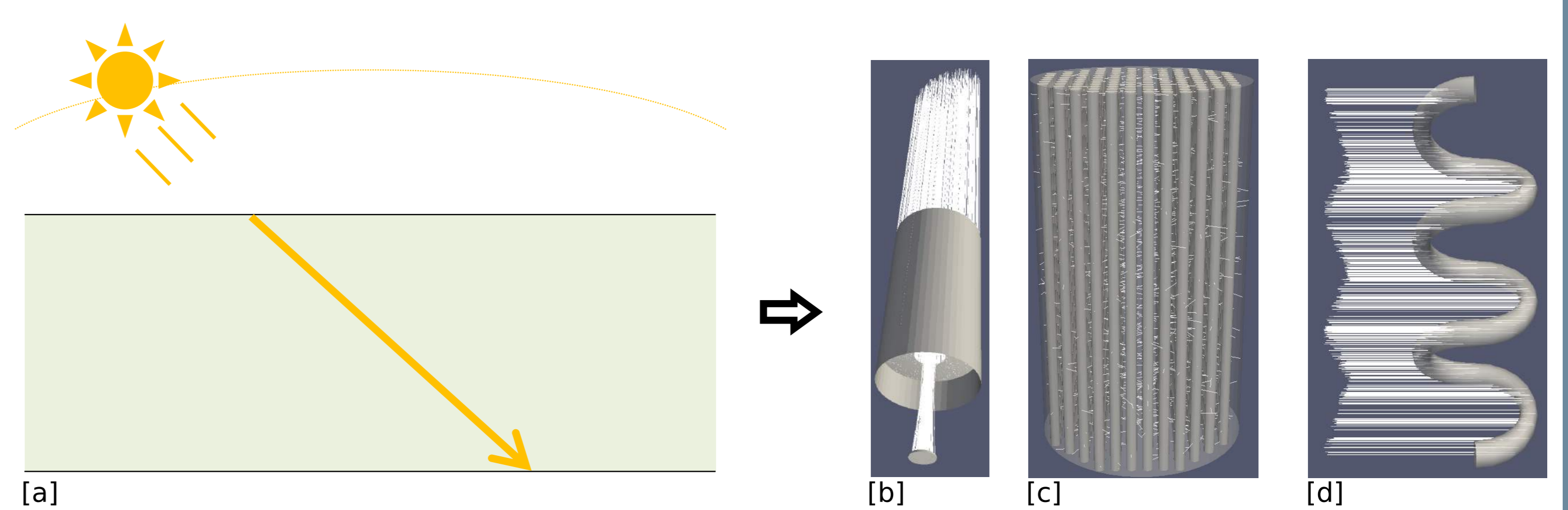


Figure 1: Development of algorithms in simple geometry and passage to complex geometry. [a] Reactor considered as a slab. [b] Ray tracing in a cassegrain telescope. [c] Ray tracing in a complex reactor with optical fibers. [d] Ray tracing on a microalgae with complex shape (*A. platensis*)

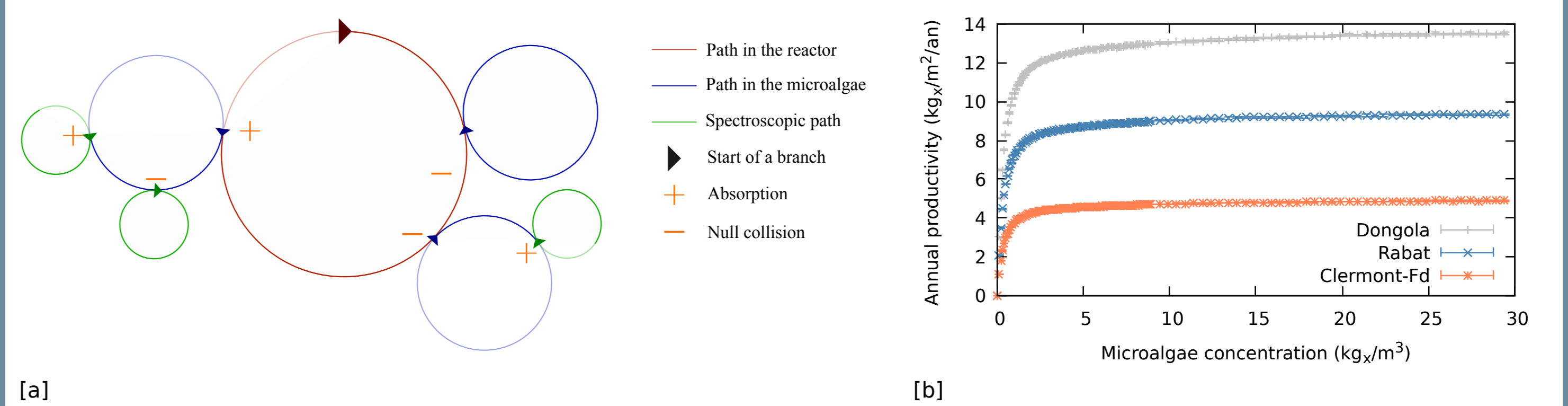


Figure 2: [a] A part of a MC realization (algorithm presented as a diagram). [b] Annual surface productivity according to the concentration of microalgae in Dongola, Rabat and Clermont-Fd (solar database www.meteonorm.com). The calculation of a point (10^7 samples on a Intel®Core™ i7-7820HQ CPU @ 2.90GHz) in complex geometry costs 1 minute.

Conclusion & perspectives

- The implementation of MC algorithms in complex geometry is conceptually simple and here validated
- MC method is a relevant and promising tool to tackle physical and engineering multi-scale problems
- Our kind of non-linear multi-scale model can be managed thanks to recent MC advances (null collision algorithm)

However, the management of non-linearities in any multi-scale model remains a bottleneck and requires further work.

References

- [1] D. E. Keyes et al., *The International Journal of High Performance Computing Applications*, 27(1):483, February 2013.
- [2] J. Delatorre et al., *Solar Energy*, 103:653681, May 2014.
- [3] M. Galtier et al., *Journal of Quantitative Spectroscopy and Radiative Transfer*, 125:5768, August 2013.
- [4] J. Dauchet et al., *Scientific Reports*, 8(1):13302, September 2018.

Acknowledgments

This work has been sponsored by the French government research program "Investissements d'Avenir" through the IDEX-ISITE initiative 16-IDEX-0001 (CAP 20-25) and the LabEx IMOB3 (ANR-10-LABX-16-01). This research was also financed by the European Union through the Regional Competitiveness and Employment program /2014-20/ (ERDF - AURA region) and by the AURA region.

Contact Information

- Web: www.tinyurl.com/y5vzce7q
- Email: victor.gattepaille@uca.fr
- Phone: +33 4 73 40 53 16

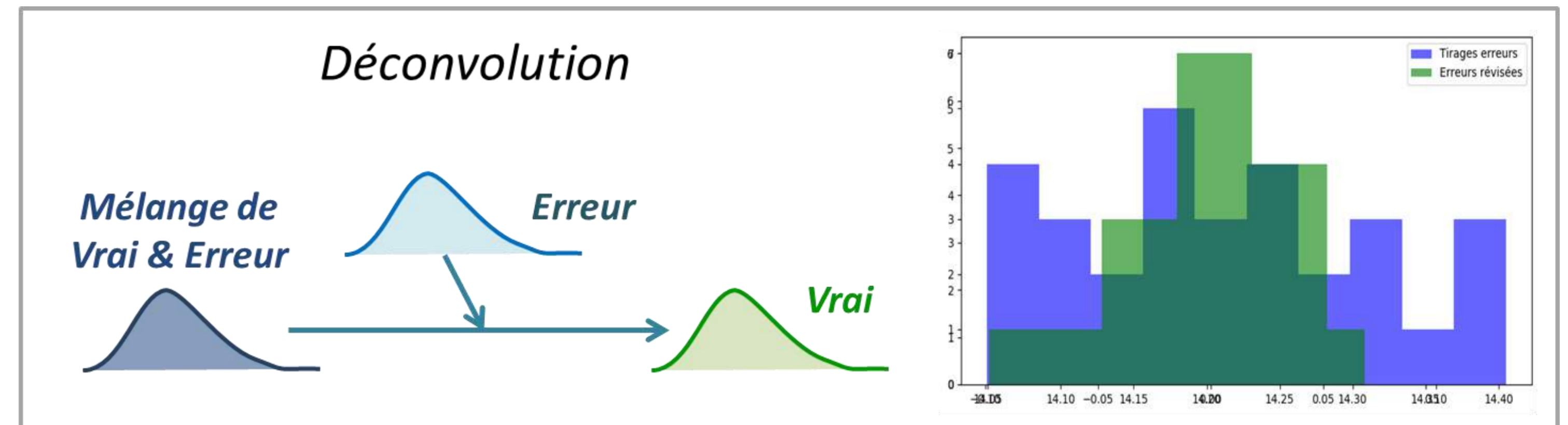
Objectifs

Motivation et enjeux

- L'industrie est amenée à répondre chaque jour à des exigences de plus en plus pointues sur la qualité de ses processus.
- Le 21e siècle est d'une part celui de l'Industrie 4.0 qui procède par l'intégration d'outils informatiques puissants et précis dans l'industrie.
- Le 21e siècle est d'autre part celui du Big Data qui profite aujourd'hui des nouvelles technologies permettant l'acquisition et le stockage peu coûteux de grands volumes de données.
- La métrologie n'a quant elle que très peu exploré ces nouvelles possibilités et aujourd'hui, face aux exigences croissantes de qualité l'erreur de mesure ne dépend toujours que de l'outil utilisé...

Enjeux

- Le projet Smart Tools for Advanced Metrology (STAM) souhaite développer et proposer un outil aux fondements statistiques et probabilistes qui répond au besoin d'affiner les mesures obtenues en métrologie.
- Pour une mesure donnée, l'outil tiendra compte du contexte dans lequel la mesure est réalisée, de la tendance des précédents résultats et d'avis experts pour proposer la valeur qui a été le plus vraisemblablement relevée.



Loi d'incertitude relative à un contexte

Il y a de l'erreur dans les mesures :

Une loi fondamentale de la Métrologie, est que la mesure est toujours entachée d'erreur. $Mesure = Valeur Vraie + Erreur$

L'erreur est composée d'un biais et d'une dispersion :

Une part des erreurs commises est constante et l'autre aléatoire. $Erreur = Biais + Dispersion$

Les causes de dispersions sont identifiées dans le contexte :

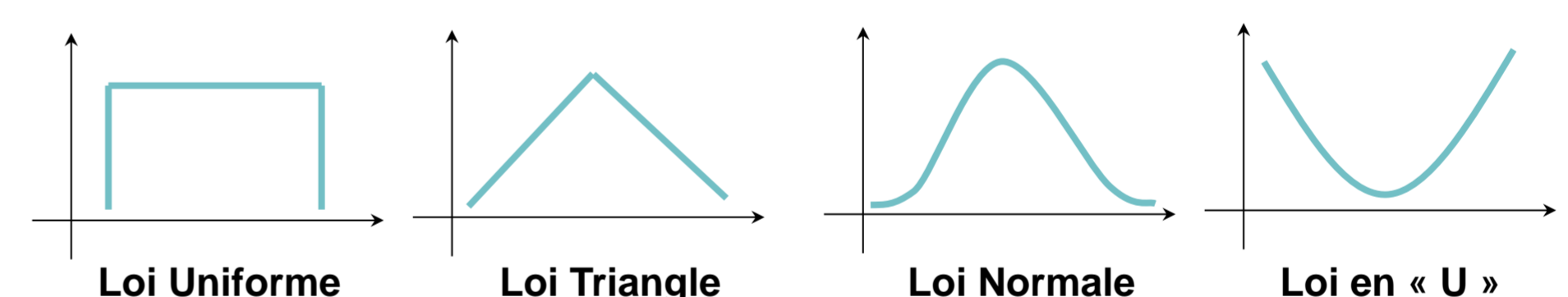
La dispersion est due à un ensemble de causes, et les causes sont lues dans le contexte singulier dans lequel la mesure a été réalisée. $Dispersion = E1 + E2 + \dots$

Quantification de la dispersion de chaque cause :

L'impact de chaque cause est défini par une expérience ou un expertise qui peut être théorique ou empirique. $\begin{cases} E1 = \dots \\ E2 = \dots \\ \dots \end{cases}$

Modélisation de la dispersion de chaque cause :

Quatre types de loi sont utilisées pour modéliser le comportement. La dispersion se transcrit de façon différente pour chaque loi de densité. Des coefficients permettent explicitement d'exprimer l'écart-type de chaque loi.



Génération d'une unique loi d'incertitude pour un contexte donné :

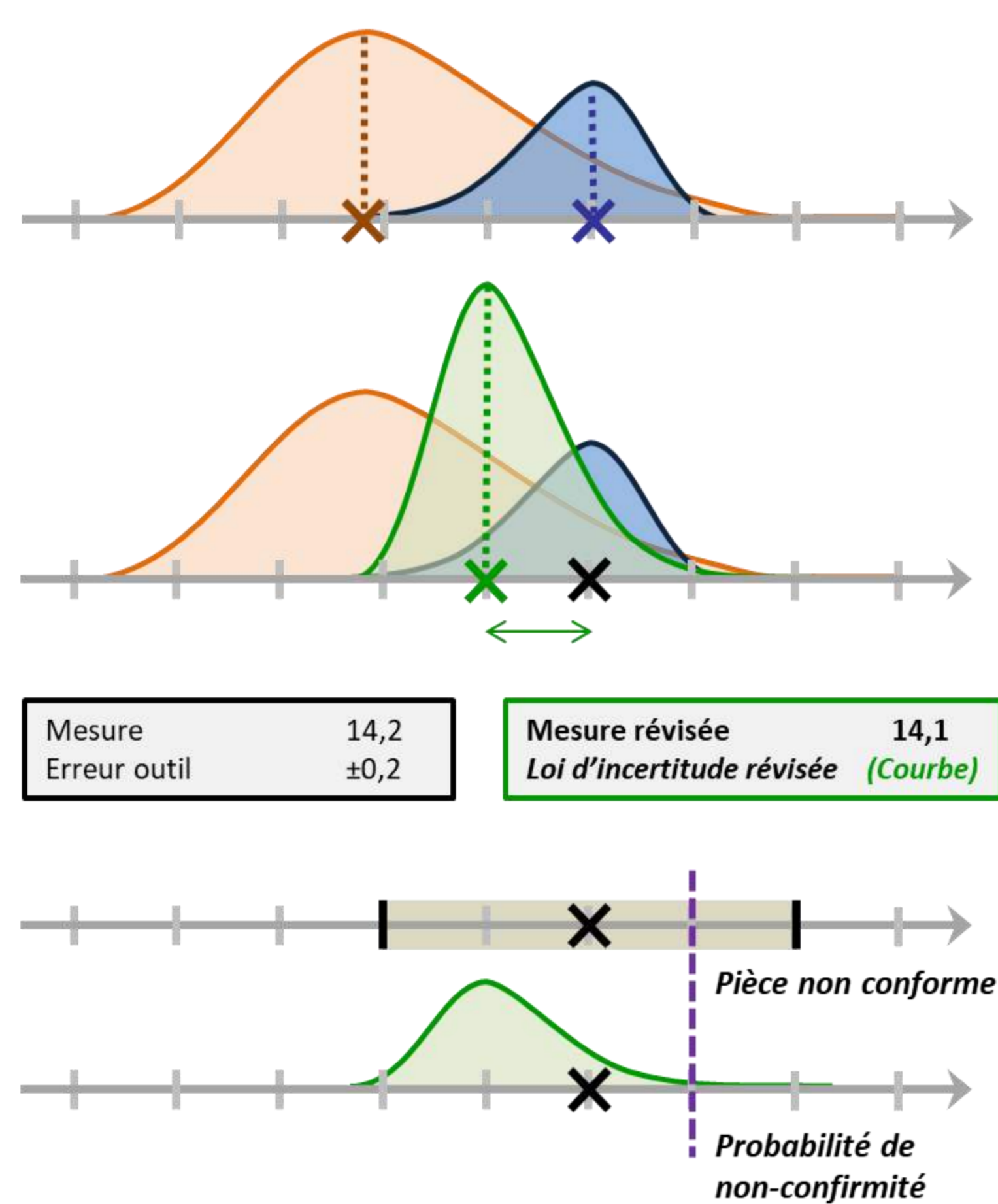
L'ensemble des causes est synthétisée dans une seule loi. Les outils qui sont utilisés dépendent quant à eux de la complexité des lois en jeu.

Complexité du modèle

Les résultats présentés graphiquement ici améliorent la qualité des mesures. Ils sont tirés d'une modélisation gaussienne « simple » : la complexification des modèles et le lissage par noyau permet d'autant plus d'en améliorer la qualité.

Valeur la plus probable

- ✗ Résultat de mesure
- ✗ Valeur vraie la plus probable selon l'a priori des valeurs vraies
- ✗ Valeur vraie la plus probable selon la plausibilité par rapport à l'a priori de l'erreur
- ✗ Loi d'incertitude révisée : Pour une valeur X (axe gris), produits des deux densités données par les courbes orange et bleu foncé.
- ✗ Mesure révisée : Valeur vraie la plus probable.
- ↔ Erreur révisée : Erreur la plus probable appelée (Mesure - Mesure révisée)
- Valeur maximale imposée hypothétique (ici 14,3).



Correction en temps réel

Statistique Bayésienne :

L'intégration des connaissances par inférence Bayésienne qui fait appel au théorème de Bayes permet de paramétrer une loi en fonction des lois prior et posterior. $P(A | B) = \frac{P(B | A) \times P(A)}{P(B)}$

Comparabilité des expériences :

Le processus de correction fait appel au savoir des expériences antérieures. Les valeurs de ces expériences sont améliorées par *Déconvolution*. La réutilisation ou non de données est définie selon la comparabilité des contextes (la comparabilité des contextes est l'objet d'une étude menée par d'autres acteurs).

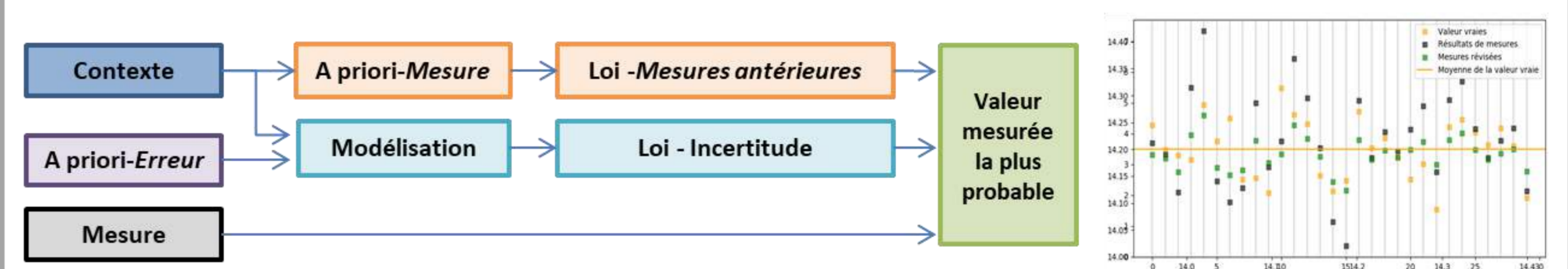
Correction par déconvolution :

La déconvolution est utilisée pour amoindrir le bruit des erreurs dans les mesures. Par simulation, on vérifie qu'en sachant la dispersion de la loi d'incertitude, qui est une connaissance imparfaite et partielle de l'erreur, les valeurs les plus probables réduisent en moyenne l'écart aux valeurs vraies.

Correction en temps réel :

Le valeur lue à la mesure n'est probablement pas celle qui a été mesurée. La loi d'incertitude donne la probabilité de l'erreur qui ait été faite. La loi des mesures antérieures donne la probabilité de la valeur mesure. La combinaison de ces deux informations donne la *Valeur la plus probable*.

Correction d'une mesure en temps réel



Conclusions

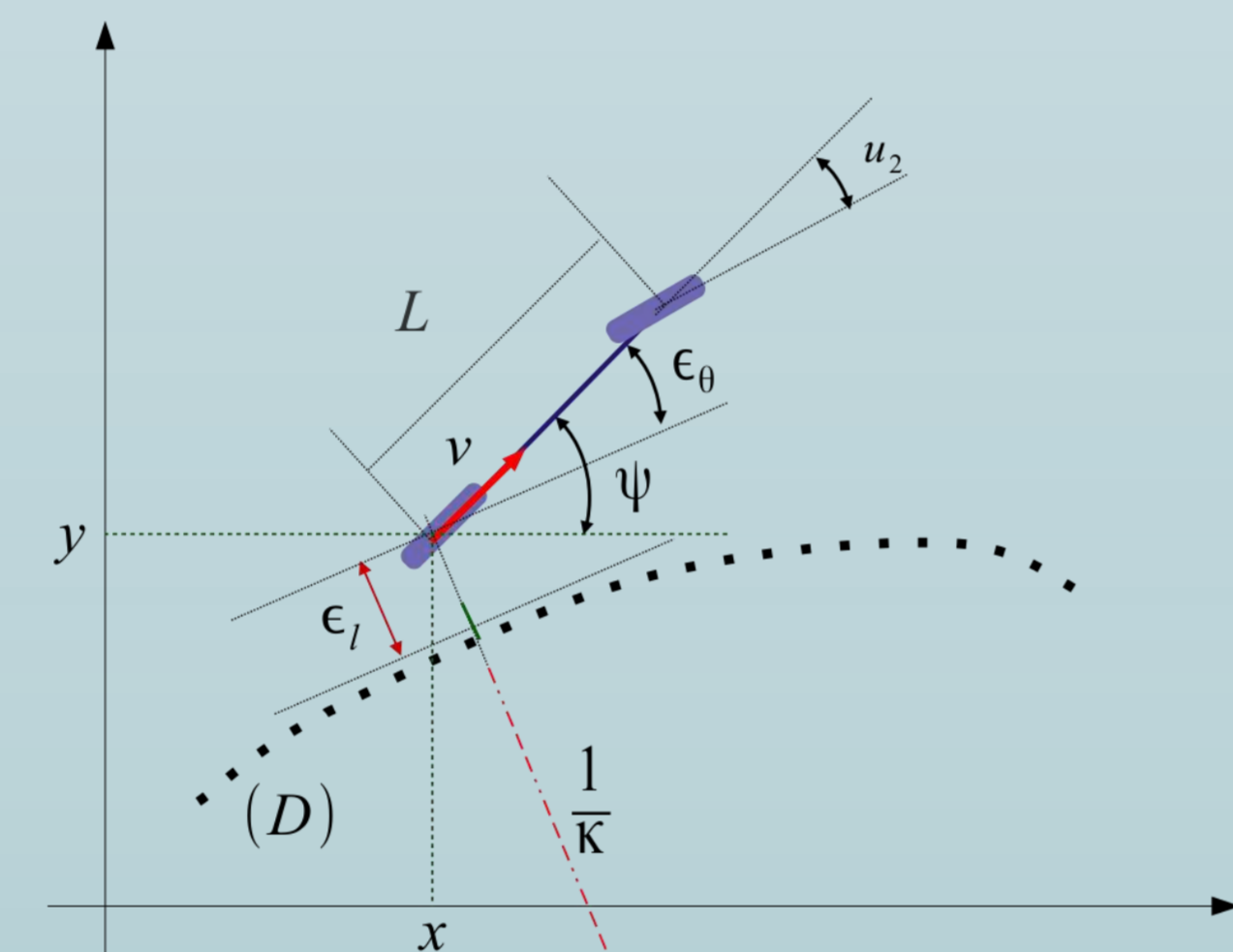
- ✓ La simulation valide l'efficacité de l'intégration de connaissances a priori par la statistique Bayésienne ainsi que les outils probabilistes ;
- ✓ Cet outil permet de suggérer en temps réels les valeurs qui ont été réellement mesurées, et ces valeurs réduisent en moyenne l'écart aux longueurs réelles ;
- ✓ Les valeurs issues de la métrologie sont ainsi affinées et accompagnées d'une caractérisation probabiliste permettant de prendre des décisions de tolérancement souple en rapport avec des seuils de risques.

Introduction

Mobile robots are used to accomplish different missions, their sensors being used to correctly and efficiently understand the robot's environment. Those sensors have varying degrees of **certainty in their measurements** depending on the environment and their properties. This **limits the efficiency** of robots using static controllers, as the tuning of their parameters takes into consideration the **nominal behavior** of the robot, which has a negative effect on the robot's efficiency when operating in sub-nominal states. Furthermore, the tuning of these controllers is done to guarantee a higher level of margins, which has a negative effect on robot performance during nominal states. This **compromise reduces the overall performance** of the robot.

The aim of the work is to integrate the **covariance of the measurement noise** and the **trajectory information** into the control policy in order to adjust the robot's behavior to its complex environment, by adjusting the **controller gain**. **Neural networks** have been used, with promising results [2,3,4]; however such methods use small neural networks that are not capable of complex inference, and are using the error or state vector as the basis for the gradient which can cause instability if noisy.

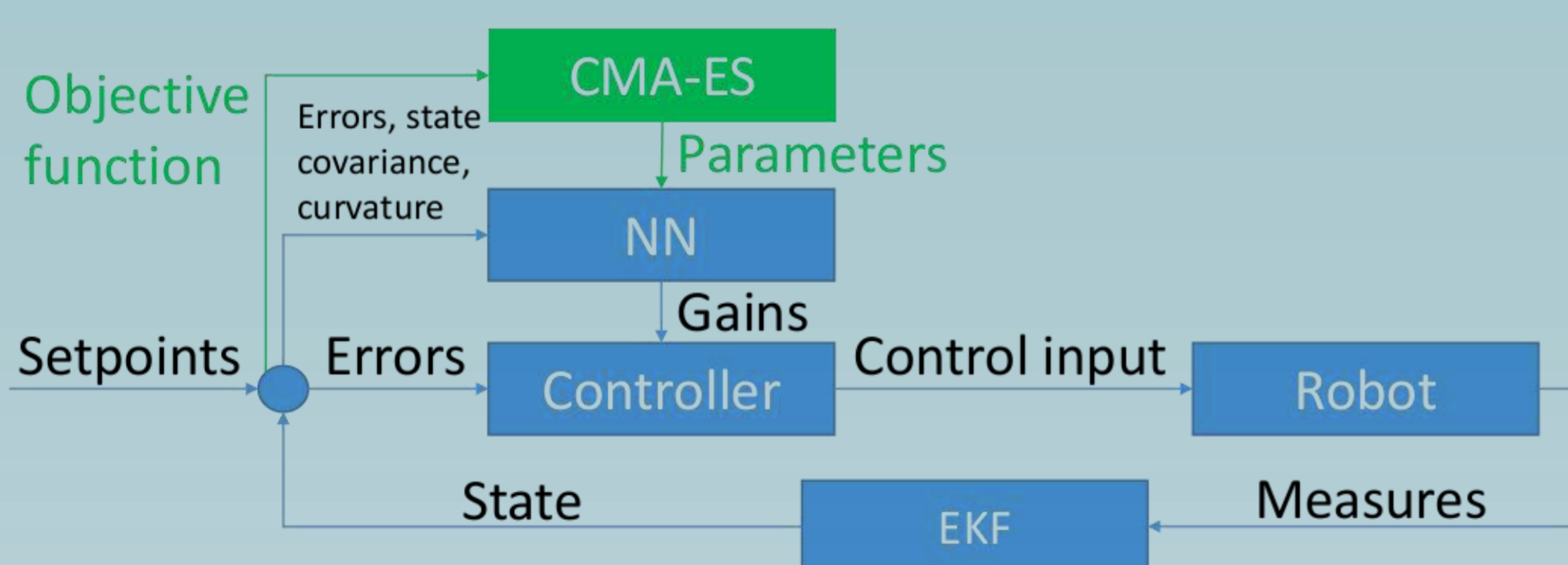
The following Robotic model with the state equations below and the controller defined by :

$$\dot{X} = \begin{pmatrix} \dot{x} \\ \dot{y} \\ \dot{\theta} \\ \dot{v} \end{pmatrix} = \begin{pmatrix} v \cos(\theta) + \alpha_x \\ v \sin(\theta) + \alpha_y \\ \frac{\tan(u_2 + \alpha_{u_2})}{L} + \alpha_\theta \\ u_1 + \alpha_{u_1} \end{pmatrix}$$


$$u_2 = \arctan \left(\frac{L \cos^3 \epsilon_\theta}{\alpha} \left(k_\theta(e_\theta) + \frac{\kappa}{\cos^2(\epsilon_\theta)} \right) \right) \text{ with } e_\theta = \tan \epsilon_\theta - \left(\frac{k_l \epsilon_l}{\alpha} \right)$$

Methods

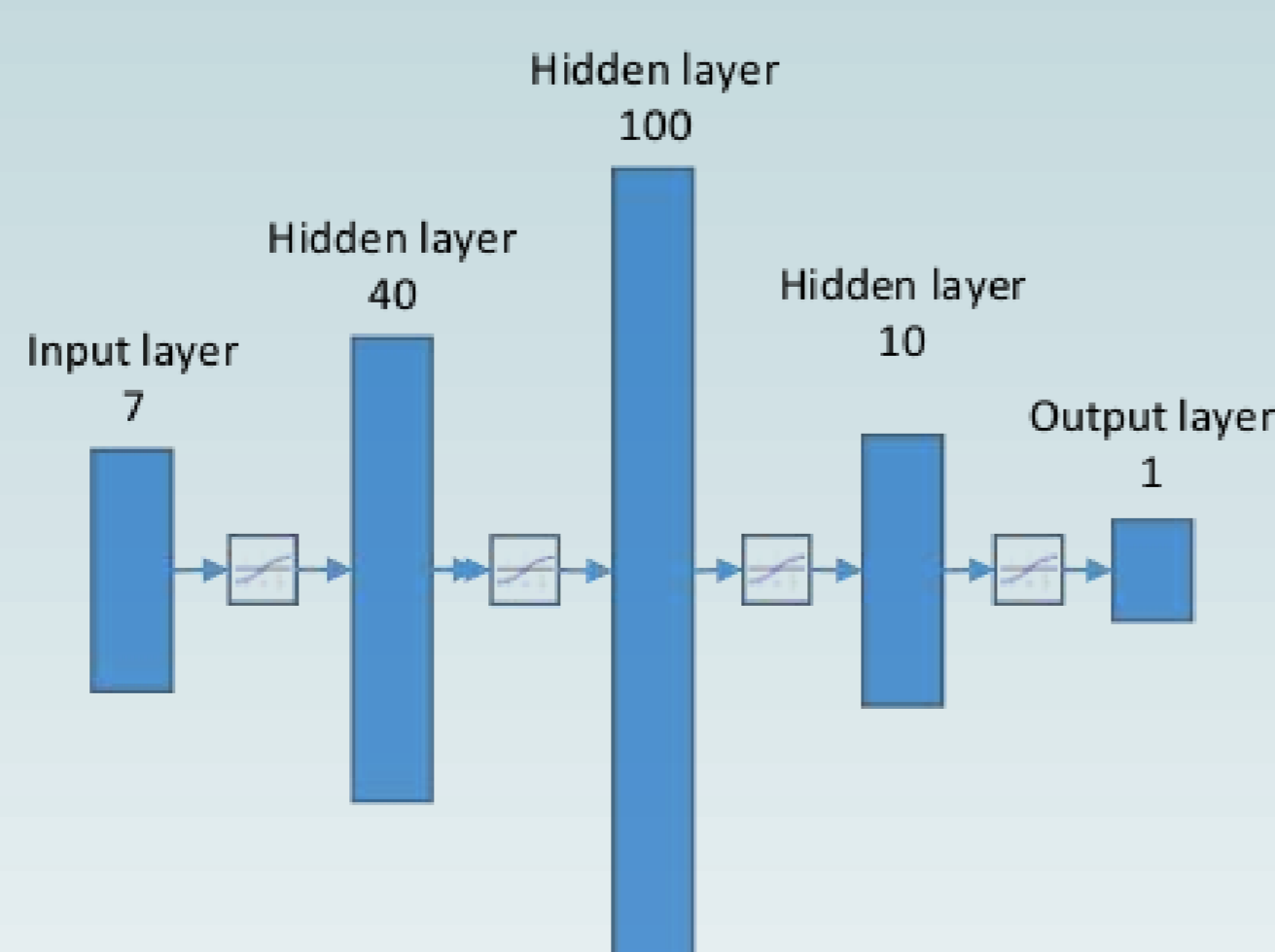
A new strategy for on-line gains adaptation is proposed :



The controller uses the gains defined by the neural network in order to effectively follow the requested trajectory. The robot's dynamics simulate the behavior of the robot. The noise applied to the measurements mimics real world conditions, and so an **extended Kalman filter** (EKF) is used to observe the state of the robot.

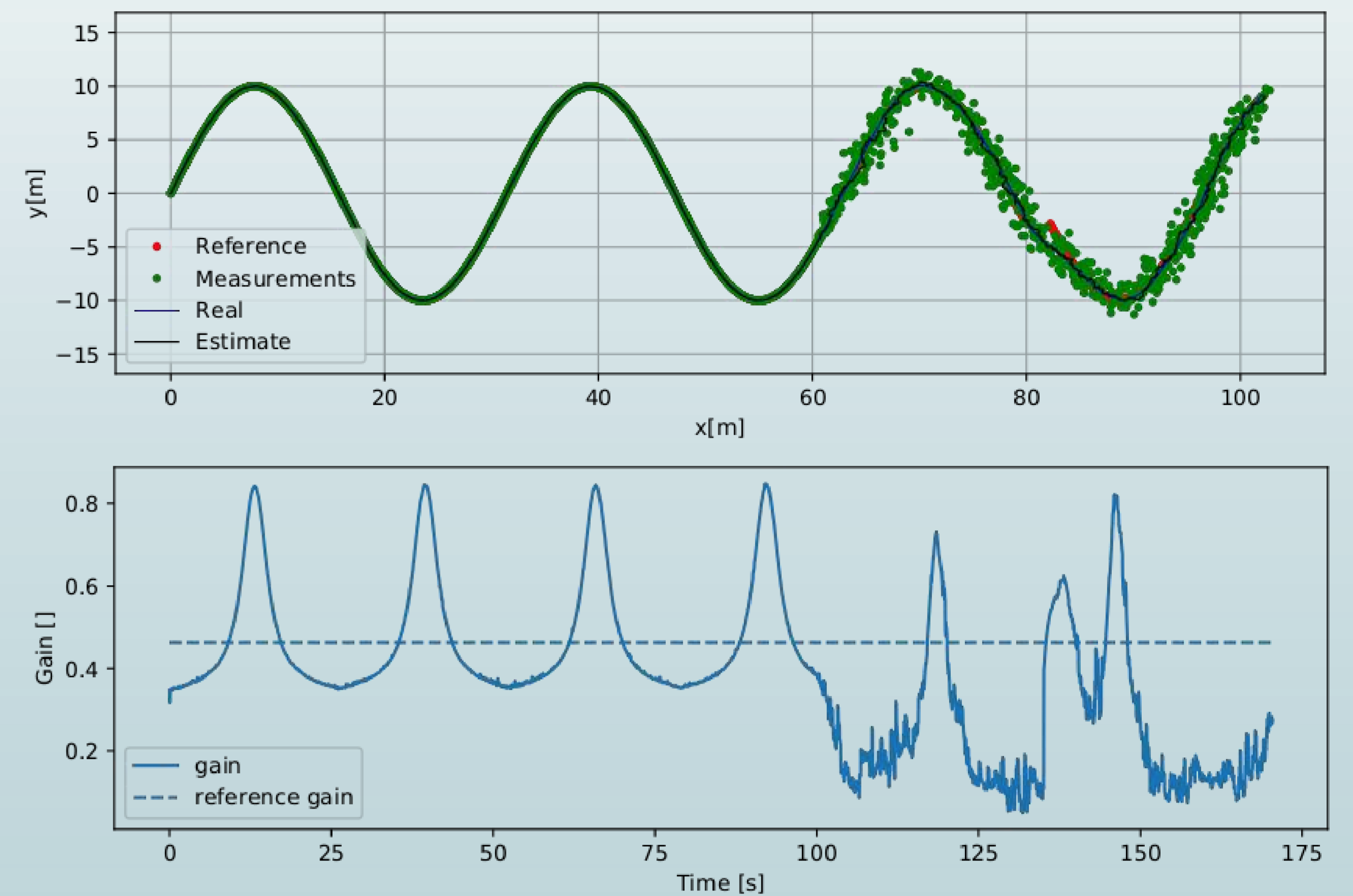
The neural network is trained using CMA-ES [1] as the optimization algorithm for the parameters of the neural network. This is commonly called **Neuroevolution**, and has shown promising results in the past [5]. However for this, objective function must be defined. In our case it is defined as the **minimization** of the lateral error, angular error, and applied steering.

The neural network is given the lateral error, angular error, Kalman covariance matrix, trajectory curvature and current speed as input, in order to determine the optimal gain.



Results

The experiments were done with a **simulation** of the robotic model and state equations, over a few trajectories. Here is an example of the gain when following a sinusoidal path :



A visible **increase** in the gain can be observed when perturbations such as corners occur, and a **reduction** of the mean gain when entering a noisy region where the robot is no longer accurately measuring its position. This allows more accurate following of the trajectory, while avoiding oscillatory behavior in sub-optimal regions.

A more quantitative measurement is required however to show the general improvement of the method. As such, simulations were run **250 times** over different trajectories, using the proposed method (named **CMA-ES NN**), compared over reinforcement learning methods and a fixed gain method. The comparative metric was the objective function defined in the method (**lower is better**) :

Trajectory	CMA-ES NN	SAC	PPO	DDPG	A2C	Fixed gain
Line	41.60 (± 2.34)	60.99 (± 22.21)	115.11 (± 57.10)	158.14 (± 4.09)	57.52 (± 15.12)	48.20 (± 2.45)
Sine	144.76 (± 2.86)	1140.52 (± 3004.65)	2403.93 (± 2824.32)	309.18 (± 5.79)	280.51 (± 175.61)	151.70 (± 2.83)
Parabola	98.73 (± 3.39)	191.48 (± 2.43)	389.65 (± 6.34)	417.99 (± 6.23)	208.80 (± 26.57)	125.29 (± 4.02)
Spline1	117.66 (± 3.04)	508.24 (± 152.24)	2864.41 (± 14.31)	272.20 (± 5.27)	542.85 (± 4.47)	142.04 (± 3.45)
Spline2	147.32 (± 3.18)	6563.63 (± 3310.81)	3169.80 (± 23.61)	258.85 (± 26.39)	437.22 (± 736.97)	164.94 (± 4.45)

Conclusions

We are currently working on a method of **neuroevolution**, which is used to train a neural network to then tune a controller in real time in order to adapt a robot's behavior to a varying level of precision in the perception. The proposed method has been shown to **improve** the overall performance in the context of mobile robotics when compared with constant gain models or reinforcement learning methods. Furthermore, the proposed method can be used with varying controllers in many different applications, such as navigation in urban landscapes, agricultural application, or even drones. Many possible variants exist of this method that could be put in application, such as variants of the CMA-ES algorithm could be used, or even the possible variants of the objective function for different tasks. First simulation tests have shown the **theoretical validity** of the proposed approach, accounting for sensors noises and low level settling times. Further experimentation with existing adaptive control algorithms, multi-gain controllers, observateurs gain tuning, and **experimentation with real world robots** are envisioned for future works, especially with respect to grip conditions.

Bibliography

- Hansen, N. (2016). The CMA evolution strategy: A tutorial. CoRR, abs/1604.00772
- Jalali, L. and Ghafarian, H. (2009). Maintenance of robot equilibrium in a noisy environment with fuzzy controller. In 2009 IEEE International Conference on Intelligent Computing and Intelligent Systems, volume 2, pages 761-766
- Jiang, L., Deng, M., and Inoue, A. (2008). Support vector machine-based two-wheeled mobile robot motion control in a noisy environment. Proceedings of the Institution of Mechanical Engineers, Part I: Journal of Systems and Control Engineering, 222(7):733-743.
- Doicin, B., Popescu, M., and Patrascioiu, C. (2016). Pidcontroller optimal tuning. In 2016 8th International Conference on Electronics, Computers and Artificial Intelligence (ECAI), pages 1-4
- Salimans, T., Ho, J., Chen, X., Sidor, S., and Sutskever, I. (2017). Evolution Strategies as a Scalable Alternative to Reinforcement Learning. ArXiv e-prints.

Objectives

1. Investigate how data quality indicators can be used in order to improve the quality of query answers,
2. Ability to reason about quality-ranked query answers,
3. Design and implement quality-aware query evaluation algorithm that enables the usage of quality indicators to compute context-dependant and quality-aware query answers,
4. Effective approach to automatically rewrite the query by taking into account the quality indicators of the involved data.

Introduction

► Conclusions are done with extracted data from stored data. From these conclusions, decisions are made. If stored data contain erroneous data, extracted data from them can also contain error. So, wrong decision can be made from conclusions that are from these extracted data. To deal with this problem, some quality indicators are introduced. Given a query and a stored data called database, extracted data is answers of this query over database. Having a database that contains error and a query, our main goal is to compute answers of query over this database with a quantity that measures level of errors arise in answers. In literature, there are some related works but they are about error quantification in stored data. Using this quantity, when one takes decision with answers of query so one has idea about the risk of result.

Overview of the problem

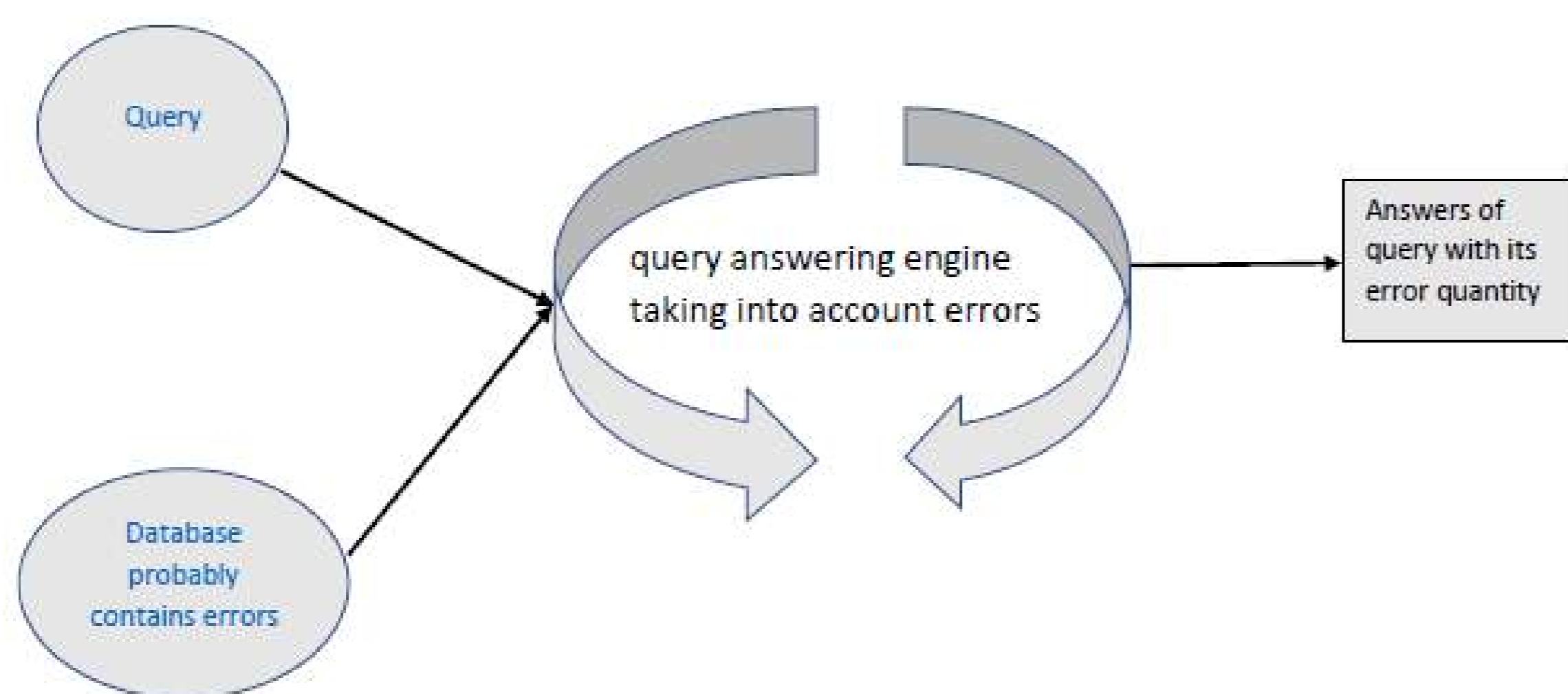


Figure 1: Overview of our the problem

► Some interesting questions are:

1. How to identify these erroneous data from database ?
2. How to quantify errors of answers of queries ?
3. What means this error quantity for answers of queries ?
4. How to compute this quantity, once it is defined ?
5. depending on the context, what are the underlying filtering problems ?

First contribution, quantify inconsistency

- First, we are interested in inconsistency,
- Inconsistency arise when some integrity constraints defined over database are violated.
- These constraints make it possible to give meaning to the data.
- Example of integrity constraint is that two students can not have the same school number or two person can not have the same social security number.
- An other example of integrity constraint is any disease is diagnosed before its surgical operation

Related works

- Measure of inconsistency in database [1, 2]. In case of [1], inconsistency is measured as the number of contradictions that can be arise in database when integrity constraints are applied over it. In [2], inconsistency measure is the number of cases that violate constraints.
- Other related works are works about consistent query answering. For more details, reader can see [3, 4, 5, 6].

Formalization of the problem

► Let I , IC and q respectively a database, a set of integrity constraints and a query.

1. Identify set of tuples in I that violate IC , it is denoted $IncT(I, IC)$
2. Compute answers of q over I , denoted $q(I)$, and during this processing compute for each tuple $t \in q(I)$ its set of set tuples in I from which it is derived, denoted $prov(I, q, t)$
3. All tuples in answers of query with their inconsistency degree, denoted $q^{IC}(I)$ is the following

$$q^{IC}(I) = \{ \langle t, m \rangle : t \in q(I) \text{ and } m = \text{Min}_{E \in prov(I, q, t)} (|E \cap IncT(I, IC)|) \} \text{ with } || \text{ the cardinal function.}$$

Running example

Diagnosis (P)				Vaccination (R)				Surgery (S)			
id	PatientID	DiseaseRef	Date	id	PatientID	DiseaseRef	Date	id	PatientID	DiseaseRef	Date
t1	P01	D1	2	t10	P01	D2	3	t17	P01	D1	1
t2	P02	D7	4	t11	P02	D4	5	t18	P02	D7	3
t3	P03	D7	10	t12	P03	D4	6	t19	P03	D7	9
t4	P04	D1	3	t13	P04	D4	7	t20	P04	D1	4
t5	P04	D4	8	t14	P02	D5	10				
t6	P02	D4	7	t15	P08	D5	7				
t7	P01	D2	5	t16	P10	D3	8				
t8	P08	D7	4								
t9	P10	D1	5								

Integrity Constraints

Query $Q(y, u) \leftarrow P(x, y, z), R(x, u, v), S(x, y, z)$

(1) not $(P(x, y, z) \text{ and } S(x, y, u) \text{ and } z > u)$
 (2) not $(P(x, 'D2', y) \text{ and } R(x, 'D2', z) \text{ and } y > z)$
 (3) not $(P(x, 'D4', y) \text{ and } R(x, 'D4', z) \text{ and } y > z)$

Tuples in answers of query and their provenance tuples			Tuples in answers of query and their inconsistency degree		
Surgery Disease	Vaccinated Disease	Provenance tuples	Surgery Disease	Vaccinated Disease	Inconsistency degree
D1	D2	{t1, t10, t17}	D1	D2	3
D7	D4	{t2, t18, t11} or {t3, t12, t19}	D7	D4	2
D1	D4	{t4, t15, t20}	D1	D4	1
D7	D5	{t2, t18, t14} or {t8, t15, t21}	D7	D5	0

Figure 2: Running example of answers of query computing with inconsistency degree of tuples in answers

Conclusion

- My thesis work is about quality of query answering over database that contains errors
- My first contribution is definition of a new measure of inconsistency of query answers.

References

- [1] John Grant and Anthony Hunter. Measuring inconsistency in knowledgebases. *Journal of Intelligent Information Systems*, 2009.
- [2] Hendrik Decker and Davide Martinenghi. Modeling, measuring and monitoring the quality of information. In *ER '09 Proceedings of the ER 2009 Workshops (CoMoL, ETheCoM, FP-UML, MOST-ONISW, QoS, RIGiM, SeCoGIS) on Advances in Conceptual Modeling*, 2009.
- [3] Leopoldo Bertossi. *Database Repairing and Consistent Query Answering*. 2011.
- [4] Marcelo Arenas, Leopoldo Bertossi, and Jan Chomicki. Consistent query answers in inconsistent databases. In *the eighteenth ACM SIGMOD-SIGACT-SIGART symposium on Principles of database systems*, pages 68–79. ACM, 1999.
- [5] Dany Maslowski and Jef Wijsen. A dichotomy in the complexity of counting database repairs. *Journal of Computer and System Sciences*, 2013.
- [6] JEF WIJSEN. Database repairing using updates. *ACM Transactions on Database Systems (TODS)*, 2005.
- [7] Todd J. Green, Grigoris Karvounarakis, and Val Tannen. Provenance semirings. In *Proceedings of the twenty-sixth ACM SIGMOD-SIGACT-SIGART symposium on Principles of database systems*, pages 31–40. ACM, 2007.

Contact Information

- Email: issaousmane7@gmail.com
- Phone: +33767128651

Micro-Lenses Array (MLA) based Plenoptic Cameras

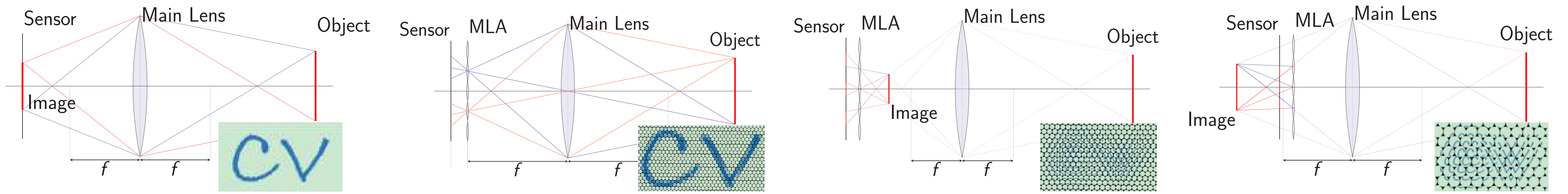


Figure 1: Comparison of optical design of a classic camera and plenoptic cameras. From left to right: classic camera, unfocused design (1.0), Keplerian design (2.0), and Galilean design (2.0).

Objectives

1. Improve the robustness and simplicity of computer vision in field robotics applications (*autonomous vehicles, drones, industrial manipulations, etc.*).
2. Investigate the use of a new type of passive vision sensor called a *plenoptic camera* in these applications.
3. Develop a localization algorithm (*Structure-from-Motion (SfM), Visual Odometry (VO), SLAM, etc.*) using a plenoptic camera to work in challenging weather conditions.

Context & Motivation

- ▶ In context of field robotics applications, challenging weather conditions (especially, *dust, rain, fog, snow, murky water* and *insufficient light*) can cause even the most sophisticated vision systems to fail.
- ▶ The robustness is usually addressed by the use of other sensors (*Lidar, radar, GPS, IMU, etc.*). But such sensors, usually active, suffer from interference. Contrarily, camera, which is a passive sensor, does not suffer from inter-sensor interference.

Imaging System

- ▶ The purpose of an imaging system is to map incoming light rays r from the scene onto pixels p_i of the photo-sensitive detector. Each pixel collects radiance \mathcal{L} from a bundle of closely packed rays in a non-zero aperture size system.
- ▶ The radiance is given by the *plenoptic function* $\mathcal{L}(x, \theta, \lambda, \tau)$ [1] where:
 - ▷ x is the *spatial* position of observation in space,
 - ▷ θ is the *angular* direction of observation in space,
 - ▷ λ is the frequency of the light and τ is the time.
- ▶ Imaging systems allow to capture only a part of this function:

Sensors	Spatial (x)	Angular (θ)	Temporal (τ)
classic camera	✓	-	-
video camera	✓	-	✓
plenoptic cameras	✓	✓	-
plenoptic video cameras	✓	✓	✓

How to acquire the plenoptic function?

- ▶ From *Lumigraph* [2] to commercial *plenoptic cameras* [3, 4], several designs have been proposed to capture the plenoptic function.

Multi-sensors	Sequential	Multiplexing
camera array	gantry, coded aperture	micro-lenses array (MLA)



Figure 2: Lytro Illum camera [3]



Figure 3: Raytrix R12 camera [4]

Main References

- [1] E. H. Adelson and J. R. Bergen. "The plenoptic function and the elements of early vision". In: *Computational Models of Visual Processing* (1991), pp. 3–20.
- [2] Gabriel Lippmann. "Integral Photography". In: *Academy of the Sciences* (1911).
- [3] Ren Ng et al. *Light Field Photography with a Hand-held Plenoptic Camera*. Tech. rep. Stanford University, 2005, pp. 1–11.
- [4] Christian Perwaß, Lennart Wietzke, and Raytrix GmbH. "Single Lens 3D-Camera with Extended Depth-of-Field". In: 49.431 (2010).

Plenoptic cameras capabilities

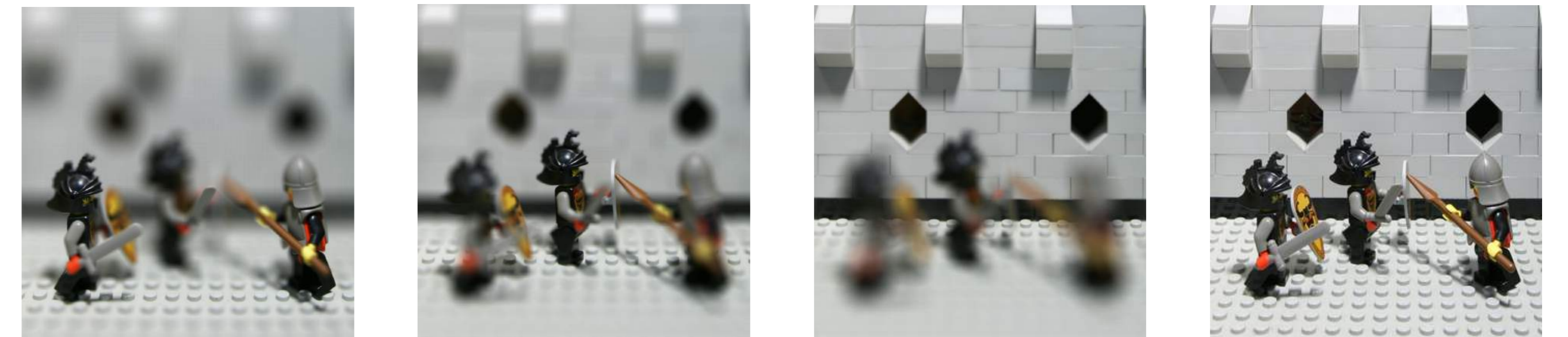


Figure 4: Post-capture refocusing and total focus reconstruction

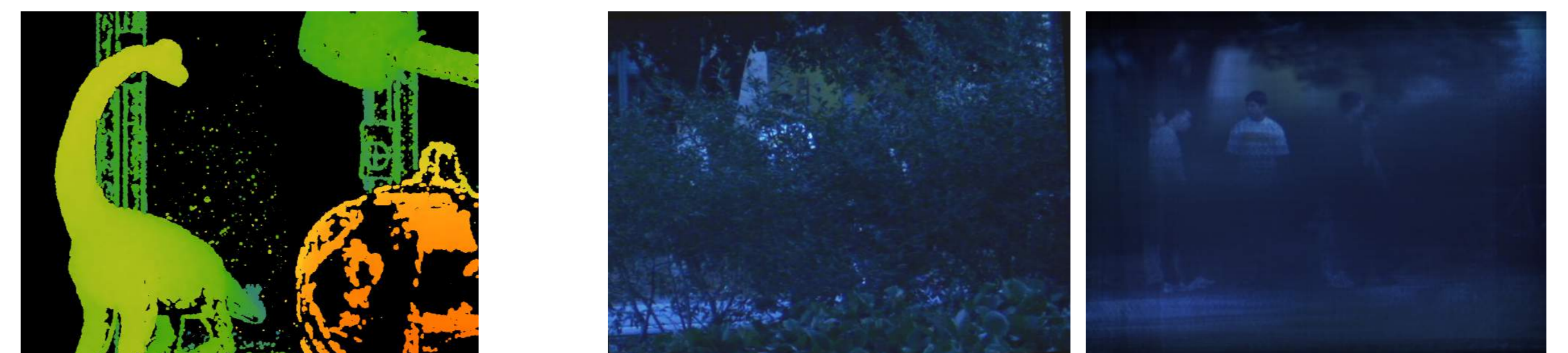


Figure 5: Depth map

Figure 6: Occlusion management

Plenoptic cameras in field robotics applications

- ▶ Taking inspiration from bio-compound-eyes, Neumann et al. established the formalism for the plenoptic-based motion estimation.
- ▶ During his thesis, Dansereau used the plenoptic function to achieve real-time navigation, introducing three distinct closed-form solutions to extract the motions parameters from the plenoptic function.
- ▶ At the same period, Dong et al. gave a complete scheme to design usable real-time plenoptic cameras for mobile robotics applications.
- ▶ Zeller et al. adapted a *SLAM* formulation to deal with plenoptic information. Derived from their calibration model, they proposed a *visual odometry* framework, later improved with scale information.
- ▶ More recently, Hasirlioglu and al. investigated the potential of plenoptic cameras in the field of automotive safety.

Roadmap

- ▶ By taking into account blur information and the multi focal lengths:
 - ▷ Propose a new model and calibration procedure (*in progress*).
 - ▷ Develop a new approach to generate more precise depth map.
- ▶ Propose a probabilistic plenoptic-based *Structure-from-Motion (SfM)* approach.
- ▶ Create a *dataset* of plenoptic images captured from a vehicle under different weather conditions.

Conclusion

- ▶ Plenoptic cameras capture rich information about a scene (*spatial* and *angular* information). Given a single snapshot, a 3D representation of a scene can be passively created. With more information the robustness of localization algorithm is improved, especially during challenging weather conditions.

Acknowledgments

- ▶ This work has been sponsored by the AURA Region and the European Union (FEDER) through the MMII project of CPER 2015-2020 MMaSyF challenge.



Context & Motivations

In a context of autonomous mobile robots, we want to

1. Evolve in the environment without taking too much 'risk'
2. Prove that the robot takes a 'risk' below a certain threshold
3. Define mathematically the notion of risk

Occupancy Grids

- Light Detection And Ranging (lidar) are often used to estimate the traversability of the environment [1].
- Using lasers, they measure the distance to the closest obstacle for several orientations.



Figure 1: Lidar LMS-1xx

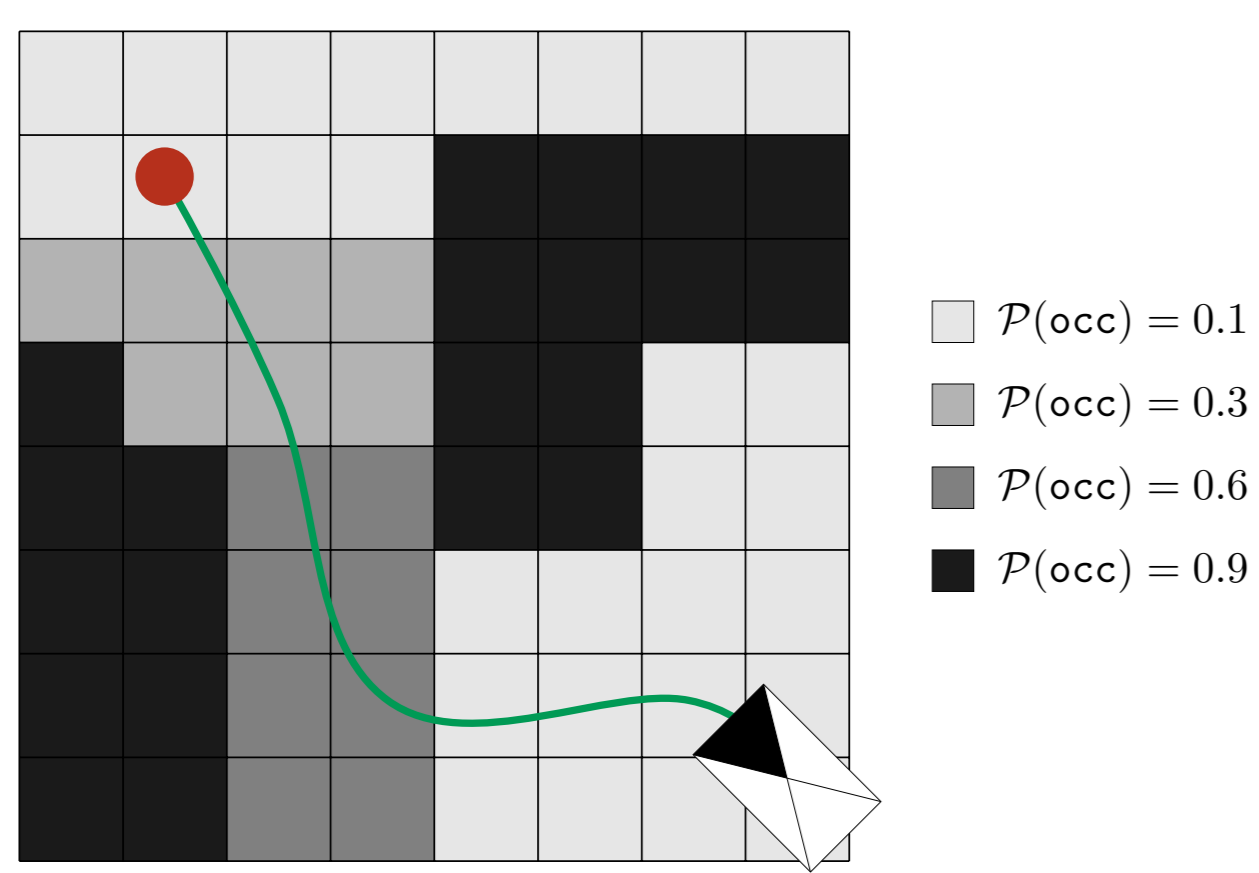


Figure 2: Example of occupancy grid

- The traversability is represented by cells of fixed size containing the probability of occupancy.
- The robot wants to go to the goal (red dot) while minimizing the probability of collision.

Lambda-Field: A Continuous Counterpart for Risk Assessment

- Occupancy grids are however not fitted to assess the probability of collision.
- The probability of collision indeed depends on the size of the cells, which is counterintuitive.

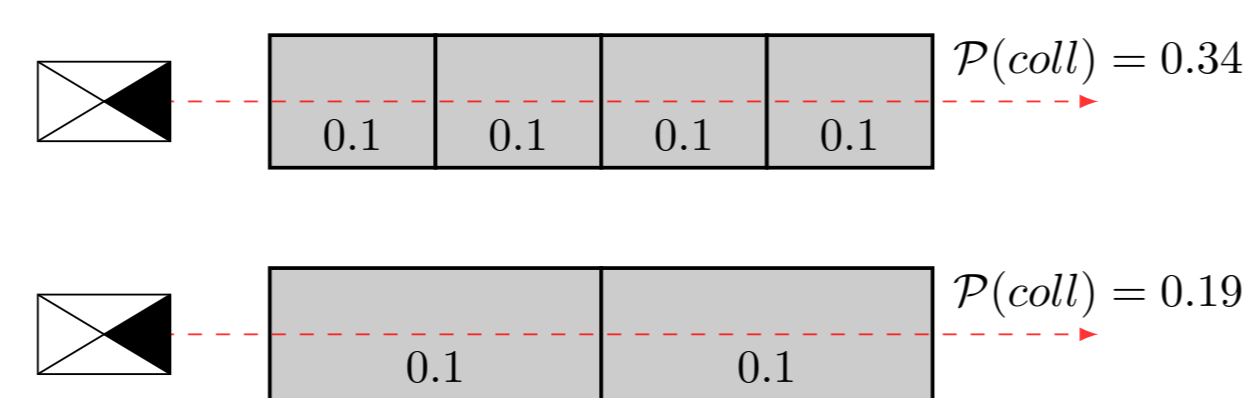


Figure 3: The robot wants to cross the same field with different discretisation sizes.

We introduce the concept of Lambda-Field, which allows the computation of path integrals over a field.

For a positive real-valued field $\lambda(s)$, $s \in \mathbb{R}^2$, the probability to encounter at least one obstacle in a path $\mathcal{P} \subset \mathbb{R}^2$ is

$$\mathbb{P}(\text{coll}|\mathcal{P}) = 1 - \exp\left(-\int_{\mathcal{P}} \lambda(s) ds\right) \approx 1 - \exp\left(-\mathcal{A} \sum_{c_i \in \mathcal{C}} \lambda_i\right) \quad (1)$$

where the approximation is valid for a discretization of the field into cells of area \mathcal{A} and the path \mathcal{P} crosses the cells $c_i \in \mathcal{C}$.

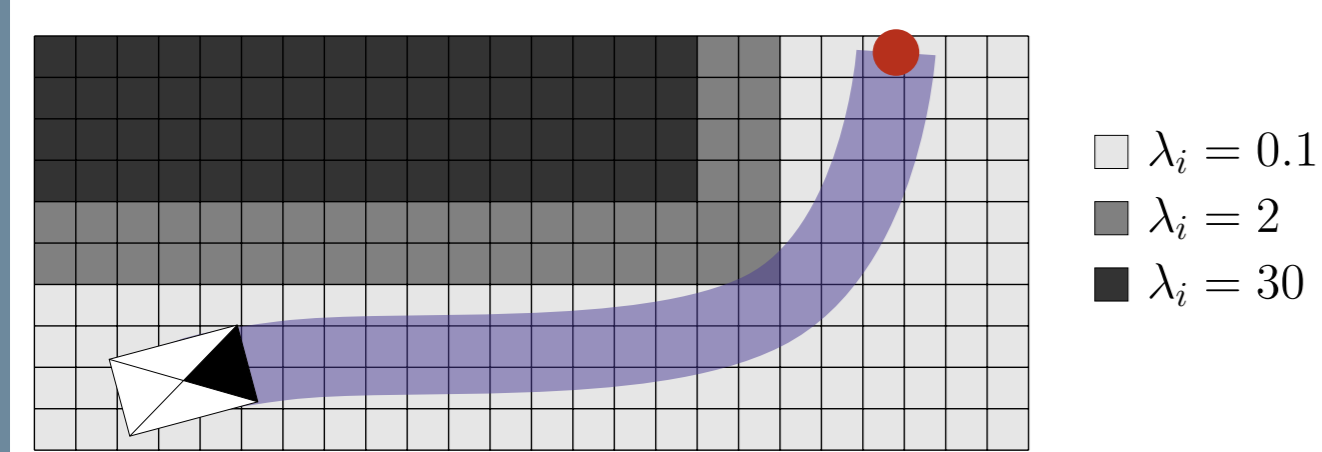


Figure 4: Example of lambda-field. The robot want to cross the path in blue, where each cell has an area of 0.04m^2 .

- Using Equation 1, the probability of collision for the blue path is $1 - \exp(-0.04(58 \cdot 0.1 + 1 \cdot 2)) \approx 0.27$

Construction of the Lambda-Field

- Under the assumption that the error region e of the lidar is small, the λ_i that maximizes the expectation is

$$\lambda_i = \frac{1}{e} \ln\left(1 + \frac{h_i}{m_i}\right) \quad (2)$$

where h_i (resp. m_i) is the number of times the cell has been counted as 'hit' (resp 'miss').

- We also define confidence intervals over the lambda field, such that

$$\mathbb{P}(\lambda_L \leq \lambda_i \leq \lambda_U) \geq 95\% \quad (3)$$

Risk Assessment in Lambda-Field

- The strength of the Lambda-Field is its ability to compute path-integrals. Under the assumption of small cells, we are able to compute the expectation of a risk $r(X)$ over a path crossing the cells $\{c_i\}_{0:N}$, where X is a random variable which stands for the position of the collision:

$$\mathbb{E}[r(X)] = \sum_{i=0}^N r(\mathcal{A}_i) \exp\left(-\mathcal{A} \sum_{j=0}^{i-1} \lambda_j\right) (1 - \exp(-\mathcal{A} \lambda_i)) \quad (4)$$

- The risk function $r(X)$ can take several shapes:
 - ▷ $r(X) = 1$ leads to the probability of collision for a given path.
 - ▷ $r(X) = m_R \cdot v(X)$, where m_R is the mass of the robot and $v(X)$ its velocity at X , leads to the expected force of collision the robot will encounter in the path for static obstacles (walls, ...).

Simulations: Robot-Follower Scenario

- The robot (black & white box) has to follow the pedestrian (green dot) knowing only its position (not the environment nor its future path).
- The robot samples trajectories every second, and chooses one such that it is sure at 95% that the expected collision is below 1 kg m s^{-1} and stays as close as possible to the pedestrian.

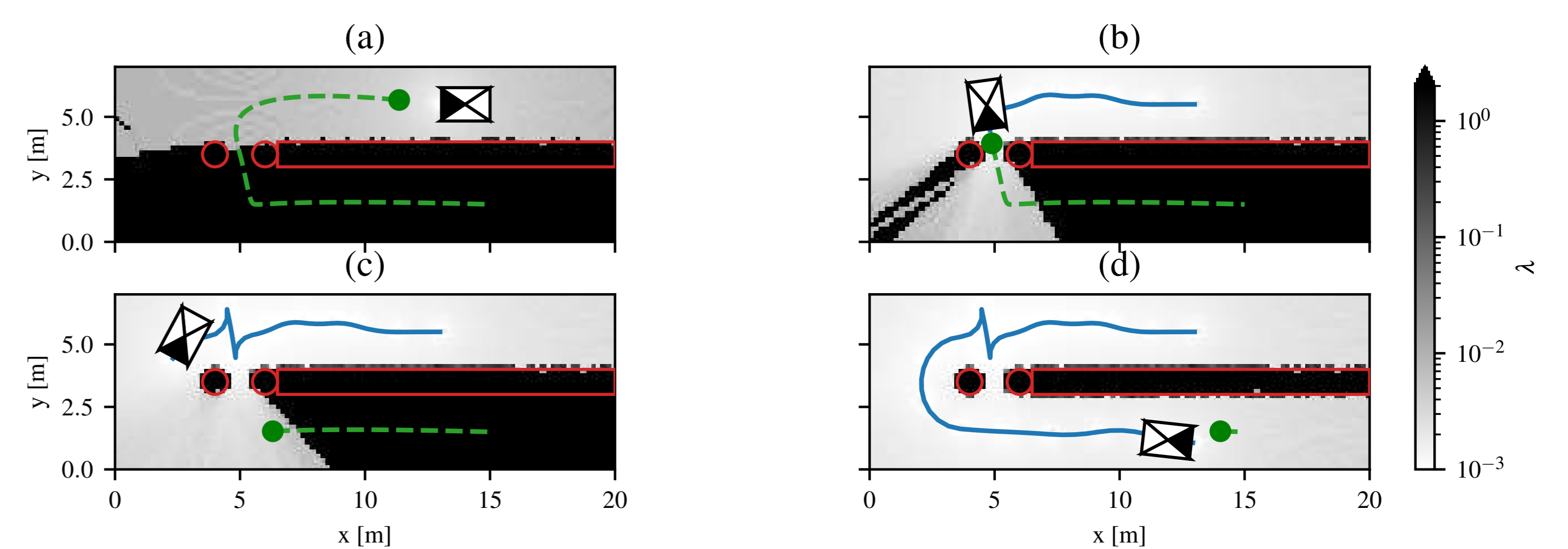


Figure 5: Simulation of a robot-follower scenario

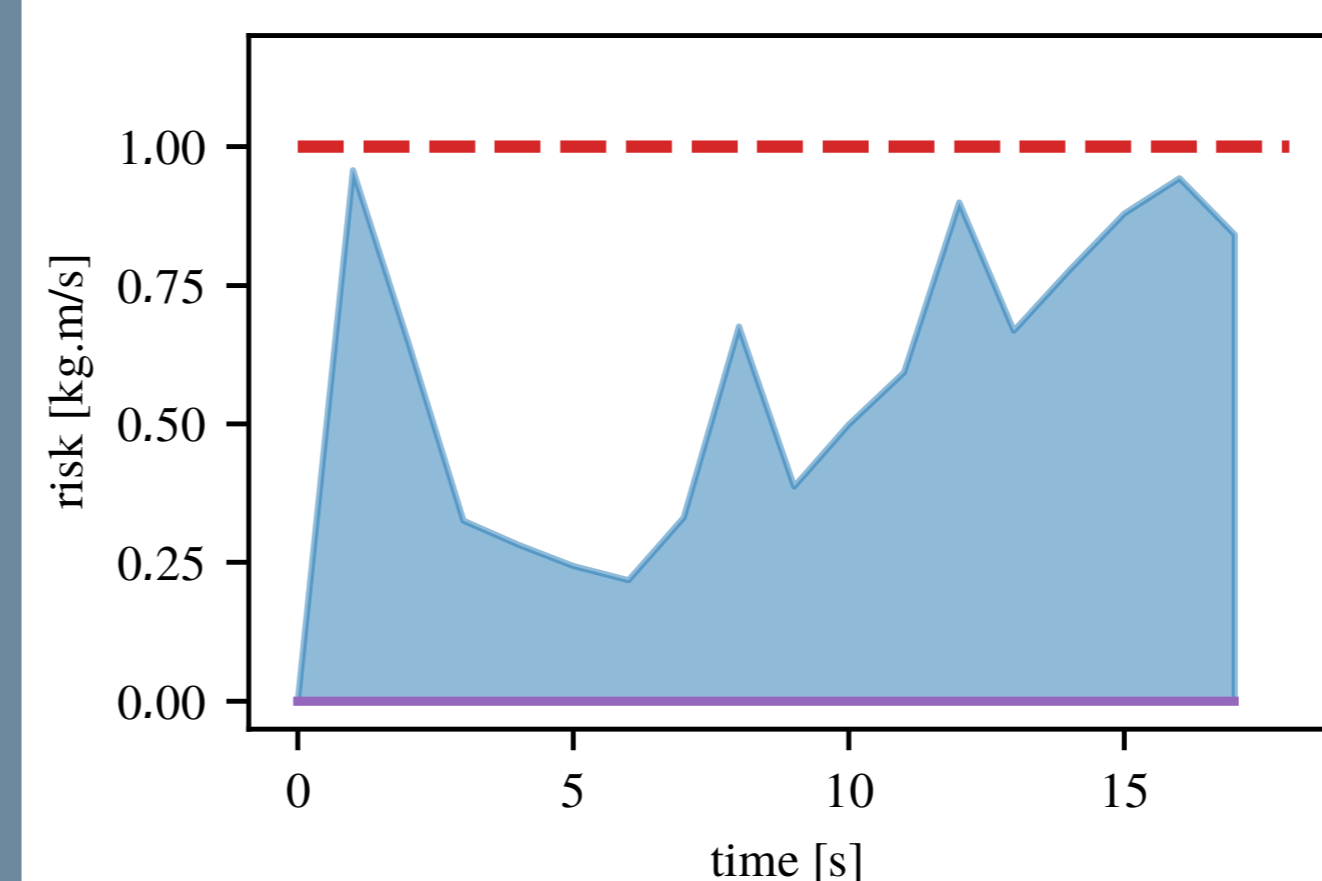


Figure 6: Expected risk (purple) taken by the robot, with its upper bound at 95% in blue. The risk is always below the maximum allowed (dashed-red).

- At $t = 6 \text{ s}$ (Figure 5b), the pedestrian goes through a passage too narrow for the robot. The risk being too high, the robot choose to go around the obstacle.
- The robot rejoins the pedestrian after the narrow passage. The upper limit risk is higher for $t > 6 \text{ s}$ because the robot has to raise its speed to quickly reach the pedestrian.

Experimentations & Future Works

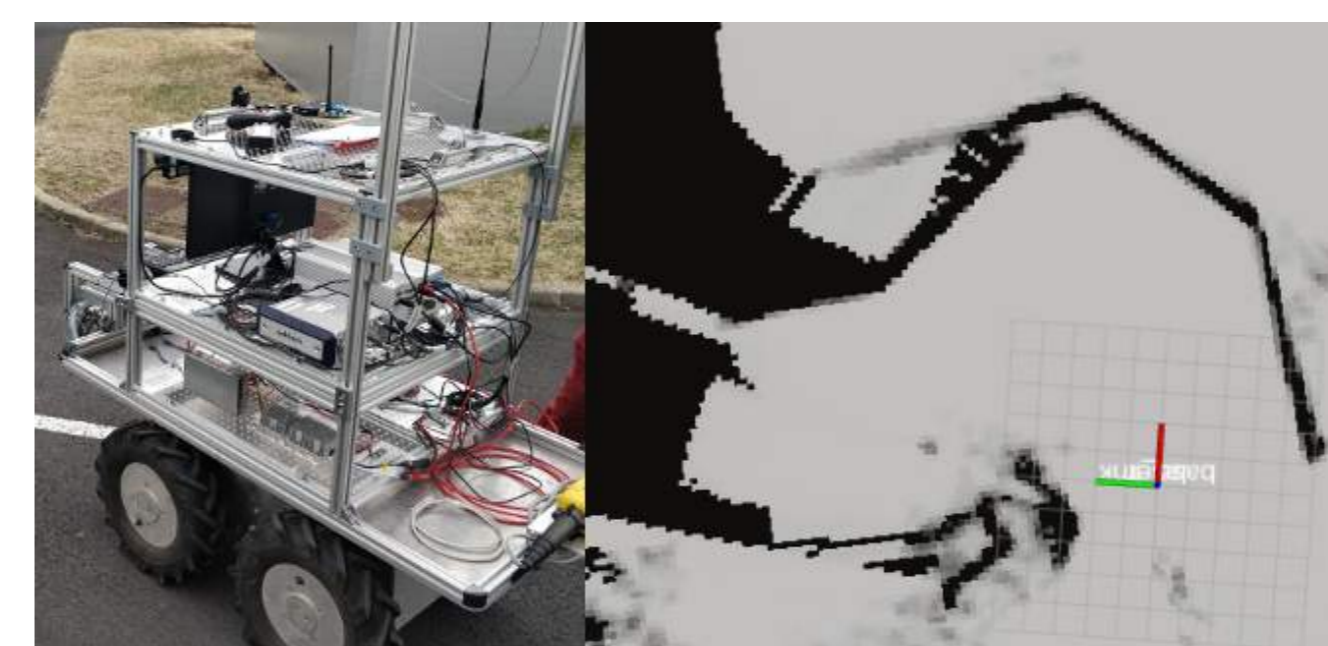


Figure 7: Left: Robot used in experimentations. Right: Lambda-Map created while the robot navigates in the environment

- We implemented our method onto a real robot, leading to promising results [2].
- Future works will add dynamic obstacles, as well as a better risk function. It is indeed far more dangerous to hit a pedestrian than tall grass!

Acknowledgments

This work has been sponsored by the French government research program 'Investissements d'Avenir' through the IDEX-ISITE initiative 16-IDEX-0001 (CAP 20-25), the IMobS3 Laboratory of Excellence (ANR-10-LABX-16-01) and the RobotEx Equipment of Excellence (ANR-10-EQPX-44). This research was also financed by the European Union through the Regional Competitiveness and Employment program 2014-2020 (ERDF-AURA region) and by the AURA region.



References

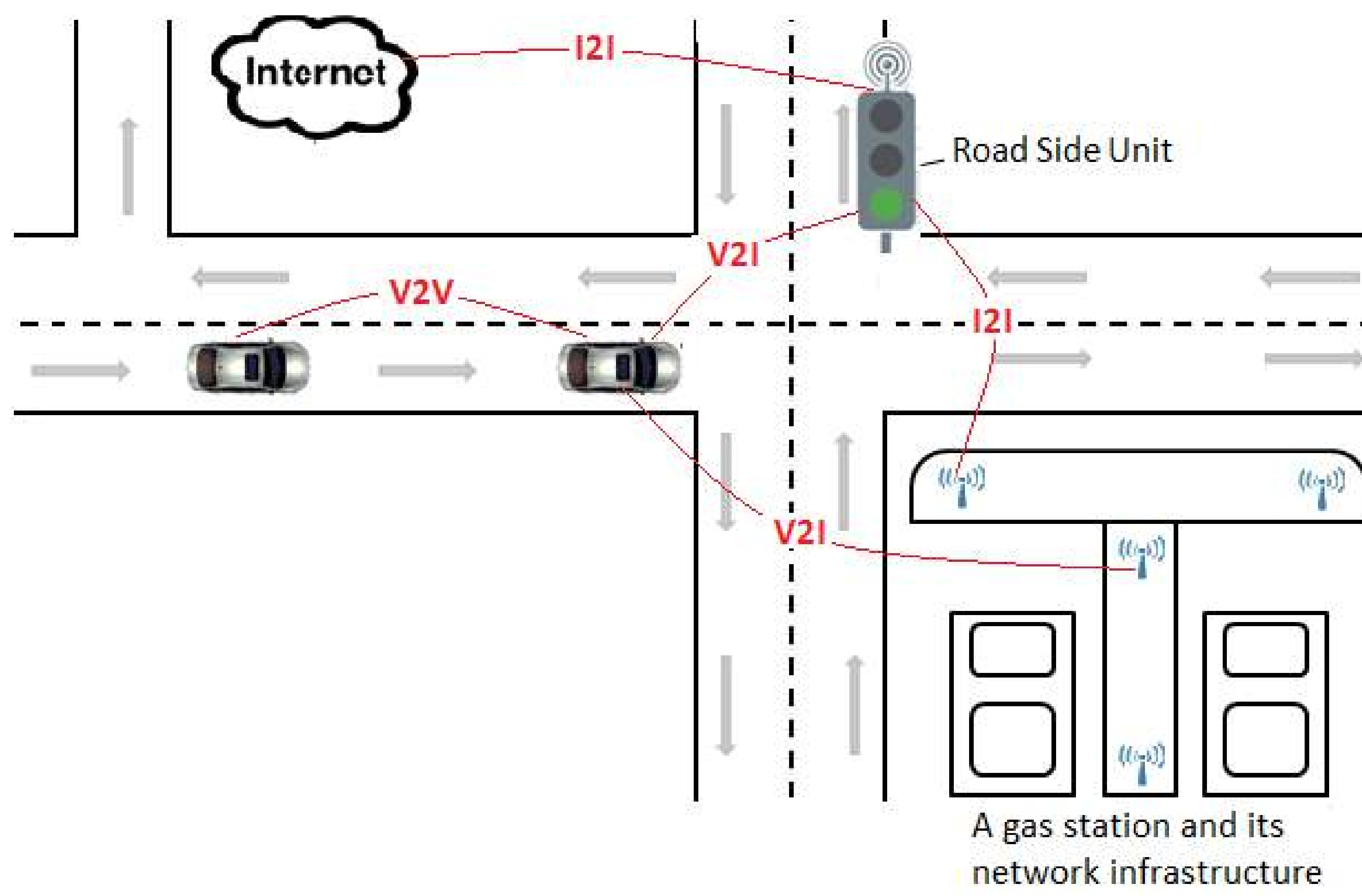
- [1] Alberto Elfes. Using occupancy grids for mobile robot perception and navigation. *Computer*, 6:46–57, 1989.
- [2] Johann Laconte, Christophe Debain, Roland Chapuis, François Pomerleau, and Romuald Aufrère. Lambda-Field: A Continuous Counterpart of the Bayesian Occupancy Grid for Risk Assessment. *Submitted to IROS 2019*.

1. General introduction: 5G networking concept

Apart from more throughput and ultra-low latency communication requirements, the wide vision and revolutionary side of the 5G networks are to enable a **seamless society connection** by bringing together all network actors and elements (e.g. people, things, cities, applications, and data) by 2020 and beyond. With 5G on the horizon, the concept of the collaborative intelligent transportation system (C-ITS) also known as the Internet of Vehicles (IoV) which relies on the coexistence and the integration of heterogeneous communication networking technologies and devices is getting a reality.

2. Our working context: connected and smart cities

The networking environment of IoV which is typically a dense urban environment of connected cities should address several communication scenarios such as Vehicle-To-Vehicle (V2V), Vehicle-To-infrastructure (V2I) or Infrastructure-To-infrastructure (I2I) as illustrated in the figure below. Disseminating information in such environment, imply the usage of various access technologies such as Bluetooth, 802.15.4, 802.11p|ac|ax, LTE-U, 802.11ah, LoRa, Sigfox, LTE-M, NB-IoT, etc.



The information in IoV environment is of various types, from various sources, and for different applications. Applications such as road safety, advanced driving assistance, autonomous vehicles, fluidification/regulation of urban traffic, environmental monitoring for security matters, and so on.

5. Opportunities and Challenges

In a dense urban environment, one can imagine the deployment scenario illustrated in the figure below, where the resources of hotspots having multi-access technology are pooled by other nodes in the vicinity (e.g. connected vehicles, surrounding sensors or mobile users). This deployment scenario implementing a resource mutualization approach would allow to increase the connectivity of the network nodes and avoid harmful interference between the devices through common radio management components within the hotspots. Thus, this would allow to efficiently cohabit the underlying access technologies. Nevertheless, these immediate questions remain open research problems: 1) the appropriate access technologies to deploy within the mutualized hotspots in order to get a maximum of efficiency of the resources. Efficiency, e.g., in terms of satisfaction of latency and throughput requirements of the underlying supported applications. 2) Scenarios (e.g. expected node density, coverage needs) for which to add more such a mutualize hotspots or to add mobility to some of them. Performance evaluation in this context is usually made through computer simulations because of expensiveness and difficulty of field tests. To the best of our knowledge, to date, there is no a platform that models and brings together all the access technologies expected under the 5G umbrella.

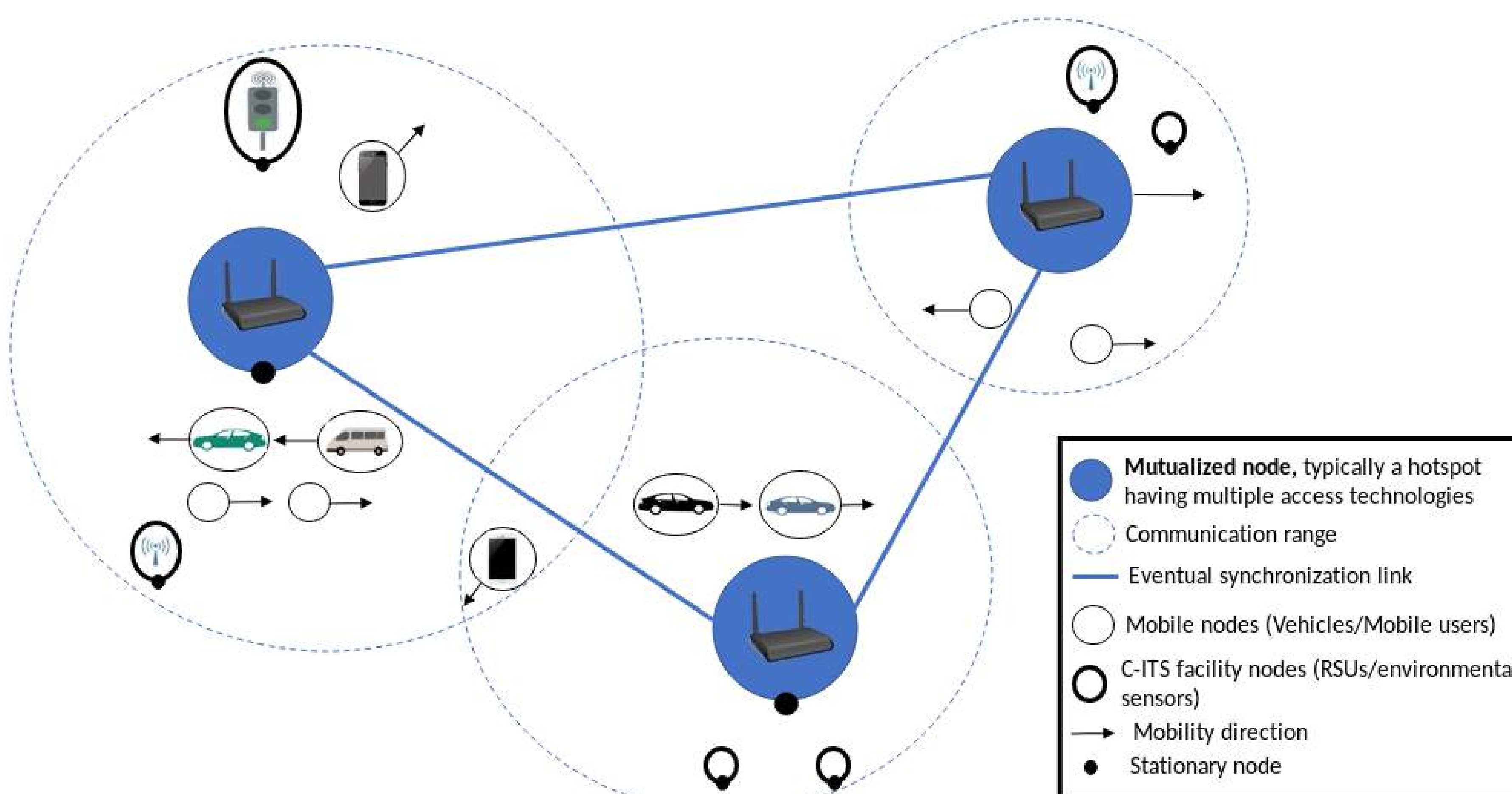


Illustration of a scenario implementing a resource mutualization approach.

3. Issues

In order to coexist, wireless access technologies have to share the scarce and naturally limited radio resource. Hence, appropriate precautions must be taken for a safe, reliable and efficient coexistence of access technologies in IoV environment which have to share very often the limited number of license-free radio bands. Technology standards toward a 5G networked world are typically in place and some deployments even stated. Nevertheless, every access technology can only optimize the usage of the resources (e.g. the radio) in its homogeneous environment and, heterogeneous networking access technologies have to coexist under the 5G umbrella, particularly in the dense urban environment of connected cities. Thus, the challenge is to efficiently cohabit heterogeneous access technologies for IoV applications, without removing the standard aspects of these technologies which guarantee the interoperability of devices.

Spectrum efficiency in 5G networks

4. Our solution approach

To deal with this aspect of wireless access technologies coexistence issue, we rely on a **framework of the mutualization of network resources of a connected city** to efficiently cohabit heterogeneous access technologies in IoV environment. In this framework, the resources are mainly the access devices within the connected vehicles, Road Side Units (RSU), and those of eventual surrounding hotspots, sensors and sensor networks. We reasonably assume that such network resources do not necessarily belong to a single entity. Thus, resource management architecture in this mutualization framework should be decentralized because the deployment of a centralized solution should be practically difficult. This concept of resource mutualization is not completely new in the field of computer networks in general. For example in Internet Exchange Points, many Internet Service Providers mutualize and share the same routing and switching infrastructures for the sake of cost and resource efficiency.

Toward a resource mutualization

Contact

Ali.MAMADOU_MAMADOU@uca.fr

Modelling and control of a collaborative robot for medical echography

Irmella Mélina MOUTSINGA

Supervised by Hélène CHANAL, Flavien PACCOT, Nicolas BOUTON

University Clermont Auvergne, SIGMA Clermont, CNRS, UMR 6602, Institut Pascal, BP 10448, F 63171 AUBIERE



This thesis is subsidized by the Gabonese Government in partnership with Campus France.

Introduction

Echography is a complex medical imaging examination that needs to be performed by a medical expert. It is all the more complex as its interpretation involves both the gesture and the image. Diagnostic errors may occur due to involuntary movements of the patient and / or doctor. In addition, they sometimes suffer musculoskeletal disorders, caused by uncomfortable positions they keep during exams, the frequency is quite high and the relatively long time. A hand-guided collaborative robot can be used to assist the doctor in the practice of his activity. Giving it a more comfortable work platform and increased freedom of movement and allow the positioning of the probe and maintain applied forces.

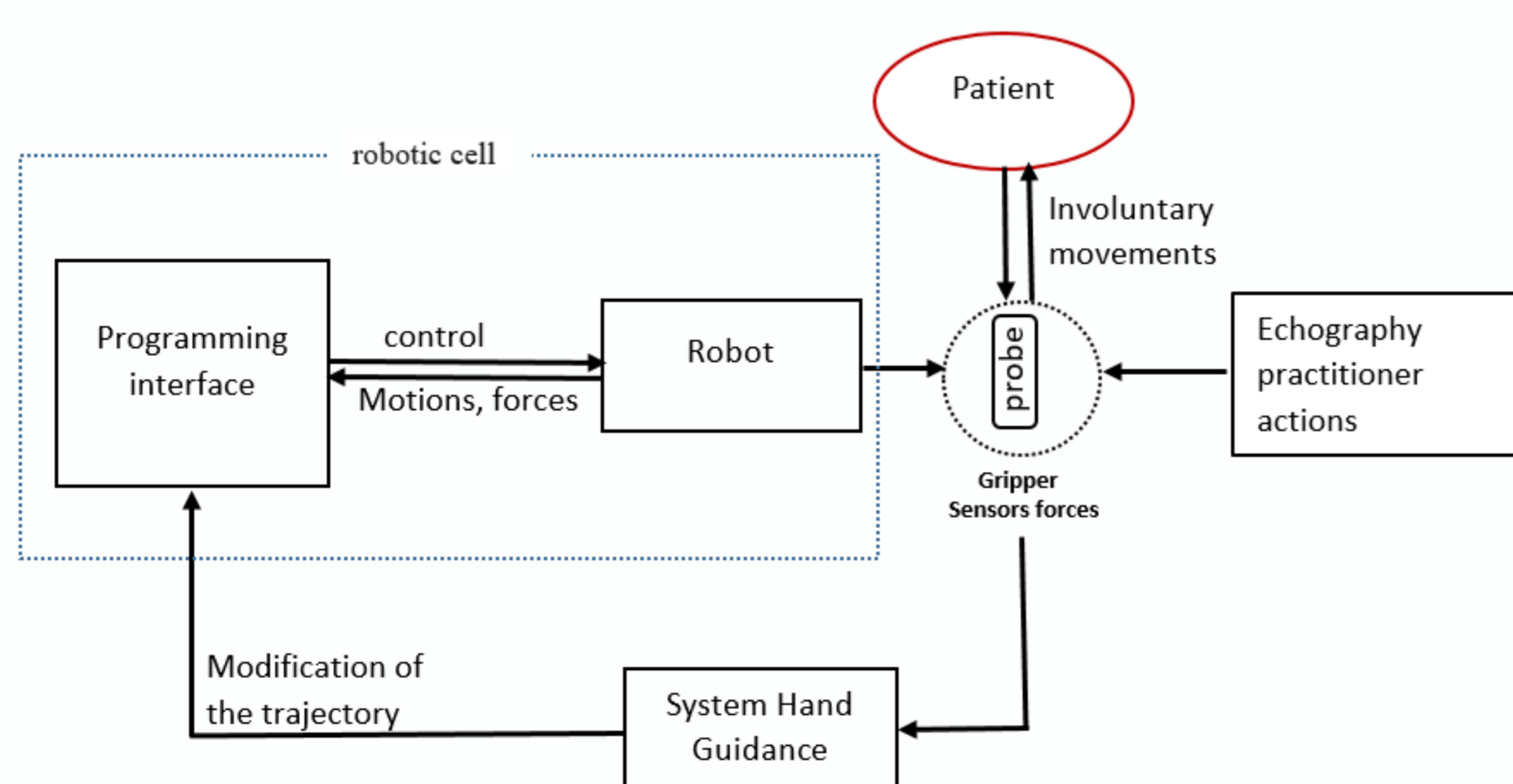


Figure1: The versatile robot Kuka for assistance tasks in the health sector



Problematics

- Adapt to the collaborative robot Staubli TX2 60, an intelligent gripper allowing the hand guidance of the robot by the doctor;
- Develop a control allowing a flexible movement of the robot and self-compensation of physiological movements of the patient;



Methodology

- Modelling:** Geometric, kinematic and dynamic modelling of the robot. the dynamic model takes into account the forces applied at the level of the effector and the friction of the actuators;
- Design:** Design a gripper and instrument it with force sensors;
- Control:** Development of a control strategy for the robot guidance, the maintenance of efforts and the compensation of parasitic movements.

Results

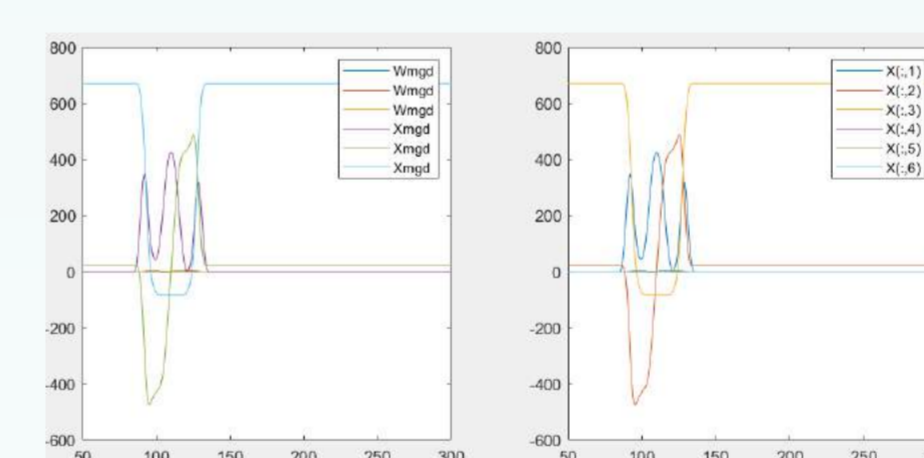
We are currently modelling TX2 60

Geometric model

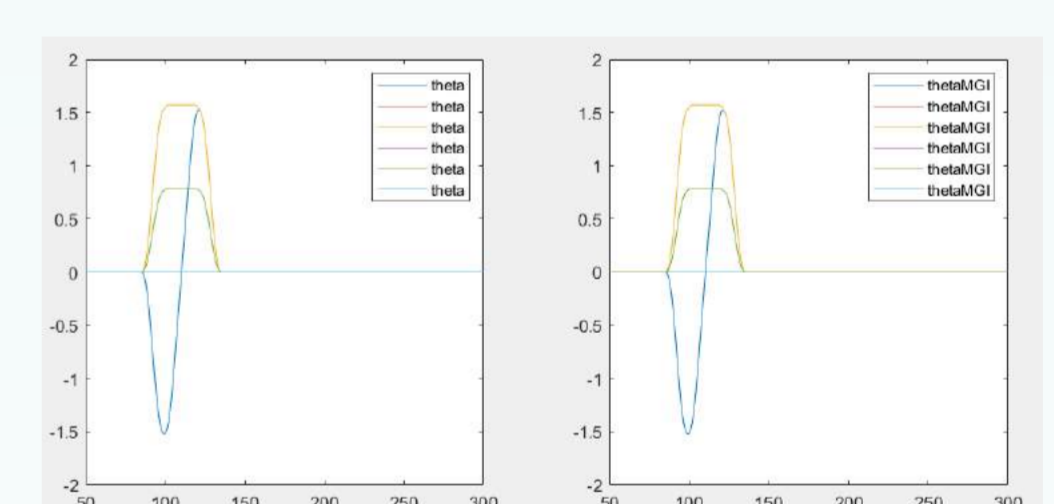
$$X = \text{MGD}(q, \xi)$$

$$T = {}_0 T^1(q_1) {}_1 T^2(q_2) {}_2 T^3(q_3) {}_3 T^4(q_4) {}_4 T^5(q_5) {}_5 T^6(q_6) T^S$$

$${}_6 T^S = \begin{bmatrix} \cos\theta_s & -\sin\theta_s & 0 & d_s \\ \cos\alpha_s \sin\theta_s & \cos\alpha_s \cos\theta_s & -\sin\alpha_s & -r_s \sin\alpha_s \\ \sin\theta_s \sin\alpha_s & \cos\theta_s \sin\alpha_s & \cos\alpha_s & r_s \cos\alpha_s \\ 0 & 0 & 0 & 1 \end{bmatrix}$$

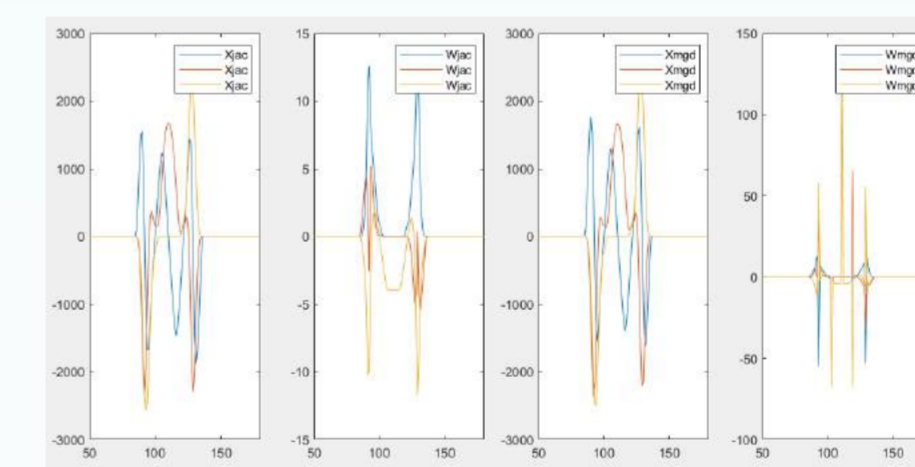


$$q = \text{MGI}(X, \xi)$$



Kinematic model

$$J_i(q) = \frac{dX}{dq_i}$$



Dynamic model

$$\Gamma = A(q)\ddot{q} + C(q, \dot{q})\dot{q} + Q(q) + F_s \text{sing}(\dot{q}) + F_v \dot{q} + J^T f_e$$

Prospect

The work on model validation is continuing. The identification of dynamic parameters allowing the development of external control for trajectory generation and dynamic modelling under Matlab-Simulink or Adams View Student is the next step.

Bibliography

- [Le Flohic, 2015] Le Flohic, Julien. *Vers Une Commande Basee Modele Des Machines Complexes: Application Aux Machines-Outils et Machines d'essais Mecaniques*. 2015, p. 165;
- [Salcudean et al., 2002] Salcudean, S. E., et al. *A Robot System for Medical Ultrasound*. no. December 2002, 2002;
- [Khalil and Dombre, 1999] Khalil, Wisama, and Etienne Dombre. *Modélisation et Commande Des Robots*. HERMES, 1999;

Introduction

Recently, much progress has been made to bring 3D-PTV outside the laboratory to apply in real-world settings; however, there are many challenges yet to be overcome. The limited measuring volume of the 3D-PTV system is one important challenge, which needs to be extended to cover all the measuring volume [1]. In buildings and in large areas such as conference halls, clean rooms, inside the plane cabin, large-scale 3D-PTV could play a significant role in order to predict the trajectory and velocity of the air and airborne pollutants.

➤ Why large scale PTV is crucial?

1. Energy: saving energy
2. Environmental efficiency: thermal comfort, predicting airborne pollutants



Clean room



Inside a plane cabin



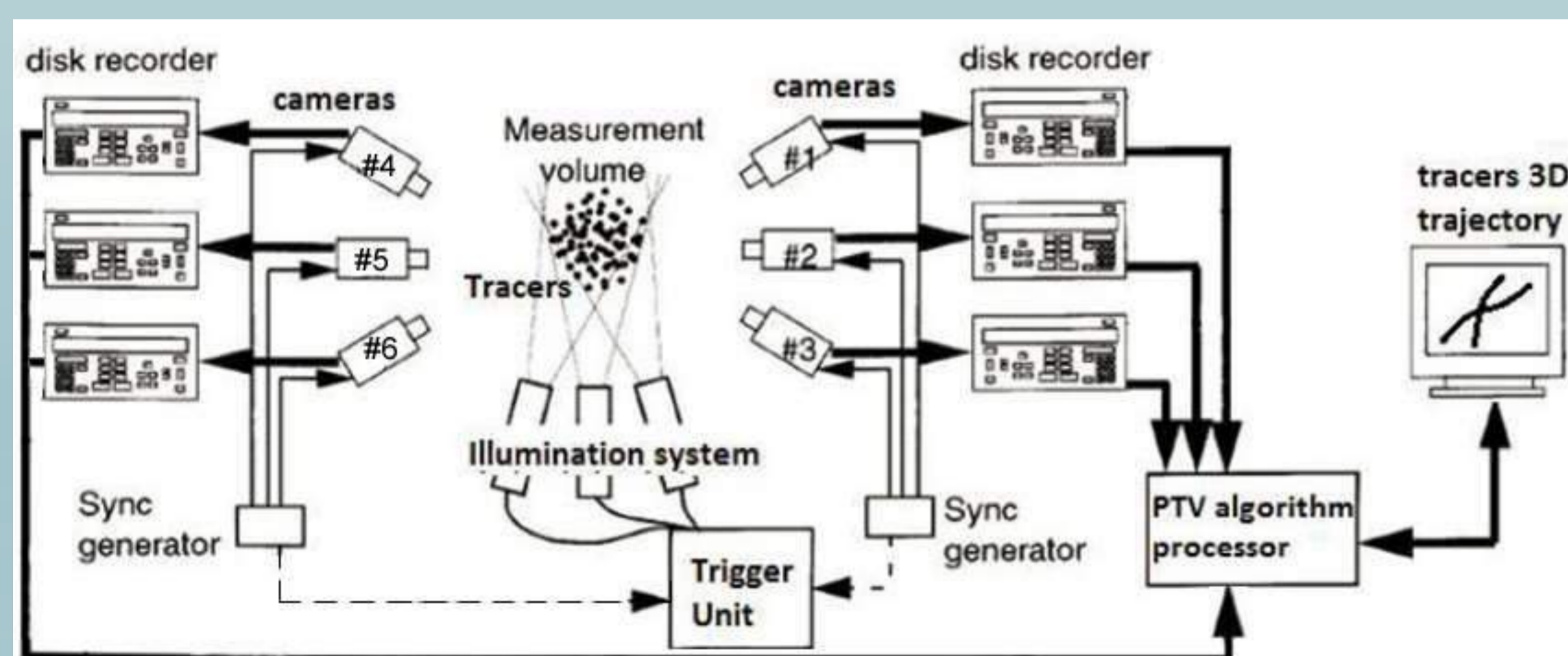
Conference hall



Inside the home

Methods

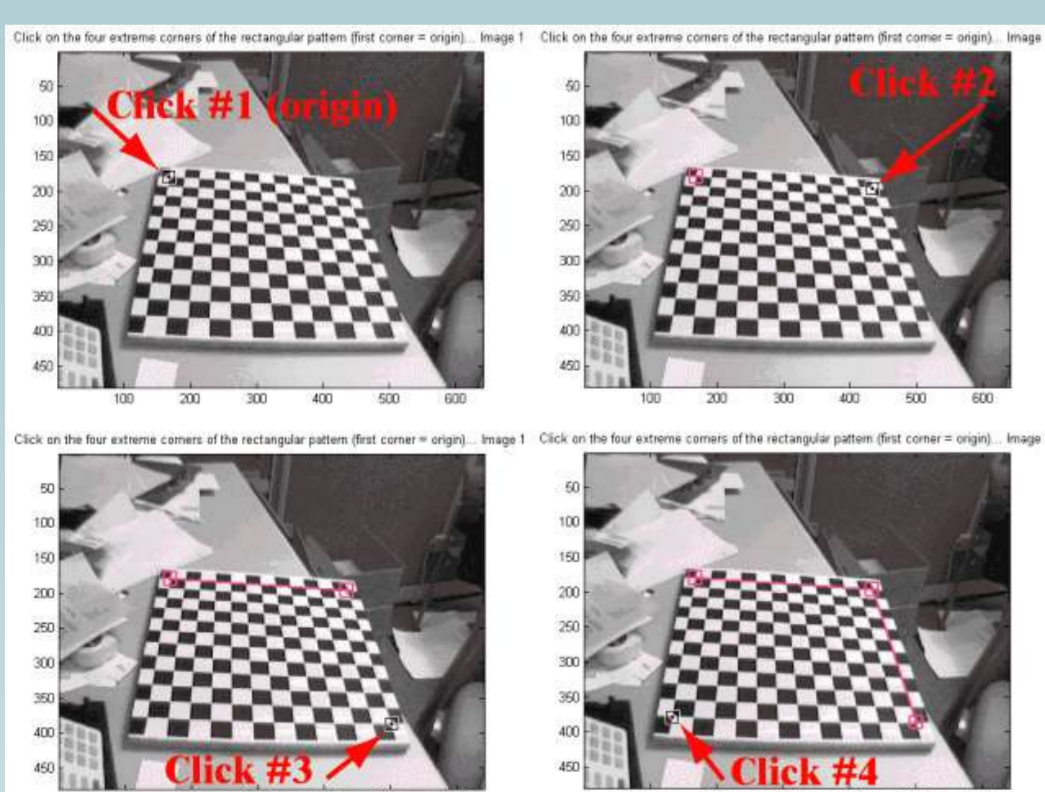
- Two 3D-PTV systems are being considered.
- Each system is composed of at least 3 cameras
- The cameras should be time synchronous



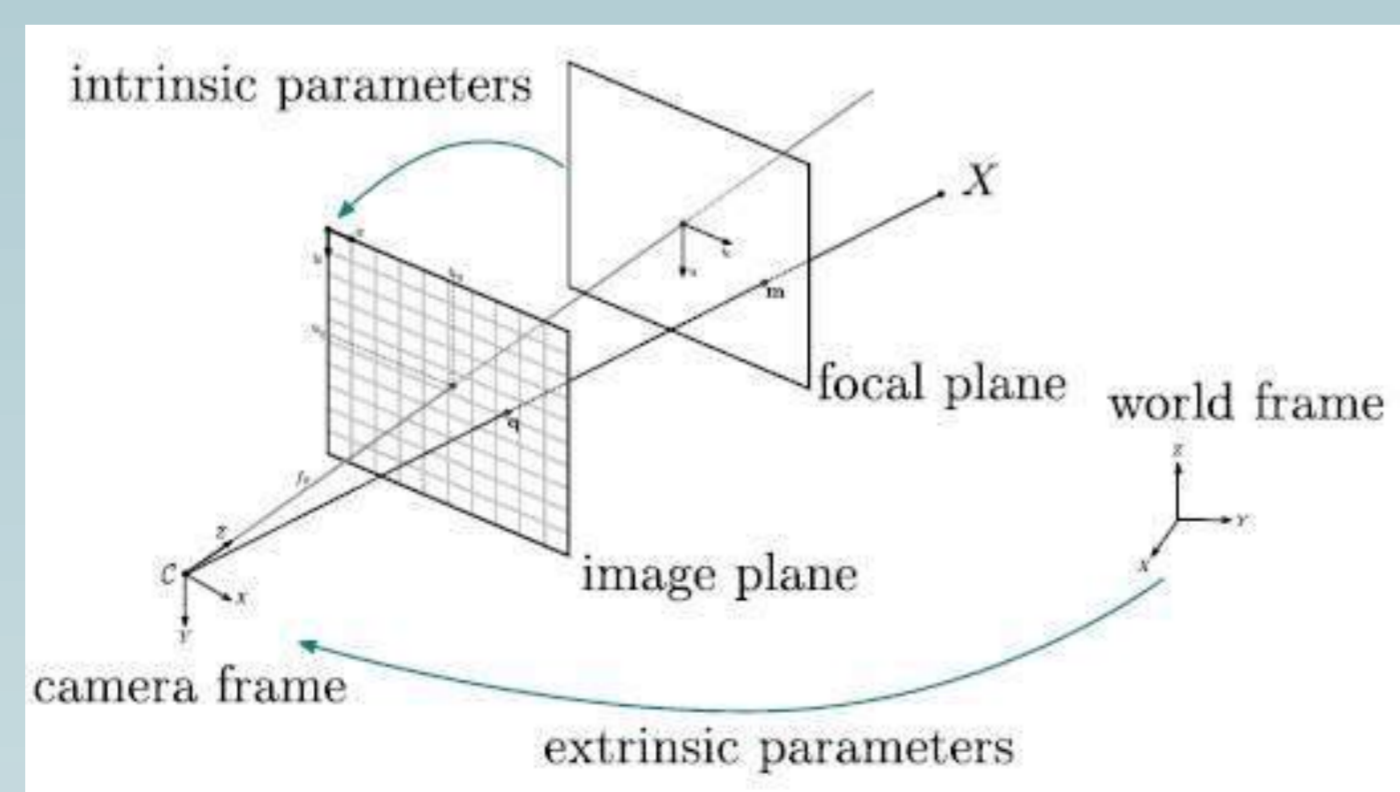
Schematic representation of the experimental setup

The main procedures performed are as follows:

- Multiple Camera Calibration: separately calculating intrinsic and extrinsic parameters using the pinhole camera model [2]
- The calibration method proposed by Zhang [3] and implemented in Matlab by Bouguet [4] in a Camera Calibration Toolbox.

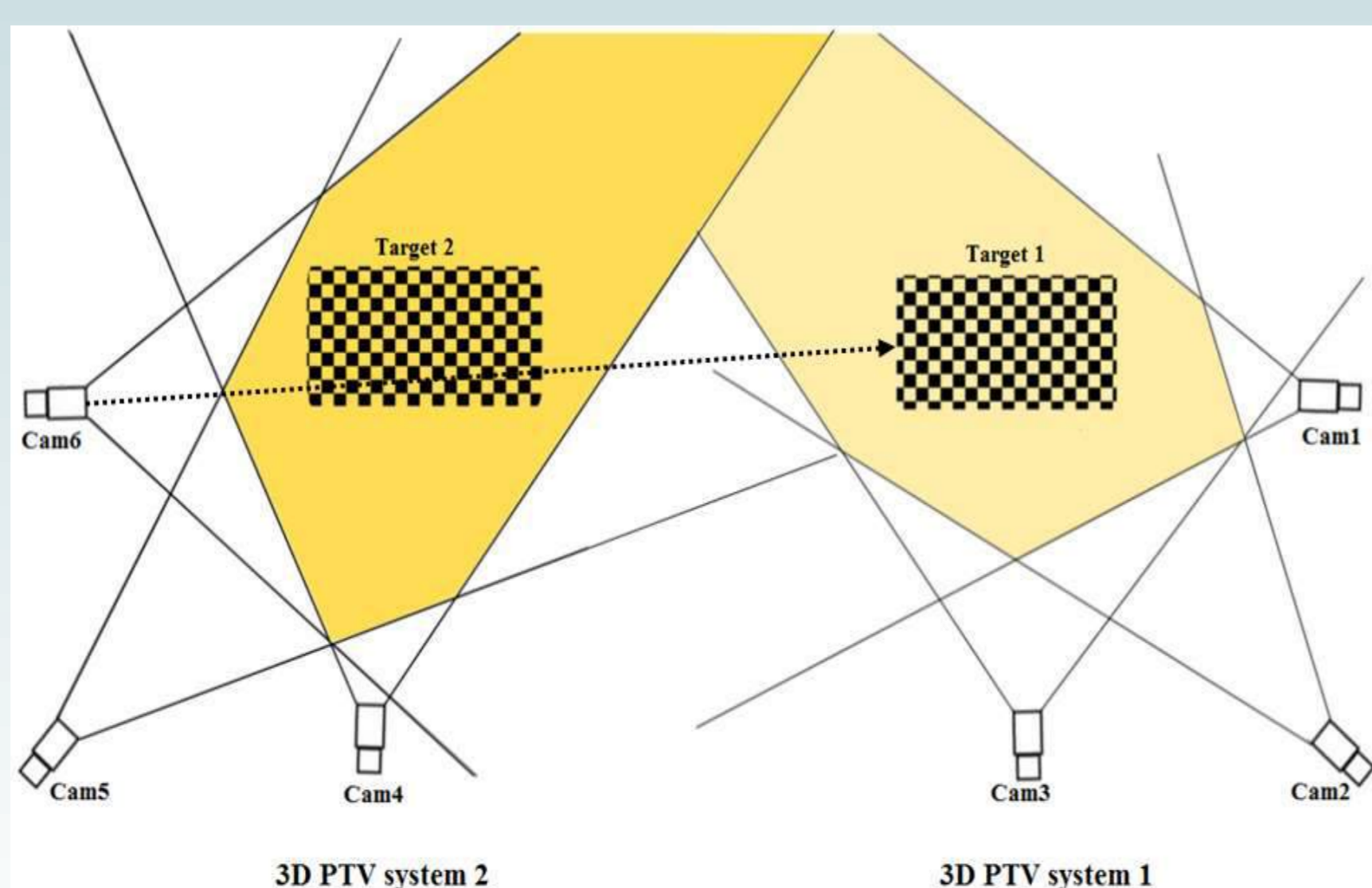


Calibration toolbox



Pinhole camera model

- At least one camera should have a view over the calibration target of the other system.



3D PTV system 2

3D PTV system 1

Results

- Transforming camera i coordinates system XX_C into the calibration target coordinate system XX :

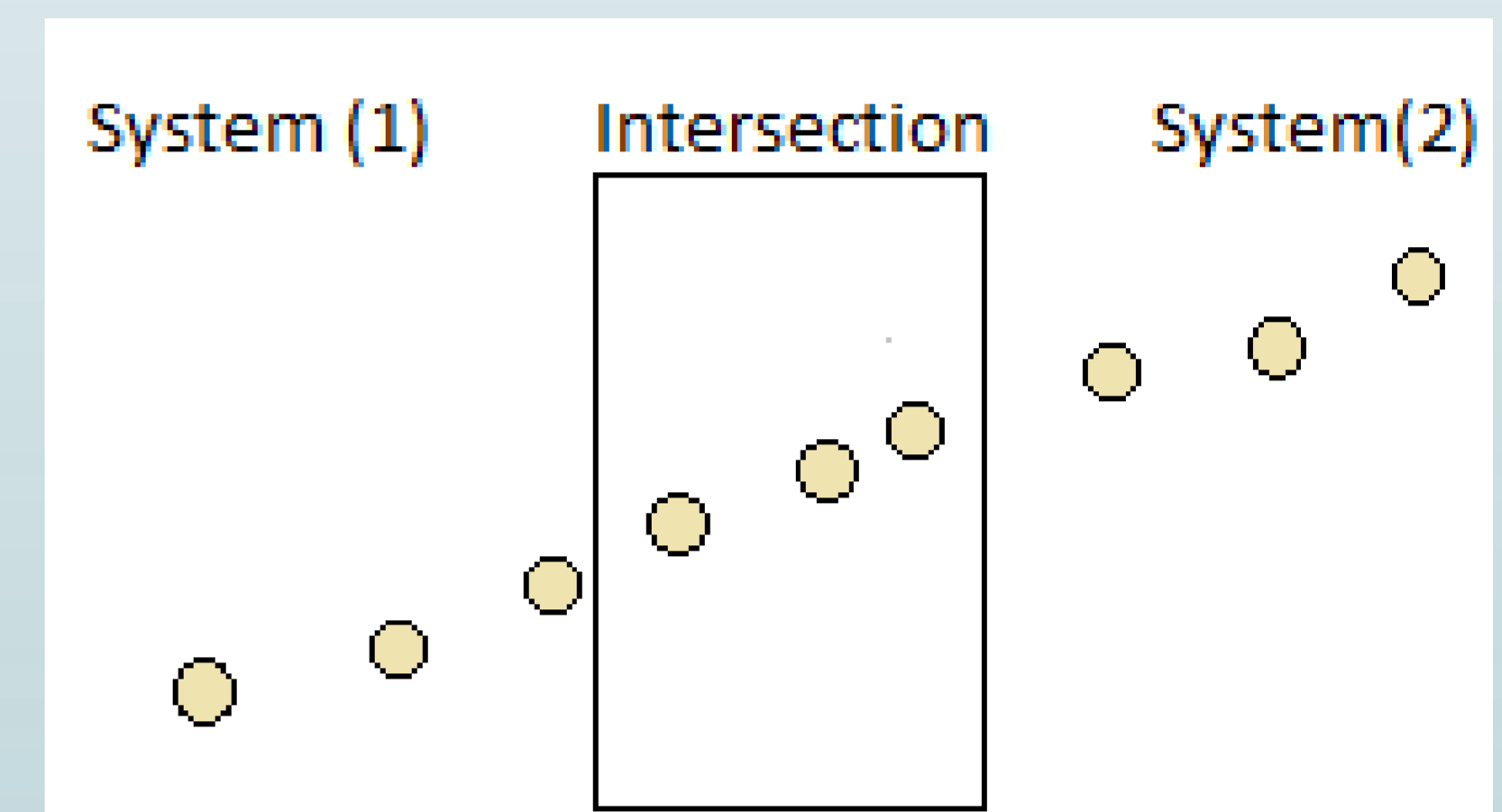
$$XX_{Ci}^n = R_i^n \cdot XX^n + T_i^n$$

- If camera i of system n sees the calibration target of system m , then the relationship between XX_{Ci}^n and XX^m can be written as:

$$XX_{Ci}^n = R_i^m \cdot XX^m + T_i^m$$

- The relationship between XX^m and XX^n can be deduced as:

$$XX^n = [R_i^n]^{-1} [R_i^m \cdot XX^m + T_i^m - T_i^n]$$



A non-zero intersection in the 3D fields observed by the two adjacent 3D-PTV systems should be assumed to establish a link between the trajectories.

- Two 3D coordinates of the two 3D-PTV systems are considered to be "similar", meaning that they correspond to the same particle, if the Euclidean distance between the 3D coordinates, noted below as A and B , is lower or equal than a threshold value s :

$$\|A - B\|_2 = \sqrt{(x_A - x_B)^2 + (y_A - y_B)^2 + (z_A - z_B)^2} \leq s$$

- ❖ s can be also specified through a physical parameter, such as the average particle diameter or according to the experiment accuracy.

- If the similarity criterion is valid for at least three consecutive instants, then the algorithm proceeds to link the trajectories related to those particles, $XX^{(1)}$ and $XX^{(2)}$. The algorithm, therefore, performs a comparison of the 3D coordinates particle by particle and at each time step.

	$XX^{(1)}$	$XX^{(2)}$
t_1	OK	-
t_2	OK	-
t_3	OK	-
t_4	OK \approx	\approx OK
t_5	OK \approx	\approx OK
t_6	OK \approx	\approx OK
t_7	-	OK
t_8	-	OK
t_9	-	OK

Conclusions and Future Studies

- A method is proposed by using multiple 3D-PTV systems applicable for large enclosures such as conference rooms. Several 3D-PTV systems located next to each other are utilized to cover the entire volume measured.
- The calibration of the cameras is described to define a common 3D coordinate system for the particle trajectories.
- An algorithm for linking the particle trajectories is developed based on a similarity criterion.
- The performance of this algorithm will be investigated using the experimental data of two 3D-PTV systems.
- In order to reduce the computational time, a parallelized programming method will be utilized by the aid of FPGAs as a future study.

Bibliography

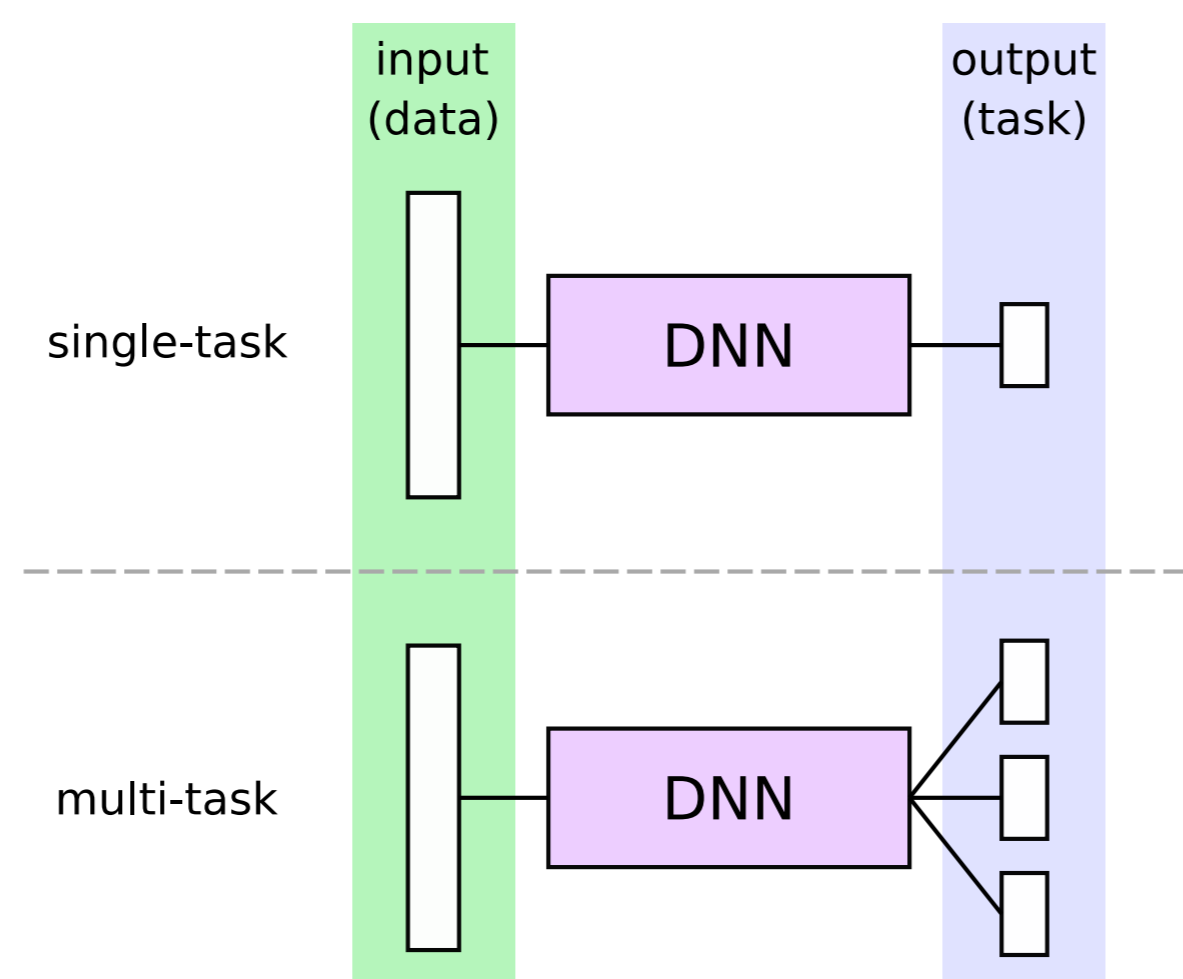
1. Biwole, P.H., Yan, W., Zhang, Y. and Roux, J.J., 2009. A complete 3D particle tracking algorithm and its applications to the indoor airflow study. *Measurement Science and Technology*, 20(11), p.115403.
2. Heikkila, J. and Silven, O., 1997, June. A four-step camera calibration procedure with implicit image correction. In *cvpr* (Vol. 97, p. 1106).
3. Zhang, Z., 1999, September. Flexible camera calibration by viewing a plane from unknown orientations. In *Iccv* (Vol. 99, pp. 666-673).
4. Bouguet, J.Y., 2004. Camera calibration toolbox for Matlab. http://www.vision.caltech.edu/bouguetj/calib_doc/index.html.

Objectives

1. Develop a **multi-task** Neural Network for autonomous vehicle **visual perception** (monocular video).
2. Devise a way to add or remove tasks on the fly without training the full network all over again.
3. Extend the application to **multi-sensor** input.

Introduction

- ▶ Multi-Task Learning (MTL) [1] encompasses the idea that similar computational tasks in deep learning should at one point share some kind of common latent representation, in a more or less pronounced fashion, depending on their relatedness.



- ▶ Learning such common representation in a single network can offer several advantages :
 - ▷ It can reduce the total size of the networks as well as the computational cost, as a portion of the weights is shared.
 - ▷ Various features can be useful to some tasks while being easier to learn by others.
 - ▷ The learnt latent representation generalise better.
 - ▷ Tasks can be specifically added to incite the network to focus on a wanted data feature.
- ▶ In autonomous driving, vision tasks such as obstacle and traffic signs detection and tracking, lane marking detection, scene segmentation, etc., occur in the same space. It is intuitively clear that they are related to some extent.

Problematic

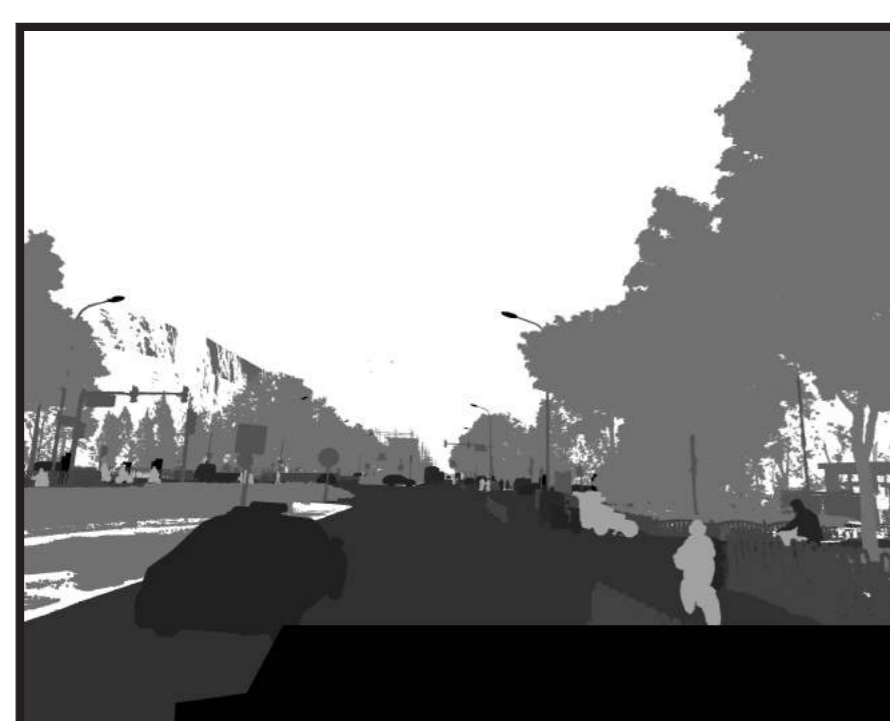
- ▶ How to select which tasks to share, and at which point ?
- ▶ Which architecture would be able to adapt to additional tasks and enable to train only a part of the network each time ?

Dataset

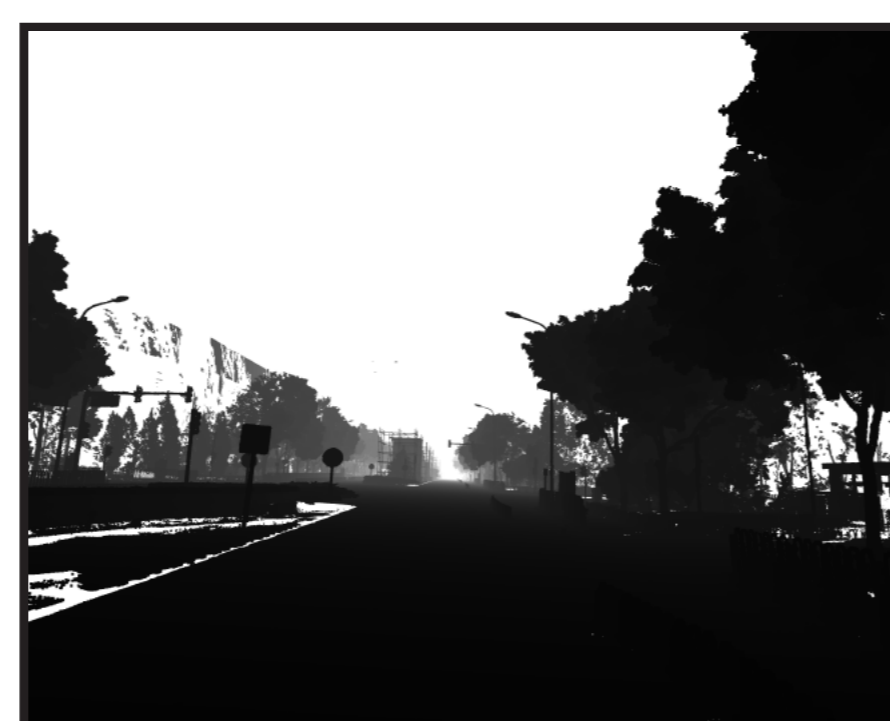
- ▶ Trials will mainly be done over Baidu's **ApolloScope** dataset, that was chosen because it exhibits some uncommon and valuable characteristics compared with other existing collections :
 - ▷ It is densely annotated, both spatially and temporally
 - ▶ Per pixel labels are given for each frames of video sequences
 - ▷ labels cover several interesting tasks :
 - ▶ Semantic segmentation
 - ▶ Instance segmentation
 - ▶ Lane marking detection
 - ▶ Depth estimation
 - ▶ Pose estimation



Color image



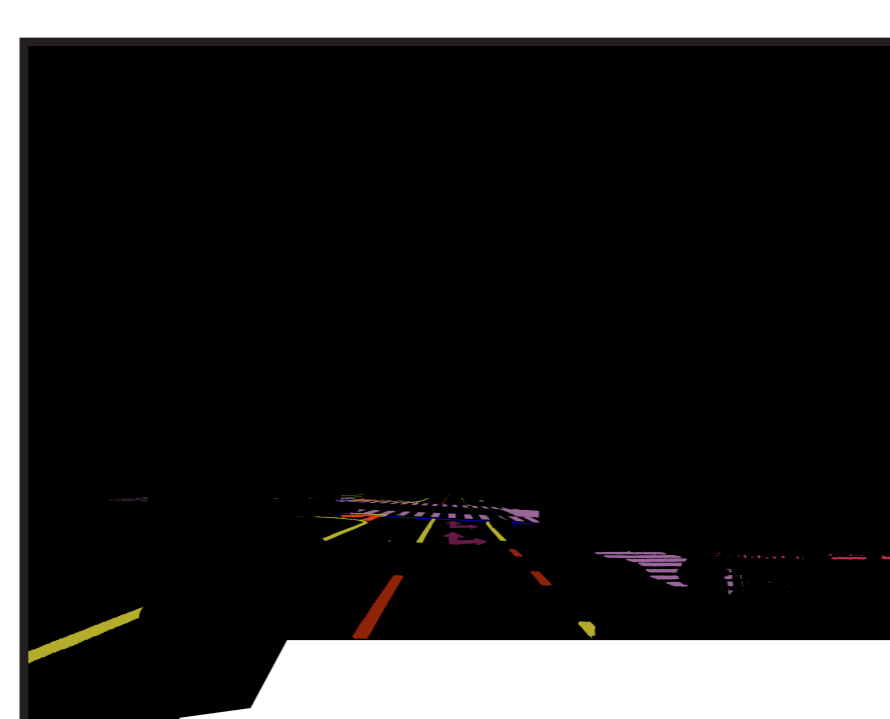
Semantic segmentation



Depth map



Instance segmentation



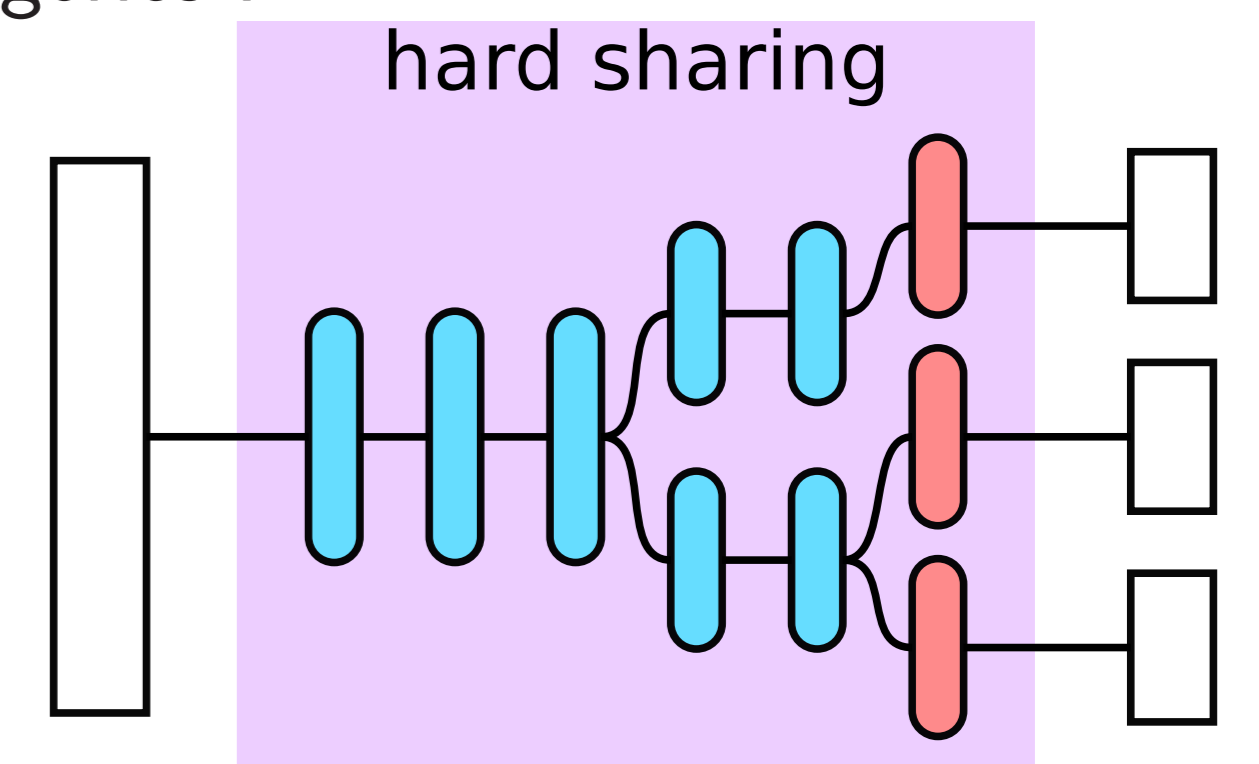
Lane markings

Methods

- ▶ MTL methods generally fit into two categories :

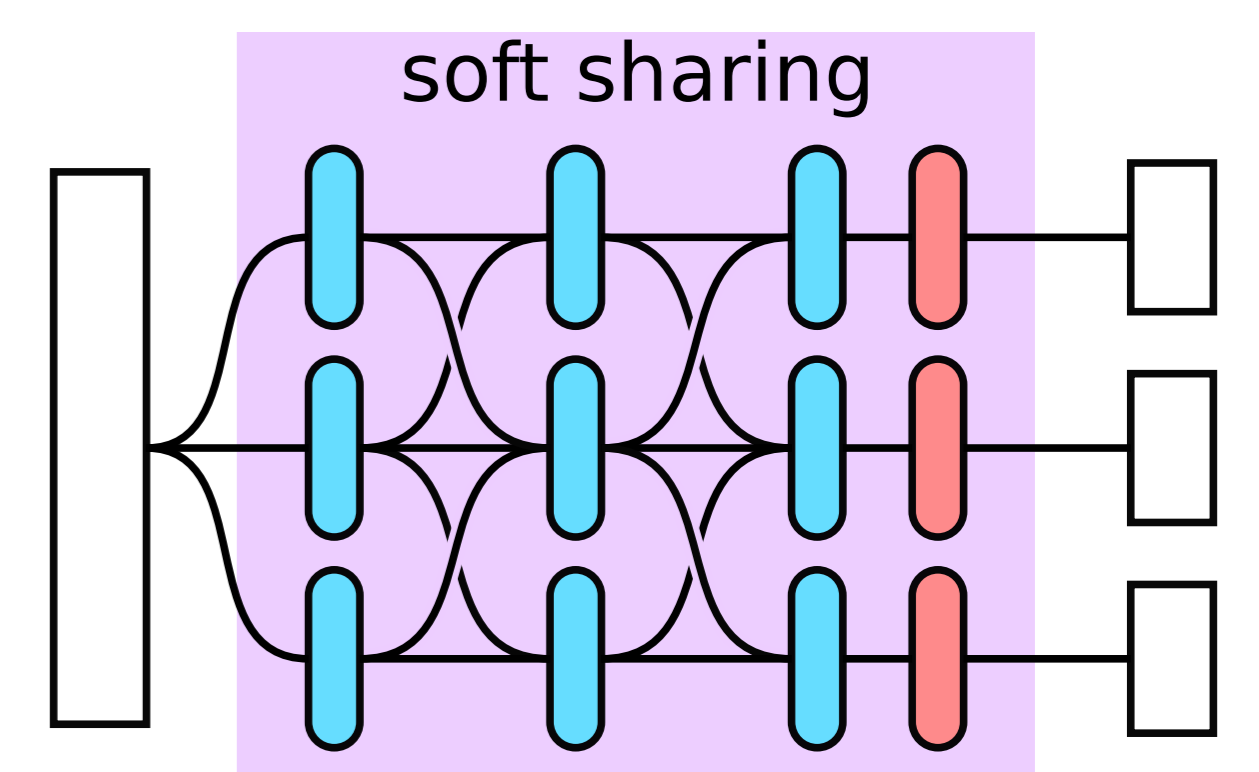
▶ Hard parameter sharing

It is the most straightforward and obvious approach to MTL, starting from a common core and branching progressively to each task. the problem is to find where to split.



▶ Soft parameter sharing

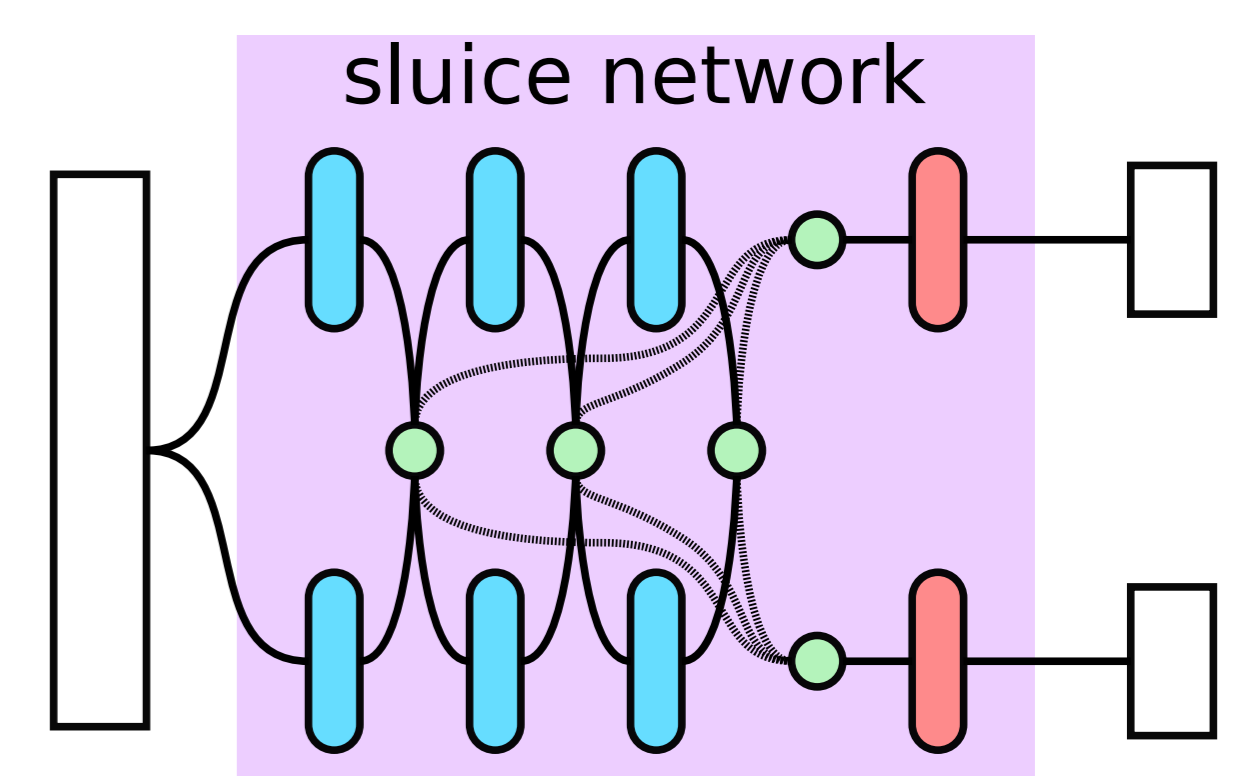
In this kind of configuration, each task retain its own specific network, but sharing happens between layers. While losing the sparing of weights, it is more flexible than hard sharing. The challenge is to define how the sharing is made.



- ▶ Traditionally, tasks are shared following an hand-crafted scheme, chosen *ad hoc* for a peculiar task set. Thus, some work has been done toward the automation and optimisation of multi-task network architectures. The difficulty lies primarily in the very large space of structures to explore.

▶ Sluice networks [2] are an attempt

at unifying previous approaches with a meta-architecture, adding linear combinations with learnable coefficients of every task at each layer in a soft sharing structure, and showing how other methods can emerge depending on the learnt coefficients, including hard parameter sharing.



- ▶ **Task taxonomy** methods [3] use a computational metric to assess tasks affinity and cluster them in a hard parameter sharing fashion.

- ▶ **Soft layer ordering** [4] tries to explore the possibilities that arise when breaking the assumption that all tasks must use the shared layers in the same order, by allowing each task to learn and use its own sequence.

Conclusion

- ▶ One of the thesis' objectives being to have a modular network, hard parameter sharing approaches are quite impractical, since there is very little space for learning when adding a new task. On the other hand, soft sharing techniques linearly grow in size with the number of tasks and can become an hassle when embedding the network in a mobile platform.
- ▶ The state of the art seems devoid of modular approaches to multi-task neural networks, Therefore it could be a future contribution if it is achieved.
- ▶ Extending the method to use multiple sources of information as input (multi-sensor) will be the last goal.

References

- [1] R. Caruana. "Multitask Learning". In: *Machine Learning* 28 (July 1997). DOI: 10.1023/A:1007379606734.
- [2] S. Ruder et al. "Latent Multi-task Architecture Learning". In: *arXiv:1705.08142 [cs, stat]* (Nov. 2018).
- [3] S. Vandenhende et al. "Branched Multi-Task Networks: Deciding What Layers To Share". In: *arXiv:1904.02920 [cs]* (Apr. 2019).
- [4] E. Meyerson and R. Miikkulainen. "Beyond Shared Hierarchies: Deep Multi-task Learning through Soft Layer Ordering". In: *arXiv:1711.00108 [cs, stat]* (Feb. 2018).

Contact

- ▶ trong-lanh.nguyen@safrangroup.com
- ▶ t-lanh.nguyen@etu.uca.fr

Introduction

➤ What is a mobile manipulator ?



Manipulator

Mobile

Mobile manipulator

➤ Interest:

- No limit in workspace → Similar tasks can be realized everywhere
- High redundancy degree → Several tasks can be realized simultaneously
- System association → One task can be realized by several mobile manipulators

➤ Exemple of application:



Vegetable picking

Weeding

Deformable objects transport

➤ Thesis objectives:

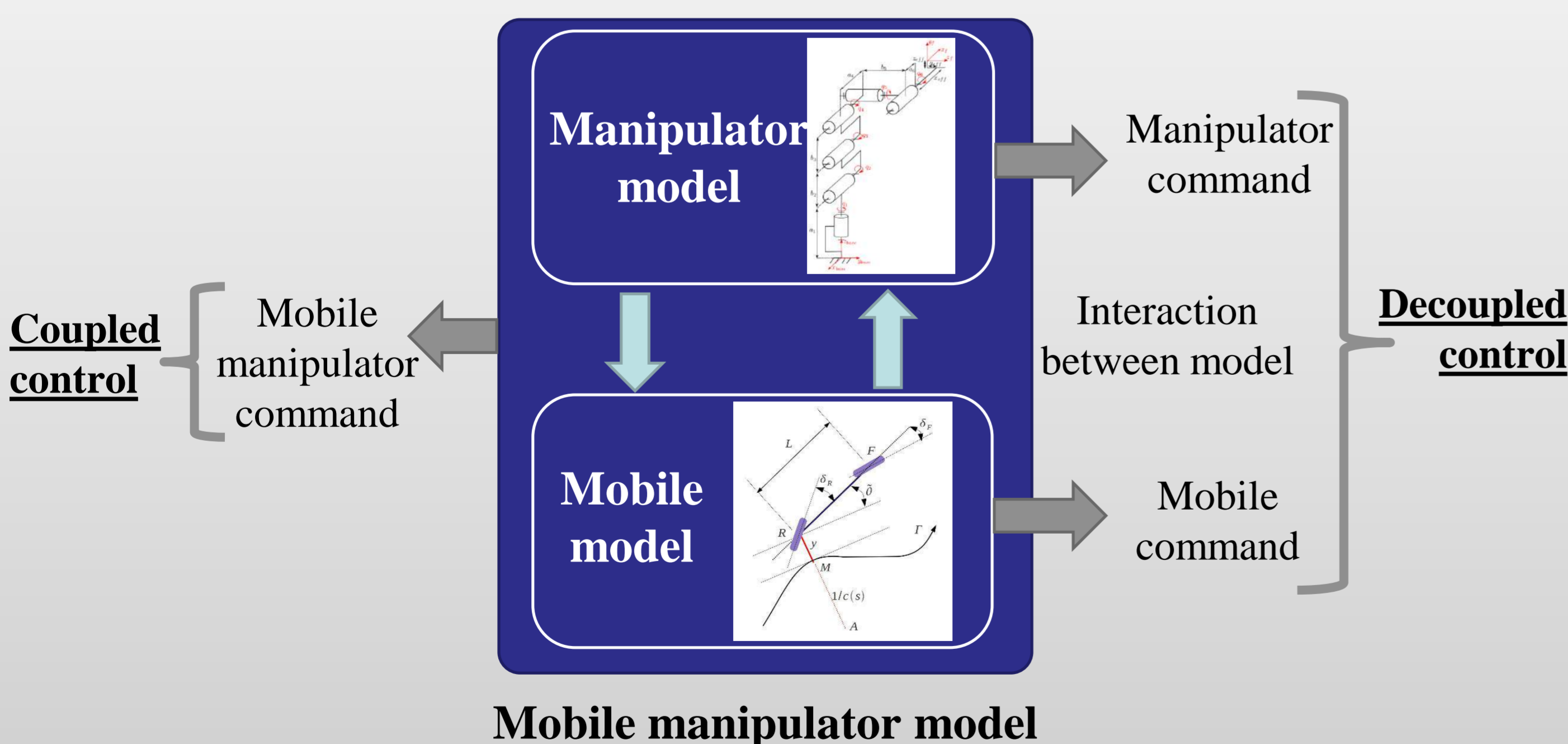
- Coordinated control between manipulator and platform for grasping deformable object.
- Optimize manipulator positionment and workspace around the object interest using redundancy.

➤ Scientific questions:

- How to coordinate motion between manipulator and platform to ensure precision of the task and stability of the system, with sliding and irregularity of the field ?
- How to adapt motion of the manipulator and counterbalance dynamic induced by object deformation ?
- How to use high redundancy degree to perform multi-criteria optimization ?

Methods

➤ Choice of model to control mobile manipulator:

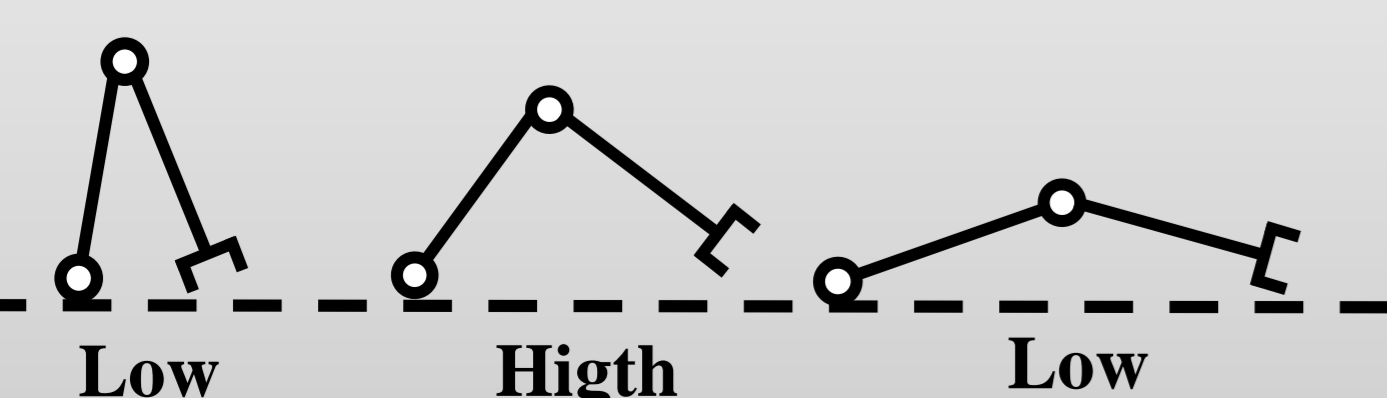


Mobile manipulator model

➤ Choice of optimization criterion to control mobile manipulator :

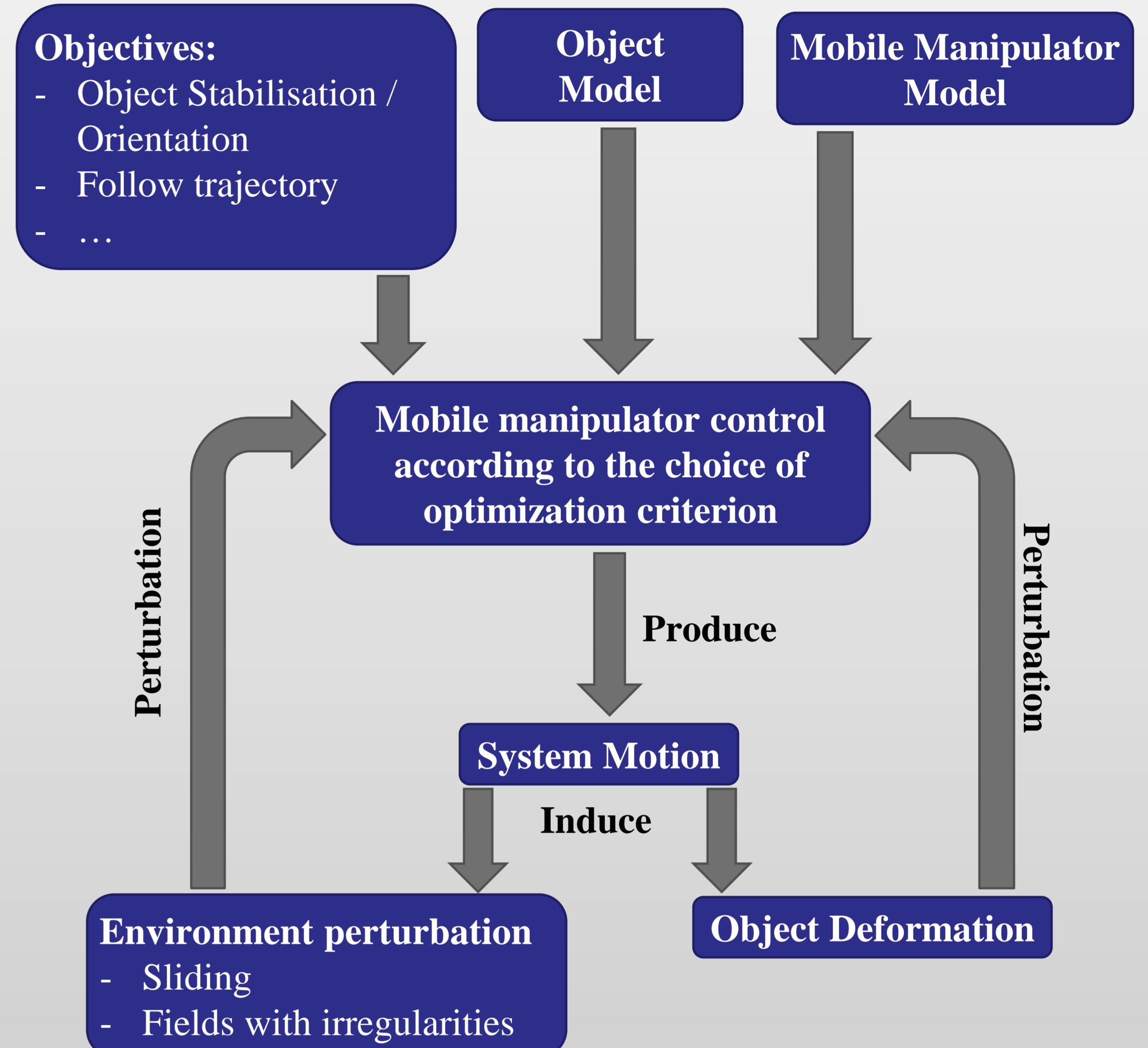
- Stability
- Manipulability
- Speed/Torque distribution
- Limit joint position
- ...

Ex : Manipulability⁽¹⁾

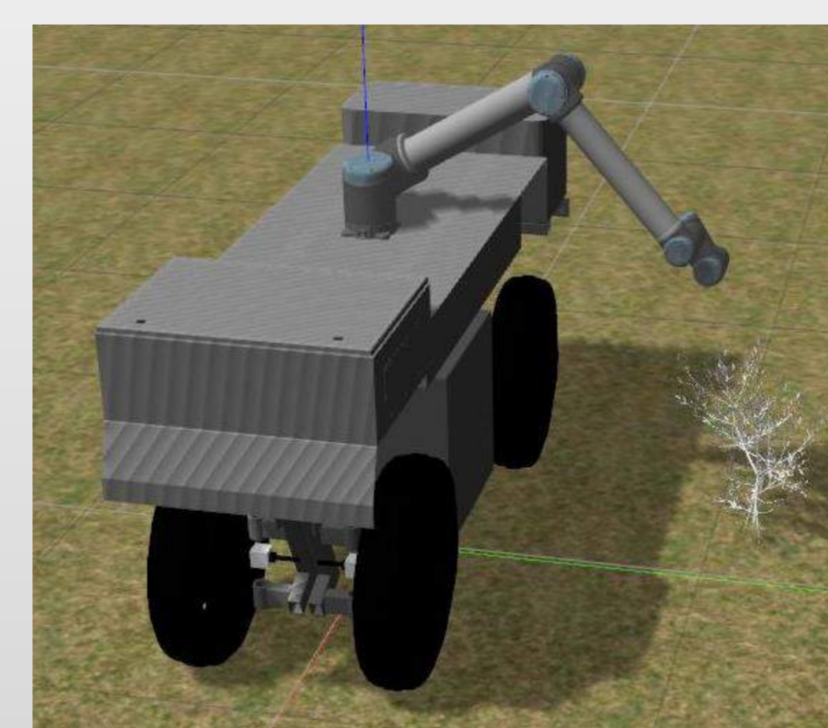


⁽¹⁾ Tsuneo Yoshikawa. Manipulability of Robotic Mechanisms. The International Journal of Robotics Research, 4(2) :3-9, June 1985.

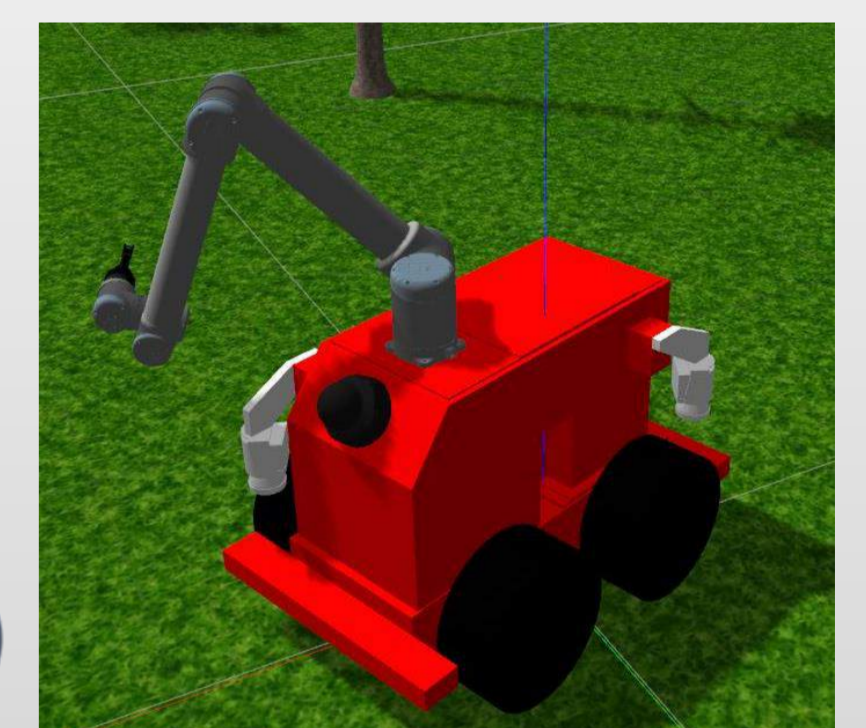
➤ Control Scheme



➤ Method evaluation in simulation:



- Adap2E (IRSTEA)
- Campero (IRSTEA/Institut Pascal)



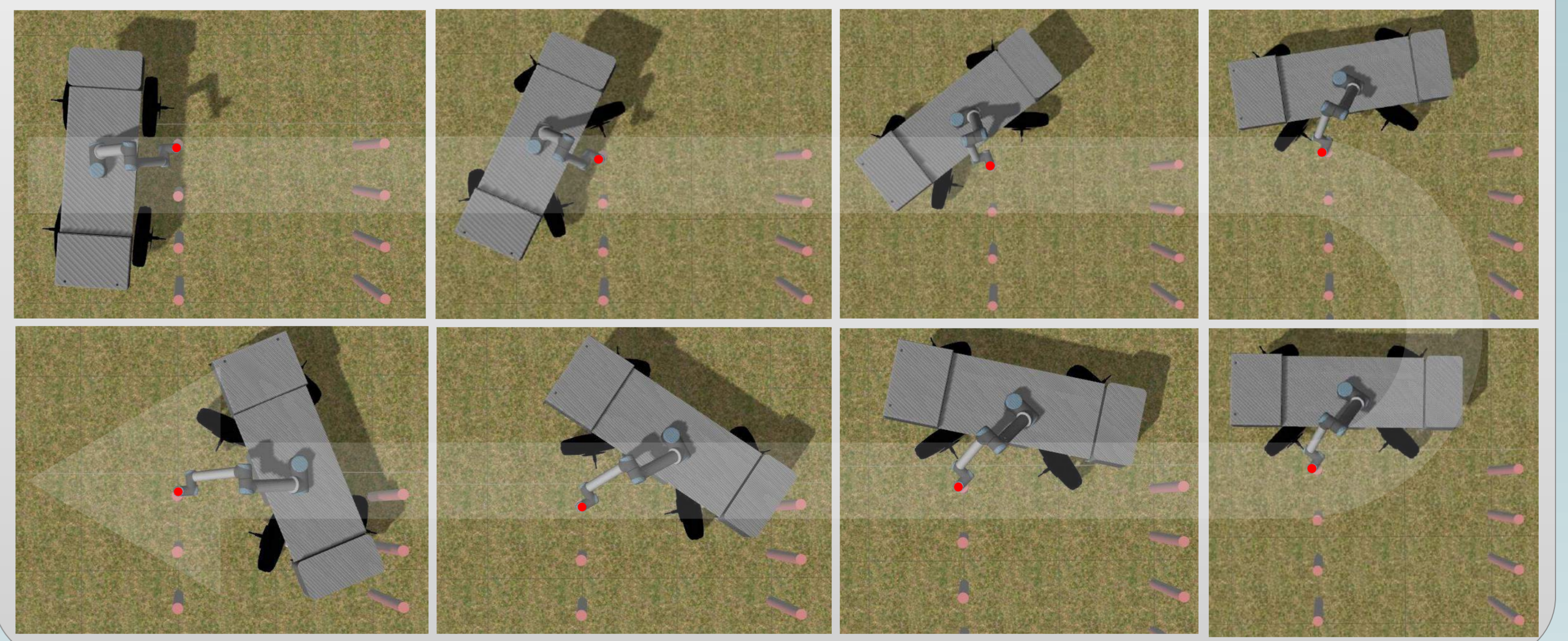
ROS

➤ Method evaluation on real platform for future test

Results

➤ First application of this scheme to demonstrate coordination:

Case : Counterbalance motion of the platform on manipulator to stabilise effector at one point in space. No perturbation was considered. Mobile has been driven manually.



Conclusions

➤ Result:

- First result on coordinated motion between mobile and manipulator with decoupled model.

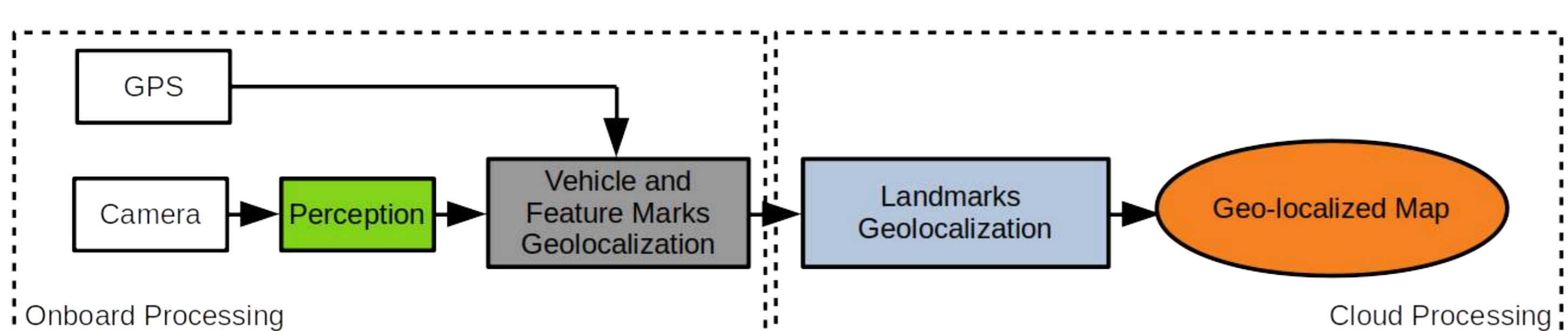
➤ Next step:

- Take into account irregularity of the field(roll and pitch axes).
- Command with unified model for mobile manipulator.

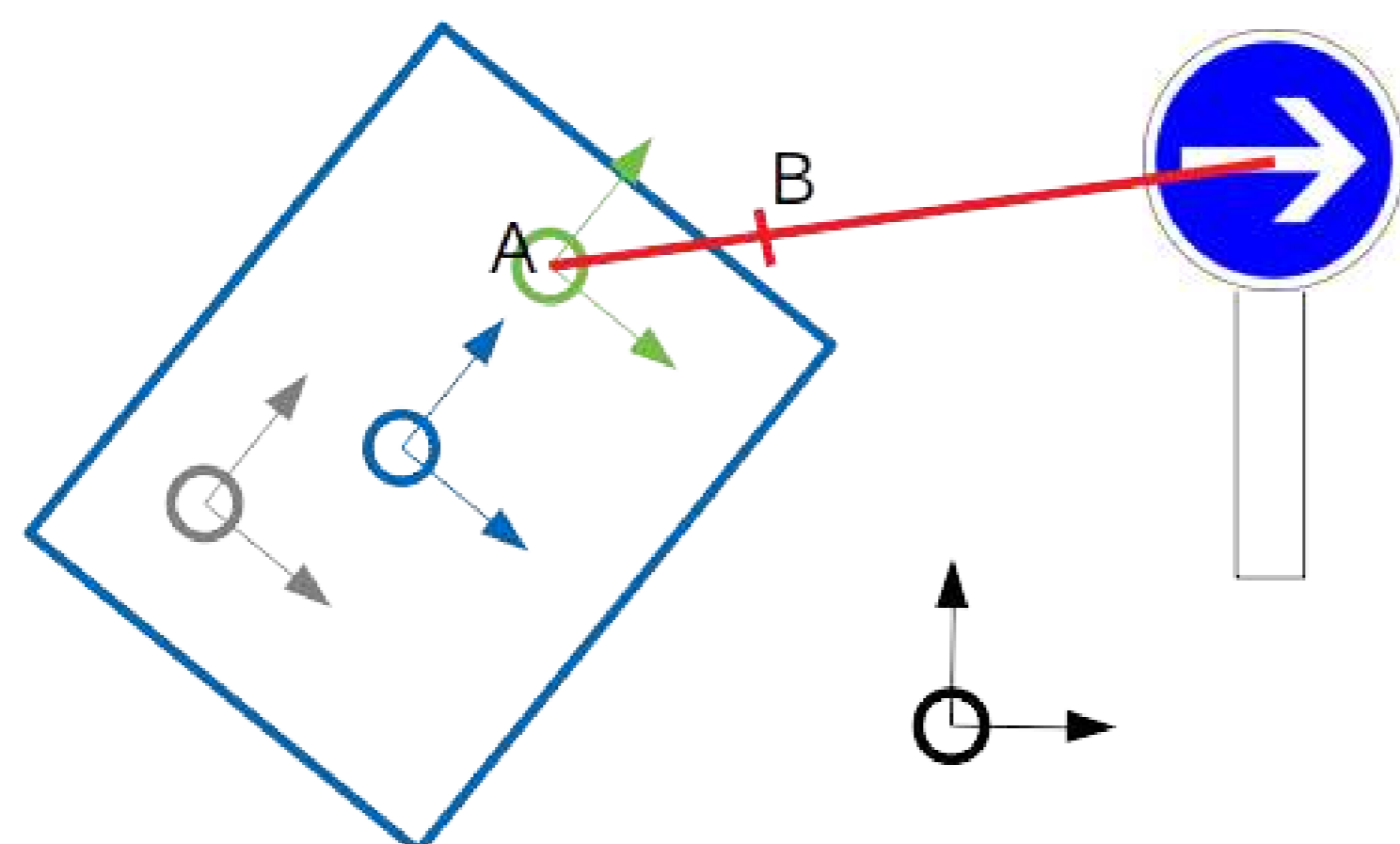
Introduction

- ▶ For connected vehicles to have a significant effect on road safety, it is required that they can be accurately geo-positioned within a common frame.
- ▶ While GNSS receivers lack of precision, another strategy consists in using visual sensors, and matching images over a map of accurately positioned landmarks.
- ▶ Major actors in the field have tried building maps by using fleets of vehicles equipped with high-quality sensors, but are now facing [1]:
 - ▷ Strong logistical costs for maintaining the fleets.
 - ▷ Slow rates for updating the maps.
- ▶ Instead, we intend to use production vehicles equipped with standard sensors, and crowdsource their individual observations.

Methods



- ▶ First, the *Perception* block receives images from the camera, uses a CNN-derived architecture to detect traffic signs and establish bounding boxes [2], and outputs their descriptions.
- ▶ Next, the *Vehicle and Feature Marks Geolocalization* block receives positions from the GPS receiver, and traffic signs descriptions as inputs. The position and orientation of the camera is estimated directly from GPS readings. As a traffic sign is detected, a projection line is established linking its bounding box center to the camera center. Traffic signs observations, consisting each of a description and a geo-positioned projection line, are outputted.



- ▶ Cloud servers receive traffic signs observations from potentially several vehicles as inputs, and match them with their corresponding traffic sign in the map.

For each traffic sign, a new estimation \hat{X} of its geo-position is computed, using all of its associated projection lines Z , and applying a least-squares optimization:

$$\hat{X} = \min_X \sum dist(X, Z) \quad (1)$$

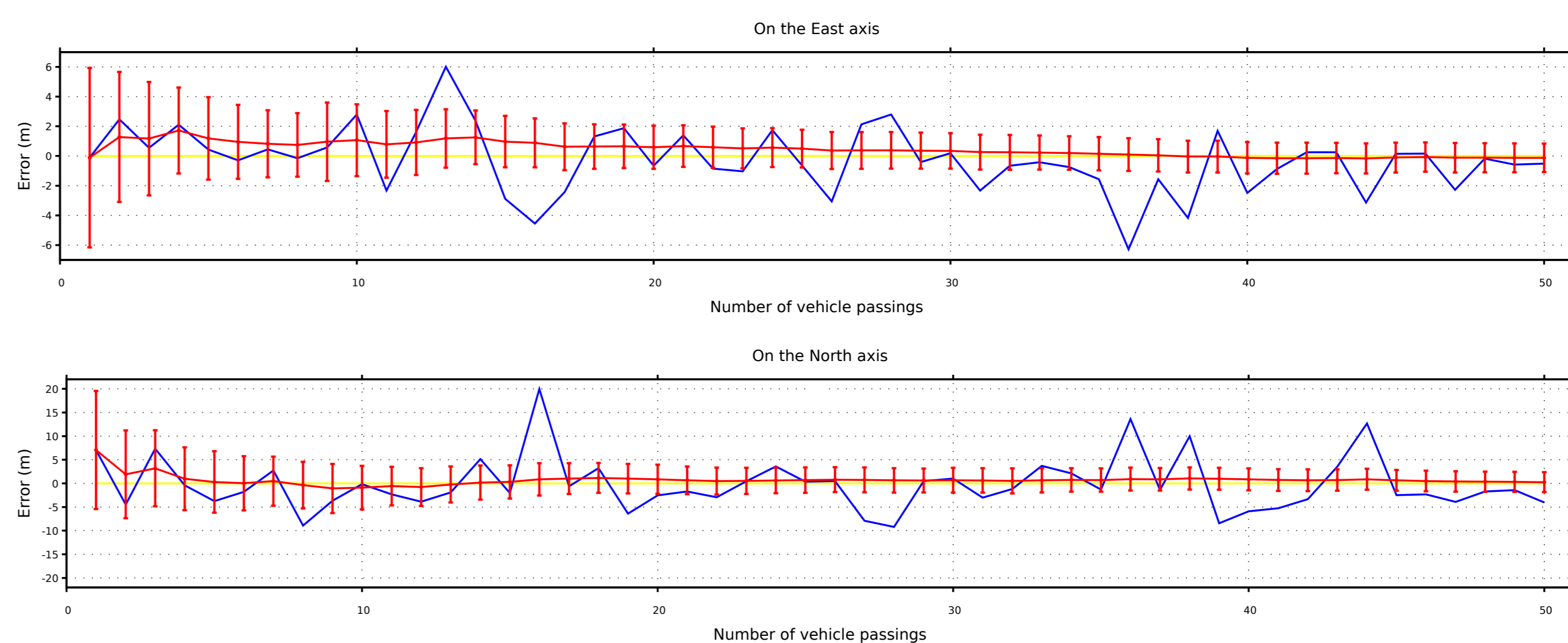
with $dist(X, Z)$ being the orthogonal distance between the geo-location X and the projection line Z .

Conclusion

- ▶ Our simulation confirmed the hypothesis holding that the map accuracy converges towards a null error, as more vehicles detect the traffic signs.
- ▶ Our real experiments, despite a limited number of passings, could show a better performance in average than single-passing measurements.
- ▶ Future works include:
 - ▷ The implementation of deviations calculations for the regular optimization applied by the *Landmarks Geolocalization* block.
 - ▷ The extension of our solution to other types of landmarks, such as road markings or buildings.
 - ▷ The dynamic management of the map's landmarks.

Simulation Results

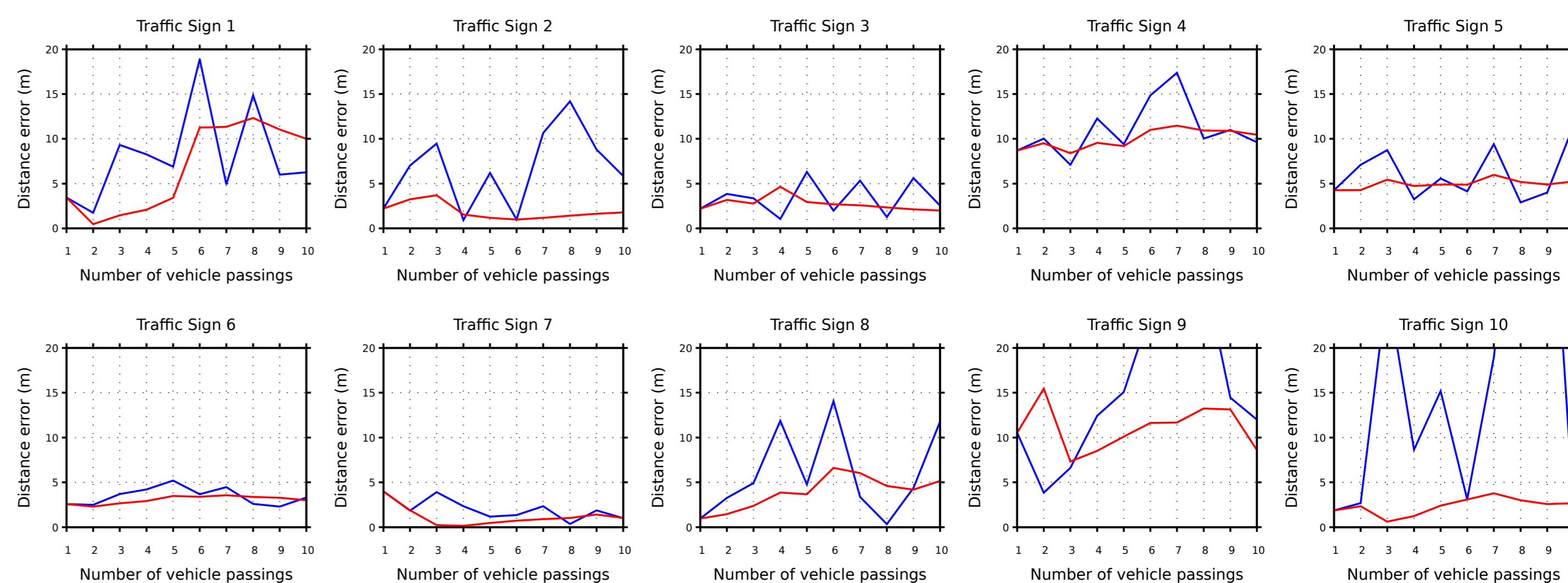
- ▶ A 2D simulation of our solution was implemented, in which a traffic sign was defined along a straight road, and vehicles trajectories were computed for several passings.
- ▶ Random, white noises of amplitude **5 m** in position and **0.35 rd** in orientation were applied around true vehicles trajectories to generate outputs from the GPS receiver.
- ▶ Random, white noises of amplitude **5 pixels** were applied around true bounding box centers to generate outputs from the *Perception* block.
- ▶ At each passing, a simplified optimization based on the yaw angles of projection lines was applied by the *Landmarks Geolocalization* block, enabling to compute associated deviations [3].



Simulation Results - Errors for single-passing measurements (blue) and for estimations of our approach (red) are shown, as well as the groundtruth (yellow). Deviations related to estimations of our approach are depicted as $[-2\delta; +2\delta]$ ranges.

Early Results

- ▶ A field-experiment was performed, in which a vehicle equipped with a standard GPS receiver and a mono-visual camera was driven for **4 hours** on a **7 km** loop, enabling to collect data for **10** passings along the loop.
- ▶ The geo-positions of **10** traffic signs were measured with an RTK-GPS receiver, constituting a groundtruth to compare our results with.
- ▶ At the end of each passing, the regular optimization was applied by the *Landmarks Geolocalization* block to estimate the geo-positions of all traffic signs:



Real Results - Distance errors for single-passing measurements (blue) and for estimations of our approach (red) are shown.

References

- [1] H. G. Seif and X. Hu, "Autonomous Driving in the iCity—HD Maps as a Key Challenge of the Automotive Industry," *Engineering*, vol. 2, pp. 159–162, jun 2016.
- [2] Z. Zhu, D. Liang, S. Zhang, X. Huang, B. Li, and S. Hu, "Traffic-Sign Detection and Classification in the Wild," in *2016 IEEE Conference on Computer Vision and Pattern Recognition (CVPR)*, pp. 2110–2118, IEEE, jun 2016.
- [3] A. Eudes and M. Lhuillier, "Error propagations for local bundle adjustment," in *2009 IEEE Conference on Computer Vision and Pattern Recognition (CVPR)*, vol. 2009 IEEE, pp. 2411–2418, IEEE, jun 2009.

Introduction

- ▶ With new technologies come new ways of learning and teaching. The theory of knowledge spaces [3] aims to benefit from computers power to improve or propose a new way to assess knowledge of students based on a mathematical structure named learning space. It has been implemented in the ALEKS system in USA, and is studied within the ProFan project in France, to which the PhD is attached. First, we explain learning spaces and thesis objectives. Then, we stick to one problem for which we state main ideas of existing results and current work.

Learning spaces with hands

- Our main context: a group of students must master a topic at school.
- ▶ For each student, we want to reveal both her/his knowledge on the subject and what he/she is ready to learn.
- ▶ The subject is divided in a group of small problems called **items**. The set of items mastered by a student is its **knowledge state**. From this state we know which items to teach next.
- ▶ Assumptions: a student can learn one item at a time (see **augmentation**), the union of two (knowledge) states is a state too (see **stability**). The collection of possible states is called a **learning space**.
- ▶ We can discover a learning space by asking queries to expert teachers (see **implications**) of the form "if a student fails this item, will she/he fails this one too?".

PhD Objectives

1. **representation**: how do we store efficiently the information of the structure ?
2. **modification**: how can we update the learning space ?

Both those questions first motivate the **theoretical** study of the mathematical structure hidden behind learning spaces. Second, results may lead to real **applications** (e.g: reducing memory costs, computation times).

Learning spaces in theory (a few)

- ▶ We give two possible definitions, see [4, 3]. They settle the more used **dual** but **equivalent** structure to learning spaces. Let Q be a finite set representing items, $F, G \subseteq Q$, $a, b \in Q$. A learning space is

- (i) an **anti-exchange closure space**: a pair (Q, ϕ) where $\phi : 2^Q \mapsto 2^Q$ is an operator satisfying
 - ▶ $F \subseteq \phi(G) \iff \phi(F) \subseteq \phi(G)$, (closure)
 - ▶ $\forall a \neq b$ s.t $a, b \notin \phi(F)$, it holds $a \in \phi(F \cup \{b\}) \implies b \notin \phi(F \cup \{a\})$ (anti-exchange), see Figure 1

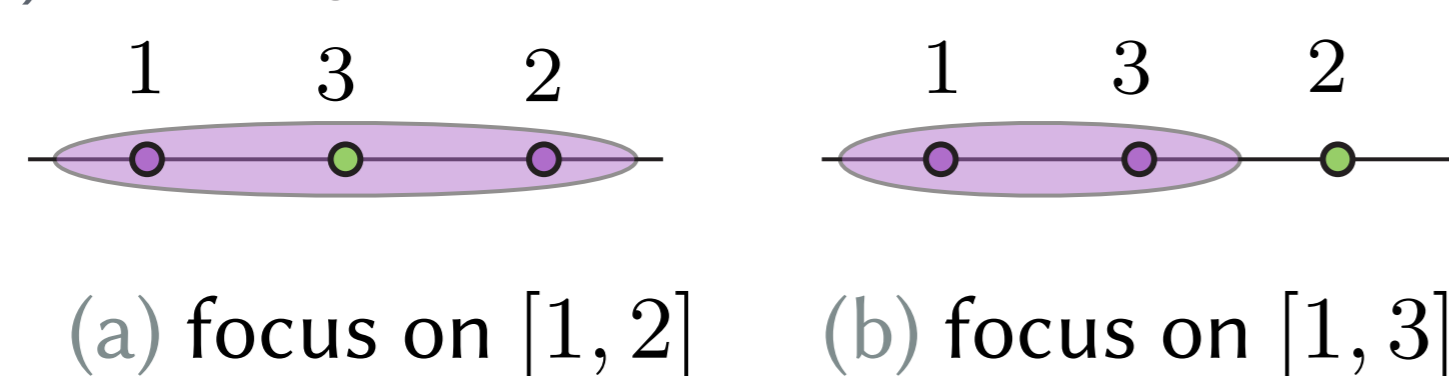
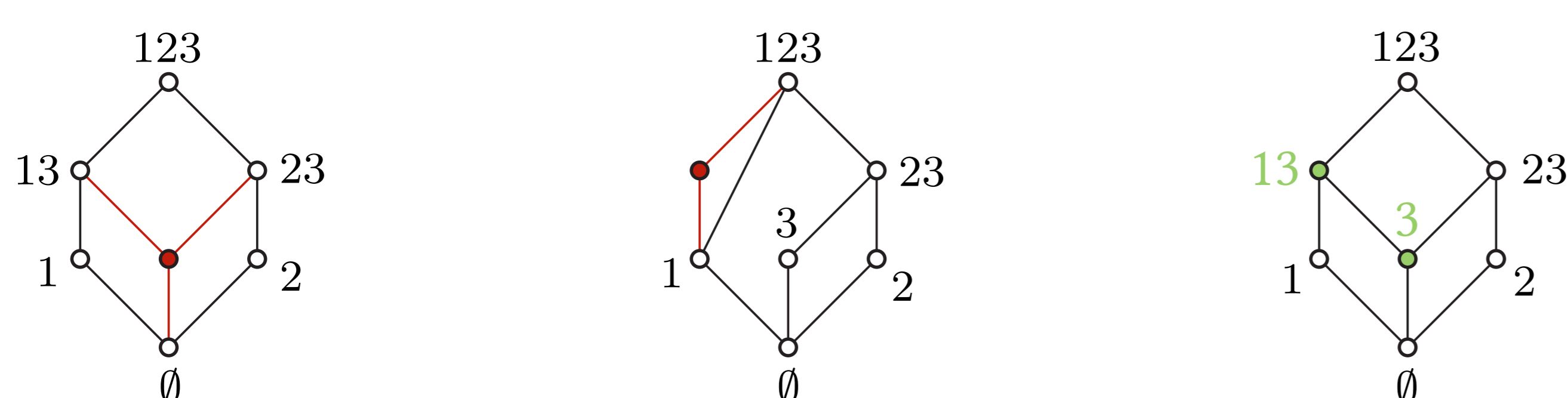


Figure 1: On this line $3 \in [1, 2]$ (a) but $2 \notin [1, 3]$ (b): they cannot be exchanged.

- (ii) a **convex geometry** (see Figure 2) which is a pair (Q, \mathcal{F}) , where $\mathcal{F} \subseteq 2^Q$ ($Q \in \mathcal{F}$) and

- ▶ $F, G \in \mathcal{F} \implies F \cap G \in \mathcal{F}$, (\cap -stability)
 - ▶ for $F \subset Q$, $F \in \mathcal{F}$, $\exists q \in Q \setminus F$ s.t $F \cup \{q\} \in \mathcal{F}$. (augmentation)
- ▶ Under inclusion order, a \cap -stable set family is a **lattice**.
 - ▶ There is a one-to-one correspondence between (Q, ϕ) and (Q, \mathcal{F}) .
 - ▶ F is **closed** or **convex** if $F = \phi(F)$ (equivalently $F \in \mathcal{F}$).



(a) failing \cap -stability (b) failing augmentation (c) valid convex geometry

Figure 2: Illustration of convex geometry properties on $Q = \{1, 2, 3\}$ through lattices of closed sets: in (a) $13 \cap 23$ is missing, in (b) 1 cannot be augmented. (c) is the geometry associated to convex sets of the line in Figure 1 (sets are ordered by inclusion and a sequence such as 123 is a shortcut for $\{1, 2, 3\}$).

Ongoing topic: representation problem

Focus on the **translation** between representations. (Q, \mathcal{F}) is a learning space.

- ▶ Two widely used representations ($[1]$):
 - ▶ a characteristic subset \mathcal{M} of \mathcal{F} from which we can reconstruct \mathcal{F} ,
 - ▶ a set Σ of **implications** $A \rightarrow B$ meaning "if a student fails A , he/she fails B too" ($A, B \subseteq Q$).
- ▶ Existing results:
 - ▶ \mathcal{M} and Σ uniquely define a learning space [5],
 - ▶ translation from one to another has unknown complexity [5],
 - ▶ existing algorithms for subclasses of closure systems [1, 2].
- ▶ Our ideas: algorithms for a subclass of convex geometries with an **acyclicity** constraint. Main tools are **lattices**, **maximum independent sets** of an hypergraph.

Example of translation

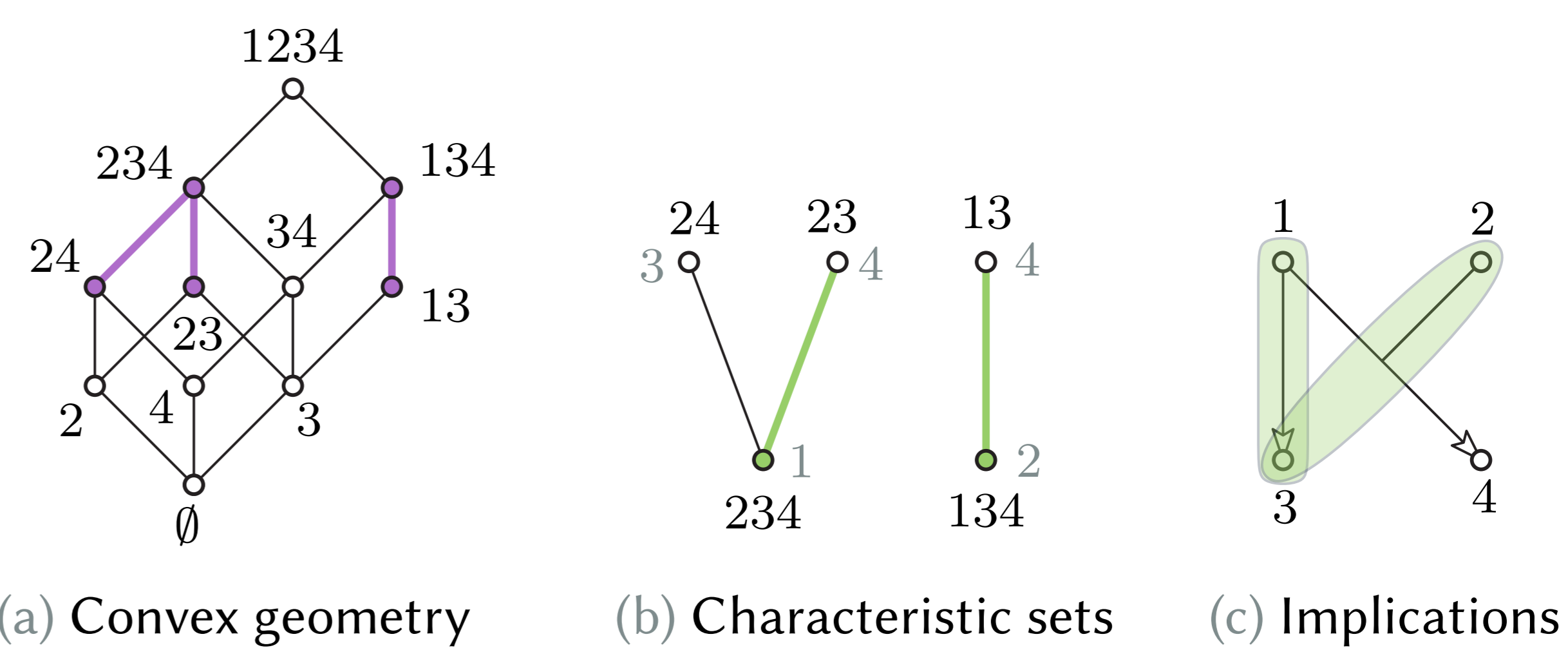


Figure 3: The lattice of (a) can be both represented by the implications $\{12 \rightarrow 4, 1 \rightarrow 3\}$ in (c) and by the characteristic sets of (b) ordered by \supseteq . These sets are also highlighted in (a) along with their relationship.

We want to switch between (b) and (c) in Figure 3. For instance with 4:

- ▶ From (b) to (c): **minimum set covering 4** in (b) is $\{234, 134\}$ associated to $\{1, 2\}$ so we derive $12 \rightarrow 4$ in (c) (the covering is denoted by highlighted arcs).
- ▶ From (c) to (b): **maximum sets** (circled) not implying 4 in (c) are 13 and 23 , they do not fire the implication $12 \rightarrow 4$. Hence, they appear in (b) and are attached to 4.

Conclusion

- ▶ **Learning spaces** model knowledge of a particular topic through particular assumptions. They help to assess skills of students and point out what they should learn next.
- ▶ This theory wishes to use new technologies to improve educational systems. As such, our research is dedicated to **representation** and **modification** in view of real life applications such as ALEKS in USA or within the ProFan project in France.
- ▶ Representation problem has unknown tractability and put the light on the study of **subclasses** of learning spaces.

References

- [1] Marcel Wild. The joy of implications, aka pure horn formulas: mainly a survey. *Theoretical Computer Science*, 658:264–292, 2017.
- [2] Karel Bertet, Christophe Demko, Jean-François Viaud, and Clément Guérin. Lattices, closures systems and implication bases: a survey of structural aspects and algorithms. *Theoretical Computer Science*, 743:93–109, 2018.
- [3] Jean-Paul Doignon and Jean-Claude Falmagne. *Knowledge spaces*. Springer Science & Business Media, 2012.
- [4] Paul H Edelman and Robert E Jamison. The theory of convex geometries. *Geometriae dedicata*, 19(3):247–270, 1985.
- [5] Roni Khardon. Translating between horn representations and their characteristic models. *Journal of Artificial Intelligence Research*, 3:349–372, 1995.

Contact Information

- ▶ Email: simon.vilmin@isima.fr
- ▶ Phone: +33 6 21 97 83 33

Conception d'un exo-squelette industriel d'assistance à l'effort pour les membres supérieurs

Anthony Voilqué^{1,2}, Jean-Christophe Fauroux², Laurent Sabourin², Olivier Guezet¹

¹ Groupe PSA, Centre technique de Vélizy, route de Gisy, Vélizy-Villacoublay, F-78140, France.

² Institut Pascal, SIGMA Clermont, Université Clermont Auvergne, CNRS, F-63000 Clermont-Ferrand, France.

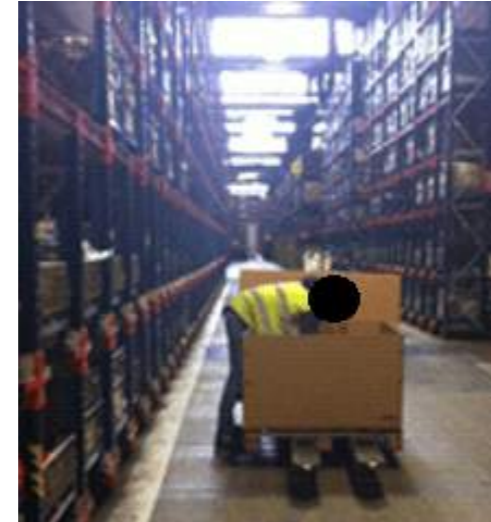
Besoins industriels

CU1: Posture/mouvement contraignant



Travail sous-caisse

CU2: Port/manipulation de charges lourdes



Logistique

CU3: Effort d'assemblage



Clippage pièces plastiques

Les Cas d'Usage (CU) issus de l'industrie automobile sont illustrés par des postes du Groupe PSA.

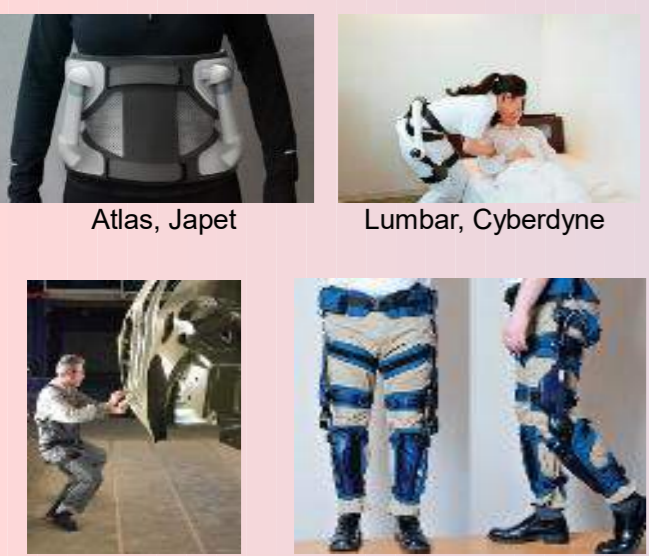
L'exo-squelette, une solution parmi d'autres

Une nouvelle approche lorsque les limites du process et des produits sont atteintes:

- Augmenter la versatilité
- Solution à faible coût et flexible
- Réduire l'absentéisme
- Réduire les coûts direct et indirect liés aux troubles musculo-squelettiques

Exosquelettes industriels

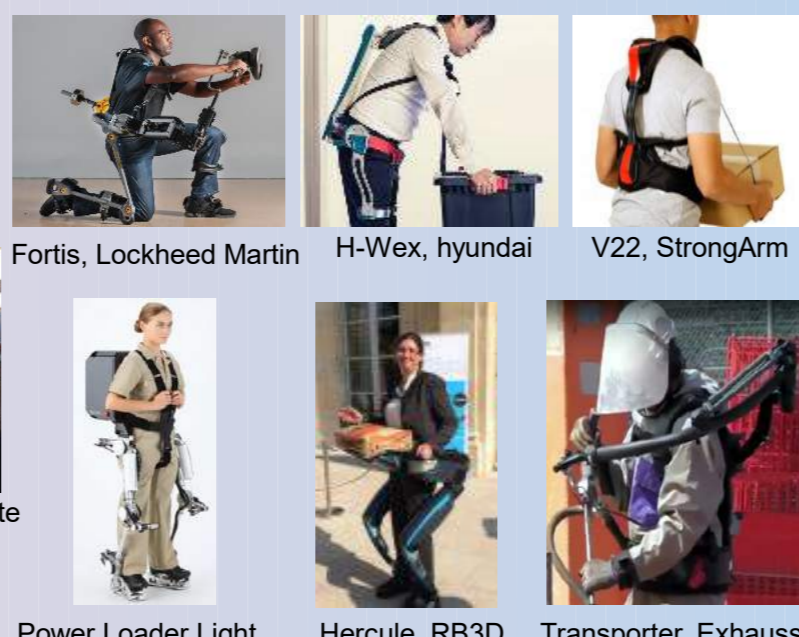
CU1: Assistance au mouvement/maintien de posture contraignante



Tête: 1
Main: 0
Bras: 5
Epaules: 11
Buste: 17
Jambes: 10

40/69 (60%)
Actif: 17
Passif: 23

CU2: Port/manutention de charges



Mains: 0
Bras: 21
Epaules: 23
Buste: 22
Jambes: 7

42/69 (63%)
Actif: 19
Passif: 23

CU3: Application d'effort à l'environnement



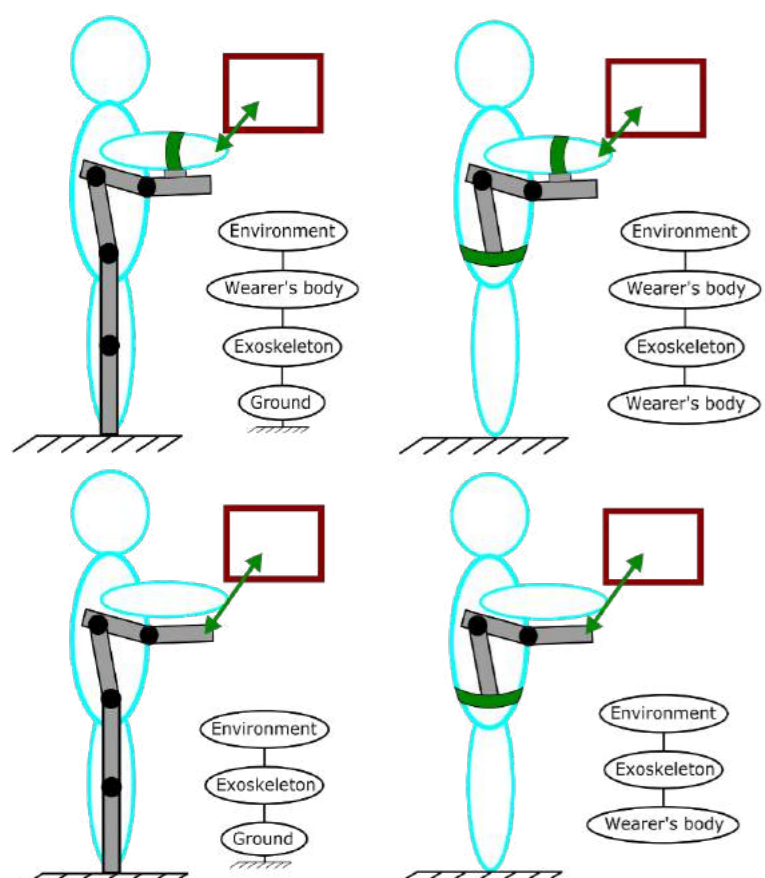
Mains: 2
Bras: 5
Epaules: 4
Buste: 3
Jambes: 3

7/69 (10%)
Actif: 7
Passif: 0

- 90% des exosquelettes industriels actuels sont destinés à CU1 et CU2
- La simplicité d'utilisation et de maintenance des exosquelettes passifs justifie leur succès
- Les systèmes actifs sont bien plus versatiles
- Les nouveaux développements tendent vers des systèmes actifs et semi-actifs (passif à raideur commandée)

Identification et proposition de formalisation du problème de conception centrée utilisateurs

2. Identification de la chaîne d'efforts



En vert, les fixations homme exo-squelette transmettant des efforts fonctionnels pour l'assistance de l'effort final (flèche verte).

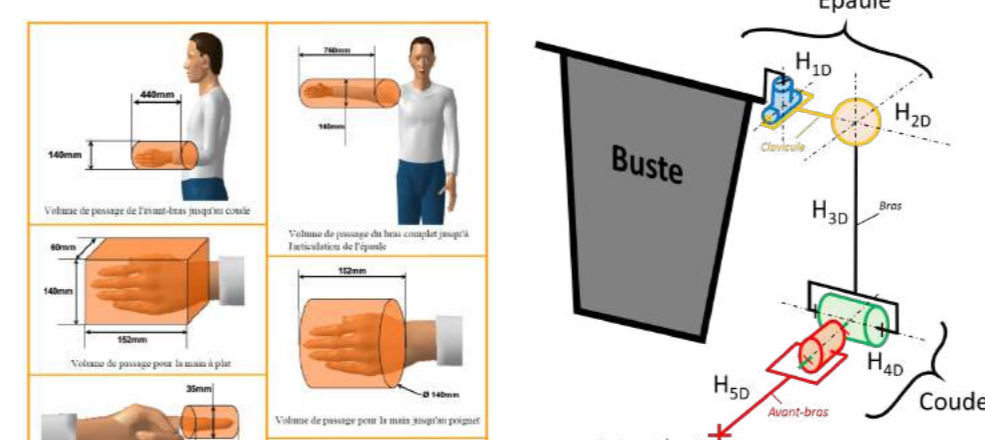
3. Types de fonctionnement possibles

- Passifs** : distribution d'efforts, mécanismes simples et légers (ressorts, etc)
- Actifs** : génère des efforts, versatiles mais lourds (servomoteurs, moteurs p.à.p, etc)
- Semi-actifs** : contrôle de l'effort résistif d'une liaison, permet de rigidifier une structure ou freiner un mouvement (embrayage, etc)

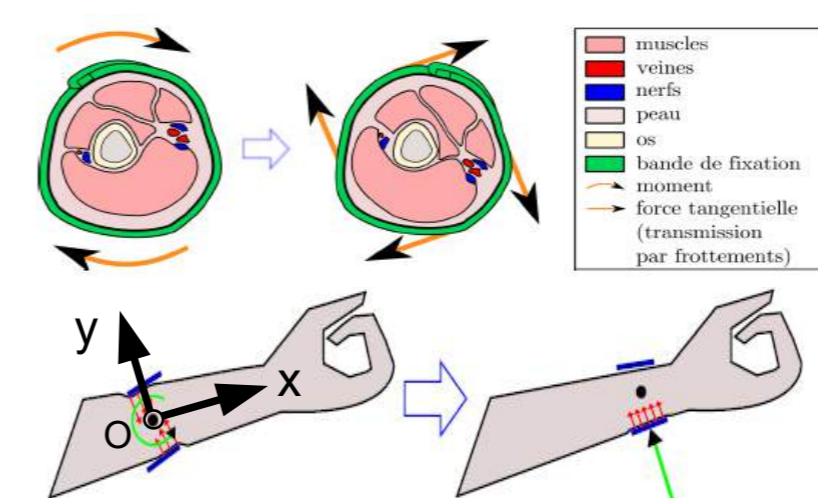
4-5. Définition du modèle cinématique

L'hyperstatisme homme exo-squelette doit être évité pour limiter les blocages mécaniques possibles.

Adaptation de l'exo-squelette à l'opérateur

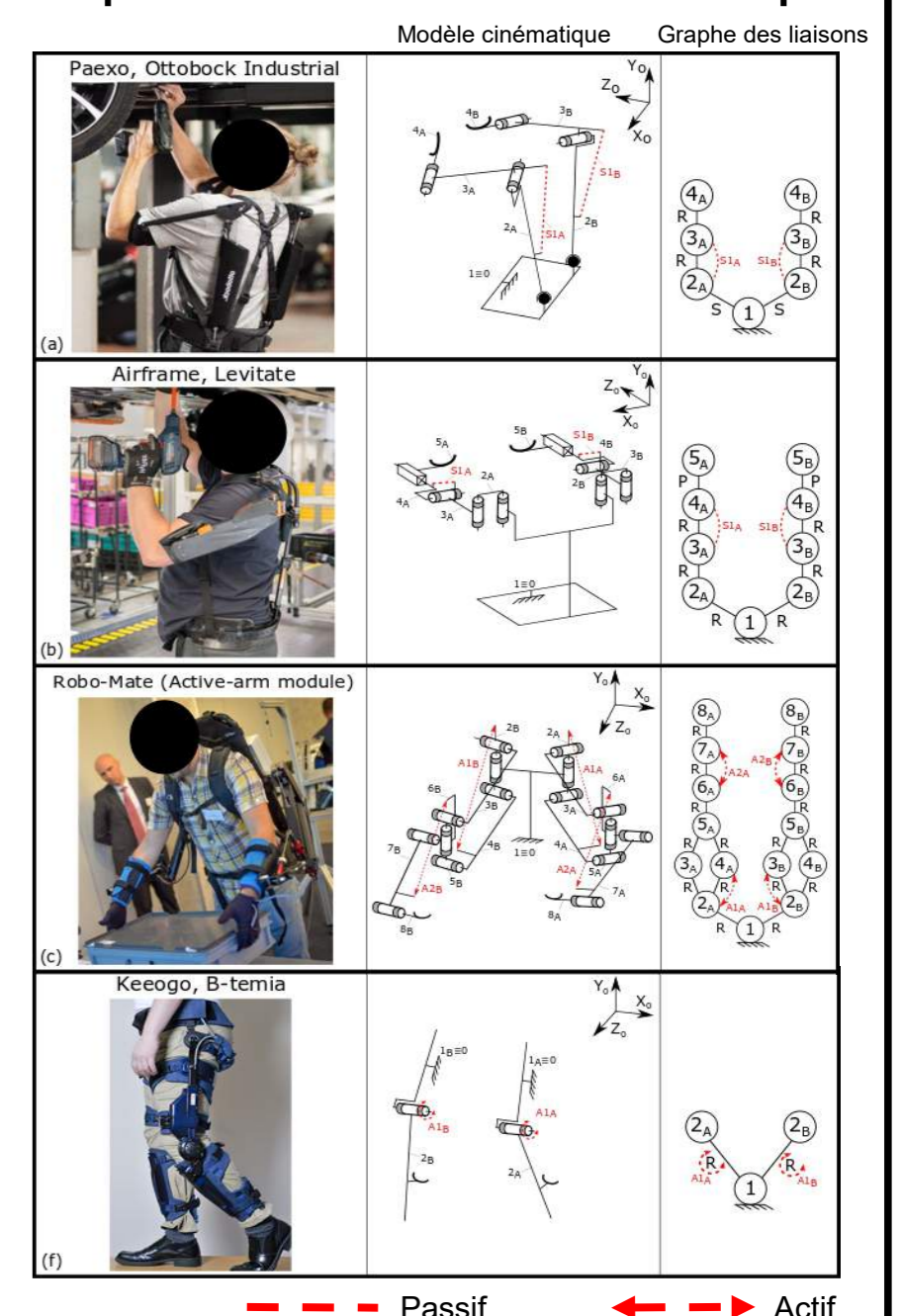


Équivalence cinématique aux fixations homme / exo-squelette



Calcul du torseur équivalent dans la fixation

Représentation cinématique



Conclusion

- Proposition d'un algorithme de conception en six étapes séquentielles
- A partir des retours d'utilisation d'exosquelettes en milieu industriel (PSA, AFNOR,...), des règles de conceptions ont été formulées et sont incluses dans l'algorithme
- Proposition d'un concept pertinent pour l'industrie automobile.

Publications internationales :

A. Voilqué, J. Masood, J-C. Fauroux, L. Sabourin, O. Guezet, 'Industrial Exoskeleton Technology: Classification, Structural Analysis, and Structural Complexity Indicator', IEEE, WearRAcon Scottsdale, USA, 2019

Perspectives

- Prototypage d'une liaison semi-active innovante :
 - Choix de matériaux et méthodes de fabrication
 - Caractérisation, commande, intégration
- Réalisation d'un prototype d'exo-squelette fonctionnel pour validation expérimentale
- Deux brevets en cours de rédaction :
 - Mécanisme innovant de la liaison semi-active
 - Fonctionnement du concept d'exo-squelette proposé
- Article de journal en cours d'écriture : IISE Transactions on Occupational Ergonomics and Human Factors

Introduction

The aim of this thesis is to detect anomalies in the activity of dairy cows. An anomaly can be a disease, an estrus, a perturbation in the barn, etc. A farmer needs to early detect the anomalies to act as fast as possible.

An indoor GPS placed on each cow detects their position in the barn per second. From these locations, three main activities are defined:

- **eating** if the cow was located new to the trough,
- **in alley** if the cow was located in the alley,
- **resting** if the cow was located in the cubicles.

These three activities are aggregated into one single value called **level of activity**. The process is described in [1]. This activity is given for each cow and for each hour. A high value corresponds to a high activity (e.g. eating) and a low value corresponds to a low activity (e.g. resting). The problem consists of detecting anomalies in the time series representing the level of activity of each cow.

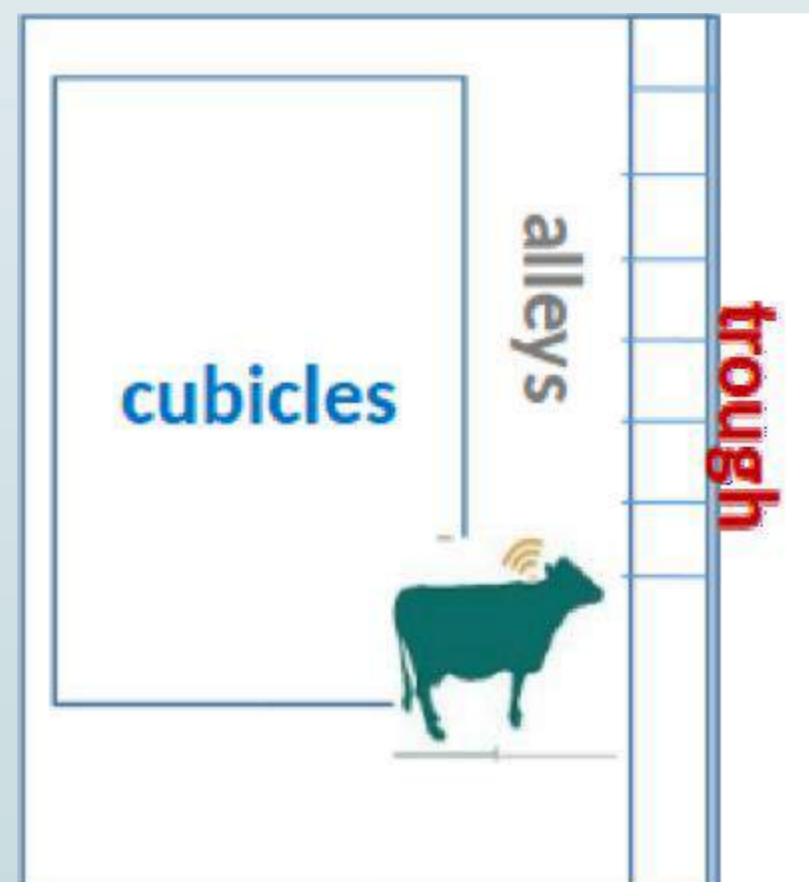


Fig 1: Structure of a barn

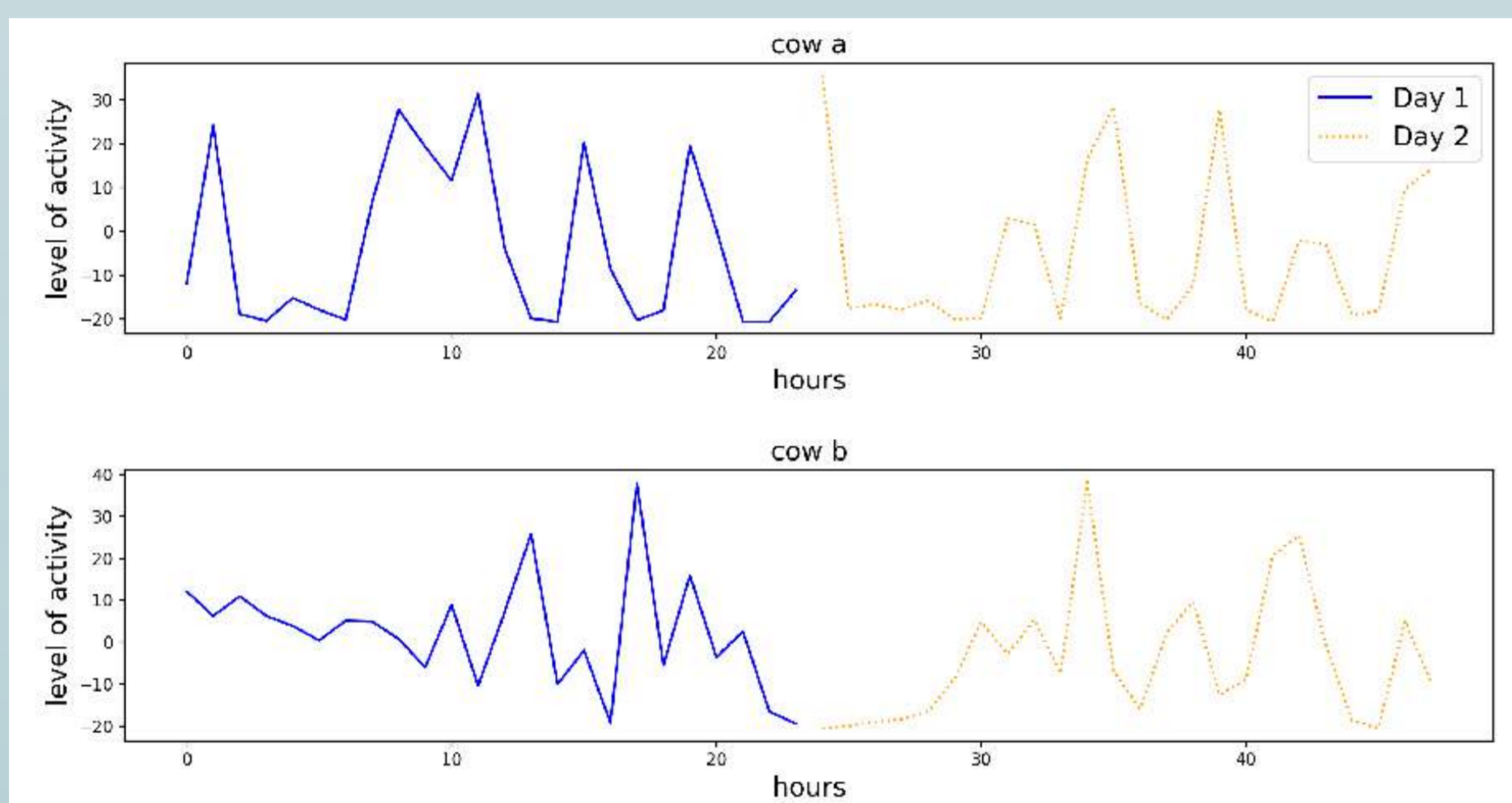


Fig 2: Example of two levels of activity time series of two different cows for 2 days

The Fig 2 underlines two main problems:

- two cows can have two different shapes of level of activity,
- the activity of a cow can change with time.

Consequently, it is impossible to define a pattern for a normal activity and a pattern for each type of anomaly. This excludes all the solutions based on classification tools. The proposed solution consists of analyzing the changes in the seasonal rhythm called **circadian cycle**. The method is called **Fourier Based Method (FBM)**.

Fourier Based Method

As illustrated in the Fig 3, the time series are sliced into time windows of size p and delayed of q ($p=24$ and $q=12$ hours in this study).

A Fast Fourier Transform is applied on each time window to obtain the harmonics h_f .

Then, a model $m(t)$ of each time window is Built according to:

$$m(t) = \sum_{f=-z}^z |h_f| \cos(2\pi f \frac{t}{p} + \arg(h_f))$$

with z , the number of harmonics to keep in the model. This is an important parameter that fix the precision of the model.

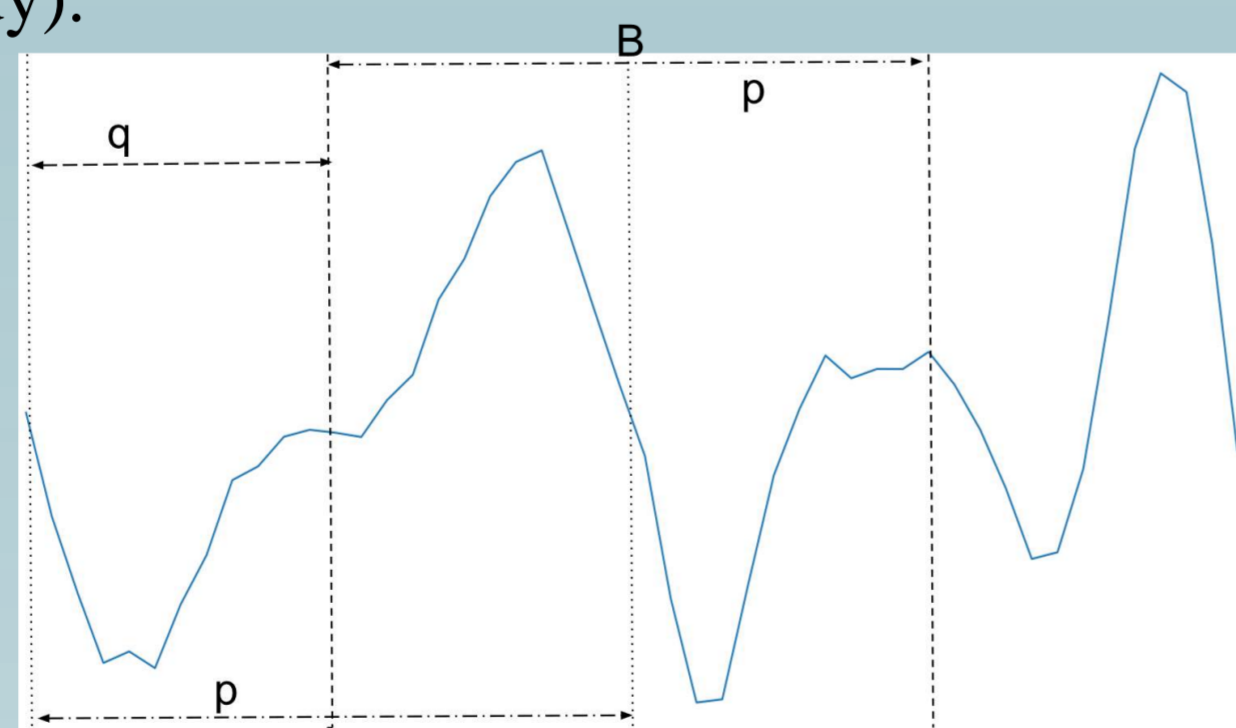


Fig 3: Illustration of the time windows slicing operation

Fourier Based Method

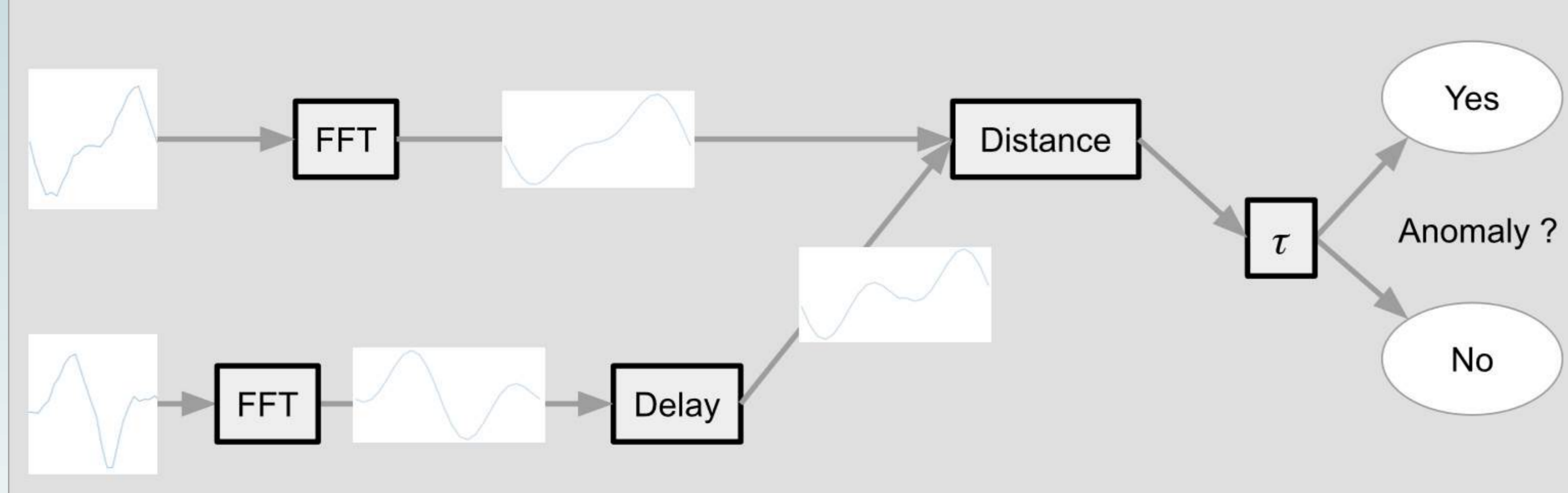


Fig 4: General framework of the Fourier Based Method

An anomaly is detected if two successive models $m_A(t)$ and $m_B(t)$ are **too** different. This difference is measured with a L_1 distance:

$$L_1 = \sum_{t=0}^{p-1} |m_B(t) - m_A(t)|$$

Notice that the model of B is delayed of q hours from A. To synchronize them, a **delay** of $-\frac{q}{p}2\pi$ is added in $m_B(t)$.

A **threshold** is computed and if the distance between two models is over this threshold, we consider the both models as abnormal.

Results

To evaluate the method, we used the True Positive Rate (TPR) and the False Positive Rate (FPR) measures. The aim is having a TPR as close to 1 as possible and a FPR as close to 0 as possible.

The method is applied on data set coming from an experimental farm of INRA.

Let's focus on the lameness (Fig 5) and estrus (Fig6) anomalies.

For each, we study the influence of the z value. For both anomalies the best is $z = 1$ and lameness are Better detected than estrus.

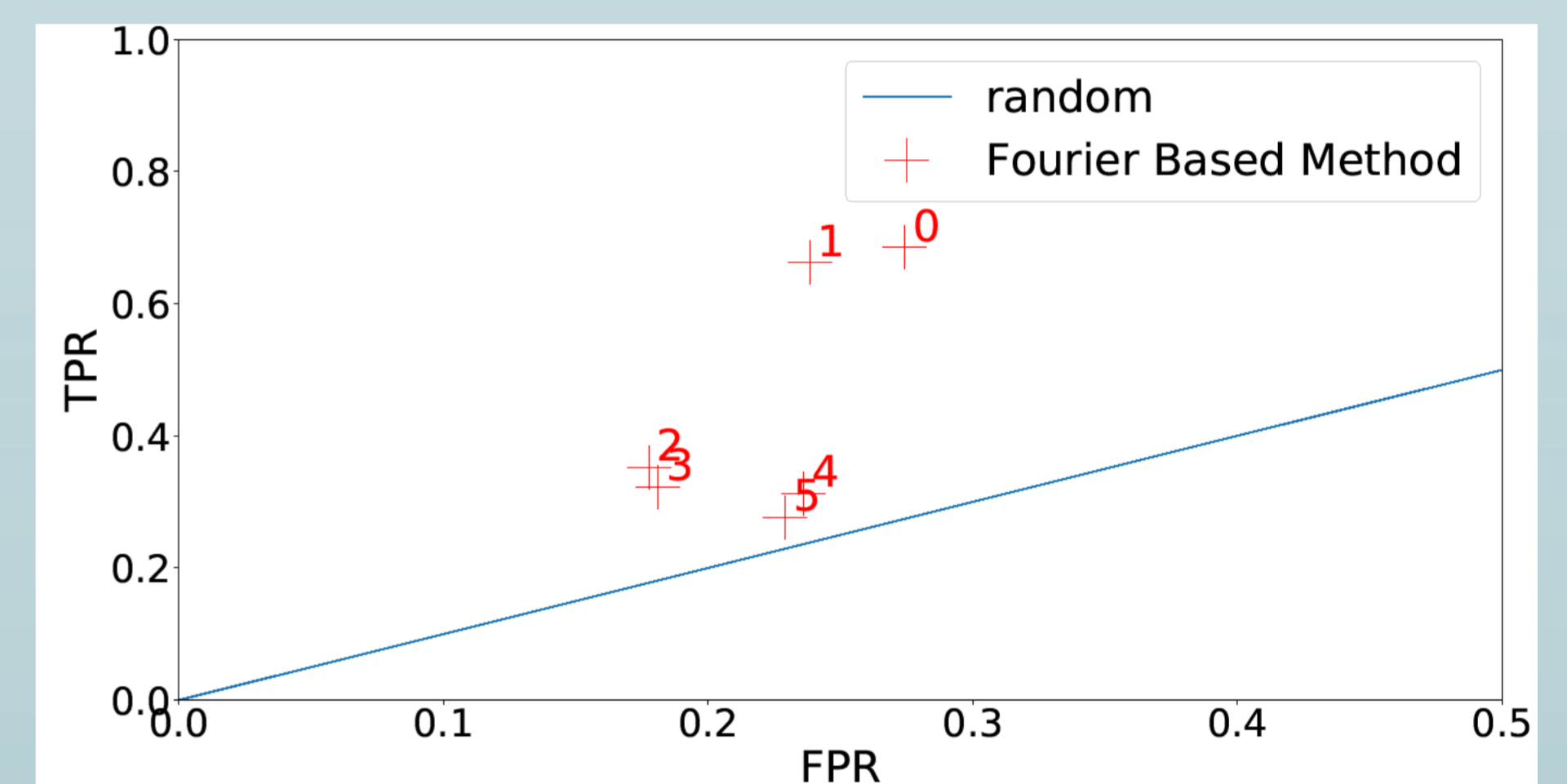


Fig 5: Results of FBM for lameness anomaly; the numbers represent the z value

The results are: lameness, TPR = 0.66, FPR = 0.24; estrus, TPR = 0.50, FPR = 0.24.

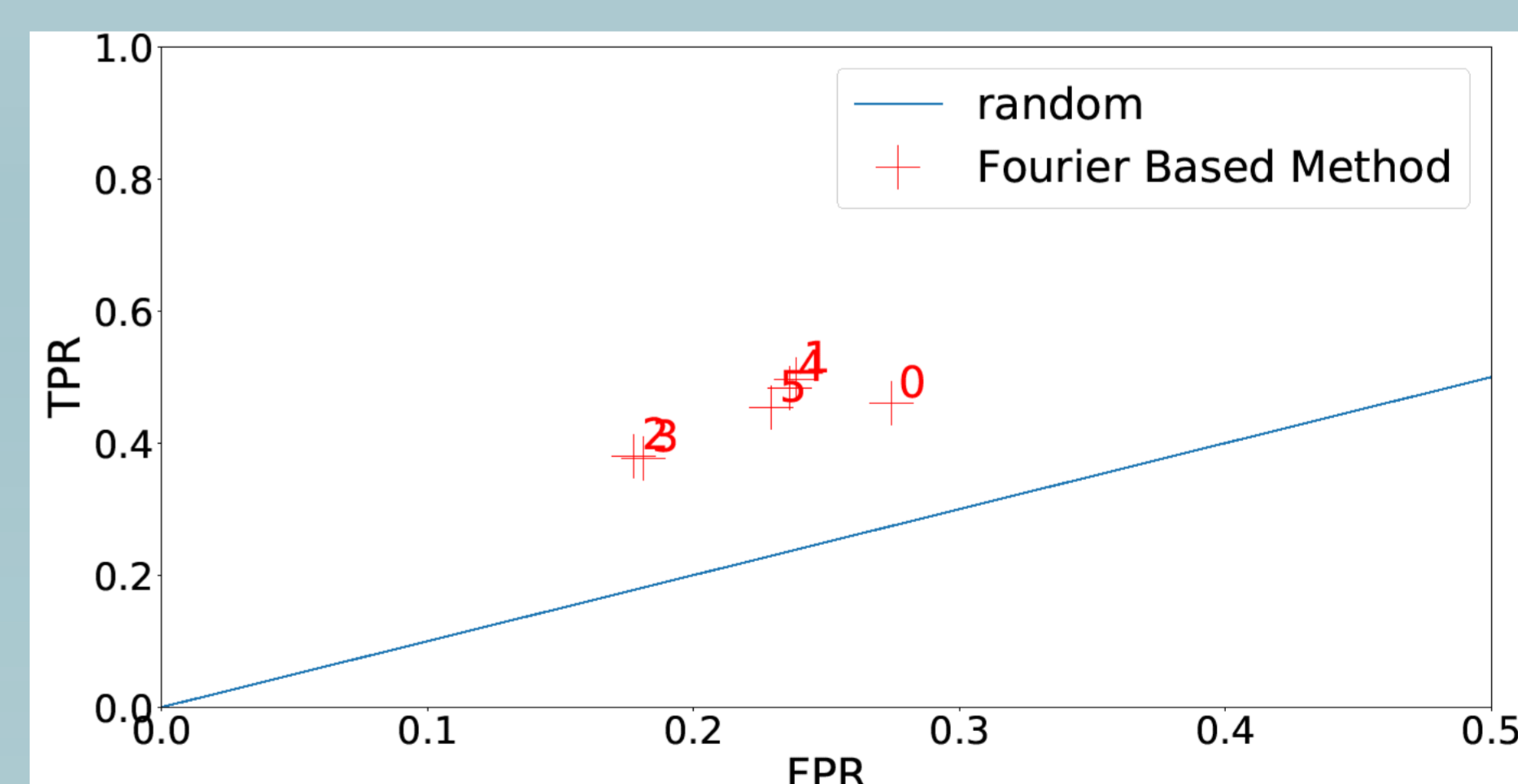


Fig 6: Results of FBM for estrus anomaly; the numbers represent the z value

The z value acts as a filter on the model. A low value of z takes the model away from the original time window but that apply a filter with a high-level of **noise reduction**.

Conclusions

This Fourier Based Method is able to detect anomalies in time series and it can perform without identifying the pattern of each anomaly. And other strength of this FBM is its capacity to apply a noise reduction by selecting a good value for the z parameter. With the tested data set, the method shows promising results [2].

Bibliography

1. Isabelle Veissier, Marie-Madeleine Mialon, and Karen Helle Sloth. *Early modification of the circadian organization of cow activity in relation to disease or estrus*. Journal of dairy science, 100(5):3969–3974, 2017.
2. N.Wagner et al., *Use of a precision-livestock-farming technology coupled with time series methods to identify abnormal circadian pattern of activity*, Measuring Behaviour, Jun 2018, Manchester, UK.

Introduction

The process of cracks propagation is strongly intensified under the action of corrosion media and cyclic load. The long-term operation deteriorates the properties of the metal and, in particular, the fatigue crack growth resistance.

To determine the service life and the residual life, of metallic structural elements under cyclic loads and under the action of corrosive media, it is necessary to have the corresponding computational models.

Fundamental investigations of short cracks were carried out by Ritchie and Miller. The whole period of the fatigue crack growth was split into three stages according to the crack size (micro structurally short, physically small, and long cracks).

Methods

Problem statement

Consider a plate with a short rectilinear crack of the initial length $2l_0$. The plate is uniformly stretched by distributed cyclical forces p perpendicular to the line of the crack.

The problem is to determine the number of loading cycles $N = N^*$ for which the corrosion-fatigue crack grows to the critical size $l = l^*$ and the plate destroys.

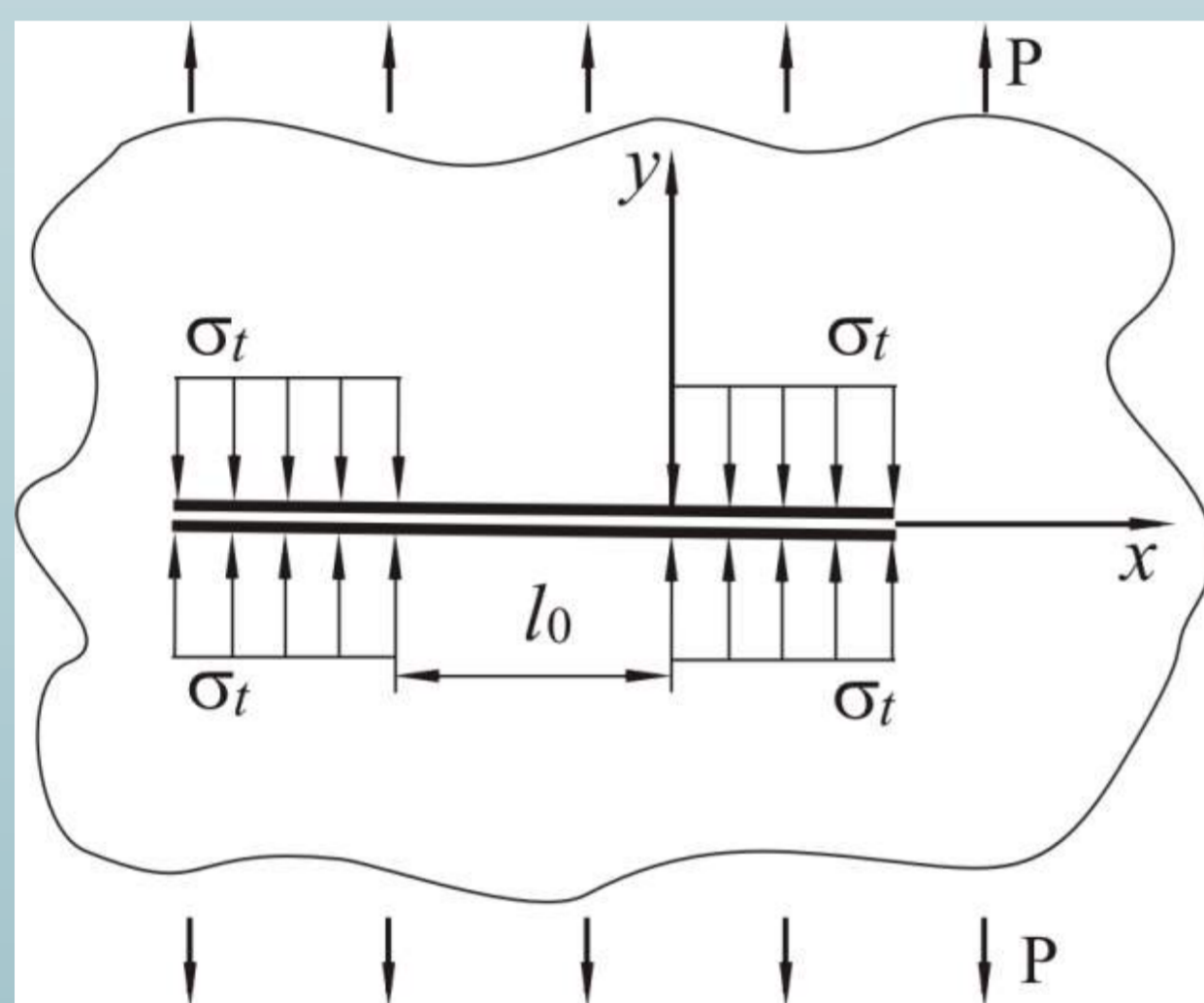


Fig. 1. Loading scheme of a cracked plate.

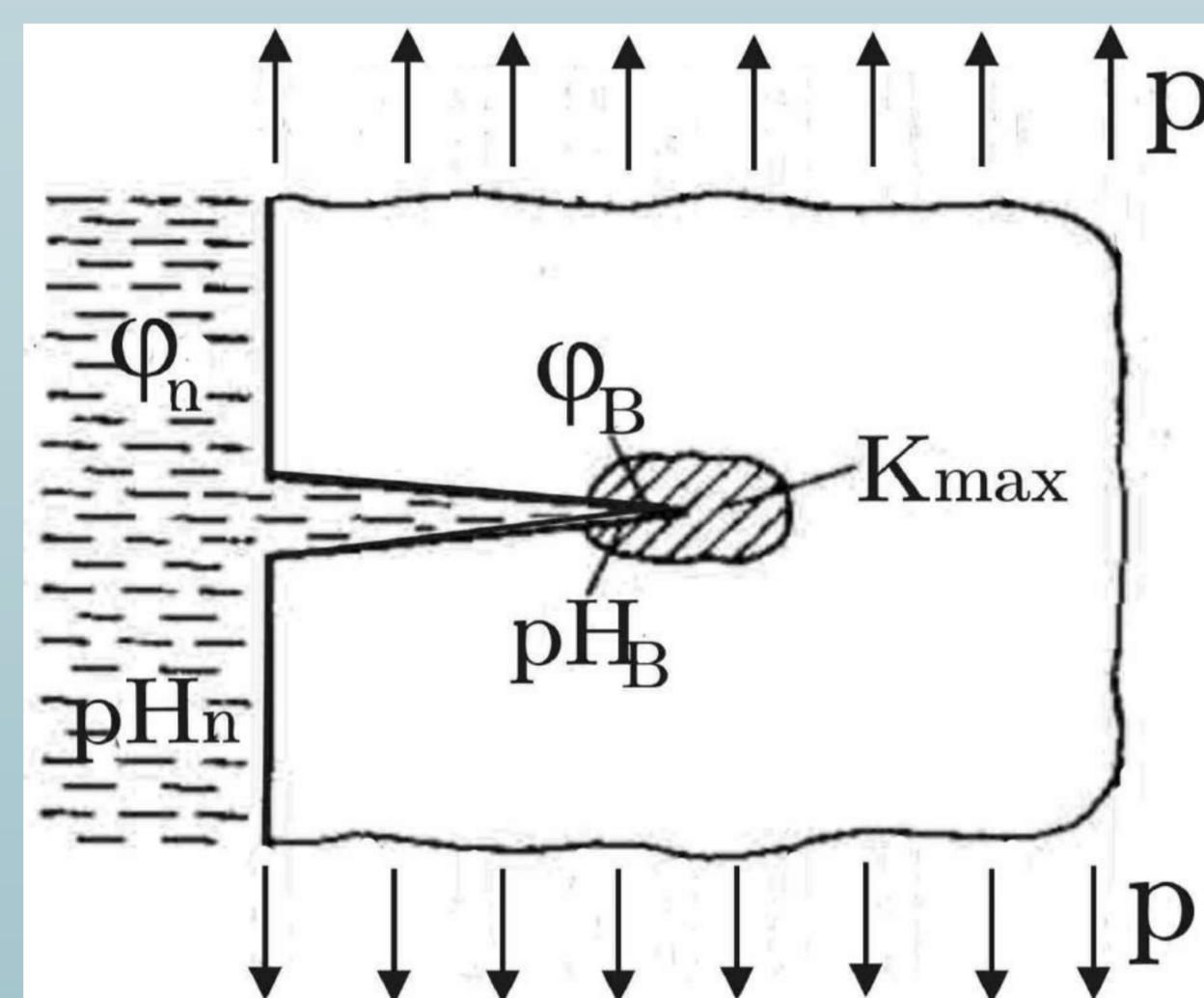


Fig. 2. Loaded plate with a rectilinear crack in a corrosive environment.

Solution method and model development

The developed model is based on the first law of thermodynamics.

Power balance method:

$$A = W + \Gamma + Q + K, \quad (1)$$

where A – work of external forces, W – deformation energy of the material in the pre-fracture zone in the vicinity of the crack tip, Γ – fracture energy of the body.

The energy of deformation of the material in the pre-fracture zone in the vicinity of the crack tip is presented as:

$$W = W_S + W_p^{(1)}(l) + W_p^{(2)}(t) - W_p^{(3)}(t),$$

where W_S is the elastic component, $W_p^{(1)}(l)$ – work of plastic deformations, which depends only on the crack length l , $W_p^{(2)}(t)$ – work of plastic deformation from external forces, which emanates at the constant crack length during the incubation period of its jump preparation, $W_p^{(3)}(t)$ – work of plastic deformation during the unloading of the body and compression of the pre-fracture zone.

Change rate of the power balance:

$$\frac{\partial A}{\partial t} = \frac{\partial W}{\partial t} + \frac{\partial \Gamma}{\partial t}.$$

Analytical model

with stress intensity factor (SIF)

$$\frac{dl}{dt} = \frac{\alpha(K_{I_{max}}^2 - K_{Scc}^2)[(1-R)^4(K_{I_{max}}^2 + K_{Scc}^2) + \eta E \sigma_t]}{E \sigma_t (K_{f_{cc}}^2 - K_{I_{max}}^2)}, \quad (2)$$

$$N = 0, l(0) = l_0; \quad N = N_*, l(N_*) = l_*; \quad K_{I_{max}}(l_*) = K_{f_{cc}}$$

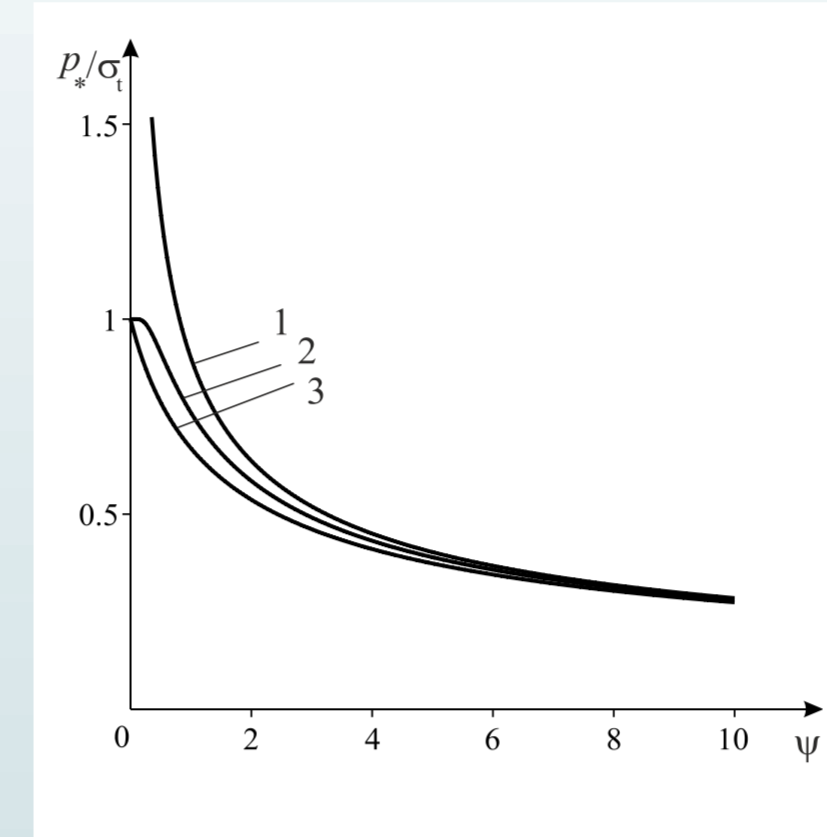
new model

$$\frac{dl}{dt} = \frac{\alpha(\delta_{t_{max}} - \delta_{scc})[(1-R)^4(\delta_{t_{max}} + \delta_{scc}) + \eta]}{\delta_{f_{cc}} - \delta_{t_{max}}}, \quad (3)$$

$$N = 0, l(0) = l_0; \quad N = N_*, l(N_*) = l_*; \quad \delta_{t_{max}}(l_*) = \delta_{f_{cc}}$$

Results

Disclosure determination in the top of a short crack under tension



$$\delta_t \approx K_I^2 [E \sigma_t (1 - \xi^2)]^{-1} \quad (4)$$

Fig. 3. Solutions comparison of the Griffiths task:
1 – via the Irwin criterion;
2 – via the δ_c -model;
3 – solution (1)

Validation of the approximate formula to determine δ

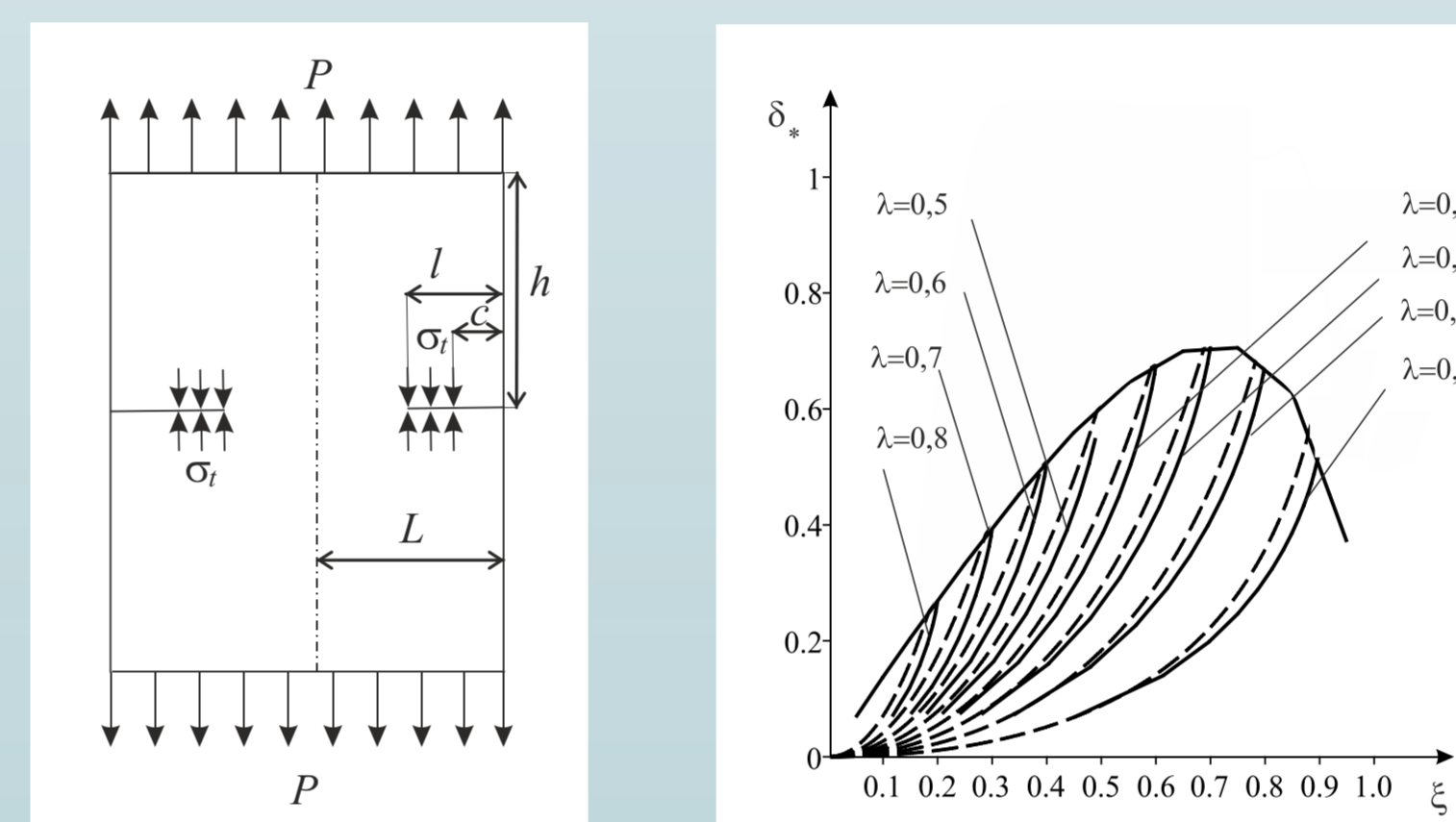


Fig. 4. Tension diagram of a plate with two side cracks (a); the dependence of the relative disclosure of the top of the cracks: solid lines – numerical data of Hayes and Williams, dotted line – dependence according to the formula (6) (b)

Determination of the short fatigue crack propagation rate in plates

$$V = dl/dt = \alpha(1-R)^4 (\delta_{t_{max}}^2 - \delta_{th}^2) (\delta_{f_{cc}} - \delta_{t_{max}})^{-1}$$

$$V = dl/dt = \alpha(1-R)^4 (K_{I_{max}}^4 - K_{th}^4) [E \sigma_t (K_{f_{cc}}^2 - K_{I_{max}}^2)]^{-1}$$

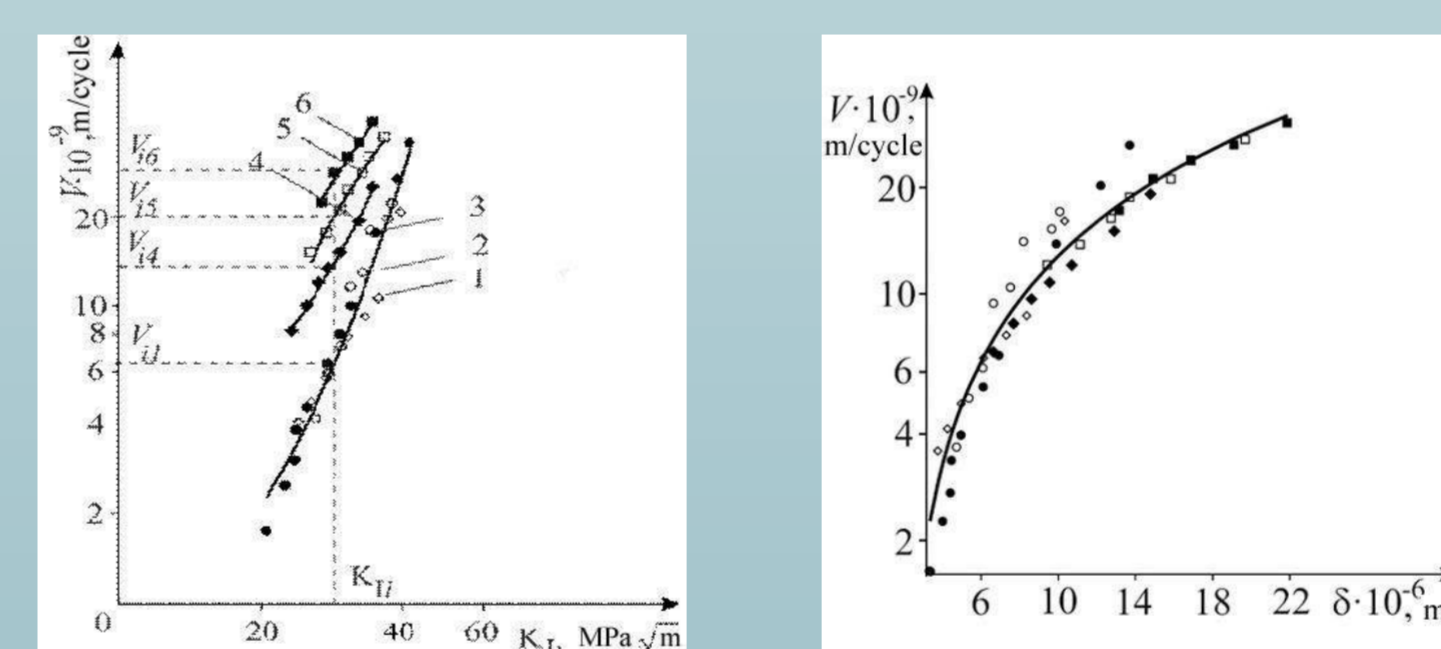


Fig. 5. Kinetic diagrams a) $V \sim K_I$ b) $V \sim \delta$
propagation of corrosion fatigue cracks in alloy Fe-3%, Si under load levels: 1- 560 MPa; 2- 640 MPa; 3- 720 MPa; 4- 800 MPa; 5- 840 MPa; 6- 880 MPa

Propagations of corrosion fatigue cracks numerical experiment

$$\alpha \approx 0,3(\text{cycle})^{-1}, \eta \approx 10^{-5} \text{ MPa} \cdot \text{m}, \delta_{scc} \approx 2 \cdot 10^{-4} \text{ mm},$$

$$\delta_{f_{cc}} \approx 0,08 \text{ mm}, R = 0,1, E = 2 \cdot 10^5 \text{ MPa}, \sigma_t = 636 \text{ MPa},$$

$$K_{f_{cc}} \approx 101 \text{ MPa} \sqrt{\text{m}}, K_{i_{cc}} \approx 9 \text{ MPa} \sqrt{\text{m}}$$

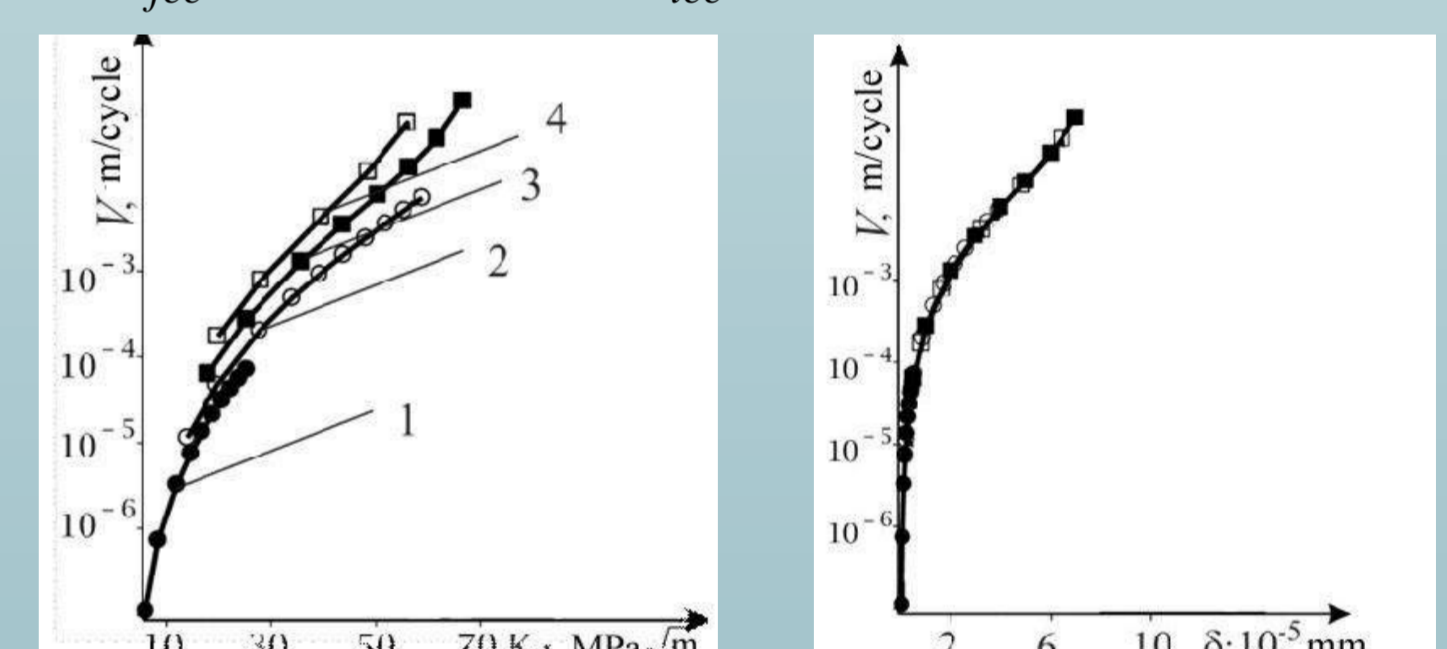


Fig. 6. Kinetic diagrams a) $V \sim K_I$, b) $V \sim \delta_t$
propagation of corrosion fatigue cracks for series of load changes in the numerical experiment: 4- 500 MPa, 3- 450 MPa, 2- 350 MPa, 1- 150 MPa

Evaluation of periods subcritical growth of short corrosion-fatigue cracks

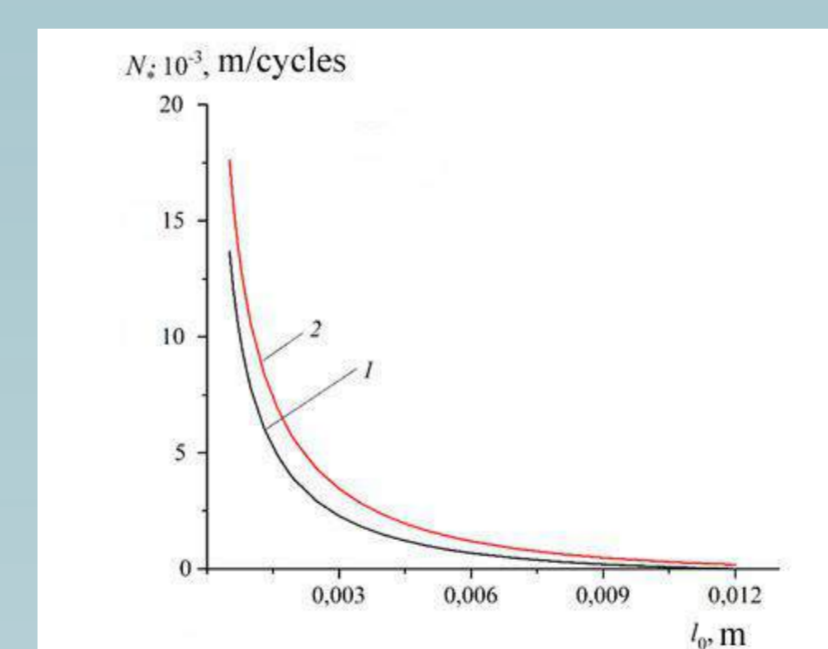


Fig. 7. Dependence of periods subcritical growth of short corrosion-fatigue cracks

$$N_* = E \sigma_t \alpha^{-1} \int_{l_0}^{l_*} \frac{(K_{f_{cc}}^2 - K_{I_{max}}^2) dl}{(K_{I_{max}}^2 - K_{scc}^2) [(1-R)^4 (K_{I_{max}}^2 + K_{scc}^2) + \eta E \sigma_t]}$$

$$N_* = E \sigma_t \alpha^{-1} \int_{l_0}^{l_*} \frac{(1 - \xi^2) (K_{f_{cc}}^2 - K_{I_{max}}^2) dl}{(K_{I_{max}}^2 - K_{scc}^2) [(1-R)^4 (K_{I_{max}}^2 + K_{scc}^2) + \eta E \sigma_t (1 - \xi^2)]}$$

Conclusions

1. A general power balance method is proposed to investigate the propagation of short fatigue crack growth in plates under the action of loading and physicochemical factors. The approach is based on the first law of thermodynamics (1) and on a simplified formula (2) for determination of crack tip opening displacement using SIF and load level of the fracture process zone.
2. Having compared the experimental data, computational models founded on SIF (2) and the approach (3) (Fig. 5,6), it was shown that SIF model describes kinetics of the short crack growth no uniquely and may lead to big inaccuracies (Fig. 7) while determining their subcritical growth.

Bibliography

1. J. Schijve, "Fatigue of structures and materials in the 20th century and state of the art," Mater. Sci., No. 3, 7-27 (2003).
2. R. O. Ritchie and S. Suresh, "Mechanics and physics of the growth of small cracks," AGARD Conf. Proc., No. 328, I.1-1.14 (1983).
3. K. J. Miller, "The behavior of short fatigue cracks and their initiation. Part II. A general summary," Fatigue Fract. Eng. Mater. Struct., 10, 93-113 (1987).
4. O. E. Andreykiv and M. B. Kit, "Determination of the subcritical growth period of cracks in structural elements under their bifrequency loading". Mashinostroyeniye, No. 2, 3-7 (2006).

Introduction

Safe and accurate coordination of multi-robots systems is a field of research of high effervescence. Indeed, this kind of system of large potentialities makes possible to carry out for example tasks which are unfeasible for only one robot or improve certain criteria related to the velocity, the robustness or the flexibility of task to achieve. The applicative focus of the proposed PhD thesis corresponds to the field of **autonomous public transportation**.

In recent years, the development of fully autonomous vehicles for transportation tasks has received even more attention from different laboratories/companies through the world[1][2]. The focus of the proposed PhD subject is passengers' transportation in midtown(e.g., to cross an intersection) or in closed/dedicated areas. **Multi-vehicle navigation and coordination** is a complex task and **need very precise design and management of vehicle interaction**. The main scientific challenges related to this PhD subject deals with cooperative autonomous vehicles management and navigation in complex environments/situations(mainly in terms of cooperative scheduling, planning and control).

Safe, efficient and flexible coordination of a group of autonomous vehicles in dynamical environments requires taking into account both inter-connected aspects: high-level and low-level. The PhD thesis will elaborate on the architecture of control/management with the **modular** and **bottom-up** manner like Brooks[3]. Multi-vehicle system(MVS) are controlled either while adopting a centralized approach or while using a distributed approach that only uses local information of the environment. The works of this PhD thesis will obtain optimal or sub-optimal balance between centralized and distributed functionalities in order to enhance the overall efficiency of the MVS based on Hierarchical control structure mentioned above.

Methodology Adopted

The main research content of the doctoral thesis in the first year is to give a hybrid multi-controller architecture for the management/control of a group of vehicles(i.e., Multi-vehicle system, MVS) in constrained and dynamical environment.

A. Robust and Generic Hybrid Multi-Controller Architecture (MCA)

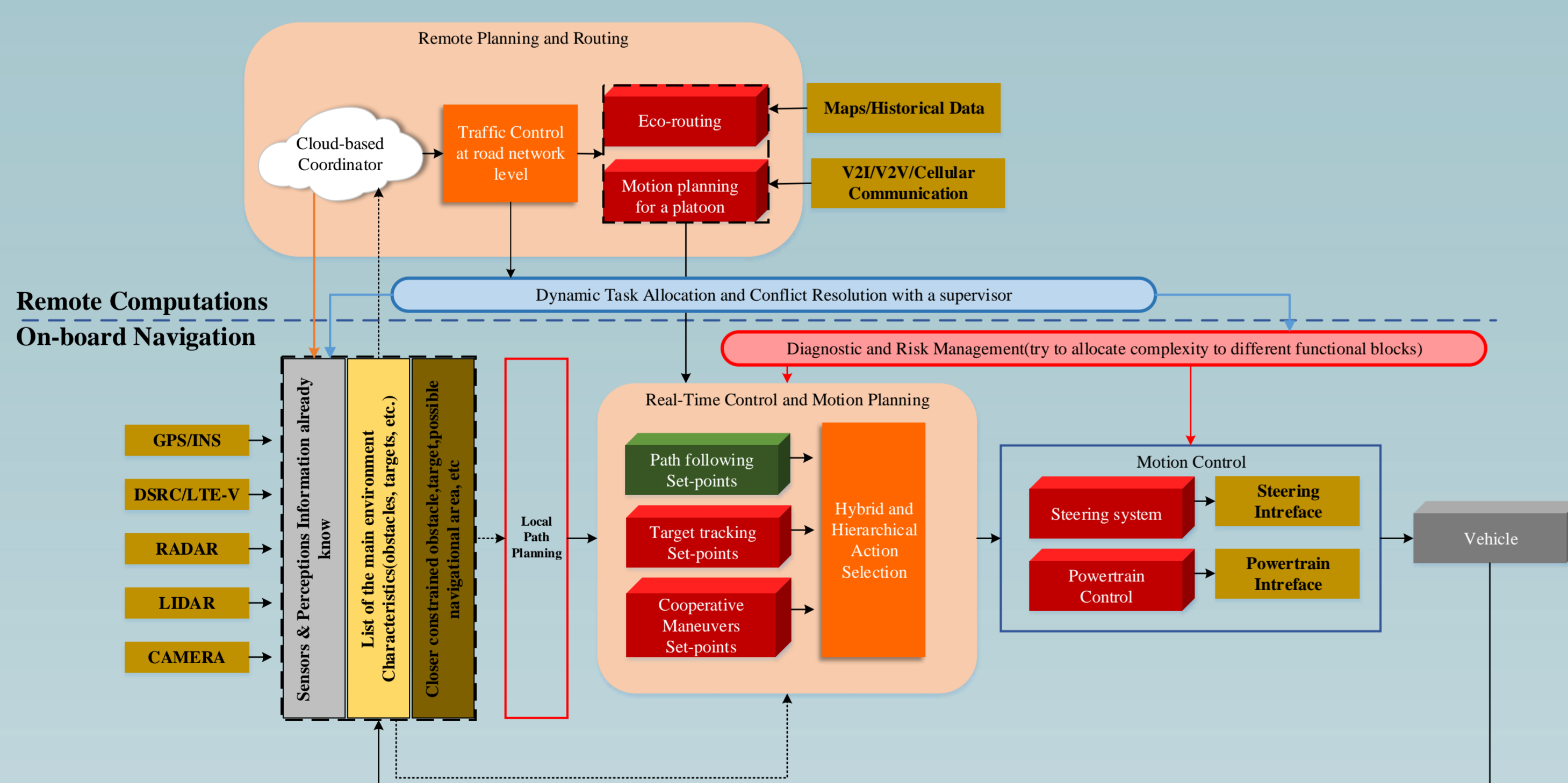


Figure 1. Examples of multi-controller architecture which could be used to manage with reliable way the coordination of autonomous multi-vehicle systems

As show in Figure. 1, a successful multi-vehicle system(MVS) in an intelligent transportation system depends both on the on-board instrumentation and on the surrounding environment, i.e. the road infrastructure and the cloud infrastructure which could supply to MVS static and dynamic road maps. Historical databases, and remote computational power.

B. Cooperative multi-vehicle navigation

The challenge consists of guaranteeing the stability and the safety of the MVS at the critic time of the **transitions between shape configurations**. This will make possible to change online the spatio-temporal configuration of the MVS according to the context of navigation. The developed concepts should be enough generic in order to be applied for **complex intersection/roundabout navigation**.

Results of Optimization-based Coordination of MVS

In the first doctoral year, the optimization problems involve MVS of variable size and these applications are at the border of traffic control(road network level).

- A pictorial classification of these applications is given

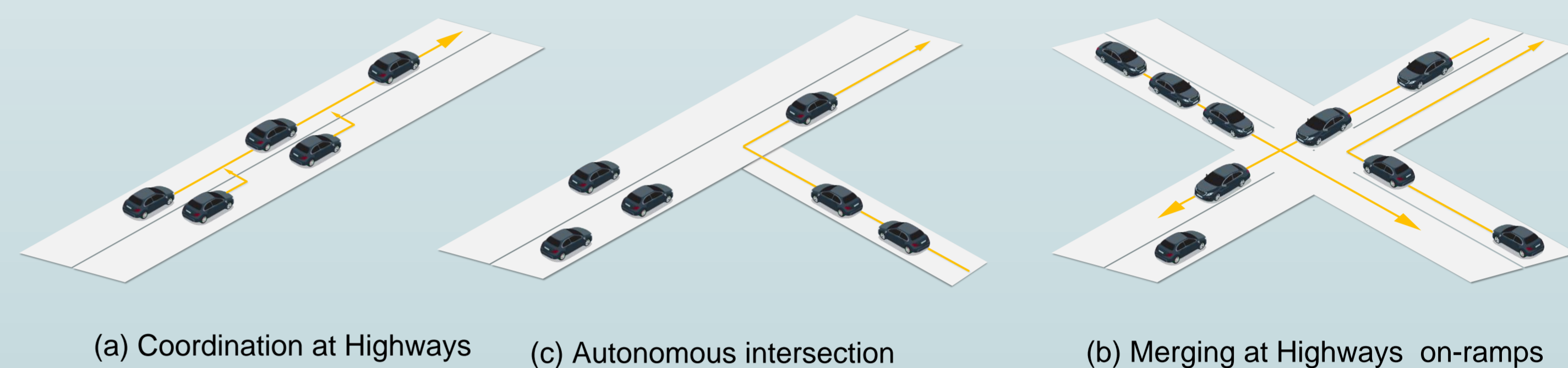


Figure 2. Coordination problems for multi-vehicle systems(MVS)

- Example: Motion planning for a platoon in Highways/Autonomous Intersection

- ① A problem of multi-vehicle coordination that arises in Highways is Proactive Speed Harmonization. If for example for each vehicle i , when it enter a control zone within time $\forall t \in [t_i^0, t_i^m]$, define the set $Y_i(t)$ (W.R.T. a state equation $\dot{x}_i = f(t, x_i, u_i)$) as

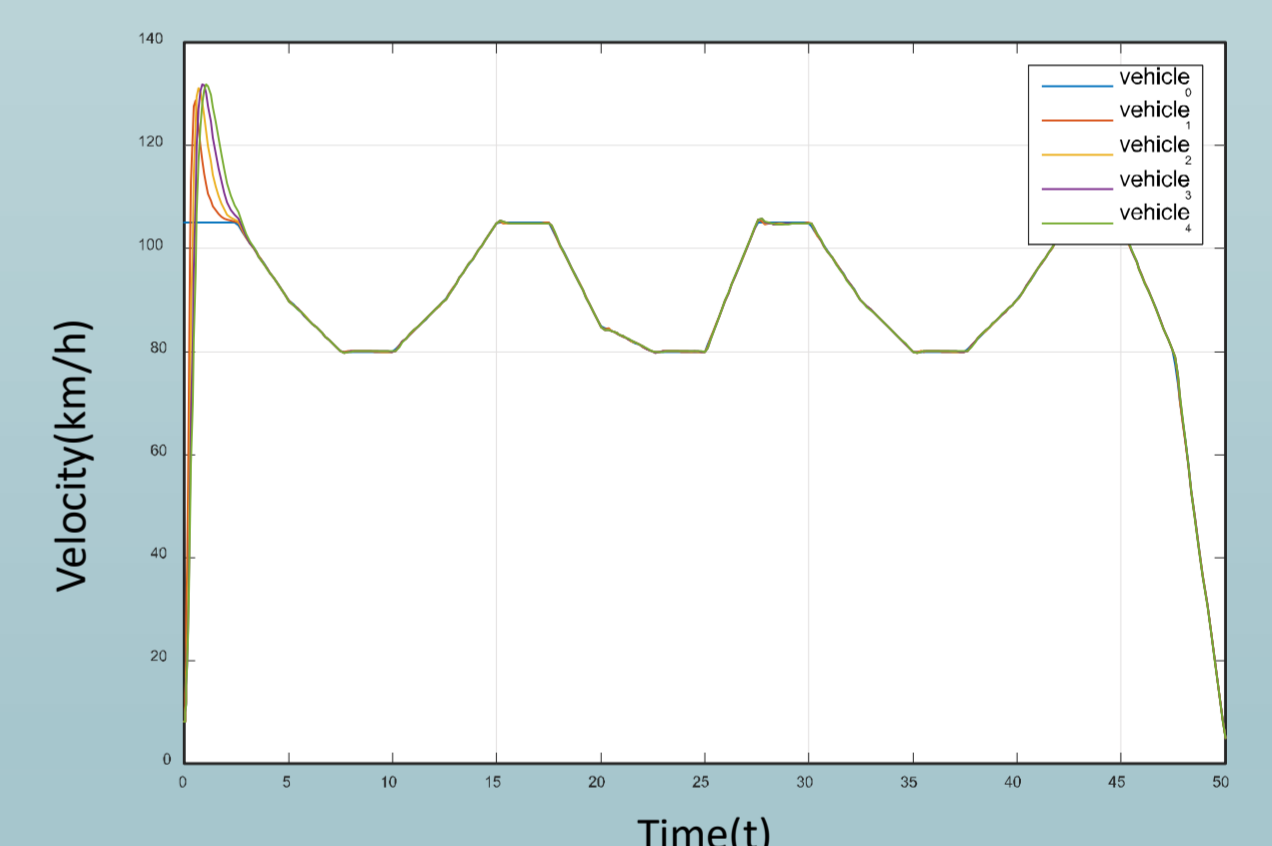
$$Y_i(t) = \{p_i(t), v_i(t), t_i^m\}, \forall t \in [t_i^0, t_i^m]$$

$$\min \frac{1}{2} \int_{t_i^0}^{t_i^m} u_i^2(t) dt, \text{ subject to}$$

$$\dot{p}_i = v_i(t), \text{ and } 0 \leq v_{\min} \leq v_i(t) \leq v_{\max}$$

$$\dot{v}_i = u_i(t), \text{ and } u_{\min} \leq u_i(t) \leq u_{\max}$$

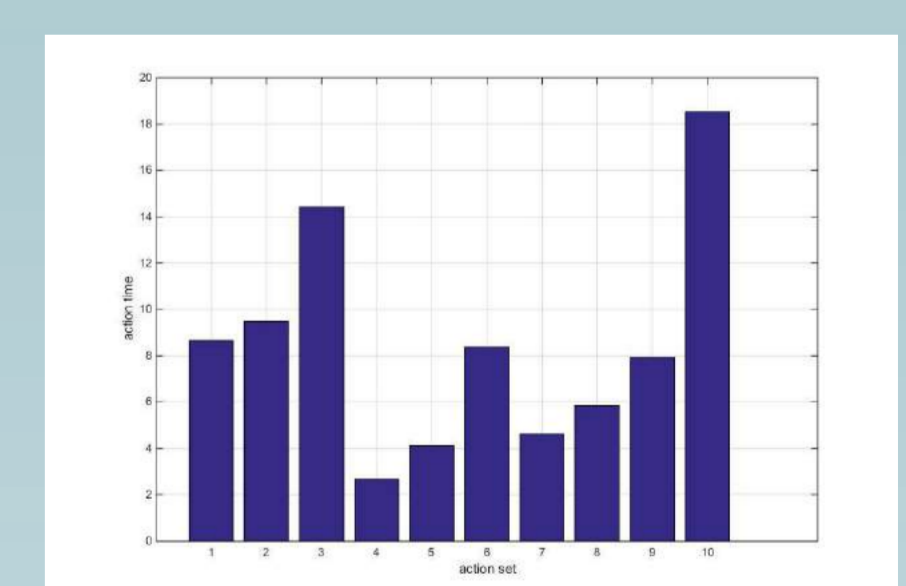
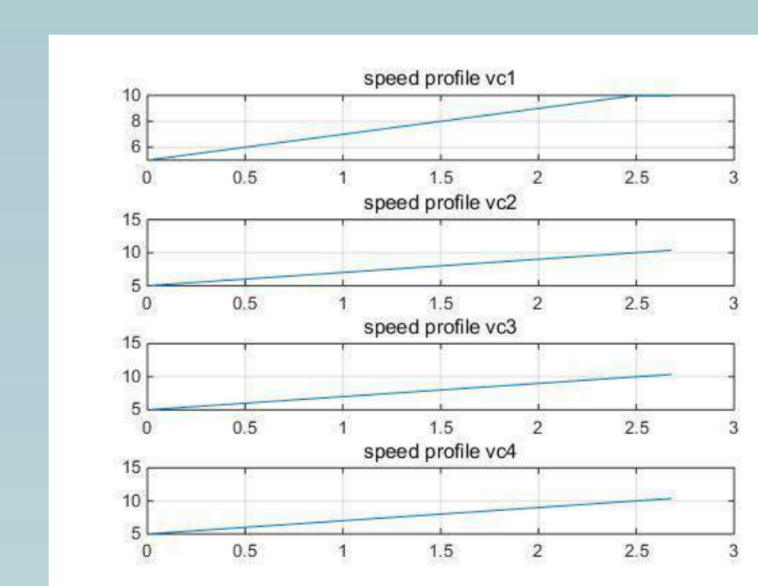
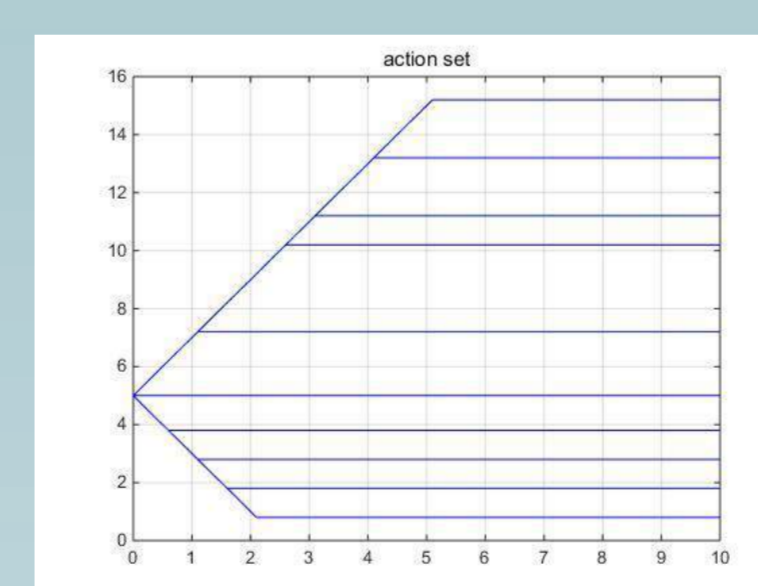
$$p_i(t) \leq p_k(t) - \delta$$



- ② A multi-vehicle probabilistic optimization algorithm is applied to the problem of multi-vehicle coordination in an intersection.

$$J(X) = W_{sep} \sum_{i \neq j} \sum_{k=1}^{k_{max}} \frac{1}{d_k(i, j, i_{self})^2} + W_{speed} (v_{max} - v_{avg})^2 + W_{control} \sum_{k=1}^{k_{max}} |v_{i_{self}}(k) - v_{i_{self}}(0)|$$

$$q^i(X^i) = \min \left(\sum_{k=1}^N q^i(X_k^i) E(J(X_k^i)) - TS(q^i(X^i)) \right)$$



what the next step of work?

- Research the motion driving planning for MVS in global road network maps;
- Integrate the multi-controller architecture from remote computations modular to on-board Navigation modular;
- Develop a Multi-level Bayesian Decision Making Network(MBDMN) for robust and reliable Decision–Action process under high level of uncertainties.

Bibliography

1. Burns, and D. Lawrence . "Sustainable mobility: A vision of our transport future." Nature 497.7448(2013):181-82.
2. B. Hichri, L. Adouane, J.C Fauroux., et al. Cooperative Mobile Robot Control Architecture for Lifting and Transportation of Any Shape Payload. Distributed Autonomous Robotic Systems., Springer Japan, 2016.
3. Brooks, and R. "A robust layered control system for a mobile robot." IEEE Journal of Robotics and Automation 2.1(1986):14-23.



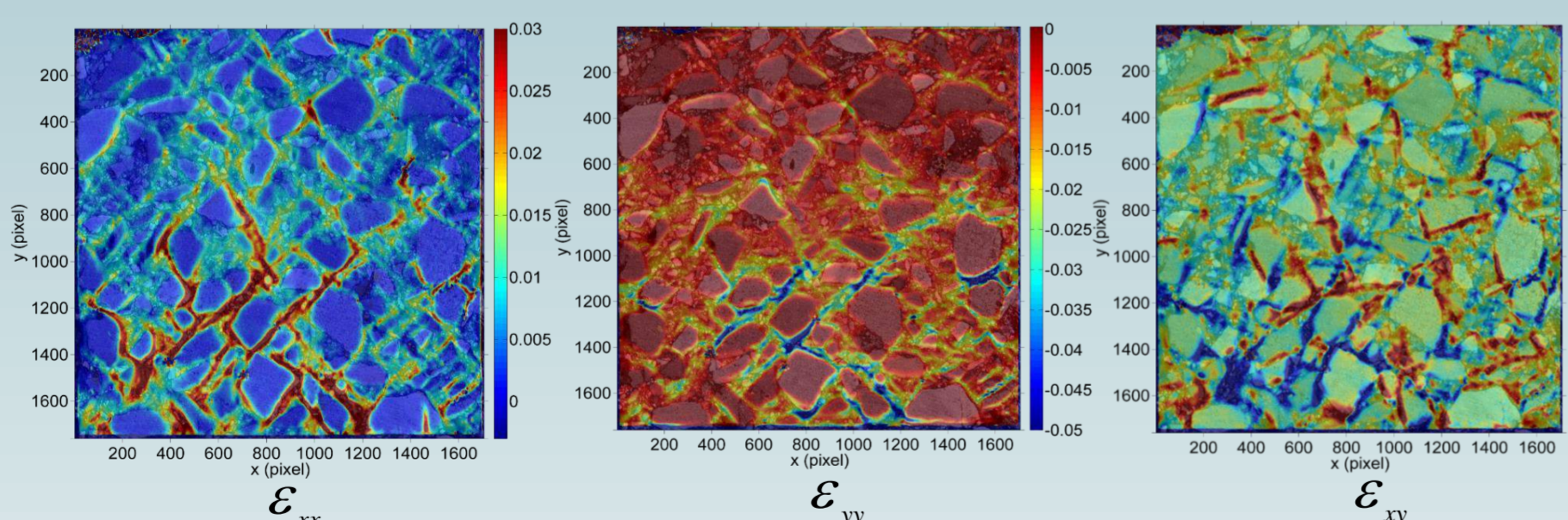
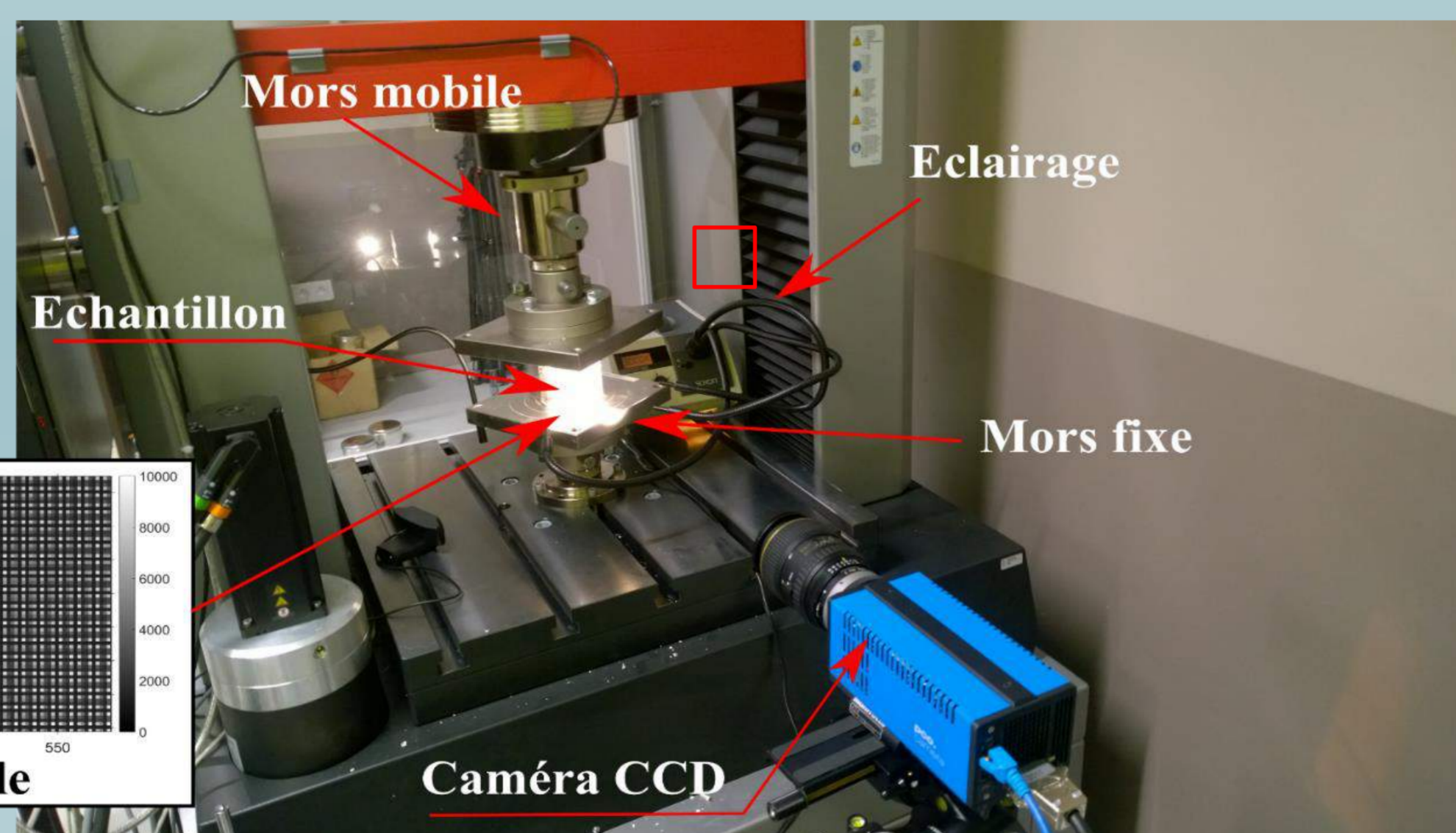
Materials and methods



Demolition and construction waste as well as industrial waste can replace virgin aggregate and bituminous binder, at different percentages, in the manufacture of roads based on recycled materials [2].



The addition of these wastes has beneficial effects on the mechanical properties of asphalt. To understand how these recycled materials work at micro-scale, a full-field measurement method was developed by the laboratory (Grid Method) and will be used during this thesis.



- Strain maps provided by the grid method help to understand the local mechanical behavior of different mixtures [3].
- The strain localization in the binder bands can be distinguished.

Objectives

General objectives :

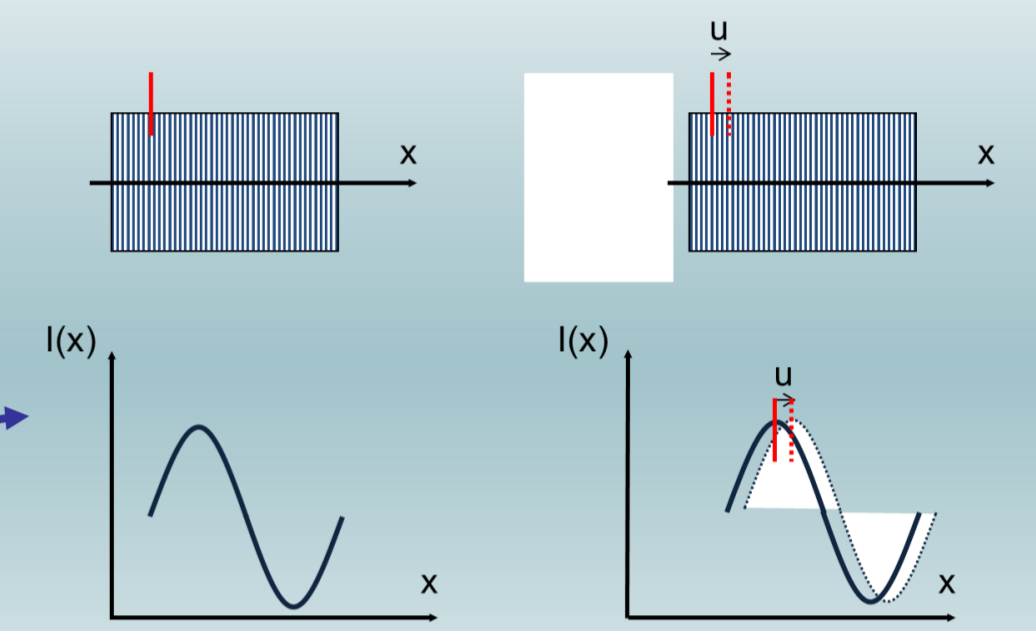
- Save non-renewable natural resources.
- Introduce waste in asphalt mixtures at an optimum rate.

Specific objectives :

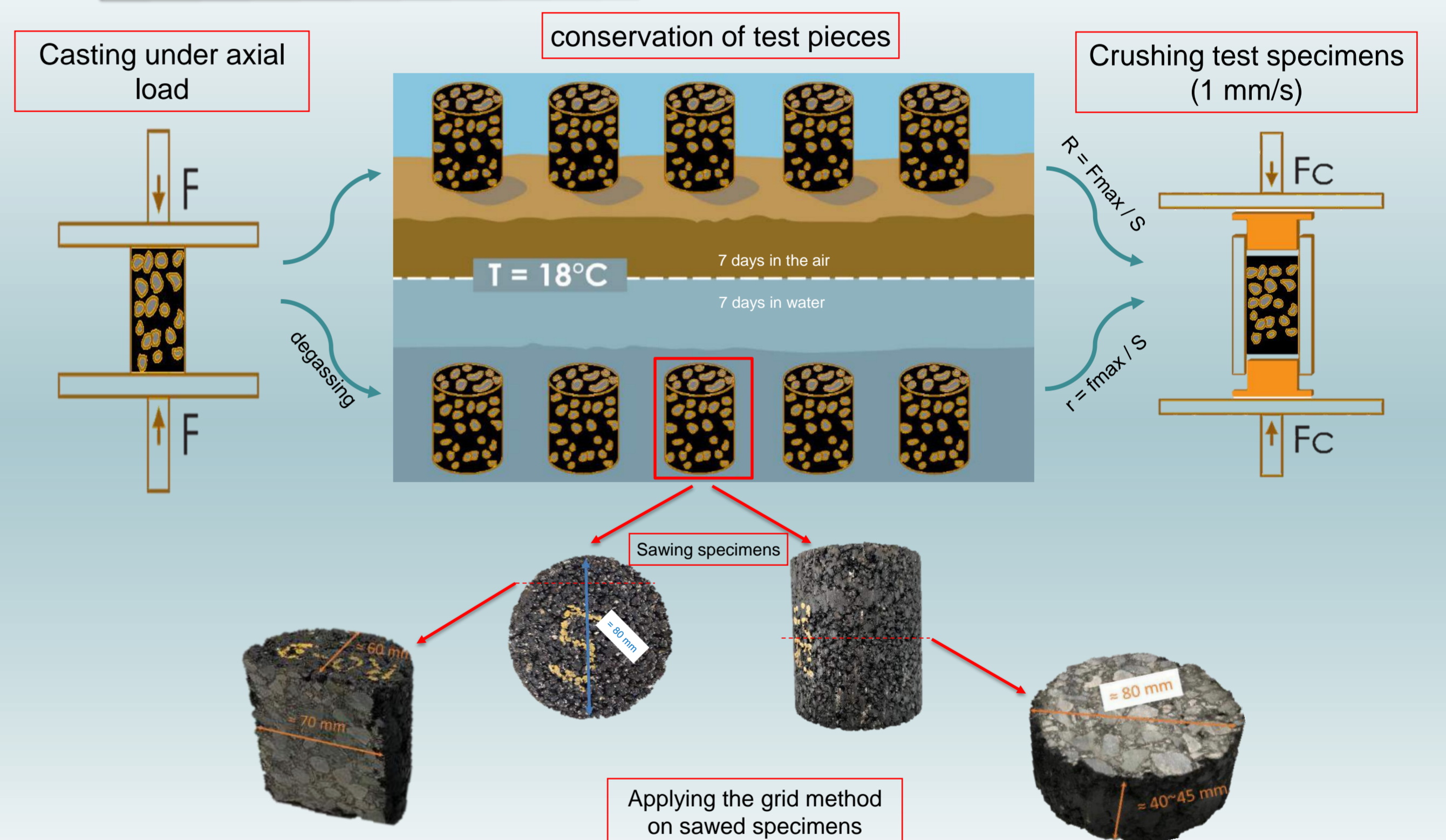
- Study local behavior of asphalt mixtures containing waste materials.
- Evaluate the mechanical behavior of these mixtures.

Grid method

- The grid method is a technique suitable for measuring in-plane displacement and strain maps in experimental mechanics.
- The displacement field is proportional to the phase change between current and reference grid images.



methodology



Expected results

- To evaluate the water sensitivity of bituminous mixes containing recycled asphalt aggregates at different recycling rates (0%, 10%, 20%, 30%, 40% and 50%).
- To obtain accurate information at micro-scale of compression behavior of samples containing recycled asphalt aggregates.
- To improve the performance of asphalt mixtures by introducing waste materials in it.
- To identify the mechanical parameters of different types of Recycled Asphalt Pavement using inverse method.
- To validate the experimental results using finite element method.

Bibliography

[1] Martins Zaumanis, Rajib B Mallick, and Robert Frank. 100% hot mix asphalt recycling : challenges and benefits. *Transportation research procedia*, 14 :3493–3502, 2016.

[2] Arabani, Mahyar, Seyed Amid Tahami, and Mohammad Taghipoor. "Laboratory investigation of hot mix asphalt containing waste materials." *Road Materials and Pavement Design* 18.3 (2017): 713-729.

[3] TEGUEDI, Mohamed Cheikh. *Comportement local des enrobés recyclés: apport des mesures de champs cinématiques*. 2017. Thèse de doctorat. Clermont Auvergne.